63-4-2

R63-23

DASA-1320

DYNAMIC STUDIES OF STRUCTURES BY MEANS OF MODELS

by
Harry G. Harris
Peter Jan Pahl
Shyam D. Sharma

Supervised by
Robert J. Hansen

September, 1962

This research was supported by the
DEFENSE ATOMIC SUPPORT AGENCY

NWER Subtask 13.06
Contract DA-49-146-XZ-025

MIT

DEPARTMEN
OF
CIVIL
ENGINEERIN

SCHOOL OF ENGINEERI
MASSACHUSETTS INSTITUTE OF TEC
Cambridge 39, Massachuse

R63-23 DASA-1320

Department of Civil Engineering

DYNAMIC STUDIES OF STRUCTURES BY MEANS OF MODELS

by

Harry G. Harris
Peter Jan Pahl
Shyam D. Sharma

Supervised by

Robert J. Hansen

September, 1962

This research was supported by the
DEFENSE ATOMIC SUPPORT AGENCY

NWER Subtask 13.06
Contract DA-49-146-XZ-025
DSR 8379

Massachusetts Institute of Technology

Cambridge, Massachusetts

ACKNOWLEDGEMENT

This research was conducted by the Department of Civil Engineering of the Massachusetts Institute of Technology under the supervision of Dr. Robert J. Hansen for the Defense Atomic Support Agency. Chapters 1, 3 and 4 of this report were written by H.G. Harris with data on plastics furnished by S. D. Sharma and Chapter 2 was written by P. J. Pahl. The dynamic tests were done by H. G. Harris and S. D. Sharma.

Thanks go to the various departments at M.I.T. whose facilities were used in the course of the research: the Materials Testing Laboratory of the Mechanical Engineering Department, the Plastics Research Laboratory, the Models Research Laboratory and the Soil Mechanics Laboratory of the Civil Engineering Department.

Special thanks go to Mr. Donald Gunn for machining many of the parts used in the testing program to Mr. Edward McCaffrey for assisting in the instrumentation of the dynamic tests.

The help received from the informal discussions which the authors had with many of their colleagues and professors is greatfully acknowledged.

Thanks also go to Misses Patricia Markee and Marguerite Bakarian for typing this report.

TABLE OF CONTENTS

TABLE OF CONTENTS (CONT.)

TABLE OF CONTENTS (CONT.)

TABLE OF CONTENTS (CONT.)

TABLE OF CONTENTS (CONT.)

LIST OF TABLES

LIST OF TABLES (Cont'd.)

LIST OF FIGURES

LIST OF FIGURES (Cont'd.)

LIST OF FIGURES (Cont'd.)

LIST OF FIGURES (Cont'd.)

LIST OF FIGURES (Cont'd.)

LIST OF FIGURES (Cont'd.)

LIST OF APPENDICES

NOTATION

a	acceleration vector
A	any material property
a_e	earth's gravitational acceleration
B	any external influence
c	specific heat
$C_1,\ldots,C_4$	constants (p.70)
C	any partial derivative in the equation of state
$D(z)$	dimension of physical quantity z
$D(z_1, z_2, z_3)$	dimensional relationship between z_1, z_2, and z_3.
$d(z)$	density function for the physical quantity z.
E	modulus of elasticity in the linear elastic range.
e	base of natural logarithm
f_z	correlation function for the physical quantity z
F	applied force (Appendix A)
g	specific mass
G	body force
h	coefficient of linear thermal expansion
H	heat
K_1, K_2	Coefficients in creep law (p. 33)
L	length
L_j	load per influence volume
P_{ult}	ultimate load carrying capacity of a structure
m	mass
M_p	ultimate moment of section at complete plastification
N	axial thrust in member
P	external force on structure
p	applied surface stress (section 2.7)

p	subscript used to denote prototype properties
q	any property of a structure
r	distance in system of spherical coordinates
$1/R$	rate of change of slope, or the curvature of the elastic curve
S_Z	standard deviation for physical quantity Z
t	time
T	temperature
u	displacement vector
v	velocity
v_j	influence volume
V	shearing component of load
V_i	function defining the i-th surface of the structure
w	specific gravity
W	Weight of structure
x	coefficient of thermal conductivity
γ	gravitational constant
δ_p	vertical deflection
δ_v	deflection along V
δ_N	deflection along N
ϵ	strain
ϵ_{max}	maximum strain that the material can undergo before rupture
ϵ_y	yield strain of the material
ϵ_s	beginning of strain hardening
μ	friction coefficient
ν	Poisson Ratio

θ	angle in system of spherical coordinates (in Chapter 2)
θ	half the joint rotation in the knee (in Chapters 1, 3 and 4)
ϕ	angle in system of spherical coordinates (in Chapter 2)
ϕ	rate of change of slope of the elastic curve
σ	stress
$\sigma_{y\ell}$	lower yield stress of a material
σ_{yu}	upper yield stress of a material
σ_{dy}	dynamic yield stress
σ_1	major principal stress
σ_2	minor principal stress
τ_{max}	maximum shear stress

ABSTRACT

The objective of this research work is the investigation of materials and techniques that can be used in model studies of structures under blast-type loads. The materials are selected on the basis of theoretical considerations, and their usefulness is demonstrated by means of actual model structure tests which are compared to prototype tests.

The theory of structural models is reviewed and extended to a very general form, with emphasis on the basic differences in the approach suitable for analysis by means of the mathematical model and the physical model respectively. This extension of the theory proves to be necessary when the large number of factors affecting a dynamic model study in the plastic range are to be taken into account in a systematic manner. A description of the general properties of a structure is followed by a dimensional analysis leading to a comparison between model and prototype. The criteria for compatibility between model and prototype materials are derived in detail. Modelling is discussed as a random process, and the theory is applied to massive structures in particular.

It is shown that plastic deformations during dynamic response impose severe restrictions on the equation of state of the model material which is to be compatible with steel as a prototype material. The properites of phosphor bronze and ethyl cellulose and their usefulness as modelling materials for steel structures under dynamic loads are discussed. Manufacturing techniques for phosphor bronze and the loading devices used in the studies are described in detail. The results of model studies of beams, joints and portal frames under static loads are compared to results

obtained from tests on full scale structures, and a technique of testing models under dynamic loads is described

Since model and prototype results generally show good agreement, it is concluded that the metal phosphor bronze can be used as a modelling material in small scale studies of welded steel structures in all cases where the model and prototype surface loads do not have to be of equal intensity. This will, for instance, be the case where the blast loading is mainly of the drag type. The use of plastics in the modeling of steel structures presents problems which cannot be overcome without a reliable error analysis of the model since in this case the model will be distorted above the proportional limit.

CHAPTER 1

INTRODUCTION

The use of physical models in the study of engineering problems has become prevalent in the past decade (1,2,3)*. Two general classes of problems lend themselves particularly to a model solution. First, in problems where the number of variables or the complexity of the situation make the analytical solution difficult or particularly cumbersome and second, in areas where the general laws governing the phenomenon have not yet been sufficiently developed and a general theory is lacking. The study of the dynamic response of structures is one area of structural mechanics where the modeling method of analysis may be used to advantage. It is the aim of this report to discuss the problems of using structural models to study the dynamic behavior of structures in general and to present specific examples in the choice of modeling materials and the modeling techniques developed for their use.

1.1 THE STRUCTURAL MODEL

A structural model is a device, which being a reproduction of the prototype following certain rules, can be used to find particular unknown quantities about the prototype. Two large classes of models emerge from this definition. One encompasses all those model studies dealing with elastic problems. In this case both model and prototype are within the elastic range and the results can be compared with those obtained analytically if such methods exist. A second group representing a more recent approach to the use of models is in closer agreement with present day concepts of structural analysis and design(31). Here, the model is

---

* Numbers in parenthesis indicate the particular reference cited as listed at the end of the report.

a faithful reproduction of the prototype following the laws of similitude and boundary conditions from which the ultimate behavior of the prototype can be predicted as well as the factor of safety which is defined as the ratio of ultimate load to the working load acting on the structure. Although the second approach by the nature of its scope places more restrictions on the model, it is the only one feasible in certain problems where plastic deformations are tolerated. Such problems arise in the study of the dynamic response of structures where energy absorption criteria allow the use of some plastic deformations in design. Two basic types of models arise in our study of structural problems. One is the stress model or a model which fails because of rupture of the material at local points, and the buckling model which becomes unstable at certain critical loads and results in large deflection. Our main concern here is the stress type of model and we shall attempt to investigate its behavior.

1.2 A HISTORICAL SURVEY OF MODEL STUDIES

Physical models have been used to some extent in structural analysis and design for many years. In general the principal external forces involved in these studies have been static in nature. Further, only the elastic behavior of the model, hence the prototype, was of interest. Model studies to verify the analytical results of complicated structural problems are recorded in the literature[50,28]. In most of these cases the importance of the project made it feasible to make a model study but in all these cases the model was used as a check. It was inconceivalbe then to base the design on the results of a thorough model study. As teaching aids in indeterminate structural analysis, models have found their place in the laboratories of many schools[50]. These, however, have been predominantly of the first class or elastic models.

More recent model studies especially in the field of arch dams have been done in Europe[32,33,38,39]. Techniques have been developed and refined to the point where the model study plays a major role in the design of arch and domed dams. Besides the extensive work on dams however, model studies of complicated buildings and earthquake effects as well as pioneering work in model studies beyond the elastic limit have also been done[36]. All being said, the European model studies have set a good precedent and have prompted many engineers to base their designs on a model study.

In the United States great impetus has been given to model studies in the postwar years. This revival stems from two main sources. Architectural taste for more complicated but pleasing structural forms and the intensive efforts to develop techniques for the design of structures and structural elements to resist dynamic loads have introduced some very interesting but difficult problems. The models in studies dealing with dynamic response have been loaded to failure in shock tubes, by impulsive loading machines and in some cases by high explosive detonations[8,18,26,42]. In the majority of cases reinforced concrete structures were modeled by the steel wire-mortar technique. Dynamic tests on model or prototype steel structures are far less. Many problems are encountered in such studies but the results up to the present (1962) seem encouraging and it is anticipated that with future research enough data will be collected to make the modeling technique an indispensible tool at the disposal of the structural engineer.

1.3 LIMITATIONS OF PRESENT DAY MODEL STUDIES

Although the general theory of structural models under the most general conditions has been known for a long time its application to specific cases has been limited. The reasons are many but among them one stands out as a limitation which must be overcome before the modeling technique can be applied with confidence to non-linear problems in structures and to distorted models. This limitation is

the lack of a comprehensive method of evaluating errors in models which may be "distorted". Thus far model studies are limited to elastic cases and to a few known rheologically compatible model materials. In many cases the same material is used in the model (to be on the safe side) and external means are employed to satisfy similitude thus introducing errors of a different nature. An error analysis of models would be a great contribution to model theory and would open new horizons in the applications of the modeling technique.

More work is needed to establish criteria on the scale limits of model studies. It is obvious that the smaller the model the bigger the chance of increasing the errors in the results. Thus if there is a correlation between percentage error and scale for a particular class of problems the experimenter would be able to pick a scale which will be within the tolerance of his overall allowable error.

Another area which needs more study is the need of a method of making the model and prototype materials compatible while satisfying the other similitude requirements. It is hoped that some light will be thrown upon this problem in the sections that follow.

CHAPTER 2

A GENERAL THEORY OF STRUCTURAL MODELS

The basic aim of the analysis of a structure is the prediction of its behavior at a time different from that at which initial conditions are specified. For the purpose of the investigation, the nature of the structure may be described either abstractly by means of a mathematical model or concretely by means of a physical model, frequently called "the structural model". Each of the two methods has its own specific advantages. The mathematical method tends to use a model in which some of the physical events occurring in the actual structure are either simplified or neglected. As a result, a speedy analysis is possible without excessive loss in accuracy. The physical model, on the other hand, permits the investigator to account accurately for a large number of physical events and variables even if they have complex space-time distributions.

This important property of the structural model can be used to full advantage only if the experiments are based on a very general theory. Indeed, direct application of formulations appropriate for use in current methods of mathematical analysis will unnecessarily limit the scope of structural model investigations. This reasoning has led to the unusual formulations encountered in some of the later sections.

The theory of structural models forms the basis for the planning, execution and interpretation of laboratory studies on a physical model which permit the prediction of the behavior of a prototype structure under static or dynamic conditions. It establishes the rules according to which the geometry, material properties, initial conditions and boundary conditions of the model and of the prototype have to be related so that the behavior of the one can be expressed as a function of the behavior of the other. The

degree of perfection with which these relationships can be maintained during the actual experiment, and the effect of any possible deviation on the accuracy of the prediction of the prototype behavior, are discussed briefly in Section 2.5.

The physical events considered in this theory are described in Sections 2.1 and 2.3. If an event occurs in either model or prototype which involves physical laws not considered in the theory presented here, the model studies will lead to erroneous results. So, for instance, electromagnetic effects are not taken into account since they play no role in the vast majority of structural problems.

2.1 DESCRIPTION OF THE MODEL AND PROTOTYPE STRUCTURES

Before a one to one correspondence between model and prototype can be established, the properties of and external influences on each of them individually must be specified. The following physical quantities in most cases fully describe the nature of a structural problem:

2.1.1 Geometric Properties. If time is not considered to be a basic dimension, a point in a structure is fully described by its three space coordinates. A general theory must, however, take the variation of geometry with time into account, so that time must be regarded as a coordinate in the same manner as the space coordinates.

If no mass is added to or removed from the structure during the time interval in which its behavior is to be studied, its geometry needs to be specified at one time t_o only. The geometry at any other time t will then be uniquely determined by the displacement vector $\bar{u}$ defined later. But if, for instance, the erection period of the structure is to be included in the model study, a complete time history of the geometry during that interval must be given.

The position of any mass particle of a structure in space may be described in any one of the many well-known coordinate systems. It is thus necessary to prove that the theory loses none of its generality if it is restricted to a single system of coordinates. Assume,

for instance, that spherical coordinates are chosen, so that the position of point P at time t is

$$P \equiv P(r, \theta, \varphi, t) \qquad (2.1.1)$$

In all other coordinate systems, P would also be fixed by at least one length and, in some cases, dimensionless ratios such as angles. Thus no new physical variables will be introduced by a coordinate transformation, and the theory may be limited to the system of equation (2.1.1).

The extent of the structure is defined by its enclosing surfaces which can be expressed by equations of the form

$$V_i (r, \theta, \varphi) = 0 \qquad (2.1.2)$$

The number i of these equations varies from one upward and is equal to the number of surfaces by which the structure is bounded. As time varies, their number may increase or decrease and the region of validity of existing V_i functions may change. Thus the limits of any two of the three space coordinates must be given in terms of the fourth coordinate, time:

$$r_j(t) \leq r_i \leq r_k(t)$$

$$\theta_j(t) \leq \theta_i \leq \theta_k(t) \qquad (2.1.3)$$

where i is the same index as in equation (2.1.2). The limits of the third space coordinate, φ, can be calculated from equation 2.1.2 and the geometry of the entire structure is now fully described.

2.1.2 Material Properties. A structure will, in the most general case, consist of several materials, each of which has its own particular physical properties that may, or may not, change with time and temperature. For the purpose of this theory it is, however, more convenient though still perfectly general to treat the structure as if it consisted of a single material whose properties change from point to

point in space as well as with time and temperature. The intrinsic properties of the material are then given by the functions:

Specific Mass:	$g = g(r, \Theta, \varphi, t, T)$
Specific Heat:	$c = c(r, \Theta, \varphi, t, T)$
Coefficient of Thermal Conductivity:	$x = x(r, \Theta, \varphi, t, T)$
Coefficient of Linear Thermal Expansion:	$h = h(r, \Theta, \varphi, t, T)$

(2.1.4)

A material is not fully specified by its intrinsic properties. Those of the material properties which are dependent on external influences are interrelated by the equation of state of the material, which will be presented in Section 2.3.

2.1.3 Initial Conditions. When the geometry of the structure is specified at time t_o, the material may already be subject to initial stresses due to prestressing or other processes that have taken place before time t_o. There will also be an initial temperature distribution so that it is necessary to specify

Initial Stress:	$\bar{\sigma}_o = \bar{\sigma}(r, \Theta, \varphi, t_o)$
Initial Temperature:	$T_o = T(r, \Theta, \varphi, t_o)$

(2.1.5)

If the history of a structure is known from the beginning of its erection period, and all events (such as shrinkage of concrete) during and immediately following this period are taken into account in the analysis, no specific initial conditions need to be specified. In some cases where the molecular processes occurring in a prototype (e.g., during curing) cannot be reproduced correctly in the physical model, the specification of initial stresses may become mandatory even if the entire history of the structure is known.

2.1.4 External Influences on a Structure. The influences acting on a structure from the outside fall into two categories:

the forces and displacements imposed on its boundary surfaces and the body forces acting as a result of the attraction between the mass of the structure and the mass of the earth.

At every location on the face of a structure, the imposed surface force (i.e. force per unit area) is defined by the vector

$$\bar{P} = \bar{P}(r, \theta, \varphi, t) \qquad (2.1.6)$$

In the literature, a distinction is sometimes made between point, line and surface forces. This distinction is artificial since all forces necessarily have to be applied over an area. It is not desirable to introduce into a structural model study without justification all the simplifications that are convenient for mathematical methods.

At some points on the surface (e.g. at a perfectly rigid support) displacements rather than forces may be applied to the structure. They are specified by the displacement vector

$$\bar{u}^i = \bar{u}(r, \theta, \varphi, t) \qquad (2.1.7)$$

where superscript i distinguishes the externally imposed displacements from those which are the result of the response of the structure to other external influences such as forces. Frequently structures are subjected to a combination of boundary forces and displacements.

The body forces caused by the earth's attraction on the structure are described by the vector

$$\bar{G}^i = \bar{G}(r, \theta, \varphi) \qquad (2.1.8)$$

where time variations in the earth's field of attraction are neglected. The nature of these body forces is quite different from that of the inertia body forces caused by the response of the structure to dynamic surface loads or support accelerations, as will be shown in more detail in Section 2.6.1.

The structure will also respond to temperature changes at its surfaces. They are specified by means of the scalar

$$T^i = T(r, \Theta, \varphi, t) \qquad (2.1.9)$$

2.1.5 Description of Structural Behavior. Once a structure with given geometric and material properties and given initial conditions is subjected to a set of external influences, its response has to be registered by measuring certain physical quantities which are indicative of the nature of the structure. Three different aspects of the behavior of a structure are of particular interest to the engineer:

a) Stress, Strain or Displacement Distribution - The stress or strain distribution in a concrete structure, for instance, is of importance in the determination of the positioning and dimensioning of the steel reinforcement. The displacement distribution is of importance in flexible structures where deformations are restricted by building codes.

Since all the properties of and influences on a structure are space and time dependent, the stress, strain or displacement distributions will be known in terms of the space and time coordinates once the following functional relationships have been determined:

$$\text{Displacements:} \quad \bar{u} = \bar{u}(V_1, g, c, x, h, \bar{\sigma}_o, T_o, \bar{P}, \bar{u}^i, \bar{G}^i, T^i)$$

$$\text{Stresses:} \quad \bar{\sigma} = \bar{\sigma}(V_1, g, c, x, h, \bar{\sigma}_o, T_o, \bar{P}, \bar{u}^i, \bar{G}^i, T^i)$$

$$\text{Strains:} \quad \epsilon = \epsilon(V_1, g, c, x, h, \bar{\sigma}_o, T_o, \bar{P}, \bar{u}^i, \bar{G}^i, T^i) \qquad (2.1.10)$$

This is the most general form of solution since it is valid for all space time distributions of the variables in the brackets. For any specified space time distribution of the variables, $\bar{u}$, $\bar{\sigma}$ and ϵ are found as functions of r, Θ, φ and t by direct substitution.

Frequently, the analysis is simplified considerably if the distribution of $\bar{u}$, $\bar{\sigma}$, and ϵ has to be found for just one specific space time distribution of the variables. These investigations are referred to as case studies, and the results are obtained directly as

$$\begin{aligned} \bar{u} &= \bar{u}(r, \theta, \varphi, t) \\ \bar{\sigma} &= \bar{\sigma}(r, \theta, \varphi, t) \\ \epsilon &= \epsilon(r, \theta, \varphi, t) \end{aligned} \qquad (2.1.11)$$

$\bar{u}$, $\bar{\sigma}$ and ϵ are actually related through the equation of state of the structural material and the definition of strain:

$$\epsilon = \frac{d\bar{u}}{dy} \qquad (2.1.12)$$

where y is the distance measured in the direction of $\bar{u}$ and ϵ. Since the stress-strain relationship is not always unique and in addition changes with the stress history of the material as will be shown in Section 2.3, and since displacements have to be obtained from strains by a frequently difficult integration, it is customary in model studies to observe them as if they were independent. The possibility of obtaining $\bar{u}$ and ϵ separately in a physical model is one of the main advantages of that method over current mathematical approaches.

b) The Ultimate Load - A knowledge of the stress, strain or displacement distribution at a load level below that required for failure in general does not constitute sufficient information to predict the failure load itself. The determination of the ultimate load, which is of paramount importance to the safety of the structure, is thus a problem of its own. It requires the specification of an exact failure criterion, which in most cases depends on the purpose of the structure studied. It may be decided to impose limits on

Frequently, the analysis is simplified considerably if the distribution of $\bar{u}$, $\bar{\sigma}$, and ϵ has to be found for just one specific space time distribution of the variables. These investigations are referred to as case studies, and the results are obtained directly as

$$\begin{aligned} \bar{u} &= \bar{u}(r, \theta, \varphi, t) \\ \bar{\sigma} &= \bar{\sigma}(r, \theta, \varphi, t) \\ \epsilon &= \epsilon(r, \theta, \varphi, t) \end{aligned} \qquad (2.1.11)$$

$\bar{u}$, $\bar{\sigma}$ and ϵ are actually related through the equation of state of the structural material and the definition of strain:

$$\epsilon = \frac{d\bar{u}}{dy} \qquad (2.1.12)$$

where y is the distance measured in the direction of $\bar{u}$ and ϵ. Since the stress-strain relationship is not always unique and in addition changes with the stress history of the material as will be shown in Section 2.3, and since displacements have to be obtained from strains by a frequently difficult integration, it is customary in model studies to observe them as if they were independent. The possibility of obtaining $\bar{u}$ and ϵ separately in a physical model is one of the main advantages of that method over current mathematical approaches.

b) The Ultimate Load - A knowledge of the stress, strain or displacement distribution at a load level below that required for failure in general does not constitute sufficient information to predict the failure load itself. The determination of the ultimate load, which is of paramount importance to the safety of the structure, is thus a problem of its own. It requires the specification of an exact failure criterion, which in most cases depends on the purpose of the structure studied. It may be decided to impose limits on

i) the absolute displacement of points in the structure to prevent excessive deflections associated with excessive strains.

ii) the relative displacement of points in the structure to prevent rupture.

iii) spacing and width of cracks in reinforced concrete structures.

It will be shown in section 2.5 that the choice of the failure criterion has considerable influence on both the outcome and the reliability of a model investigation.

c) The Buckling Load - Thin structures such as shells and thin structural elements such as flanges of I-beams sometimes undergo large deflections without excessive strains if they are subjected to compressive loads. They are then said to have buckled. The determination of a satisfactory general buckling criterion for the mathematical model is at present still one of the major problems of structural engineering. The physical model here shows a very marked superiority. It is possible in most cases to recognize a buckling failure by direct observation. Most shells, for instance, show a sudden snap-through. If the material is still in its elastic range when buckling occurs, the original shape of the structure is regained once the load is removed.

2.2 THE RELATIONSHIP BETWEEN MODEL AND PROTOTYPE

It is essential to keep in mind at all times that the information eventually to be obtained from a structural model study concerns the behavior of the prototype, not that of the model. Since all the measurements are, however, carried out on the model, it is necessary to develop laws according to which the model results can be extrapolated to the prototype. For the derivation of these laws, assume that both model and prototype are fully described by the physical quantities defined in Section 2.1. Model and prototype will

then be related if the relationship of each of these quantities individually is described by means of a "correlation function" f. In the literature [3,31], these correlation functions are frequently defined as constant ratios. In a more general theory, they may be made functions of the basic coordinates r, θ, φ and t. It will then be possible, for instance, to use distorted models without violating any of the similitude requirements derived later in this section. The correlation function concept will also be found useful in Section 2.5 when structural model analysis is considered as a random process.

2.2.1 Geometric Properties. The distance r and time t are the only physical quantities required for the description of the geometric properties. Thus model and prototype are related if

$$r_m = f_r(r, \theta, \varphi, t)\, r_p$$

$$t_m = f_t(r, \theta, \varphi, t)\, t_p \qquad (2.2.1)$$

where the following conventions are observed:

i) Subscript m denotes model property

ii) Subscript p denotes prototype property

iii) f_z denotes correlation function for the physical quantity z and is evaluated at r, θ, φ and t of the prototype.

Since angles are dimensionless ratios, it follows that

$$\theta_m = \theta_p$$

and

$$\varphi_m = \varphi_p$$

2.2.2 Material Properties. Model and prototype are related as follows:

Specific Mass: $g_m = f_g(r, \theta, \varphi, t) g_p$

Specific Heat: $c_m = f_c(r, \theta, \varphi, t) c_p$

Coefficient of Thermal Conductivity: $x_m = f_x(r, \Theta, \varphi, t)x_p$

Coefficient of Thermal Expansion: $h_m = f_h(r, \Theta, \varphi, t)h_p$

(2.2.2)

2.2.3 Initial Conditions. Model and prototype are related if

Initial Stress $\bar{\sigma}_{o_m} = f_\sigma(r, \Theta, \varphi, t_o)\bar{\sigma}_{o_p}$

Initial Temperature $T_{o_m} = f_T(r, \Theta, \varphi, t_o)T_{o_p}$

(2.2.3)

2.2.4 External Influences on a Structure. Model and prototype are related if

Surface Forces: $\bar{P}_m = f_p(N, \Theta, \varphi, t)\bar{P}_p$

Displacements: $\bar{u}^i_m = f_u(r, \Theta, \varphi, t)\bar{u}^i_p$

Body Forces: $\bar{G}^i_m = f_G(r, \Theta, \varphi, t)\bar{G}^i_p$

Temperature: $T^i_m = f_T(r, \Theta, \varphi, t)T^i_p$

(2.2.4)

It should be noted that the correlation functions defined in Sections 2.2.1 to 2.2.4 are independent of the state of stress or strain of the materials involved.

2.2.5 Comparison of Structural Behavior. In addition to the quantities described in Section 2.1.5, the acceleration

$$\bar{a} = \frac{\partial^2 \bar{u}}{\partial t^2} \qquad (2.2.5)$$

which occurs in many applications, will also be considered. The required correlation functions thus are

Displacements: $\bar{u}_m = f_u(r, \Theta, \varphi, t)\bar{u}_p$

Stresses: $\bar{\sigma}_m = f_\sigma(r, \Theta, \varphi, t)\bar{\sigma}_p$

Coefficient of Thermal Conductivity: $x_m = f_x(r, \Theta, \varphi, t)x_p$

Coefficient of Thermal Expansion: $h_m = f_h(r, \Theta, \varphi, t)h_p$

(2.2.2)

2.2.3 Initial Conditions. Model and prototype are related if

Initial Stress $\bar{\sigma}_{o_m} = f_\sigma(r, \Theta, \varphi, t_o)\bar{\sigma}_{o_p}$

Initial Temperature $T_{o_m} = f_T(r, \Theta, \varphi, t_o)T_{o_p}$

(2.2.3)

2.2.4 External Influences on a Structure. Model and prototype are related if

Surface Forces: $\bar{P}_m = f_{\underline{p}}(N, \Theta, \varphi, t)\bar{P}_p$

Displacements: $\bar{u}^i_m = f_u(r, \Theta, \varphi, t)\bar{u}^i_p$

Body Forces: $\bar{G}^i_m = f_G(r, \Theta, \varphi, t)\bar{G}^i_p$

Temperature: $T^i_m = f_T(r, \Theta, \varphi, t)T^i_p$

(2.2.4)

It should be noted that the correlation functions defined in Sections 2.2.1 to 2.2.4 are independent of the state of stress or strain of the materials involved.

2.2.5 Comparison of Structural Behavior. In addition to the quantities described in Section 2.1.5, the acceleration

$$\bar{a} = \frac{\partial^2 \bar{u}}{\partial t^2} \qquad (2.2.5)$$

which occurs in many applications, will also be considered. The required correlation functions thus are

Displacements: $\bar{u}_m = f_u(r, \Theta, \varphi, t)\bar{u}_p$

Stresses: $\bar{\sigma}_m = f_\sigma(r, \Theta, \varphi, t)\bar{\sigma}_p$

Accelerations: $$\bar{a}_m = f_a(r, \theta, \varphi, t)\bar{a}_p \qquad (2.2.6)$$

It follows from equation (2.1.12) that

$$\epsilon_m = \frac{\bar{u}_m}{y_m} = \frac{f_r \bar{u}_p}{f_r y_p} = \epsilon_p \qquad (2.2.7)$$

so that no correlation function for strains needs to be specified.

2.2.6 Dimensional Analysis. If all the correlation functions defined in the previous sections were independent, the prototype behavior could not be predicted from the model behavior. An analysis of the dimensions of the physical quantities defining a structure will, however, reveal that only a few of the correlation functions can be considered as independent. Thus the correlation functions in equation (2.2.6) comparing model and prototype behavior can be expressed in terms of the other correlation functions, and a prediction of the prototype behavior is possible.

Before the dimensional analysis is carried out, a special type of model study that does not require this approach will be discussed for the sake of completeness of presentation. Suppose that quantity y describing the structural behavior is known as a function of other quantities x_1, x_2 ..., i.e., the physical event controlling y is known. Say

$$y = \frac{x_1 x_2}{x_3} + \frac{x_4}{x_5} - \ldots \qquad (2.2.8)$$

Chose x_1, x_2 ... in the model and prototype in such a manner that

$$\frac{x_{1m} x_{2m}}{x_{3m}} = k \frac{x_{1p} x_{2p}}{x_{3p}}$$

$$\frac{x_{4m}}{x_{5m}} = k \frac{x_{4p}}{x_{5p}} \qquad \text{etc.}$$

Then equation (2.2.8) can be used to predict the prototype behavior y_p from the model behavior y_m since

$$y_m = k\, y_p \tag{2.2.9}$$

The usefulness of this method, which has been very popular in the past, is restricted since equation (2.2.8) must first be found by mathematical investigation. The physical model is degraded to become an "analog computer" for the mathematical model and in this manner is deprived of its main advantage of generality.

Full generality is maintained if the model to prototype relationship is based on an analysis of the dimensions of the physical quantities describing the structure. The following concepts are of importance:

Dimension: The dimension is that part of the description of a variable which specifies the type of physical measurement that has to be carried out to determine its magnitude. The dimension is dictated by nature and is therefore independent of the basic unit adopted for measurement, which may be arbitrarily chosen by man. If the respective magnitudes of two physical quantities with the same dimension are determined by comparison to two different basic units, they cannot be compared directly. Yet the quantities are not totally unrelated since their magnitudes can be compared once the ratio between the basic units is specified. This principle forms the basis for dimensional analysis of structural models.

Dimensional Relationship: Some basic physical laws such as Newton's second law relating mass M, length L

and time t to force F make it possible to regard certain quantities as physically completely equivalent to a product of other terms, e.g.,

$$F = \frac{ML}{t^2} \tag{2.2.10}$$

The magnitude of each of the four quantities in this equation is determined by expressing it as a multiple of a chosen basic unit, such as a foot, a pound, a meter, etc. The numerical values that are to be substituted into the equation thus change with the basic units of measurement that are chosen. The type of measurement to be performed, e.g., determining a length, determining a mass, is, however, independent of the basic units that are chosen. The type of measurement required to determine the magnitude of a given variable is called its dimension. If we let F represent the magnitude only of the variable (e.g. 10 feet, 20 pounds) and D (F) the dimension only (e.g., length, mass) then, in addition to equation (2.2.10), we can write

$$D(F) = D\left(\frac{ML}{t^2}\right) = \frac{D(M)\ D(L)}{D(t)^2} \tag{2.2.11}$$

The left and right hand sides of this equation are independent of the basic units chosen for the variables, so that the equation is more characteristic of the phenomenon than equation (2.2.10) was. Equation 2.2.10 could also be written

$$Ft^2 = ML$$

so that equation (2.2.11) would become

$$D(F)\ \left[D(t)\right]^2 = D(M)\ \ D(L)$$

Thus multiplication and division of dimensions are both defined.

Fundamental Physical Quantities: There exist a number of quantities such as length, mass and time whose magnitude can be determined by one specific type of physical measurement only. They will be called the fundamental physical quantities. Their number depends on the type of experiment performed since heat, for instance, may be considered a fundamental quantity only if thermodynamic transformations are not studied in the experiment.

If a physical quantity is not fundamental, its magnitude can be determined by several types of measurement. Force, for instance, can be determined from measurements of mass, length and time or mass and acceleration or directly by comparison to a unit force.

Dimensional Independence: It follows from the definition of fundamental physical quantities that the magnitude of none of them can be determined by a combination of the types of measurement used to determine the other fundamental quantities. Thus the fundamental quantities are considered dimensionally independent. The set of all the fundamental quantities for a specific experiment will thus contain all the types of measurement to be carried out during the experiment, and is thus a basis for the dimensions of the other quantities describing the phenomenon.

Consider the dimensions $D(q_i)$ of all the quantities q_i that play a role in a specific experiment. Let i range from 1 to n. If K_j with $j = 1, 2, \ldots, r$ is the complete set of fundamental physical quantities for the experiment ($\therefore n \geq r$), each of the dimensions $D(q_i)$ can be expressed as a function of all the $D(K_j)$, in the manner demonstrated by equation (2.2.11). Thus

$$D(q_i) = D_i(K_1, K_2, \ldots, K_r) \qquad (2.2.12)$$

where $i = 1, 2, \ldots, n$

Since the processes of multiplication and division of dimensions are defined, the laws for the inversion of mathematical functions can be applied to equations (2.2.12). Thus if any r of the n equations (2.2.12) are selected in such a manner that the Jacobian

$$\frac{\partial(q_1, q_2, \ldots, q_r)}{\partial(k_1, k_2, \ldots, k_r)} \neq 0 \qquad (2.2.13)$$

it is possible to write explicitly

$$D(K_j) = D_j(q_1, q_2, \ldots, q_r) \qquad (2.2.14)$$

where $j = 1, 2, \ldots, r$

Since the K_j form a complete set of dimensionally independent quantities, equation (2.2.14) guarantees that $q_1, q_2, \ldots, q_r$ also form a complete set of dimensionally independent quantities for the experiment. Thus functional independence is not restricted to the fundamental quantities. Substitution of equation (2.2.14) into the remaining (n-r) equations of expression (2.2.12) shows that

$$D(q_h) = D_h(q_1, q_2, \ldots, q_r) \qquad (2.2.15)$$

where $h = r, (r + 1), \ldots, n.$

Dimensional Analysis - Equation (2.2.15) indicates which quantities have to be measured before q_h is known. As discussed in the section on dimensional relationships, equation (2.2.15) must be augmented by an equation relating the magnitudes of the quantities concerned:

$$q_h = F_h(q_1, q_2, \ldots, q_r) \qquad (2.2.16)$$

D_h in equation (2.2.15) and F_h in equation (2.2.16) are functions of identical form, i.e., if

$$D_h(q_1, q_2, q_3) = \frac{[D(q_1)]^a [D(q_2)]^b}{[D(q_3)]^c}$$

then it follows that

$$F_h(q_1, q_2, q_3) = \frac{(q_1)^a (q_2)^b}{(q_3)^c}$$

The number of variables in the event has in effect been reduced from n to r. While the basic units of measurement for $q_1, q_2, \ldots, q_r$ can still be chosen arbitrarily, the basic unit of measurement for q_h must now be calculated

from equation (2.2.16). This is the basic principle of dimensional analysis.

2.2.7 The Laws of Similitude. Suppose that the same physical events occur in both the model and the prototype. Then the form of function D_h, and therefore also the form of function F_h, is the same for both structures. Let subscripts m and p denote model and prototype properties respectively. Then

$$\frac{q_{hm}}{q_{hp}} = \frac{F_h(q_{1m}, q_{2m}, \cdots, q_{rm})}{F_h(q_{1p}, q_{2p}, \cdots, q_{rp})}$$

Since the relationship between model property q_m and prototype property q_p has already been defined as

$$q_m = f_q q_p$$

the preceding equation can be rewritten

$$\frac{f_{qh} q_{hp}}{q_{hp}} = \frac{F_h(f_{q1} q_{1p}, f_{q2} q_{2p}, \cdots, f_{qr} q_{rp})}{F_h(q_{1p}, q_{2p}, \cdots, q_{rp})}$$

Since F_h is always a product or quotient of the variables in the brackets, it will always be possible to factor

$$f_{qh} = \frac{F_h(f_{q1}, f_{q2}, \cdots, f_{qr})\, F_h(q_{1p}, q_{2p}, \cdots, q_{rp})}{F_h(q_{1p}, q_{2p}, \cdots, q_{rp})}$$

so that

$$f_{qh} = F_h(f_{q1}, f_{q2}, \cdots, f_{qr}) \qquad (2.2.17)$$

where

$$h = r, (r + 1), \ldots, n.$$

The original goal of the dimensional analysis, to establish the relationship between the correlation functions, has been achieved in equation (2.2.17). The correlation functions may simply be regarded as the relationship between the

basic units of measurement in model and prototype. It is thus possible to conclude that

i) there are as many independent correlation functions as there are dimensionally independent physical quantities.

ii) the relationship between the correlation functions is of a form identical to that of the relationship between the dimensions of the corresponding physical quantities.

The laws of similitude are defined as the relations which must exist between corresponding physical quantities if a one to one correspondence between model and prototype is to exist. They are easily derived from equation (2.2.17):

$$q_{hm} = f_{qh} q_{hp} = q_{hp} F_h(f_{q1}, f_{q2}, \ldots, f_{qr}) \qquad (2.2.18)$$

where $h = r, (r+1), \ldots, n$.

If the (n-r) laws of similitude (2.2.18) are obeyed; model measurements can be used to predict prototype behavior.

2.2.8 Laws of Similitude for Quantities in Section 2.1.

Both the number of variables and the number of fundamental physical quantities vary from experiment to experiment and have to be guessed intuitively by the experimenter. If superfluous variables are considered, unnecessary restrictions are imposed on the model since the number of laws of similitude (2.2.18) will be larger than actually required. If an essential variable is neglected, the model will not satisfy one of the essential laws of similitude and the prediction of the prototype behavior will be erroneous.

The reasoning outlined in Sections 2.2.7 and 2.2.8 will now be illustrated by the study of a specific case: a structure fully described by the quantities defined in Section 2.1. To conform with practice, it is assumed that the model will not be used to investigate thermodynamic transformations. Then all the types of physical measurement

employed in the experiment are contained among the dimensions of the following five fundamental physical quantities:

Table 2.2.1 - The fundamental physical quantities for the properties described in Section 2.1.

Quantity	Symbol	Ft, Lb, Sec Unit	Mkgs Unit
Length	L	Ft	Meter
Mass	M	Lb Sec^2/Ft	Kg Sec^2/M
Time	t	Sec	Sec
Temperature	T	°F	°C
Heat	H	B.T.U.	Calorie

Equations (2.2.12) are summarized in Table 2.2.2.

Table 2.2.2 - Powers to which quantities in equation (2.2.12) have to be raised.

k \ q	r	t	g	c	x	h	σ	T	G	a
L	1	0	-3	0	-1	0	-1	0	-2	1
M	0	0	1	-1	0	0	1	0	1	0
t	0	1	0	0	-1	0	-2	0	-2	-2
T	0	0	0	-1	-1	-1	0	1	0	0
H	0	0	0	1	1	0	0	0	0	0

It will be noted that

i) The equation of state does not contribute any additional variables to Table 2.2.2, as will be shown in Section 2.3.

ii) $\bar{P}$ and $\bar{u}$ are not listed in Table 2.2.2 since they are dimensionally identical with σ and r respectively. This guarantees that $f_p = f_\sigma$ and $f_u = f_r$. (where p is the surface stress) The independent quantities $q_1, \ldots, q_r$ must now be chosen subject to condition 2.2.13. Suitable choices are discussed in Section 2.3; in this example r, c, h, G and a are used:

$$D(r) = D(L) \qquad D(G) = D\left(\frac{M}{L^2t^2}\right)$$

$$D(c) = D\left(\frac{H}{MT}\right) \qquad D(a) = D\left(\frac{L}{t^2}\right)$$

$$D(h) = D\left(\frac{1}{T}\right) \tag{2.2.19}$$

Condition 2.2.13 becomes

$$\frac{\partial(r,\ c,\ h,\ G,\ a)}{\partial(L,\ M,\ t,\ T,\ H)} = \begin{bmatrix} 1 & 0 & 0 & 0 & 0 \\ 0 & -\frac{H}{M^2T} & 0 & -\frac{H}{MT^2} & \frac{1}{MT} \\ 0 & 0 & 0 & -\frac{1}{T^2} & 0 \\ -\frac{2M}{L^3t^2} & \frac{1}{L^2t^2} & -\frac{2M}{L^2t^3} & 0 & 0 \\ \frac{1}{t^2} & 0 & -\frac{2L}{t^3} & 0 & 0 \end{bmatrix}$$

$$= \frac{2}{M\ L\ T^3\ t^5} \neq 0$$

Thus equations (2.2.19) can be inverted to yield

$$D(L) = D(r) \qquad D(M) = D\left(\frac{Gr^3}{a}\right)$$

$$D(T) = D\left(\frac{1}{h}\right) \qquad D(H) = D\left(\frac{Gcr^3}{ah}\right)$$

$$D(t) = D\left(\sqrt{\frac{r}{a}}\right) \tag{2.2.20}$$

The dimensionally dependent variables can now be expressed in terms of the dimensionally independent variables as in equation (2.2.15):

$$D(t) = D\left(\sqrt{\frac{r}{a}}\right) \qquad D(\sigma) = D(Gr)$$

$$D(g) = D(\frac{G}{a}) \qquad D(T) = D(\frac{l}{h})$$

$$D(x) = D(\frac{Gcr^{\frac{3}{2}}}{a^{\frac{1}{2}}}) \qquad (2.2.21)$$

The form of functions D_h is thus known. The form of functions F_h is therefore also known so that the laws of similitude can be written down directly:

$$t_m = \sqrt{\frac{f_r}{f_a}}\, t_p \qquad \sigma_m = f_G f_r \sigma_p$$

$$g_m = \frac{f_G}{f_a} g_p \qquad T_m = \frac{l}{f_h} T_p$$

$$x_m = \frac{f_c f_G f_r^{\frac{3}{2}}}{f_a^{\frac{1}{2}}}\, x_p \qquad (2.2.22)$$

Equations (2.2.22) are the equivalent of equation (2.2.18) in the general theory.

2.3 THE EQUATIONS OF STATE OF THE MODEL AND PROTOTYPE MATERIALS

The equation of state relates those of the quantities describing the material which are dependent on the external influences acting on the structure. This relationship may be time and temperature dependent, it may, or may not, vary from point to point in the material and it may, or may not, be different for different directions at the same point. In addition, the events occurring in one direction may, or may not, affect the events occurring in all other directions (Poisson effect). There is some question as to whether the events occurring at one point affect the events occurring at neighboring points, eg. whether the stress gradient has an effect on the crack formation in concrete[10]. The general form of the equation of state will be developed in stages.

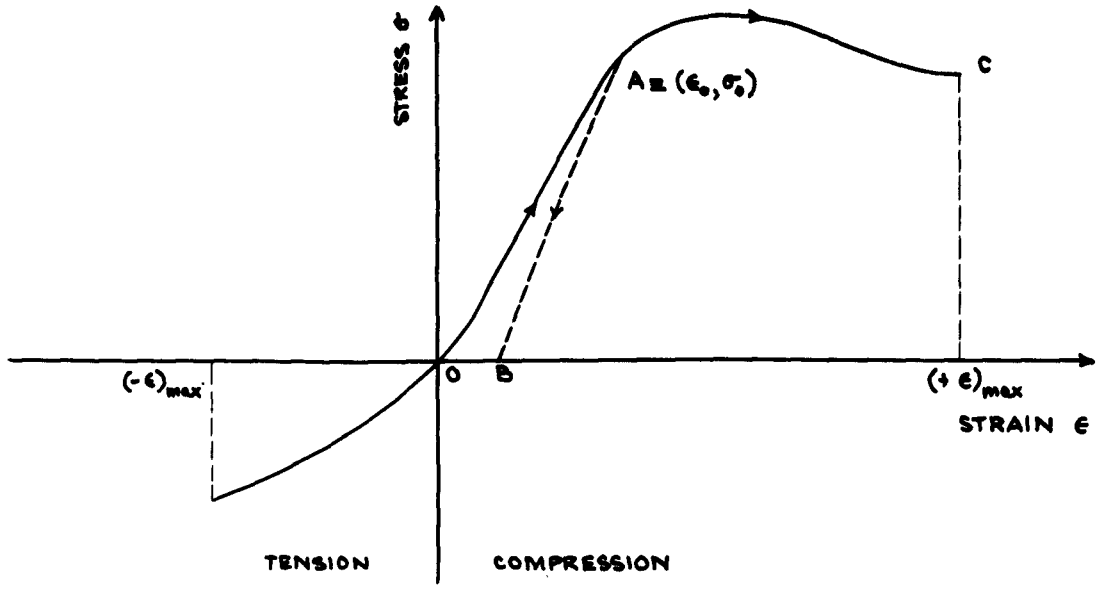

FIGURE 2.3.1

STRESS – STRAIN DIAGRAM OF A FICTITIOUS MATERIAL

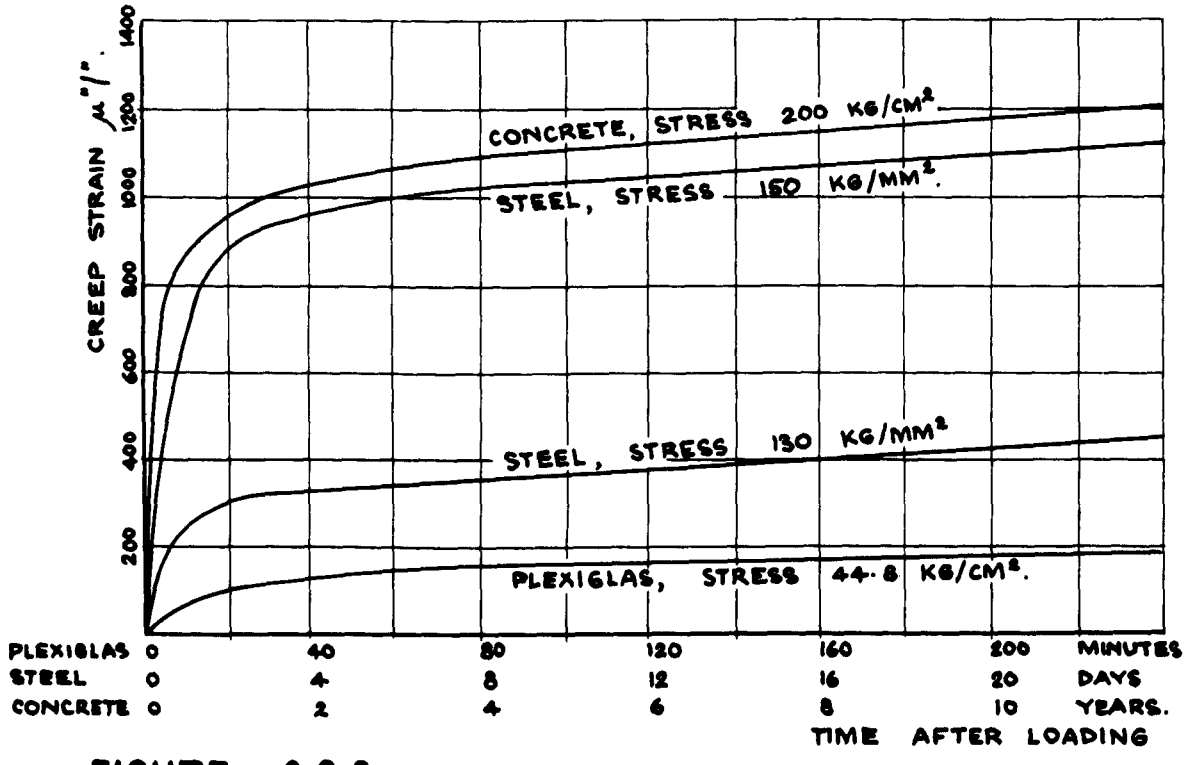

FIGURE 2.3.3

VARIATION OF CREEP STRAIN WITH TIME FOR CONCRETE, STEEL AND PLEXIGLAS. NOTE THAT THE CURVES ARE AFFECTED CONSIDERABLY BY MATERIAL COMPOSITION, EVIRONMENT AND OTHER FACTORS.

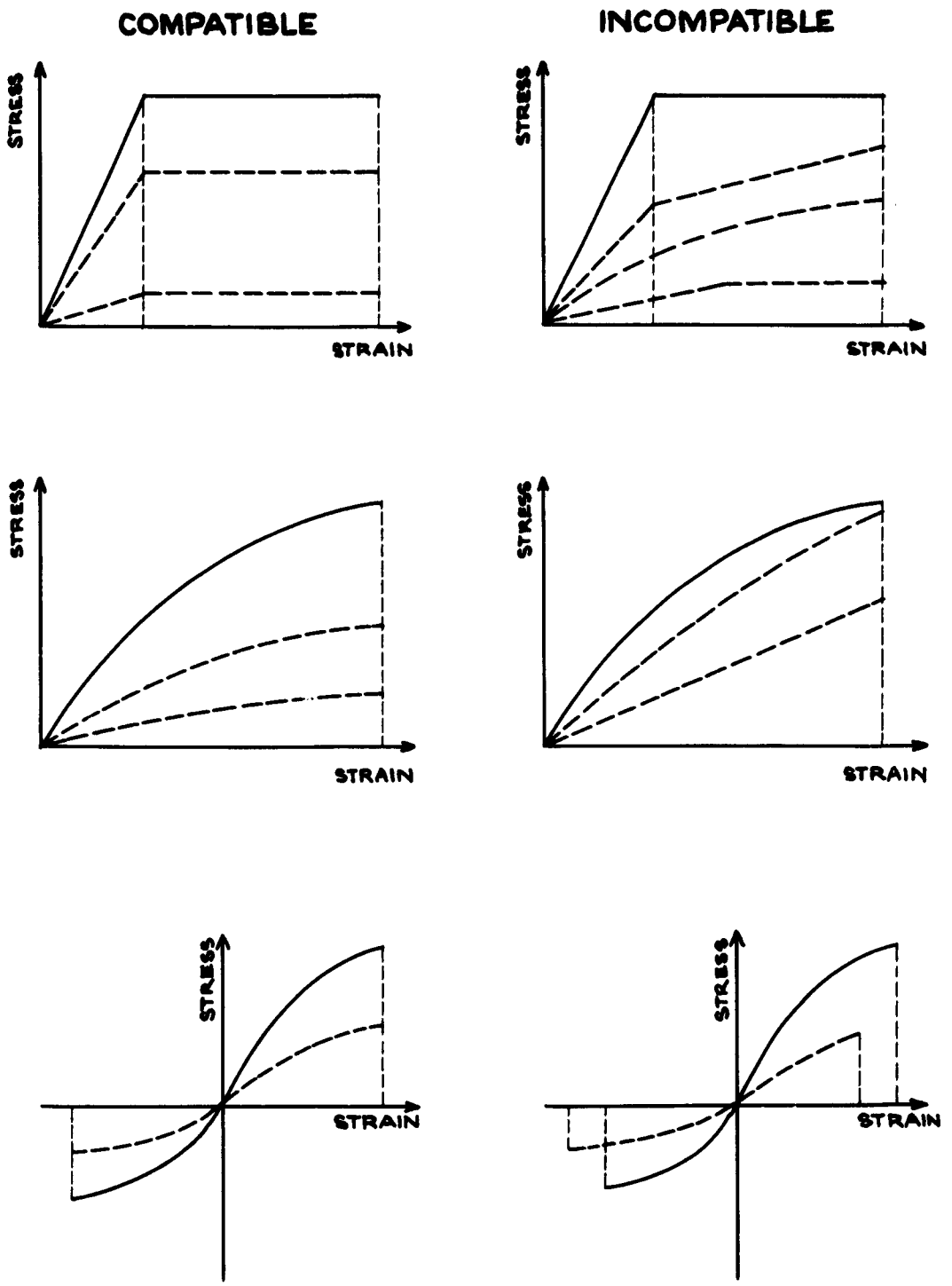

FIGURE 2.3.2.

EXAMPLES OF COMPATIBLE AND INCOMPATIBLE MODEL AND PROTOTYPE MATERIALS

---- MODEL MATERIAL ——— PROTOTYPE MATERIAL

2.3.1 The Stress-strain Relationship. Assume that a material is very gradually subjected to an external influence for the first time in its history in such a manner that all material properties except the state of stress and strain are kept constant. The event may be described by the graph in Figure 2.3.1. This curve, which is particular for the material studied, can be described mathematically as

$$\sigma = a\epsilon + b\epsilon^2 + \ldots \qquad (2.3.1)$$

The physical nature of the event is not evident from this equation, since it is not dimensionally homogeneous if a and b are constants. A better form is

$$\sigma = \sum_{n=1}^{\infty} \frac{\epsilon^n}{n!} \left.\frac{\partial^n \sigma}{\partial \epsilon^n}\right|_{\sigma=0} \qquad (2.3.2)$$

where n is a constant and the equation is dimensionally homogeneous. If, in a more general case, the derivatives $\frac{\partial^n \sigma}{\partial \epsilon^n}$ are known at point $A \equiv (\epsilon_o, \sigma_o)$, this equation becomes

$$\sigma = \sigma_o + \sum_{n=1}^{\infty} \frac{(\epsilon - \epsilon_o)^n}{n!} \left.\frac{\partial^n \sigma}{\partial \epsilon^n}\right|_{\sigma=\sigma_o} \qquad (2.3.3)$$

where $(-\epsilon)_{max} \leq \epsilon \leq (+\epsilon)_{max}$.
Both equation (2.3.3) and its limits of validity (i.e., $\pm \epsilon_{max}$) may vary from point to point in the structure. The superiority of equation (2.3.3) over equation (2.3.1) will become evident when the equations of state of model and prototype materials are compared later.

2.3.2 The Effect of Time. The time variable affects the equation of state in two different manners:

a) Aging may change the shape of the curve in Fig. 2.3.1:

$$\frac{\partial^n \sigma}{\partial \epsilon^n}(t) = \frac{\partial^n \sigma}{\partial \epsilon^n}(t_o) + \sum_{j=1}^{\infty} \frac{(t-t_o)^j}{j!} \left.\frac{\partial^{n+j} \sigma}{\partial \epsilon^n \partial t^j}\right|_{t=t_o} \qquad (2.3.4)$$

and $$\epsilon_{max}(t) = \epsilon_{max}(t_o) + \sum_{j=1}^{\infty} \frac{(t-t_o)^j}{j!} \frac{\partial^j \epsilon_{max}}{\partial t^j}\Bigg|_{t=t_o}$$

b) The rate at which the external influences are applied may affect the shape of the curve in Fig. 2.3.1. The rate of application is measured by means of the strain rate $\frac{\partial \epsilon}{\partial t}$ so that

$$\frac{\partial^n \sigma}{\partial \epsilon^n}\left(\frac{\partial \epsilon}{\partial t}\right) = \frac{\partial^n \sigma}{\partial \epsilon^n}\left(\frac{\partial \epsilon}{\partial t}\Big|_o\right) + \sum_{k=1}^{\infty}\left\{\frac{\left(\frac{\partial \epsilon}{\partial t} - \frac{\partial \epsilon}{\partial t}\Big|_o\right)^k}{k!} \frac{\partial^k}{\partial\left(\frac{\partial \epsilon}{\partial t}\right)^k}\left[\frac{\partial^n \sigma}{\partial \epsilon^n}\right]\right\}$$

and

$$\epsilon_{max} = \epsilon_{max}\left(\frac{\partial \epsilon}{\partial t}\Big|_o\right) + \sum_{k=1}^{\infty}\left\{\frac{\left(\frac{\partial \epsilon}{\partial t} - \frac{\partial \epsilon}{\partial t}\Big|_o\right)^k}{k!} \frac{\partial^k \epsilon_{max}}{\partial\left(\frac{\partial \epsilon}{\partial t}\right)^k}\right\} \qquad (2.3.5)$$

2.3.3 The Effect of Temperature. The effect of temperature on the equation of state is twofold like that of time:

a) It may change the shape of the curve in Fig. 2.3.1:

$$\frac{\partial^n \sigma}{\partial \epsilon^n}(T) = \frac{\partial^n \sigma}{\partial \epsilon^n}(T_o) + \sum_{l=1}^{\infty} \frac{(T-T_o)^l}{l!} \frac{\partial^{l+n} \sigma}{\partial \epsilon^n \partial T^l}\Bigg|_{T=T_o} \qquad (2.3.6)$$

and

$$\epsilon_{max}(T) = \epsilon_{max}(T_o) + \sum_{l=1}^{\infty} \frac{(T-T_o)^l}{l!} \frac{\partial^l \epsilon_{max}}{\partial T^l}\Bigg|_{T=T_o}$$

b) A change in temperature may cause the material to expand or shrink, setting up internal stresses and strains. This fact has already been taken into account by the definition of the coefficient of linear expansion.

2.3.4 Materials Subjected to Several Load Cycles. If the material in Fig. 2.3.1 is stressed to point A $\equiv (\epsilon_o, \sigma_o)$ and the load is then removed, it may follow curve AB rather than curve AO. Thus the stress-strain curve at A cannot be described uniquely, but is dependent on a logical decision: Follow OA on first loading cycle, continue along AC if load is increased further, follow AB if load is decreased. AB can be described in a manner similar to the description of OA:

$$\bar{\sigma} = \sigma_o + \sum_{n=1}^{\infty} \frac{(\bar{\epsilon}-\epsilon_o)^n}{n!} \frac{\partial^n \bar{\sigma}}{\partial \bar{\epsilon}^n}\Bigg|_{\sigma=\sigma_o}$$

where the bars in $\frac{\partial^n \bar{\sigma}}{\partial \bar{\epsilon}^n}$ indicate that the "curve when unloading" is described.

The permanent deformation associated with this phenomenon may lead to a considerable reduction of the initial stresses caused by the manufacture of the structure. Therefore, if a prototype structure is put through several load cycles before it is subjected to the maximum load of its lifetime, and the model has been manufactured in a manner analogous to the prototype construction, the loading history should be faithfully copied in the model.

2.3.5 The General Equation of State. The results obtained so far can be combined if it is assumed that the effects of time and temperature are independent. The general equation of state then is

$$\sigma(r,\Theta,\varphi,t,T,\frac{\partial \epsilon}{\partial t}) = \sigma_o(r,\Theta,\varphi,t_o,T_o,\frac{\partial \epsilon}{\partial t}\Big|_o) + \sum_{n=1}^{\infty}\frac{(\epsilon-\epsilon_o)^n}{n!}\left\{\frac{\partial^n \sigma}{\partial \epsilon^n}(t_o,T_o,\frac{\partial \epsilon}{\partial t}\Big|_o) + \sum_{j=1}^{\infty}\frac{(t-t_o)^j}{j!}\times\frac{\partial^{n+j}\sigma}{\partial \epsilon^n \partial t^j}\Bigg|_{t=t_o} + \sum_{\ell=1}^{\infty}\frac{(T-T_o)^\ell}{\ell!}\frac{\partial^{n+\ell}\sigma}{\partial \epsilon^n \partial T^\ell}\Bigg|_{T=T_o} + \sum_{k=1}^{\infty}\frac{(\frac{\partial \epsilon}{\partial t}-\frac{\partial \epsilon}{\partial t}\Big|_o)^k}{k!}\times\frac{\partial^k}{\partial(\frac{\partial \epsilon}{\partial t})^k}\left[\frac{\partial^n \sigma}{\partial \epsilon^n}\right]\right\}\Bigg|_{\sigma=\sigma_o} \tag{2.3.7}$$

where the limits of the maximum positive strain, for instance, are given by:

$$\epsilon_{max}(r,\Theta,\varphi,t,T,\frac{\partial \epsilon}{\partial t}) = \epsilon_{max}(r,\Theta,\varphi,t_o,T_o,\frac{\partial \epsilon}{\partial t}\Big|_o) + \sum_{j=1}^{\infty}\frac{(t-t_o)^j}{j!}\frac{\partial^j \epsilon_{max}}{\partial t^j}\Bigg|_{t=t_o} + \sum_{\ell=1}^{\infty}\frac{(T-T_o)^\ell}{\ell!}\frac{\partial^\ell \epsilon_{max}}{\partial T^\ell}\Bigg|_{T=T_o} + \sum_{k=1}^{\infty}\frac{(\frac{\partial \epsilon}{\partial t}-\frac{\partial \epsilon}{\partial t}\Big|_o)^k}{k!}\frac{\partial^k \epsilon_{max}}{\partial(\frac{\partial \epsilon}{\partial t})^k} \tag{2.3.8}$$

Similar equations can be written for the "curve when unloading". They are far too complicated for use in mathematical investigations, but can be used to advantage in the determination of the similitude requirements for the equations of state of the model and prototype materials. It should, however, be noted that material properties such as creep, relaxation, the Poisson effect, etc. which are discussed in Sections 2.3.7 to 2.3.10 are not reflected in these equations.

It has been shown in Section 2.2 that

$$\epsilon_m = \epsilon_p \qquad \sigma_m = f_\sigma \sigma_p$$

$$t_m = f_t t_p \qquad T_m = f_T T_p \tag{2.3.9}$$

Term by term comparison of equation (2.3.7), written once for the model and once for the prototype, yields the following similitude requirements if equation (2.3.9) is used:

$$\begin{aligned}
&\sigma_{om} = f_\sigma \, \sigma_{op} \\
&\frac{\partial^n \sigma_m}{\partial \epsilon_m^n} = f_\sigma \, \frac{\partial^n \sigma_p}{\partial \epsilon_p^n} \\
&\frac{\partial^i}{\partial t_m^i}\left(\frac{\partial^n \sigma_m}{\partial \epsilon_m^n}\right) = \frac{f_\sigma}{f_t^i} \times \frac{\partial^i}{\partial t_p^i}\left(\frac{\partial^n \sigma_p}{\partial \epsilon_p^n}\right) \\
&\frac{\partial \epsilon_m}{\partial t_m} = \frac{1}{f_t} \, \frac{\partial \epsilon_p}{\partial t_p} \\
&\frac{\partial^\ell}{\partial T_m^\ell}\left(\frac{\partial^n \sigma_m}{\partial \epsilon_m^n}\right) = \frac{f_\sigma}{f_T^\ell} \times \frac{\partial^\ell}{\partial T_p^\ell}\left(\frac{\partial^n \sigma_p}{\partial \epsilon_p^n}\right) \\
&\frac{\partial^k}{\partial\left(\frac{\partial \epsilon_m}{\partial t_m}\right)^k}\left(\frac{\partial^n \sigma_m}{\partial \epsilon_m^n}\right) = f_\sigma f_t^k \, \frac{\partial^k}{\partial\left(\frac{\partial \epsilon_p}{\partial t_p}\right)^k}\left(\frac{\partial^n \sigma_m}{\partial \epsilon_m^n}\right)
\end{aligned} \tag{2.3.10}$$

Similarly, the similitude requirements for equation (2.3.8) are

$$\epsilon_{max}(r, \theta, \phi, t_o, T_o)_m = \epsilon_{max}(r, \theta, \phi, t_o, T_o)_p$$

$$\frac{\partial^j (\epsilon_{max})_m}{\partial t_m^j} = \frac{1}{f_t^j} \times \frac{\partial^j (\epsilon_{max})_p}{\partial t_p^j}$$

$$\frac{\partial^\ell (\epsilon_{max})_m}{\partial T_m^\ell} = \frac{1}{f_T^\ell} \frac{\partial^\ell (\epsilon_{max})_p}{\partial T_p^\ell}$$

$$\frac{\partial^k (\epsilon_{max})_m}{\partial \left(\frac{\partial \epsilon}{\partial t}_m\right)^k} = f_t^k \frac{\partial^k (\epsilon_{max})_p}{\partial \left(\frac{\partial \epsilon}{\partial t}_p\right)^k} \qquad (2.3.11)$$

Once the requirements of equations (2.3.10) and (2.3.11) are satisfied for all points (Ψ, Φ, φ) and all values of n, j, k and ℓ, the model and prototype materials are compatible.

2.3.6 Examples of Equations of State.

a) Suppose equations (2.3.7) and (2.3.8) for a particular prototype material have the form

$$\sigma_p = \left[a + b t_p + c T_p^2 + d \frac{\partial \epsilon}{\partial t}_p\right] \epsilon_p + \left[e + g T_p\right] \epsilon_p^2$$

$$(\epsilon_{max})_p = a_1 + b_1 t_p + c_1 T_p + d_1 \frac{\partial \epsilon}{\partial t}_p$$

It is desired to determine the equation of state for the model material if the values of f_σ, f_t and f_T are prescribed. Comparison to equations (2.3.7) and (2.3.8) shows that for the prototype

$$\frac{\partial \sigma}{\partial \epsilon}\left(t_o, T_o, \frac{\partial \epsilon}{\partial t}\Big|_o\right) = a \qquad \frac{\partial^2 \sigma}{\partial \epsilon^2 \partial T} = g$$

$$\frac{\partial^2 \sigma}{\partial \epsilon \partial t} = b \qquad \frac{\partial \epsilon_{max}}{\partial t} = b_1$$

$$\frac{\partial^2 \sigma}{\partial \epsilon \partial T^2} = 2c \qquad \frac{\partial \epsilon_{max}}{\partial T} = c_1$$

$$\frac{\partial}{\partial \left(\frac{\partial \epsilon}{\partial t}\right)}\left(\frac{\partial \sigma}{\partial \epsilon}\right) = d \qquad \frac{\partial \epsilon_{max}}{\partial \left(\frac{\partial \epsilon}{\partial t}\right)} = d_1$$

$$\frac{\partial^2 \sigma}{\partial \epsilon^2}\left(t_o, T_o, \frac{\partial \epsilon}{\partial t}\Big|_o\right) = 2e$$

According to equations (2.3.10) and (2.3.11) the corresponding values for the model are

$$\frac{\partial \sigma}{\partial \epsilon}\left(t_o, T_o, \frac{\partial \epsilon}{\partial t}\Big|_o\right) = f_\sigma a \qquad \frac{\partial^2 \sigma}{\partial \epsilon^2 \partial T} = \frac{f_\sigma}{f_T} g$$

$$\frac{\partial^2\sigma}{\partial\epsilon\,\partial t} = \frac{f_\sigma}{f_t}\,b \qquad \frac{\partial\epsilon}{\partial t}_{max} = \frac{b_1}{f_t}$$

$$\frac{\partial^2\sigma}{\partial\epsilon\,\partial T^2} = 2\,\frac{f_\sigma}{f_T^2}\,c \qquad \frac{\partial\epsilon}{\partial T}_{max} = \frac{c_1}{f_T}$$

$$\frac{\partial}{\partial\left(\frac{\partial\epsilon}{\partial t}\right)}\cdot\left(\frac{\partial\sigma}{\partial\epsilon}\right) = f_\sigma f_t\,d \qquad \frac{\partial\epsilon_{max}}{\partial\left(\frac{\partial\epsilon}{\partial t}\right)} = f_t\,d_1$$

$$\frac{\partial^2\sigma}{\partial\epsilon^2}\left(t_o, T_o, \frac{\partial\epsilon}{\partial t}\Big|_o\right) = 2 f_\sigma e$$

Thus the equation of state for the model material is

$$\sigma_m = \left[f_\sigma a + \frac{f_\sigma}{f_t} b t_m + \frac{f_\sigma}{f_T^2} c T_m^2 + f_\sigma f_t d \frac{\partial\epsilon_m}{\partial t_m} \right] \epsilon_m + \left[f_\sigma e + \frac{f_\sigma}{f_T} g T_m \right] \epsilon_m^2$$

$$(\epsilon_{max})_m = a_1 + \frac{b_1}{f_t} t_m + \frac{c_1}{f_T} T_m + f_t d_1 \frac{\partial\epsilon_m}{\partial t_m}$$

b) Assume that due to technological considerations, both model and prototype material are specified. It is desired to determine under which conditions the two materials will be compatible. Suppose

$$\sigma_p = a\epsilon_p + \left[b + c\left(\frac{\partial\epsilon_p}{\partial t_p} - \frac{\partial\epsilon_p}{\partial t_p}\Big|_o \right) \right] \epsilon_p^2 \qquad \text{(i)}$$

$$\sigma_m = \left[d + e\,(T_m - T_{om}) \right] \epsilon_m + g\left(\frac{\partial\epsilon_m}{\partial t_m} - \frac{\partial\epsilon_m}{\partial t_m}\Big|_o \right) \epsilon_m^2 \qquad \text{(ii)}$$

According to equation (2.3.10)

$$f_\sigma = \frac{a}{d} \qquad f_t = \frac{g}{c f_\sigma} = \frac{gd}{ac}$$

Equation (i) does not contain a term corresponding to $e(T_m - T_{o_m})\epsilon_m$ in equation (ii). Thus the model material will satisfy the similitude requirements only if the model is kept at a constant temperature $T_m = T_{o_m}$ so that this term vanishes. Equation (ii) does not contain a term corresponding to $b\epsilon_p^2$ in equation (i). Since $\epsilon_p \neq 0$, the two materials are not compatible.

c) Fig. 2.3.2 shows several examples of compatible and incompatible model and prototype materials. Proofs of compatibility and incompatibility proceed as in Sections (a) and (b) above.

2.3.7 Creep and Relaxation. Creep and relaxation are time dependent phenomena which have not been taken into account in the general equation of state. Creep describes those phenomena which occur in the material if an external force of constant magnitude remains applied for some period of time, and to some extent after the influence has been removed (creep recovery). According to F. Leonhardt[24] the total creep strain in concrete is

$$\epsilon_k = \Phi \times k_1 \times k_2 \times \epsilon_{el} \qquad (2.3.12)$$

where

ϵ_{el} = elastic strain

Φ = variable dependent on relative humidity.

k_1 = variable dependent on the duration of load application.

k_2 = variable depending on the composition of the concrete and the thickness of the member.

Whereas it appears possible to control the variables on which Φ and k_1 are dependent in a model study, research remains to be done on factor k_2.

Relaxation occurs where a constant displacement is applied to a structure. In steel prestressing cables, for instance, it is dependent on both the initial stress and the composition of the material. Thus if $f_\sigma \neq 1$, relaxation may be very difficult to model. Plexiglas, a frequently used model material also displays creep properties. Fig. 2.3.3. compares typical creep properties of steel, concrete (taken from[24], Fig. 2.54 and 2.20) and plexiglas (taken from[19], Fig. 1, p. 316).

2.3.8 The Poisson Effect. The effect of the events occurring in one direction at a point in a material on the events occurring in another direction at the same point is described by Poisson's Ratio ν. Since this ratio is dimensionless, it must have the same value in both the model and the prototype structure. Different values for ν in model and prototype can lead to serious errors:

Consider a case of plane strain where strains ϵ_x and ϵ_y have been measured in orthogonal directions at a particular point. Then the stress in the direction of ϵ_x for a linear elastic homogeneous material is

$$\sigma_x = \frac{E}{(1+\nu)(1-2\nu)}\left[(1-\nu)\epsilon_x + \nu\epsilon_y\right]$$

If

$$\nu_m = 0.40 \text{ (eg. a plastic)} \quad \nu_p = 0.15 \text{ (eg. concrete)}$$

and

$$\epsilon_x = 1000\ \mu\text{in/in}, \quad \epsilon_y = 500\ \mu\text{in/in}$$

then

$$(\sigma_x)_m = 2860\ E_m$$

$$(\sigma_x)_p = 1150\ E_p$$

Since $f_\sigma = \frac{\epsilon_m}{\sigma_p} = \frac{E_m}{E_p}$, the model leads to a prediction which is in error by 150%. In cases where the shape and boundary conditions of a structure do not indicate if it will be in a state of plane stress or plane strain, the Poisson Effect makes it necessary to measure strains at a point in three mutually orthogonal directions before the stress distribution can be determined.

2.3.9 Crack Formation and Deflections. It has already been shown that similitude of deflections in model and prototype can be maintained only if the strains in the two structures are the same. The concrete structures where the

deflections are affected considerably by the formation of cracks, further requirements have to be met before deformations will be similar:

a) Strain Level at Which Crack Formation Starts - A crack will start at a point in a structure if $\epsilon = \epsilon_{max}$ where ϵ_{max} has been defined in Section 2.3.5. If relationships 2.3.11 are satisfied, similitude requirements for the initiation of cracks will be satisfied. This is due to the fact that the stress gradient $\frac{\partial \sigma}{\partial r}$, which in the most general case will be different in model and prototype, has no effect on the crack formation, as discussed in Ref. 10

b) Distance Between Cracks - It is shown in Ref. 10 that for $f_r \geq \frac{1}{4}$, the distance between cracks in the model will be f_r times the distance in the prototype, as required by similitude, if

i) the diameter of the individual reinforcing bars is scaled correctly.

ii) the percentage reinforcement over the entire section is the same in model and prototype. Hence, if several bars in the prototype are replaced by a single bar in the model, similitude requirements with respect to crack formation may not be satisfied.

c) Width of Cracks. - The width of the cracks, which has considerable influence on the deflection, is scaled by f_r if $f_r \geq \frac{1}{4}$.

2.3.10 Damping. If a structure is subjected to dynamic loads, its behavior is considerably affected by the damping properties of its material. Since the ratio of the actual damping in the material to the critical damping is dimensionless, it must have the same value in model and prototype.

2.4 THE DESIGN AND USE OF STRUCTURAL MODELS

The theory presented in Sections 2.1, 2.2 and 2.3 can be used to make the design of structural models a systematic

process. This section presents two different methods of design, one for cases where the model material is specified, the other for cases where the model material can be chosen freely. In both cases it will be assumed that the influences on and properties of the prototype structure are known. Where this is not the case, as discussed in Section 2.6.2, additional problems are encountered.

Method I - Suppose that technological considerations make the use of a particular model material mandatory. Then the value of f_σ will be prescribed, as demonstrated in example (b) of Section 2.3.6. The value of f_t and f_T may or may not be prescribed. The design then proceeds as follows:

i) Decide which fundamental physical quantities are involved in the experiment. Let their number be r.

ii) Decide which variables are involved in the experiment.

iii) Since there are r fundamental quantities, r of the properties of the model may be chosen arbitrarily as a dimensionally independent set as long as they satisfy equation (2.2.13). If f_σ, f_t and f_T are prescribed by the compatibility requirements of the equations of state, as in example 2.3.6 b, only (r - 3) of the model properties may be chosen arbitrarily.

iv) Calculate the correlation functions corresponding to the r dimensionally independent properties of step (iii) above.

v) Find the laws of similitude as demonstrated in the example of Section 2.2.8.

vi) Find the value of the remaining model properties from the laws of similitude and the known values of the correlation functions from step (iv).

Method II - Suppose that no particular material has been specified for the model study. The design then proceeds as follows:

i) Decide which fundamental physical quantities are involved in the experiment. Let their number be r.

ii) Decide which variables are involved in the experiment.

iii) Choose r of the model properties arbitrarily, but so that equation (2.2.13) is satisfied. These quantities then form a complete dimensionally independent set for the experiment.

iv) Calculate the correlation functions corresponding to the quantities in step (iii).

v) Find the laws of similitude as demonstrated in the example of Section 2.2.8.

vi) Find the value of the remaining model properties from the laws of similitude and the known values of the correlation functions from step (iv).

vii) Find the equation of state for the model material from the known values of f_σ, f_t and f_T and the known equation of state of the prototype material, as demonstrated by example 2.3.6 (a). The method usually breaks down at this stage because a model material with the required equation of state cannot be found.

- - - - - -

It should be noted that dimensional analysis can be used in case studies only, i.e., it can be used to obtain equations (2.1.11). The example of Section 2.2.8 will be used to demonstrate that dimensional analysis cannot be used directly to obtain equations (2.1.10), i.e., the general solution to the problem. Equations (2.2.22) show that

$$f_\sigma = f_G f_r$$

But it will be equally correct to use the remaining equations of (2.2.22) to write

$$f_\sigma = f_\epsilon f_\nu \left(\frac{f_t^2 f_h}{f_T}\right)^{a_1} \left(\frac{f_t f_a}{f_\epsilon}\right)^{a_2} \left(\frac{f_\nu f_a^{1/2}}{f_c f_\epsilon f_T^{1/2}}\right)^{a_3} (f_T f_h)^{a_4} \quad (2.4.1)$$

where a_1 to a_4 are constants. In addition, since f_p has the same value as f_σ, another factor $\left(\frac{f_p}{f_\sigma f_T}\right)^{a_5}$ could be multiplied into the right hand side. The value of the constants a_1 to a_5 cannot be found by dimensional analysis since the value of each of the brackets according to equations (2.2.22) cannot be different from one. The model can, however, be used to find the relationship

$$\sigma = F(G, r, t, a, g, x, c, T, h, P) \qquad (2.4.2)$$

This is achieved by varying the terms on the right hand side one by one, keeping the others constant, and noting the corresponding changes in σ. If expression (2.4.2) is in the form of a product, it can be used to determine a_1 to a_5 in equation 2.4.1 by forming the quotient

$$f_\sigma = \frac{\sigma_m}{\sigma_p} = \frac{F(G_m, \ldots, P_m)}{F(G_p, \ldots, P_p)} \qquad (2.4.3)$$

2.5 MODEL ANALYSIS AS A RANDOM PROCESS

In the derivation of the Laws of Similitude it was assumed tacitly that

i) physical phenomena in the prototype can be represented by a "certain" scheme of knowledge, i.e., each property can be described by a fixed number at a particular point in space at a particular time.

ii) physical phenomena in the model can be represented by a "certain" scheme of knowledge.

iii) the model to prototype relationships are "certain" numbers.

None of these assumptions hold in actual situations since such random processes as manufacture and loading of model and prototype are always involved. It therefore becomes necessary to use the concepts of mean, variance, standard deviation and statistical independence as defined in the Theory of Statistics, Ref. 16. Instead of equations (2.1.10)

and (2.1.11) it becomes necessary to find

i) the variance of the mean of the prototype outcome as predicted from the mean outcome of the model, its variance and the variance of the correlation functions.

ii) the standard deviation of the prototype outcome as predicted from the standard deviation of the model outcome and the correlation functions.

While a statistical investigation is very essential to the usefulness and reliability of a model test, particularly in cases such as blast loading where errors may occur in the modelling of a large number of properties, investigations so far have been very limited due to the great number of difficulties encountered. This section will be restricted to a presentation of basic principles and the outline of a method of solution.

2.5.1 Determination of Stress, Strain or Deflection Distribution. The deviation of the actual prototype behavior from that predicted by a model study will be due to a combination of the deviations of the assumed model and prototype properties.

i) Deviations in Geometry - The position of a point may deviate from its mean position in any direction in 3-dimensional space. This can be represented by a 3-dimensional density function $d(r, \theta, \varphi)$ which may vary from point to point in the structure, i.e.

$$d(r,\theta,\varphi) = \left[d(r,\theta,\varphi)\right](r,\theta,\varphi) \qquad (2.5.1)$$

Whether or not r, θ and φ are statistically independent variables depends on the method of manufacture. If the method of manufacture is such that r, θ, and φ for each point are determined independently, equation (2.5.1) can be rewritten

$$\left[d(r,\theta,\varphi)\right](r,\theta,\varphi) = \left[d_1(r), d_2(\theta), d_3(\varphi)\right](r,\theta,\varphi) \qquad (2.5.2)$$

The notation on the right hand side indicates that $d_1(r)$,

$d_2(\theta)$ and $d_3(\varphi)$ may all vary from point to point in the structure.

ii) Deviations in Material Properties - Consider any material property, denoted by A. Both the mean and the variance of A may be different for different points on the structure so that

$$d(A) = \left[d(A)\right] (r, \theta, \varphi) \qquad (2.5.3)$$

Both the nature of density function d(A) and its change with r, θ and φ depend on the method of manufacture of the material and the method of fabrication of the structure. So, for instance, the variation in material properties of a welded steel structure will depend on both the quality control of the steel mill and the workmanship of the individual welds.

iii) Deviations in External Influences - The uncertainty in the exact nature and amount of such external influences as earthquakes or blast loading is very large since, contrary to cases (i) and (ii) above, there is little human control over them. Deviations in any specific influence B may again be different from point to point in the structure, i.e.

$$d(B) = \left[d(B)\right] (r, \theta, \varphi) \qquad (2.5.4)$$

iv) Deviations in the Equation of State - Any of the partial derivatives used in Section 2.3 to specify the equation of state may deviate from its assumed value. This can again be represented by a density function

$$d(C) = \left[d(C)\right] (r, \theta, \varphi) \qquad (2.5.5)$$

v) Deviations in the Correlation Functions - The necessity of using correlation functions rather than ratios to define the relationship between model and prototype can now be demonstrated. Assume, for instance, that the material property A has a normal distribution in both model and prototype. Then its density function is

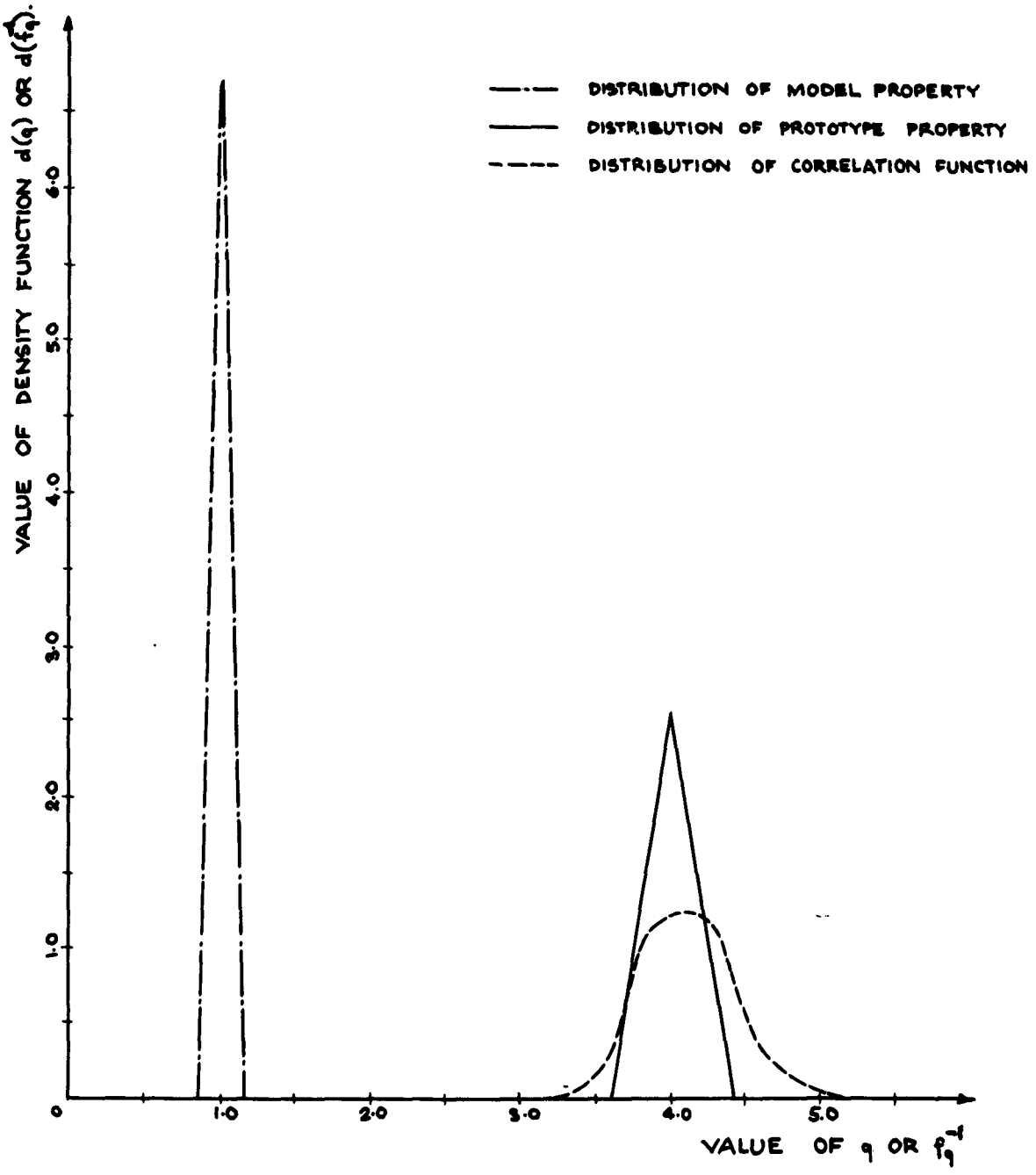

FIGURE 2.5.1

COMPARISON OF THE DISTRIBUTION OF A MODEL PROPERTY q_m, A PROTOTYPE PROPERTY q_p AND THEIR CORRELATION FUNCTION f_q^{-1}.

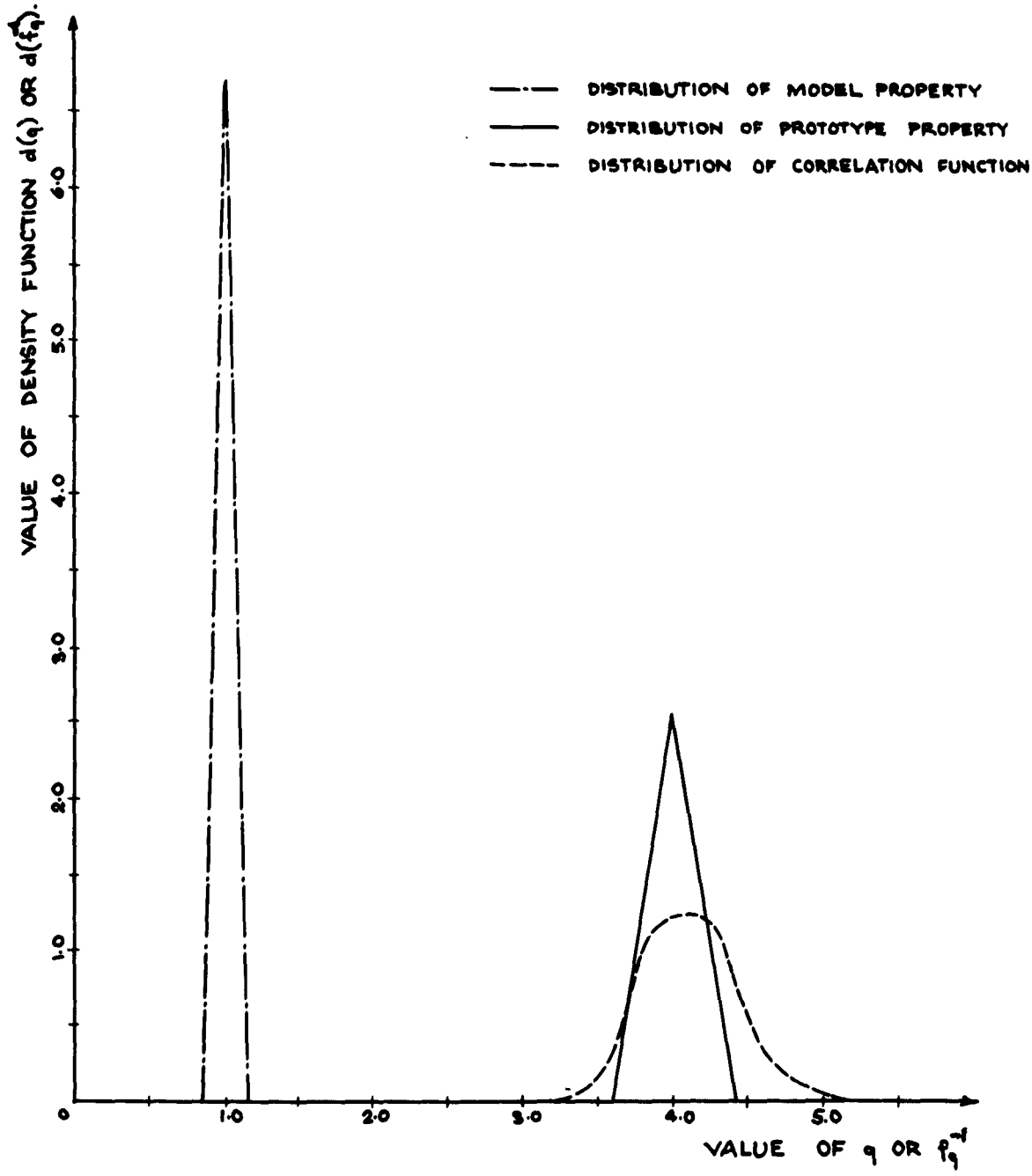

FIGURE 2.5.1

COMPARISON OF THE DISTRIBUTION OF A MODEL PROPERTY q_m, A PROTOTYPE PROPERTY q_p AND THEIR CORRELATION FUNCTION f_q^m.

$$d(A) = \frac{1}{\sqrt{2\pi}\, s_A} e^{-\frac{(A-\mu_A)^2}{2s_A^2}} \qquad (2.5.6)$$

On account of equation (2.5.3) the standard deviation S_A and the mean μ_A will be functions of r, $\blacklozenge$ and φ in both model and prototype. The correlation function

$$f_A = \frac{A_m}{A_p}$$

will thus also have a mean and a standard deviation depending on r, $\blacklozenge$, φ so that f itself must in fact in the most general case be a function of r, $\blacklozenge$ and φ.

The density function for f_A will not be geometrically similar to that of A. Assume, for instance, that material property A has mean values of 4 and 1 in prototype and model respectively. Let the density functions have a triangular graph and maximum deviations of $\pm$ 10% in the model and $\pm$ 15% in the prototype, as shown in Fig. 2.5.1. The density function for f_A can then be determined numerically as shown in Tables 2.5.1 and 2.5.2.

Table 2.5.1 - The table gives values of $\frac{A_p}{A_m}$.

$d(A_m)\times\Delta A_m$ \ $d(A_p)\Delta A_p$	A_p / A_m	0.0312	0.0935	0.156	0.219	0.219	0.156	0.0935	0.0312
		3.65	3.75	3.85	3.95	4.05	4.15	4.25	4.35
0.055	0.875	4.16	4.29	4.40	4.51	4.63	4.75	4.86	4.97
0.167	0.925	3.95	4.06	4.16	4.27	4.38	4.49	4.59	4.70
0.278	0.975	3.75	3.85	3.95	4.05	4.15	4.26	4.36	4.46
0.278	1.025	3.56	3.66	3.76	3.86	3.95	4.05	4.15	4.25
0.167	1.075	3.40	3.49	3.58	3.68	3.77	3.86	3.96	4.05
0.055	1.125	3.25	3.34	3.43	3.52	3.60	3.69	3.78	3.87

d(A) x Δ A is the probability that A lies between (A-½ΔA) and (A + ½ΔA), where $\Delta A_p = 0.1$, $\Delta A_m = 0.05$. Subscript m denotes model, p denotes prototype.

Table 2.5.2 - Calculation of $d(f_A^{-1})$ for Various Values of f_A^{-1} .

f_A^{-1}	3.3	3.5	3.7	3.9	4.1	4.3	4.5	4.7	4.9
Summation of Probabilities $d(A_p)\Delta A_p$ x $d(A_m)\Delta A_m$ x 10^4	17 51 52	86 153 210 120	86 260 434 365 260 434	52 260 434 609 609 210 153 17	17 153 210 609 609 434 260 52	51 86 365 365 434 260 86	120 210 153 86	120 86 52	17 51
$d(f_A^{-1})$ x Δf_A^{-1} 10^4	120	569	1839	2344	2344	1647	569	258	68
Corrected Values	123	583	1884	2403	2403	1688	583	264	70
$d(f_A^{-1})$	0.062	0.292	0.942	1.201	1.201	0.844	0.292	0.132	0.035
$d(f_A^{-1})$ x $f_A^{-1}\Delta f_A^{-1}$	0.040	0.204	0.695	0.940	0.982	0.732	0.262	0.124	0.035

In each column,

$$d(f_A^{-1})\,\Delta f_A^{-1}\,10^4 = \sum d(A_p)\,\Delta A_p * d(A_m)\,\Delta A_m * 10^4$$

Corrected values have been obtained from the previous row by direct scaling so that

$$\sum d(f_A^{-1})\,\Delta f_A^{-1}\,10^4 = 10^4$$

as required by theory of statistics. Then

$$d(f_A^{-1}) = \frac{1}{10^4 \Delta f_A^{-1}} \times \text{CORRECTED VALUE}$$

The last row is used to obtain the mean for f_A^{-1}.

$$\mu_{fA} = \sum f_A^{-1}\, d(f_A^{-1})\,\Delta f_A^{-1} = 4.00$$

The graph of the density function $d(f_A^{-1})$ is shown in Fig. 2.5.1. It may be concluded that

a) The mean of f_A^{-1} equals the quotient of the means of the model and prototype properties.

b) The maximum deviations of the correlation function f_A^{-1} are considerably larger than those of either the model or the prototype property: + 28% and - 22%.

c) The distribution of the correlation function is skew whereas that of the properties themselves was symmetric.

vi) <u>The Statistical Model Investigation</u> - The statistical model investigation proceeds as follows:

a) Density functions for the geometric and material properties, the external influences and the equations of state are either assumed or determined experimentally. They will depend on the particular manufacturing process, loading process, etc. Little work appears to have been done in this direction up to the present.

b) The density functions for the correlation functions of the properties in (a) are determined as demonstrated in Tables 2.5.1 and 2.5.2. The amount of computation involved is large, and will increase if $d(A_m)$ and $d(A_p)$ change from point to point in the structure.

c) The model output D_m is measured a considerable number of times so that its density function $d(D_m)$ can be found.

d) The density function $d(f_D)$ must be found before the density function $d(D_p)$ of the prototype output D_p can be determined. But this requires that f_D be known as a function of all the other correlation functions of the experiment, since D may be statistically dependent on all the other structural properties, i.e., variations in any of the structural properties may cause D to vary statistically. We come to the important conclusion that statistical analysis demands a knowledge of the general equations (2.1.11) governing the phenomenon: a case study alone is not sufficient. Methods to obtain equations (2.1.11) have already been discussed in Section 2.4. Suppose that it has been found that

$$f_\sigma = f_G^{b_1} f_\tau^{b_2} f_\tau^{b_3} \cdots f_p^{b_{10}} \qquad (2.5.7)$$

If it is assumed that the variables on the right are statistically independent, the density function for f can be found from

$$d(f_\sigma) = d(f_G^{b_1})\, d(f_\tau^{b_2}) \cdots d(f_p^{b_{10}}) \qquad (2.5.8)$$

If the right hand members of equation (2.5.8) vary from point to point on the structure, $d(f_\sigma)$ has to be obtained for each point individually. The amount of numerical work involved makes the use of a computer desirable.

e) Once $d(f_\sigma)$ is known, it is possible to determine $d(\sigma_p)$ in the manner of Tables 2.5.1 and 2.5.2, using the relationship

$$d(\sigma_p) = d\left(\frac{\sigma_m}{f_\sigma}\right) \qquad (2.5.9)$$

vii) Conclusions -

a) If the variables involved in the experiment are statistically independent, the mean of the prototype outcome will have the same value as the outcome when a "certain" scheme of knowledge is assumed.

b) Since the correlation functions tend to have a broad distribution as shown in the example of Fig. 2.5.1,

the prototype outcome will have a much larger deviation than the model outcome.

c) Conclusions (a) and (b) prove the importance of taking a large number of readings of the same outcome in the model experiment. Only in this manner can the effect of the wide distribution of the correlation functions be eliminated through the determination of a reliable mean value.

2.5.2 Ultimate Load Models. Ferry Borges, Ref. 11, has investigated the effect of f_r on the distribution of the prototype results as predicted from ultimate load model studies. His conclusions are

a) An increase in dimensions considerably decreases dispersions, regardless of the failure criterion adopted.

b) The transformation of the mean values depends largely on the failure criterion adopted. In brittle rupture, the mean values decrease as the dimensions increase. In ductile rupture, the behavior of the mean values depends on the number of failure surfaces. Finally, in the theory of similitude for failure by deformation the mean values remain constant with changes of scale. The latter result agrees with the deduction in Section 2.5.1.

Since there are factors besides f_r which affect the prediction of the prototype results from the model study, this investigation is by no means complete.

2.6 STATIC AND DYNAMIC STUDIES OF MASSIVE STRUCTURES

In this section, the theory derived in preceding sections will be applied specifically to structures whose mass plays a significant part in their behavior.

2.6.1 The Effect of Mass on Structural Behavior. The mass of a structure affects its behavior in two different ways:

a) It causes body forces due to the earth's attraction. The concept of an "earth acceleration" causing these forces is conventional and frequently convenient, but it may give the erroneous impression that model studies involving earth attraction are dynamic in character. It is preferable to base similitude of model and prctotype on Newton's Law of Mass Attraction:

$$G = \gamma \frac{mM}{r^2} \qquad (2.6.1)$$

where G = force of attraction between masses m and M
r = distance between masses
γ = gravitational constant

Since in most cases the earth's mass M as well as γ and r, the distance from the object to the earth's center, are the same for model and prototype, the ratio between the earth attraction on them is entirely determined by the ratio of their total masses. Earth attraction must therefore be considered a static phenomenon.

b) The mass of a structure or of its loads also gives rise to inertia forces once the structure as a whole or parts of it are subjected to accelerations. These accelerations may be caused by dynamic surface loads, support accelerations or free vibrations of the structure. According to Newton's Second Law

$$\bar{F} = m\bar{a} = -\bar{F}_i \qquad (2.6.2)$$

where $\bar{F}$ = force applied to particle mass m
$\bar{a}$ = acceleration of m due to $\bar{F}$
$\bar{F}_i$ = inertia force, equal in magnitude but opposite in direction to $\bar{F}$.

Since the acceleration $\bar{a}$ is the second derivative of distance with time, inertia forces are a dynamic phenomenon.

2.6.2 Types of Model Studies Involving Mass. The physical laws outlined in the preceding section make the subdivision of model studies involving mass into two categories natural. Each of the two categories will be treated separately in more detail in later sections.

i) Static Studies Involving Mass - The body forces are caused by earth attraction only, all surface loads are static and the supports do not move. Typical examples are

a) Massive concrete structures such as dams.

b) Structures designed mainly to carry their own dead weight, e.g. large span bridges.

c) Structures subjected to loads caused by heavy masses, e.g. grain silos and coal bunkers.

ii) Dynamic Studies Involving Mass. If the prototype structure is subjected to dynamic surface forces, support accelerations or free vibrations, a dynamic model study with proper regard to inertia forces has to be undertaken. Dynamic studies may, or may not, include also the effects of static surface loads and earth attraction acting on the prototype, depending on the relative size of the forces involved. Earth attraction can, for instance, frequently be disregarded. Since concrete, for example, has a mass attraction per cubic foot roughly equivalent to one psi acting on the surface, the dead weight stresses of say 12" thick shells subjected to blast load pressures of 25 to 200 psi can safely be neglected.

Typical examples of dynamic studies are

a) Surface structures such as dams or shells responding to dynamic surface loads.

b) Articulated structures such as bridges, transmission towers or radar antennae subjected to drag loads caused by atomic explosions.

c) Structures supporting heavy masses and subjected to either blast loads or seismic support motion.

As in the case of model studies where mass is not of importance, the following types of structural behavior may be investigated:

i) Stress or strain distributions and deformations if a structure is linearly elastic (i.e., superposition valid if deformations are small) or if the structure is nonlinearly elastic or plastic (superposition not valid).

ii) Ultimate load bearing capacity of the structure.

iii) Determination of the loading causing elastic or inelastic structural instability.

In addition, however, the gravity and inertia forces on masses supported by the structure should be faithfully reproduced in the model. Both the effect of their inertia forces on the overall structural action and their destructive action as missiles are of importance. It is thus important to reproduce the interaction between the masses themselves, such as friction forces, as well as the interaction between the masses and the structure.

2.6.3 The Laws of Similitude for Massive Structures.

It will be assumed in this section that the correlation functions can be chosen independently of the model material, i.e., method II of Section 2.4 is used. The following relationships between the correlation functions have already been derived in Section 2.2.8:

Accelerations: $$f_a = f_r f_t^{-2} \qquad (2.6.3)$$

Body Forces: $$f_G = f_g f_a = f_g f_r f_t^{-2} \qquad (2.6.4)$$

Surface Forces: $$f_\sigma = f_G f_r = f_g f_a f_r = f_g f_r^2 f_t^{-2} \qquad (2.6.5)$$

These equations are valid for both static and dynamic studies. Generally f_r has to have a value considerably less than unity to make a model study possible. This can be achieved by varying either the parameter f_a which is dependent on the external influences or the parameters f_σ and f_g which are dependent on the model material.

The difference between the laws of similitude for static and dynamic studies lies in the freedom that may be exercised in the choice of the correlation functions. In a static study where no time measurements need to be carried out on the model, equation (2.6.3) is automatically satisfied since f_t can be given an arbitrary value. In a dynamic model study, the time correlation function f_t is of much more importance since the prototype load-time function and support acceleration-time function must be scaled for the model according to f_t. The choice of f_t depends largely upon the nature of the dynamic load. It is convenient to distinguish between the following types:

Load Type I - The applied surface forces are known as a function of both space and time. If it is assumed that the technical problems which arise, e.g. in the modeling of load rise times of about 2 milliseconds, can be solved, this type of dynamic load imposes no restrictions on the correlation functions.

Load Type II - The applied surface forces are not known as a function of both space and time, but are caused by phenomena subject to known physical laws, e.g. those of aerodynamics. The model must then be subjected to the actual physical event that causes the loading, but the variables involved (e.g. overpressure) may be scaled down according to the chosen values of the correlation functions. The laws of similitude must now cover not only the model itself, but also the events leading to the loading. In many cases it will still be possible to chose f_σ and f_t different from unity.

Load Type III - The dynamic surface forces and the physical laws of the events by which they are caused, are not exactly known, as in some types of blast loading. The model must then be subjected to the actual prototype loading which implies that $f_t = f_\sigma = 1$, so that the choice of model materials now becomes very limited. There is,

in addition, no guarantee that f_r is not also one of the parameters affecting the space-time distribution of the loading, so that in effect structures subjected to type III loads cannot always be modelled with confidence.

2.6.4 Static Model Studies with Natural Earth Attraction. According to Newton's Gravitational Law, (2.6.1), applied to the earth (mass M) and model or prototype respectively, the body forces are

$$G_m = \frac{Mg_m}{r^2}\gamma$$

$$G_p = \frac{Mg_p}{r^2}\delta \qquad (2.6.6)$$

so that

$$f_G = \frac{G_m}{G_p} = \frac{g_m}{g_p} = f_g \qquad (2.6.7)$$

Substitution into equation (2.6.5) yields

$$f_\sigma = f_g f_r \qquad (2.6.8)$$

The value of f_g can generally be varied within very narrow limits only, as is shown in Table 2.6.1.

Table 2.6.1 - Typical Average Values of Density Ratio f_g.

Model Material		Prototype Material			
		Steel	Aluminum	Concrete	Masonry
	Spec. Mass	7.75	2.65	2.40	2.00
Mortar	1.65	0.213	0.621	0.687	0.825
Gypsum	2.30	0.296	0.869	0.959	1.150
Plexiglas	1.20	0.165	0.454	0.500	0.600
Rubber	1.10	0.142	0.415	0.458	0.550
Steel	7.75	1.000	2.920	3.230	3.875
Aluminum	2.65	0.341	1.000	1.100	1.325
Ph. Bronze	8.90	1.150	3.360	3.710	4.450

The table shows that the density ratio is less than 5 whereas the length ratio is normally less than 0.125. It therefore follows from equation (2.6.8) that the stress

ratio f_σ is less than 1. But according to the second of equations (2.3.10), the stress ratio for linearly elastic model and prototype materials is

$$f_\sigma = \frac{E_m}{E_p} \qquad (2.6.9)$$

Thus the model material must be less rigid than the prototype material. It is suggested that instead of choosing f_r and then searching for a model material which is such that f_σ and f_g satisfy equation (2.6.8), the inverse procedure is followed, as demonstrated in the following example.

- - - - - -

Example: A plexiglas model of a steel bridge is tested in the linear elastic range. If it is assumed that $E = 450{,}000$ psi for plexiglas
$E = 30 \times 10^6$ psi for steel,
find the length correlation function f_r required so that static body forces are correctly reproduced in the model.

Solution: From equation (2.6.9):

$$f_\sigma = \frac{0.45 \times 10^6}{30 \times 10^6} = 0.015$$

From Table 2.6.1: $f_g = 0.165$

From equation (2.6.8): $f_r = \frac{0.015}{0.165} = \frac{1}{11}$ (Ans.)

- - - - - -

This example demonstrates that unless f_g or f_a are artificially increased, relatively large models are required to reproduce gravity stresses faithfully. Where very flexible materials are used, e.g., rubber models of concrete dams[4], smaller models are feasible, but the high Poisson Ratio of the model material frequently makes the test results unreliable (see Section 2.3.8).

2.6.5 Technical Aspects of Static Studies with Natural Earth Attraction. If the model study is concerned with the ultimate load bearing capacity or with the stability of a structure, direct observation without the use of sensors and recording devices for strains and deflections will be sufficient, so that both the problems of body force loading and of model observation are automatically solved. If the stress distribution in the structure is to be determined, considerable difficulties both in the determination of the strain distribution and the derivation of the corresponding stress distribution are experienced.

1) Strain Distribution - The strains caused by the dead weight of a model are extremely small. Consider for instance the extremely favorable case of a mortar model (E = 75,000 psi, w = 100 pcf) of a 500' high concrete wall with $f_r = 0.01$. Then the maximum strain at the foot of the model is of the order

$$\epsilon = \frac{5 \times 100}{144 \times 75{,}000} \times 10^6 \cong 50 \mu\text{in/in.}$$

Not even the highly developed electrical strain measuring devices are capable of reliable detection at such low strain levels. Another problem is the determination of a zero reading, i.e., a strain gage reading for zero body forces. To overcome this serious problem and at the same time to increase the strain levels, tests have been carried out where the strains are first measured with the model in an upright position, and then with the model inverted[40]. In this manner, strain readings are doubled. In addition to the mechanical problems caused by the rotation of large models about a horizontal axis, the method possesses an inherent inaccuracy where the stress-strain properties of the model are different in tension and in compression. In most cases, the strain level remains too low for accurate sensing and recording. Additional difficulties are encountered if strains inside the model are to be measured. Since it is

2.6.5 Technical Aspects of Static Studies with Natural Earth Attraction. If the model study is concerned with the ultimate load bearing capacity or with the stability of a structure, direct observation without the use of sensors and recording devices for strains and deflections will be sufficient, so that both the problems of body force loading and of model observation are automatically solved. If the stress distribution in the structure is to be determined, considerable difficulties both in the determination of the strain distribution and the derivation of the corresponding stress distribution are experienced.

1) Strain Distribution - The strains caused by the dead weight of a model are extremely small. Consider for instance the extremely favorable case of a mortar model (E = 75,000 psi, w = 100 pcf) of a 500' high concrete wall with $f_r = 0.01$. Then the maximum strain at the foot of the model is of the order

$$\epsilon = \frac{5 \times 100}{144 \times 75{,}000} \times 10^6 \cong 50 \mu\text{in/in.}$$

Not even the highly developed electrical strain measuring devices are capable of reliable detection at such low strain levels. Another problem is the determination of a zero reading, i.e., a strain gage reading for zero body forces. To overcome this serious problem and at the same time to increase the strain levels, tests have been carried out where the strains are first measured with the model in an upright position, and then with the model inverted[40]. In this manner, strain readings are doubled. In addition to the mechanical problems caused by the rotation of large models about a horizontal axis, the method possesses an inherent inaccuracy where the stress-strain properties of the model are different in tension and in compression. In most cases, the strain level remains too low for accurate sensing and recording. Additional difficulties are encountered if strains inside the model are to be measured. Since it is

seldom possible to make the sensing device out of the model material, the presence of the device will cause discontinuities and changes in the strain field which frequently may lead to erroneous results.

ii) The problems encountered in deriving the stress distribution of a 3-dimensional model from its strain distribution are of a technical nature. They have already been discussed in Section 2.3.8.

2.6.6 Static Model Studies with Earth Attraction Artificially Induced by Acceleration. The large models required by the method of Section 2.6.4 and the unsatisfactorily low strain levels obtained lead to the use of artificial methods of simulating earth attraction. Consider equation (2.6.5):

$$f_\sigma = f_g f_a f_r$$

Suppose that in a particular model study it is considered essential to reproduce both the stress-strain characteristics and shrinkage and creep properties of the prototype material, and that this can be achieved only by using the prototype material as model material. Then

$$f_\sigma = f_g = 1$$

and equation (2.6.5) becomes

$$f_a f_r = 1 \qquad (2.6.10)$$

The model must therefore be subjected to very considerable accelerations, to which it will respond dynamically. In order to demonstrate the implications of the dynamic response, a typical though simplified example is given: consider a 3'0" x 4" x 1" mortar beam ($E = 3 \times 10^6$ psi, $w = 100$ pcf) which is simply supported on a sleigh as shown in Fig. 2.6.1. If the sleigh is given a constant acceleration $\ddot{z}$ along a straight line, the beam is subjected to constant forces:

$$F = \tfrac{1}{2} \rho \ddot{z} L$$

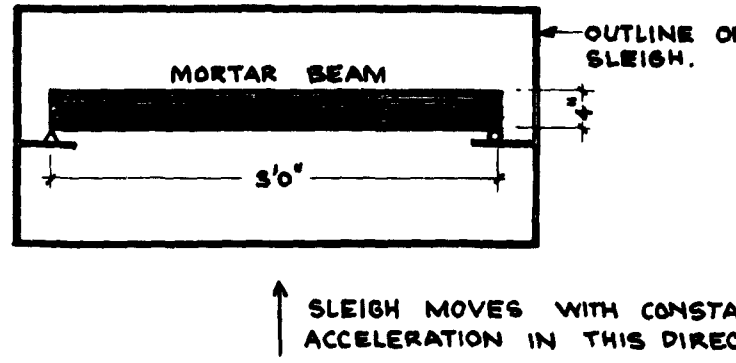

FIGURE 2.6.1

PLAN OF SLEIGH CARRYING MORTAR BEAM.

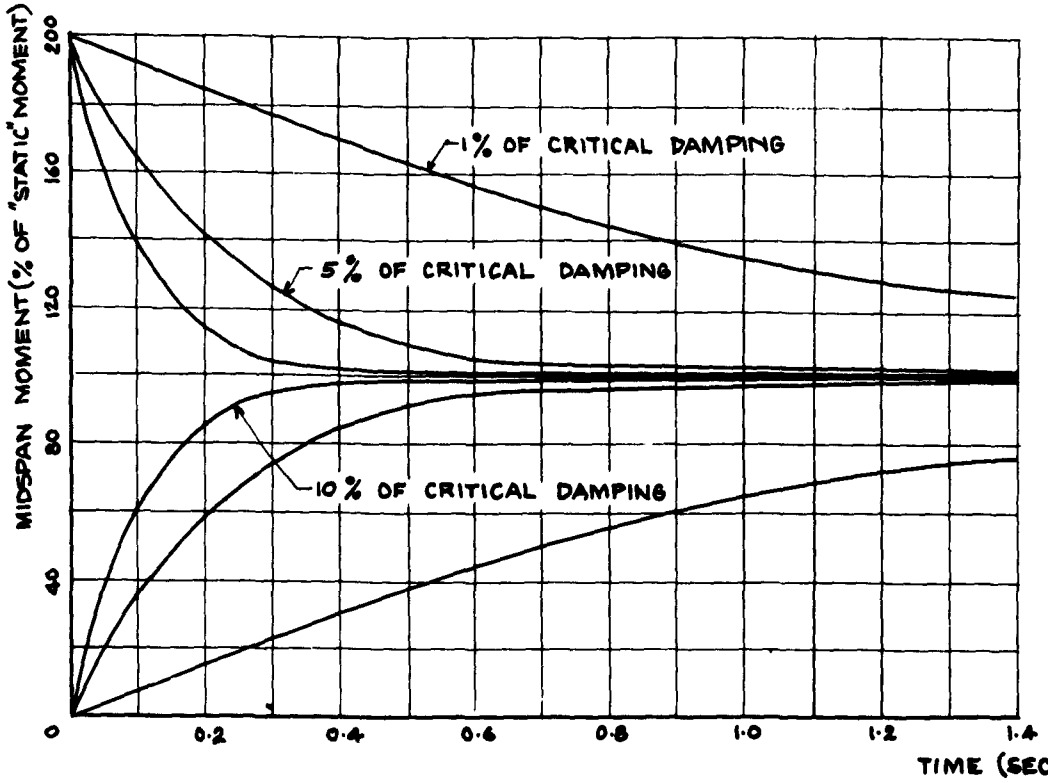

FIGURE 2.6.2

THE GRAPH SHOWS THE ENVELOPES ONLY OF THE CURVES DESCRIBING VARIATION OF MIDSPAN BENDING MOMENT WITH TIME OF THE BEAM IN FIG. 2.6.1

at each of the supports, where

ϱ = mass of beam per unit length
L = length of beam.

The dynamic response of the beam is analysed in Appendix A. The actual bending moment at midspan is calculated and compared to the static bending moment caused by a load $\varrho \frac{\pi}{2}$ per unit length of the beam. Since $\varrho \frac{\pi}{2}$ is the body force per unit length which we actually wish to obtain, and which would have been obtained if the beam were perfectly rigid, the calculations give the error caused by the dynamic response of the beam.

The results are presented in Fig. 2.6.2. It may be concluded that

i) The model is subjected to stresses far exceeding those of the steady state, represented by 100% in Fig. 2.6.2. The method is thus not suited to ultimate strength tests.

ii) Models frequently have less than 5% of the critical damping. No readings should therefore be taken before the model has been accelerated for at least 2 seconds. If 2 more seconds are required to take readings, and the model is subjected to 20 x earth acceleration, the distance travelled is

$$s = \tfrac{1}{2} a t^2 = 5150 \text{ ft.}$$

Since the model has to be decelerated more gradually, the total test run becomes very long. Linear acceleration may be eliminated as a practical method of model testing.

- - - - - -

Accelerations can also be achieved by means of centrifuges. In addition to economic problems and technical difficulties such as strain measurement on fast moving models, the method possesses an inherent source of error, which will be demonstrated by means of an example:

Suppose that the gravity stress distribution in a 1200' wide and 400' high concrete dam is to be determined. A model material is chosen so that $f_g = 1$ and $f_\sigma = 0.2$.

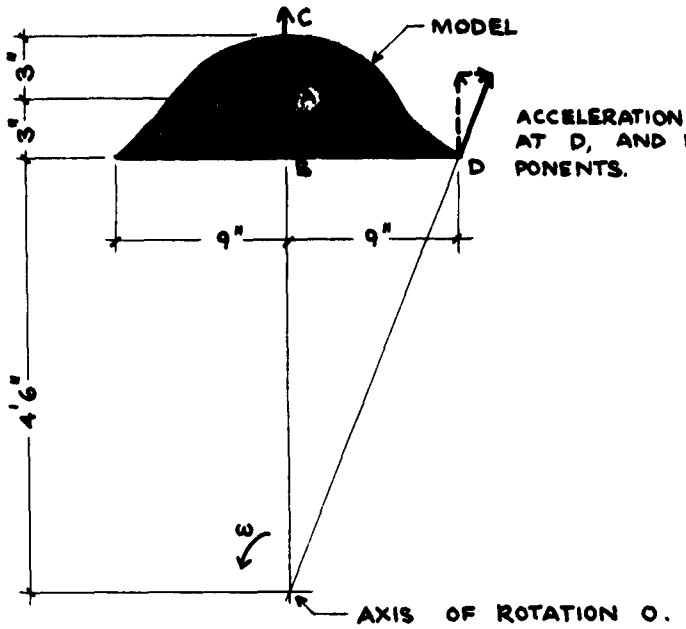

FIGURE 2.6.3

MODEL SUBJECTED TO "GRAVITY STRESSES" IN CENTRIFUGE.

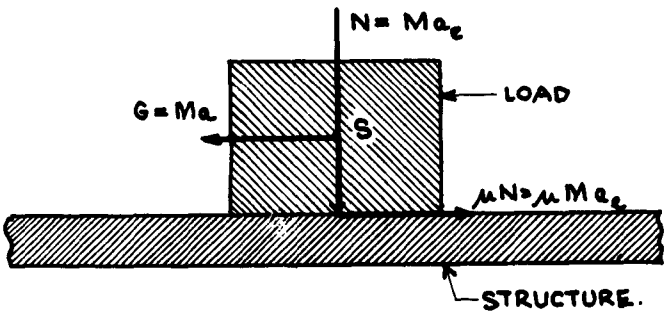

FIGURE 2.6.4

FORCES ACTING BETWEEN LOAD AND STRUCTURE.

N	NORMAL FORCE	μ	FRICTION COEFFICIENT
M	MASS OF LOAD	G	BODY FORCE
a_e	EARTH ACCELERATION	a	ACCELERATION OF LOAD

LIMITING CONDITION FOR RELATIVE MOTION.

$$G = Ma = \mu N = \mu M a_e.$$

A 10' 0" diameter centrifuge is available and accuracy in model manufacture and strain measurements limits f_r to 1 in 800. Then

$$f_a = \frac{f_\sigma}{f_r} = \frac{800}{5} = 160.$$

A particle moving along a circle with radius r at a constant angular velocity ω is subjected to a constant centripetal acceleration

$$a = \omega^2 r$$

Thus if point A in figure 2.6.3 is to have an acceleration of 160 x 32.2 ft/sec^2, the frequency of the centrifuge must be

$$f = \frac{1}{2\pi}\sqrt{\frac{160 \times 32.2}{4.75}} = 5.25 \text{ rps}$$

At points B and C on the center line, the acceleration will be about 5% in error, but will act in the correct direction. At D, the component parallel to OC will be 5% in error, and there is an additional acceleration equal to 16% of the acceleration at A acting in direction DB. The inherent errors are thus not excessive and the method will be useful if the technical difficulties can be overcome.

2.6.7 Static Model Studies with Earth Attraction Artificially Induced by Surface Forces. The earth attraction on the prototype material can also be simulated by the application of surface loads at discrete locations on the model. The method has, for instance, been used in model studies of concrete arch dams by Rocha, Serafim and Ferreira[34]. If the forces are applied to the face of the model, the continuity of the model material need not be disturbed, but considerable errors in the stress distribution in thick models may result. If they are applied inside the model, the stiffness of the structure is affected. A quantitative analysis of these problems is given in Section 2.7.

The effect of the surface loads on the model can be represented by assigning the model material an artificial specific mass $\bar{g}_m$. Suppose

P_m = total surface load applied to entire model.

W_m = total weight of model.

V_m = total volume of model.

a_e = earth acceleration

Then

$$\bar{g}_m = \frac{P_m + W_m}{V_m a_e} = \frac{P_m}{V_m a_e} + g_m \qquad (2.6.11)$$

If

$\bar{f}_g$ = artificial specific mass correlation function

w_p = specific gravity of prototype

then

$$\bar{f}_g = \frac{\bar{g}_m}{g_p} = \frac{P_m}{V_m w_p} + f_g \qquad (2.6.12)$$

It is now possible to select both the size of the model (i.e., f_r) and the model material (i.e. f_σ and f_g) then to determine the required $\bar{f}_g$ from equation (2.6.5) and finally to compute P_m from equation (2.6.12). The rules according to which P_m should be distributed over the model will be discussed in Section 2.7.

Artificial increase of model specific mass could also be achieved by making the model of a magnetic material and placing it in a magnetic field. The method has the basic limitation that magnetic lines of force leave a surface normally, i.e., the direction of the forces would not agree with the direction of earth attraction. In addition, the magnetic force is not uniformly distributed over the thickness of the model.

2.6.8 Dynamic Model Studies with Natural Earth Attraction. A model study becomes dynamic as soon as dynamic surface forces or support accelerations must be reproduced. The

structure may, or may not, at the same time be subjected to static surface loads and earth attraction. It now becomes of importance to differentiate between loads having significant mass, and thus subject to inertia forces like the structure itself, and loads whose force only needs to be simulated. The relationship between the correlation functions and the importance of f_t have already been discussed in Section 2.6.3. In this case, as in Section 2.6.4,

$$f_G = f_g$$

so that $$f_\sigma = f_g f_r \qquad (2.6.13)$$

In addition, $$f_a = 1$$

so that $$f_r = f_t^2 \qquad (2.6.14)$$

Once the model material has been chosen, f_σ and f_g are known and f_r can be determined from equation (2.6.13). Then f_t is given by equation (2.6.14). Since surface loads must be scaled according to the stress correlation function f_σ, the load-time curve for the model is now uniquely determined.

This method therefore permits the effect of both earth attraction and dynamic surface loads to be exactly reproduced in the model, but it is tacitly assumed that the loading is of Type I. If the prototype is subjected to support accelerations, these must be applied to the model in the ratio $f_a = 1$. The technical difficulties are the same as in Section 2.6.5. Data recording will, however, become more complicated since strain versus time curves must now be obtained.

2.6.9 Dynamic Model Studies with Artificially Induced Earth Attraction. In many model studies, the previous method may not be suitable because the models become too large or because the loading is not of Type I. It will then be necessary to simulate earth attraction artificially. While the earth attraction body forces must be reproduced artificially

it should be noted that the inertia body forces will automatically satisfy the laws of similitude as is demonstrated by the following example:

Consider a point load P_p acting on a particle of unit volume with specific mass g_p, giving it an acceleration a_p according to Newton's Second Law:

$$P_p = g_p a_p \tag{2.6.15}$$

A model of the particle is made at scale f_r and the surface forces are scaled in ratio f_σ. We wish to prove that the model is automatically subjected to the correct inertia body forces but that the laws of similitude for earth attraction are not satisfied unless $f_a = 1$, a case which we have excluded in this section.

The model properties are

$$\begin{aligned} P_m &= f_\sigma f_r^2 P_p \\ g_m &= f_g g_p \\ V_m &= f_r^3 \end{aligned} \tag{2.6.16}$$

According to Newton's Second Law

$$P_m = V_m g_m a_m$$

Substituting from equation (2.6.16):

$$f_\sigma f_r^2 P_p = f_r^3 f_g g_p a_m$$

Using equation (2.6.15):

$$a_m = \frac{f_\sigma}{f_r f_g} a_p$$

$$\therefore \quad f_\sigma = f_r f_g f_a \tag{2.6.17}$$

Equations (2.6.17) and (2.6.5) are identical so that inertia forces are always correctly modeled.

The earth attraction on the prototype is

$$A_p = \gamma \frac{Mg_p}{r^2} \qquad (2.6.18)$$

where γ, M and r for Newton's Gravitational Law have been defined previously. The earth attraction on the model is

$$A_m = \gamma \frac{Mf_r^3 f_g g_p}{r^2} \qquad (2.6.19)$$

But since A_m is a point force, it follows that

$$A_m = f_\sigma f_r^2 A_p \qquad (2.6.20)$$

Equations (2.6.18) to (2.6.20) yield

$$f_\sigma = f_r f_g \qquad (2.6.21)$$

Equation (2.6.21) is a special case of equation (2.6.5) which proves that the earth attraction is modelled correctly only if $f_a = 1$.

If $f_a \neq 1$, artificial methods can be used to reproduce the earth attraction body forces. It is considered impractical to apply both a blast load and an artificial acceleration to the model, and the discussion will therefore be restricted to the use of surface forces for the simulation of earth attraction.

As shown in Section 2.6.7, both the size of the model (i.e., f_r) and the model material (i.e., f_σ and f_g) may be chosen arbitrarily or in such a manner that they satisfy the conditions imposed by the dynamic surface loads, Type II or III. Then f_g is determined from equation (2.6.5) and P_m from equation (2.6.12). As shown previously, the inertia body forces due to the dynamic surface loads are automatically reproduced correctly in the model. The inertia body forces due to support accelerations will be scaled correctly if the support accelerations of the model are calculated using f_a as determined from equation (2.6.5).

The problem of reproduction of gravity stresses in models is thus basically the same in static and in dynamic studies. One technical problem is, however, added in the latter case since the surface loads simulating earth acceleration have to remain constant when the model vibrates.

2.6.10 Modelling of Heavy Masses Supported by Structures. A great variety of important public, industrial and military structures support heavy masses e.g., warehouses, grain silos, oil storage tanks, etc. Since the dynamic structural action in these cases is largely determined by the supported masses, their effect may not be neglected in a model study. In particular, it is necessary to take into account:

a) the earth attraction on them.

b) inertia forces due to dynamic response.

c) friction forces acting between individual loads and between the loads and the structure.

d) their destructive action if dynamic response of the structure, or direct exposure to dynamic external loads, turns them into projectiles.

Factors (a) and (b) may be studied in the same manner as the dead weight and inertia forces of the structure itself, as discussed previously. Factors (c) and (d) are discussed individually in the following two sections.

i) Modelling of Friction Forces - Consider a prototype mass M_p supported by a structure so that the coefficient of friction between them is μ_p. The maximum acceleration a_p to which the prototype structure may be subjected before the mass starts moving relative to the structure can be deduced from Fig. 2.6.4

$$a_p = \mu_p a_e$$

where a_e = earth acceleration.

Similarly for the model

$$a_m = \mu_m a_e$$

so that

$$\frac{a_m}{a_p} = \frac{\mu_m}{\mu_p} \qquad (2.6.22)$$

As discussed previously, accelerations in the model frequently are considerably larger than in the prototype, but generally $\mu_m \approx \mu_p$. In these cases, similarly with regard to friction forces can be achieved by artificial methods only.

a) Increase the normal force N. An additional force P normal to the surface between model structure and load is provided so that

$$N = P + M_m a_e$$

and

$$M_m a_m = \mu_m (P + M_m a_e)$$

so that

$$\frac{a_m}{a_p} = \frac{\mu_m}{\mu_p} \left[\frac{P}{M_m a_e} + 1 \right] \qquad (2.6.23)$$

Once f_a and f_μ are known, the required value of P can be calculated from equation (2.6.23). The force P can be obtained by using magnets as loads and making the model of a magnetic substance where the loads rest on it. The method has the advantage that, once the load starts moving relative to the structure, the full friction force will remain acting between their surfaces and the load will again come to rest relative to the structure once the inertia forces become less than the maximum available friction force. This is of importance where a structure goes through several cycles of vibration before it reaches maximum stress or sometimes ultimate failure conditions.

b) Increase coefficient of friction. The mass representing the prototype load may also be glued to the model, particularly if it is reasonable to assume that the load on the prototype will not move relative to the structure, so that it is only necessary to obtain a sufficiently

large friction force in the model. It must, however, be remembered that, once the bond is broken, the behavior of model and prototype loads is no longer similar. These artificial methods will not be necessary where natural earth attraction is employed in the model study, i.e., $f_a = 1$.

ii) Modeling of Projectile Action - Once a load moves relative to the structure, it becomes a projectile which, upon impact with parts of the structure or with its contents, may cause considerable damage. True modeling of this phenomenon is particularly important since a general analytical treatment of the problem is not available (see Ref. 30, p. 127 et seq.) The following limitations are imposed upon the correlation functions for the geometry and material properties of the masses representing the model loads:

a) Since the size of the impact area may be of importance, the model load must be geometrically similar to the prototype load, and f_r for load and structure must be the same.

b) While the load is still moving with the structure, it is subjected to the same acceleration so that f_a is the same for both, and thus f_t must also be the same (since f_r is already fixed).

c) The ratio between the prototype and model kinetic energies ($\frac{1}{2}mv^2$) has to be the same for structure and load so that in addition to the preceding, $f_g = 1$.

d) The percentage of the kinetic energy which must be absorbed by the structure depends largely upon the nature of the impact if the projectile mass is considerably smaller than that of the structure and the masses still adhering to it. It is considerably less for plastic than for elastic impacts. For this phenomenon to be correctly reproduced, it is essential that f_σ is the same for structure and load.

It may thus be concluded that, for missile action to be correctly modeled, the correlation functions f_r, f_t, f_g

and f_r have to be identical for the structure and its loads. In addition, the requirements of Section (a) have to be met. These conditions are not, however, sufficient to guarantee similitude for impulsive action since factors such as the crystalline structure of the prototype structural material and load may be of importance.

2.7 THE SIMULATION OF BODY FORCES BY SURFACE LOADS

It has been shown in previous sections that it frequently becomes desirable to replace the body forces due to earth attraction by a series of discrete surface loads. This section is devoted to an analysis of the errors resulting from the approximation, and to methods that may be employed to compensate for, or at least to minimize, the error.

Consider a structure loaded with n discrete surface forces L_j such that their sum P_m satisfies the relationship

$$P_m = \sum_{j=1}^{n} L_j = V_m w_p (\bar{f}_g - \dot{f}_g) \qquad (2.7.1)$$

derived in Section (2.6.7). Divide the total volume V_m of the structure into n subvolumes V_j, each proportional to its load L_j, so that

$$V_j = L_j \frac{V_m}{P_m} = \frac{L_j}{w_p(\bar{f}_g - \dot{f}_g)} \qquad (2.7.2)$$

The subdivision has to be carried out in such a manner that the influence volumes are as geometrically similar as possible. Assume that a typical influence volume, as shown in plan in Fig. 2.7.1, is small enough so that its thickness t can be considered constant. Let load L_j be applied as a uniform stress p over area a_j such that the centers of gravity of V_j and a_j coincide in plan. The problem now becomes the determination of the stresses caused in element v_j by the replacement of the uniformly

distributed body force, which should exist according to the requirements of the exact theory of similitude, by the surface force L_j. In the model, these stresses will be added vectorially to the stresses caused by the overall structural action.

Consider a section ZZ through the center of gravity of element V_j, taken so that the length $(\ell_1 + \ell_2)$ is a minimum for the figure. If shape ABCD is not too irregular, the direction of ZZ will be a good approximation to the direction of maximum stiffness of the element. To obtain an upper limit to the error stress field, it will thus be safe to consider a slice of unit thickness, as shown in Fig. 2.7.2, where ℓ is the smaller of lengths ℓ_1 and ℓ_2. The analysis will be based on the following assumptions and conditions:

i) Since an upper limit to the error stress field is sought, a condition of plane stress over EFGH may be assumed.

ii) The model material is homogeneous and linearly elastic in the range considered. This implies either that the entire stress-strain diagram is linear, or that the additional stresses caused by the approximation of the body forces are so small that within that particular range the stress-strain diagram is linear.

iii) Deformations are small. This does not imply that the model as a whole has to undergo small deflections, but rather that the relative deflections of points within EFGH have to be small.

iv) Except for stress p, faces EH and FG are free of external loads.

v) Element V_j is restrained along EF and GH in such a manner that E and H do not displace and

$$\frac{\partial u}{\partial y} = \frac{\partial v}{\partial x} = 0$$

along EF and GH. This condition satisfies symmetry requirements if all influence volumes V_j are identical and carry identical loads. F and G do displace due to the elastic deformation of lines EF and GH.

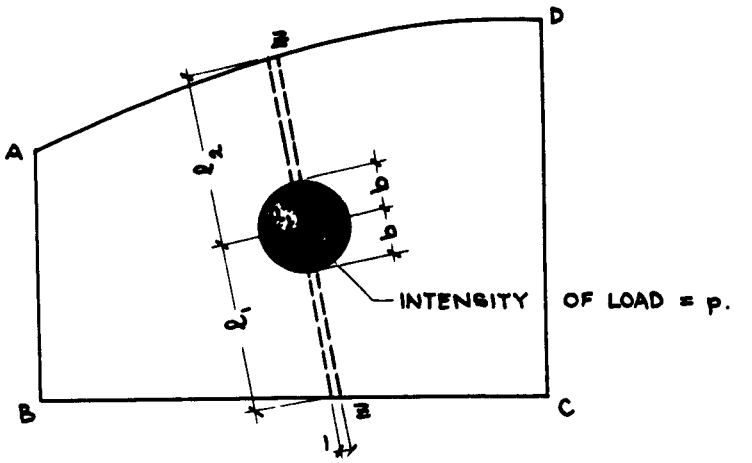

FIGURE 2.7.1

PLAN OF TYPICAL INFLUENCE VOLUME V_{ij}

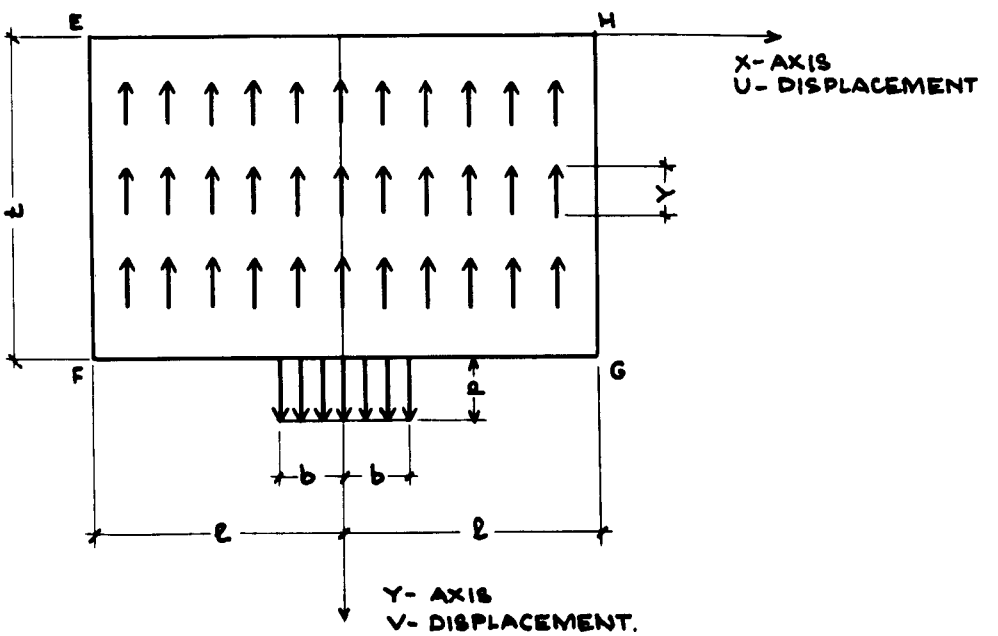

FIGURE 2.7.2

SECTION THROUGH TYPICAL INFLUENCE VOLUME V_{ij}.

vi) The nature of the supports of the structure as a whole does not affect the error stress field significantly since

a) the external loads are balanced by the body forces so that no edge reactions are required.

b) condition (v) eliminates the effect of restraints against edge rotation.

c) small errors are caused if edge EF is not rigidly restrained at the support.

Since the body forces Y are balanced by the applied load, equilibrium requires that for unit thickness of element EFGH

$$2t\ell Y = -2bp$$

$$Y = -\frac{b}{\ell t}p \qquad (2.7.3)$$

Using Timoshenko's Notation (12), the equilibrium equations are

$$\frac{\partial \sigma_x}{\partial x} + \frac{\partial \tau_{xy}}{\partial y} = 0$$

$$\frac{\partial \tau_{yx}}{\partial x} + \frac{\partial \sigma_y}{\partial y} + Y = 0 \qquad (2.7.4)$$

and the strains will be compatible if

$$\left(\frac{\partial^2}{\partial x^2} + \frac{\partial^2}{\partial y^2}\right)(\sigma_x + \sigma_y) = 0 \qquad (2.7.5)$$

The boundary conditions are

$y = 0$: $\sigma_y = \tau_{xy} = 0$ $\quad -\ell \leq x \leq +\ell$ (2.7.6)

$y = t$: $\tau_{xy} = 0$ $\quad -\ell \leq x \leq +\ell$ (2.7.7)

$\sigma_y = 0$ IF $|x| > b$, $\sigma_y = p$ IF $|x| < b$ (2.7.8)

$x = \pm\ell$ $\quad u = \frac{\partial u}{\partial y} = \frac{\partial v}{\partial x} = 0$ $\quad 0 \leq y \leq t$ (2.7.9)

The solution is simplified considerably by the introduction of the Airy Stress Function ϕ:

$$\frac{\partial^2 \phi}{\partial x^2} = \sigma_y + y_y Y$$

$$\frac{\partial^2 \phi}{\partial y^2} = \sigma_x$$

$$\frac{\partial^2 \phi}{\partial x \partial y} = -\tau_{xy} \qquad (2.7.10)$$

The equilibrium equations are identically satisfied and the compatibility condition (2.7.5) reduces to

$$\nabla^4 \phi = 0$$

A solution to this partial differential equation is

$$\phi = \cos ax \left[c_1 \cosh ay + c_2 \sinh ay + c_3 y \cosh ay + c_4 y \sinh ay \right]$$

Using (2.7.10):

$$\sigma_x = \cos ax \left[c_1 a^2 \cosh ay + c_2 a^2 \sinh ay + c_3 a (2 \sinh ay + ay \cosh ay) + c_4 a (2 \cosh ay + ay \sinh ay) \right]$$

$$\sigma_y = -a^2 \cos ax \left[c_1 \cosh ay + c_2 \sinh ay + c_3 y \cosh ay + c_4 y \sinh ay \right] - yY$$

$$\tau_{xy} = -a \sin ax \left[c_1 a \sinh ay + c_2 a \cosh ay + c_3 (\cosh ay + ay \sinh ay) + c_4 (\sinh ay + ay \cosh ay) \right]$$

Using (2.7.9): $\tau_{xy} = \dfrac{\partial u}{\partial y} + \dfrac{\partial v}{\partial x} = 0$ ON $x = \pm \ell$

$$\therefore a\ell = n\pi$$

$$a = \frac{n\pi}{\ell}$$

Using (2.7.6): $c_1 = 0$

$$c_2 a + c_3 = 0$$

Using (2.7.7): $c_4 = \dfrac{at \sinh at}{\sinh at + at \cosh at} c_3 = d_n c_3$

To satisfy (2.7.8), a Fourier Series for σ_y is required. Using the last three results, and replacing for Y from equation (2.7.3)

$$\sigma_y = \frac{bp}{t\ell} y + \sum_{n=1}^{\infty} c_n a^2 \cos ax \left[\frac{1}{a} \sinh ay + y \cosh ay + y d_n \sinh ay \right]$$

BUT FOR $y = t$, $\sigma_y = \dfrac{bp}{\ell} + \sum_{n=1}^{\infty} \dfrac{2p}{n\pi} \sin \dfrac{n\pi b}{\ell} \cos \dfrac{n\pi x}{\ell}$

$$\therefore c_n = \frac{2p \sin ab}{a^2 \ell \left[\sinh at + at \cosh at + a d_n t \sinh at \right]}$$

All the coefficients have thus been determined, and substitution yields

$$\frac{\sigma_x}{p} = -\sum_{n=1}^{\infty} \left\{ \sinh ay + ay \cosh ay + d_n \left(2 \cosh ay + ay \sinh ay \right) \right\} e_n \cos ax \qquad (2.7.11)$$

$$\frac{\sigma_y}{p} = \frac{by}{tl} + \sum_{n=1}^{\infty} \left\{ \sinh ay + ay \cosh ay + d_n\, ay \sinh ay \right\} e_n \cos ax \qquad (2.7.12)$$

$$\frac{\tau_{xy}}{p} = \sum_{n=1}^{\infty} \left\{ ay \sinh ay + d_n\, (\sinh ay + ay \cosh ay) \right\} e_n \sin ax \qquad (2.7.13)$$

where $e_n = \dfrac{2 \sin ab}{\pi n \left[\sinh at + at\, (\cosh at + d_n \sinh at) \right]}$ (2.7.14)

with $d_n = \dfrac{at \sinh at}{\sinh at + at \cosh at}$ AND $a = \dfrac{n\pi}{l}$ (2.7.15)

The results are in non-dimensional form, depending on the ratios t/l and b/l. It remains to prove that boundary condition 2.7.9 is satisfied.

The displacement in the y-direction is

$$v = \frac{1}{E} \int (\sigma_y - \nu \sigma_x)\, dy + f(x)$$

$$\therefore \frac{\partial v}{\partial x} = \frac{1}{E} \int \left(\frac{\partial \sigma_y}{\partial x} - \nu \frac{\partial \sigma_x}{\partial x} \right) dy + f'(x)$$

Since $\dfrac{\partial \sigma_x}{\partial x}$ and $\dfrac{\partial \sigma_y}{\partial y}$ contain $\sin \dfrac{n\pi x}{l}$, the series vanishes on $x = \pm l$ so that $\dfrac{\partial v}{\partial x} = \dfrac{\partial}{\partial x} \left[\int \dfrac{bp}{tlE} \cdot y\, dy \right] + g'(x) = g'(x)$

Choosing $g'(x) = 0$ ensures that $\dfrac{\partial v}{\partial x} = 0$ for all y on $x = \pm l$. Since $\tau_{xy} = 0$, this also ensures that $\dfrac{\partial u}{\partial y} = 0$ for all values of y on $x = \pm l$. The condition that $u = 0$ on $\pm l$ cannot be met since

$$u = \frac{1}{E} \int (\sigma_x - \nu \sigma_y)\, dx + f(y) = -\frac{\nu bp}{tlE} xy + f(y)$$

Choosing $f(y) = 0$ shows that u is caused by Poisson effects only. This deviation from the original conditions will be neglected.

Examples: Equations (2.7.11) to (2.7.13) will now be used to derive the error stress distribution for

i) $t = \ell$ (shear type structure)

ii) $t = 0.1\,\ell$ (bending type structure)

In each case, three alternate widths of load distribution are investigated:

$$b = 0.1\,\ell,\ b = 0.25\,\ell \text{ and } b = 0.50\,\ell$$

The case $b = \ell$ is trivial since the series terms in equations (2.7.11) to (2.7.13) vanish.

2.7.1 Error Stress Field if Height t Equals Halfspan ℓ. This case is typical of massive structures where earth attraction forces may be of great importance. It is considered of interest to determine both the error in strain readings on the surface, and the distribution of major principal stress and maximum shear stress throughout the mass. In order to facilitate similar calculations for other ratios of $t:\ell$, typical examples of the computations are given below. It will be noted that the first four terms of the series solution are evaluated with slide rule accuracy. Convergence is good except at $x = 0$, $b = 0.1\,\ell$, $y = t$ where extra terms were added.

Table 2.7.1 - The information contained in Table 2.7.1 and Table 2.7.2 is valid for all values of y.

Table 2.7.2 - The values of σ_x, σ_y and τ_{xy} have been calculated for $y = 0$, $0.4t$, $0.6t$, $0.8t$ and t, for each of the three values of b. The major and minor principal stresses σ_1 and σ_2, the maximum shear stress τ_{max} and the angle α between σ_1 and σ_x were then found from

$$\tau_{max} = \pm\sqrt{\left(\frac{\sigma_x - \sigma_y}{2}\right)^2 + \tau_{xy}^2}$$

$$\sigma_1 = \frac{\sigma_x + \sigma_y}{2} + \tau_{max}$$

$$\sigma_2 = \frac{\sigma_x + \sigma_y}{2} - \tau_{max}$$

$$\alpha = \frac{1}{2}\,\text{arctan}\,\frac{2\tau_{xy}}{\sigma_y - \sigma_x}$$

Table 2.7.1 Typical Calculations for the Error Stress Field

$\frac{x}{\ell}$	$\frac{\pi x}{\ell}$ Degrees	$\cos \frac{n\pi x}{\ell}$				$\sin \frac{n\pi x}{\ell}$			
		n = 1	n = 2	n = 3	n = 4	n = 1	n = 2	n = 3	n = 4
0.0	0.0	1.000	1.000	1.000	1.000	0.0	0.0	0.0	0.0
0.125	22.5	0.921	0.705	0.382	0.0	0.382	0.705	0.921	1.000
0.250	45	0.705	0.0	-0.705	-1.000	0.705	1.000	0.705	0.0
0.375	67.5	0.381	-0.705	-0.921	0.0	0.921	0.705	-0.382	-1.000
0.500	90	0.0	-1.000	0.0	1.000	1.000	0.0	-1.000	0.0
0.625	112.5	-0.381	-0.705	0.921	0.0	0.921	-0.705	-0.382	1.000
0.750	135	-0.705	0.0	+0.705	-1.000	0.705	-1.000	0.705	0.0
0.875	157.5	-0.921	0.705	-0.382	0.0	0.382	-0.705	0.921	-1.000
1.000	180	-1.000	1.000	-1.000	1.000	0.0	0.0	0.0	0.0

Table 2.7.2 Typical Calculations for the Error Stress Field

n	πn	sinh $n\pi$	$n\pi$ sinh $n\pi$	$\sin \frac{n\pi b}{\ell}$ $b = 0.1\ \ell$	$\sin \frac{n\pi b}{\ell}$ $b = 0.25\ \ell$	$\sin \frac{n\pi b}{\ell}$ $b = 0.50\ \ell$
1	3.14	11.5	36.0	0.308	0.705	1.000
2	6.28	265	1660	0.587	1.000	0
3	9.42	6050	56900	0.806	-0.705	-1.000
4	12.56	140000	1.76×10^6	0.950	0	0

n	d_n	$\frac{e_n}{\sin \frac{n\pi b}{\ell}}$	$b = 0.1\ \ell$ e_n	$b = 0.25\ \ell$ e_n	$b = 0.50\ \ell$ e_n	
1	0.759	8.51×10^{-3}	2.64×10^{-3}	6.00×10^{-3}	8.51×10^{-3}	
2	0.865	9.45×10^{-5}	5.52×10^{-5}	9.45×10^{-5}	0	
3	0.905	1.86×10^{-6}	1.50×10^{-6}	-1.31×10^{-6}	-1.86×10^{-6}	
4	0.930	4.50×10^{-8}	4.27×10^{-8}	0	0	

Only the computations for $y = 0.6t$, $b = 0.25\,\ell$ will be shown here. Values of maximum normal and shear stresses for other values of y and b:ℓ can be read off Figs. 2.7.1 to 2.7.3 and Tables in Appendix .B. Since

$$\sinh 0.6n\pi \approx \cosh 0.6n\pi$$

equations (2.7.11 to(2.7.13) reduce to

$$\frac{\sigma_x}{p} = -\sum_{n=1}^{\infty}\left\{1+0.6n\pi+d_n(2+0.6n\pi)\right\}e_n \sinh 0.6n\pi \cos ax$$

$$\frac{\sigma_y}{p} = 0.15 + \sum_{n=1}^{\infty}\left\{1+0.6\pi n(1+d_n)\right\}e_n \sinh 0.6n\pi \cos ax$$

$$\frac{\tau_{xy}}{p}_{y} = \sum_{n=1}^{\infty}\left\{0.6n\pi + d_n(1+0.6n\pi)\right\}e_n \sinh 0.6n\pi \sin ax$$

n	$0.6n\pi$	$e_n \sinh 0.6n\pi$	Coefficient of Cos ax or Sin ax for σ_x/p	σ_y/p	τ_{xy}/p
1	1.88	1.97×10^{-2}	-0.1150	0.0850	0.0800
2	3.77	2.05×10^{-3}	-0.0200	0.0165	0.0161
3	5.67	-1.90×10^{-4}	+0.0026	-0.0022	-0.0022
4	7.54	0.0	0.0	0.0	0.0

Using the table for $\sin\frac{\pi nx}{\ell}$ and $\cos\frac{\pi nx}{\ell}$, we find the following results.

Table 2.7.3 Typical Calculations for the Error Stress Field

$\frac{x}{\ell}$	Coefficient × cos ax				$\frac{\sigma_x}{p}$
	n=1	n=2	n=3	n=4	
0	-0.1150	-0.0200	+0.0026	0	-0.1324
0.125	-0.1060	-0.0141	+0.0010	0	-0.1191
0.250	-0.0810	0	-0.0018	0	-0.0828
0.375	-0.0439	+0.0141	-0.0024	0	-0.0322
0.500	0	+0.0200	0	0	+0.0200
0.625	+0.0439	+0.0141	+0.0024	0	+0.0604
0.750	+0.0810	0	+0.0018	0	+0.0828
0.875	+0.1060	-0.0141	-0.0010	0	+0.0909
1.000	+0.1150	-0.0200	-0.0026	0	+0.0924
$\frac{x}{\ell}$	Coefficient × cos ax				$\frac{\sigma_y}{p}$
	n=1	n=2	n=3	n=4	
0	0.0850	0.0165	-0.0022	0	0.2493
0.125	0.0783	0.0116	-0.0008	0	0.2391
0.250	0.0600	0	+0.0016	0	0.2116
0.375	0.0324	-0.0116	+0.0020	0	0.1728
0.500	0	-0.0165	0	0	0.1335
0.625	-0.0324	-0.0116	-0.0020	0	0.1040
0.750	-0.0600	0	-0.0016	0	0.0884
0.875	-0.0783	0.0116	+0.008	0	0.0841
1.000	-0.0850	0.0165	+0.0022	0	0.0837

Table 2.7.4 Typical Calculations for Error Stress Field

	$\frac{x}{\ell}$	Coefficient x sin ax n=1	n=2	n=3	n=4	$\frac{\tau_{xy}}{p}$		
	0	0	0	0	0	0		
	0.125	0.0305	0.0113	-0.0020	0	0.0398		
	0.250	0.0563	0.0161	-0.0016	0	0.0708		
	0.375	0.0738	0.0113	+0.0008	0	0.0859		
	0.500	0.0800	0	+0.0022	0	0.0822		
	0.625	0.0738	-0.0113	+0.0008	0	0.0628		
	0.750	0.0563	-0.0161	-0.0016	0	0.0387		
	0.875	0.0305	-0.0113	-0.0020	0	0.0172		
	1.000	0	0	0	0	0		

$\frac{x}{\ell}$	$\frac{\sigma_x}{p}$	$\frac{\sigma_y}{p}$	$\frac{\tau_{xy}}{p}$	$\frac{\sigma_x - \sigma_y}{2p}$	$\frac{\sigma_x + \sigma_y}{2p}$	tan 2α	α	$\frac{\tau_{max}}{p}$	$\frac{\sigma_1}{p}$	$\frac{\sigma_2}{p}$
0	-0.1334	0.2493	0	-0.1913	0.0579	0	90	0.1913	0.2492	-0.1334
0.125	-0.1191	0.2391	0.0398	-0.1792	0.0600	+0.216	96.1	0.1835	0.2435	-0.1235
0.250	-0.0828	0.2116	0.0708	-0.1472	0.0644	+0.477	102.8	0.1634	0.2278	-0.0990
0.375	-0.0322	0.1728	0.0859	-0.1025	0.0703	+0.840	110.0	0.1331	0.2034	-0.0628
0.500	+0.0200	+0.1335	0.0822	0.0567	0.0768	+1.450	117.6	0.0999	0.1767	-0.0231
0.625	+0.0604	0.1040	0.0628	-0.0218	0.0822	+3.450	126.9	0.0665	0.1487	0.0157
0.750	+0.0828	0.0884	0.0387	-0.0028	0.0856	+13.8	133.0	0.0390	0.1246	0.0466
0.875	+0.0909	0.0841	0.0172	0.0034	0.0895	-5.05	150.6	0.0176	0.1071	0.0719
1.000	+0.0924	0.0837	0	0.0044	0.0880	0	180	0.0044	0.0924	0.0836

The results of the rest of the computations are summarized in Appendix B, Tables B2 to B6. The major principal and maximum shear stresses given in Tables .B.2 to .B.6 are presented graphically in Figures 2.7.3, 2.7.4 and 2.7.5. The variation of horizontal stress σ_x on the lower face is shown in Figure 2.7.6, but the variation of σ_x on the upper face (y = 0) is so small that no graph has been drawn.

Conclusions

i) The additional stresses introduced into the model by the replacement of body forces by a surface load are of the same order of magnitude as the applied stress p, rather than the total applied load. If a 1:24 mortar model of a 24" thick concrete shell is loaded on a 2" x 2" grid (... ℓ=t), and $f_a = f_\sigma = 1$, $f_g = 0.6$ then from Eqn. 3.6.5 $\bar{f}_g = 24$ and from Eqn. 2.7.1 the load applied to each influence area is

$$L_j = v_j \, w_p \, (\bar{f}_g - f_g)$$

$$\therefore L_j = 4 \times \frac{100}{12^3} \times 23.4 = 5.42 \text{ lb.}$$

For b = 0.10 ℓ:	p =	135 psi
b = 0.25 ℓ:	p =	22 psi
b = 0.50 ℓ:	p =	5 psi

A great reduction in the additional (undesirable) stresses can thus be achieved by distributing the applied load over a large percentage of its influence area.

ii) Strain gage readings on the upper face of the element in Fig. 2.7.2 will not be affected appreciably by the replacement of body forces by surface forces ($\sigma_x < 1.3\%$ of p). Strain gage readings on the lower face are affected considerably ($\sigma_x < 115\%$ of p). Strain gages should thus always be mounted on the face opposite to that on which the load is applied.

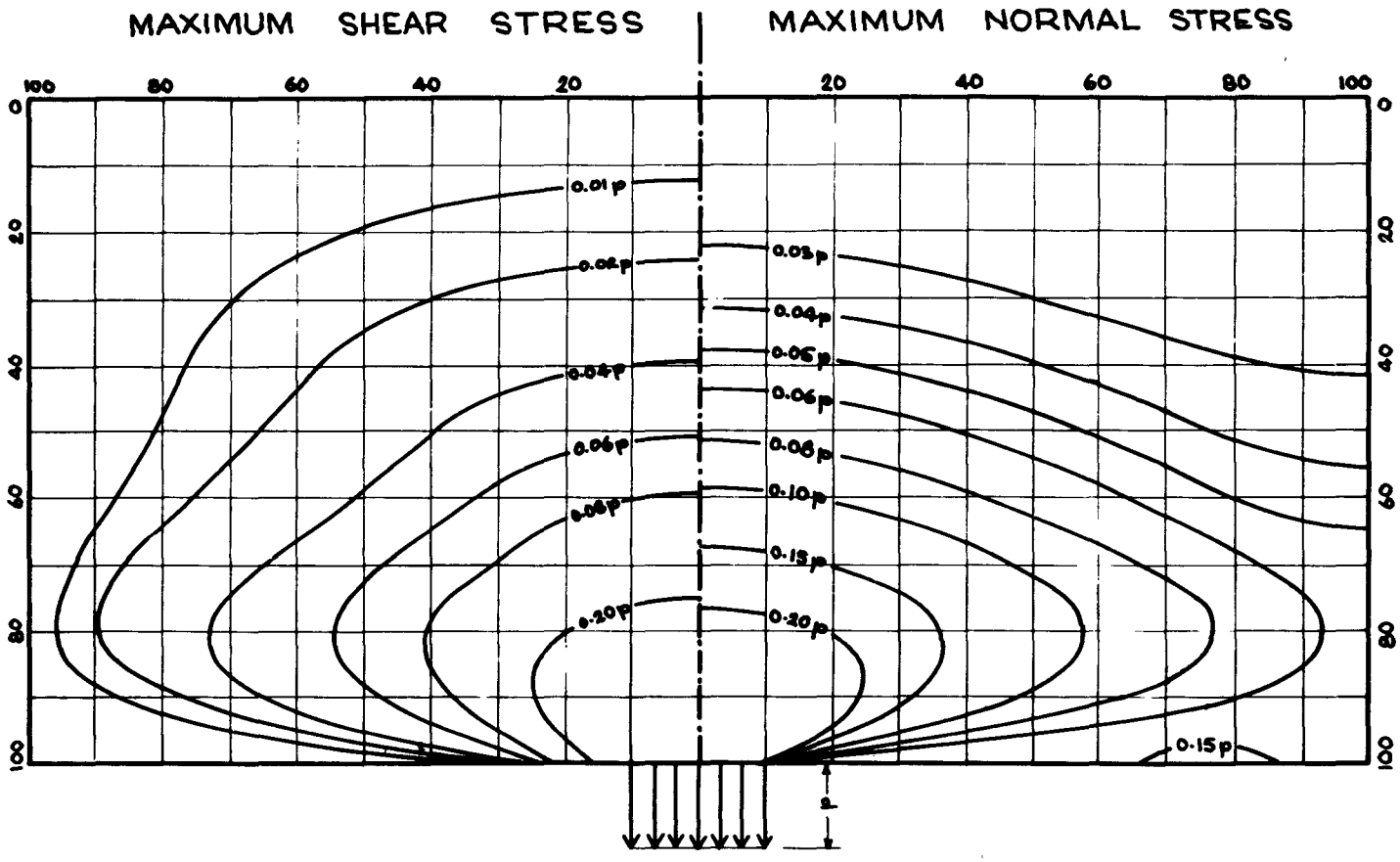

FIGURE 2.7.3

STRESSES IN A TYPICAL INFLUENCE VOLUME DUE TO THE REPLACEMENT OF BODY FORCES BY A SURFACE LOAD IF THE HEIGHT t EQUALS THE HALFSPAN ℓ.

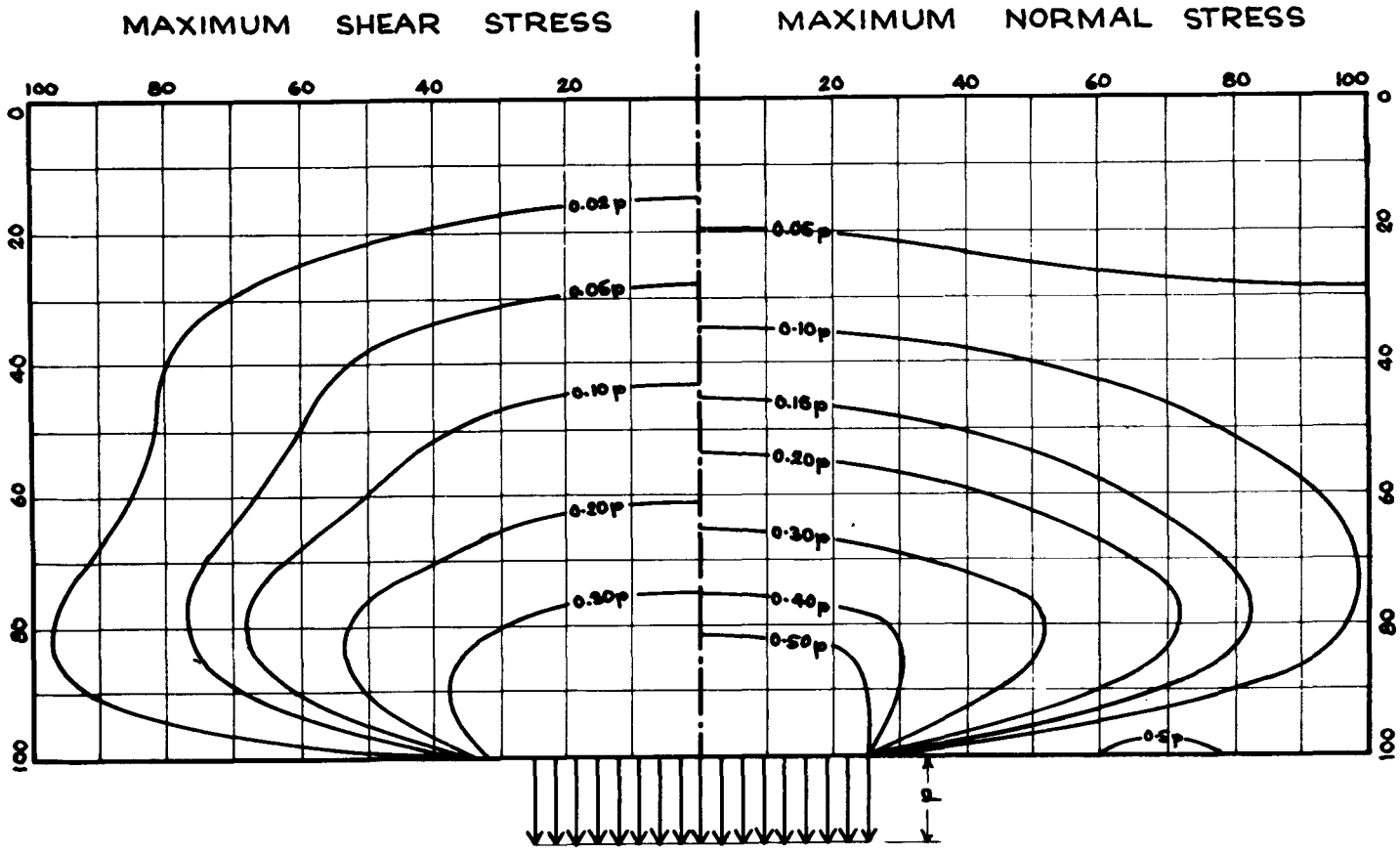

FIGURE 2.7.4

STRESSES IN A TYPICAL INFLUENCE VOLUME DUE TO THE REPLACEMENT OF BODY FORCES BY A SURFACE LOAD IF THE HEIGHT t EQUALS THE HALFSPAN ℓ.

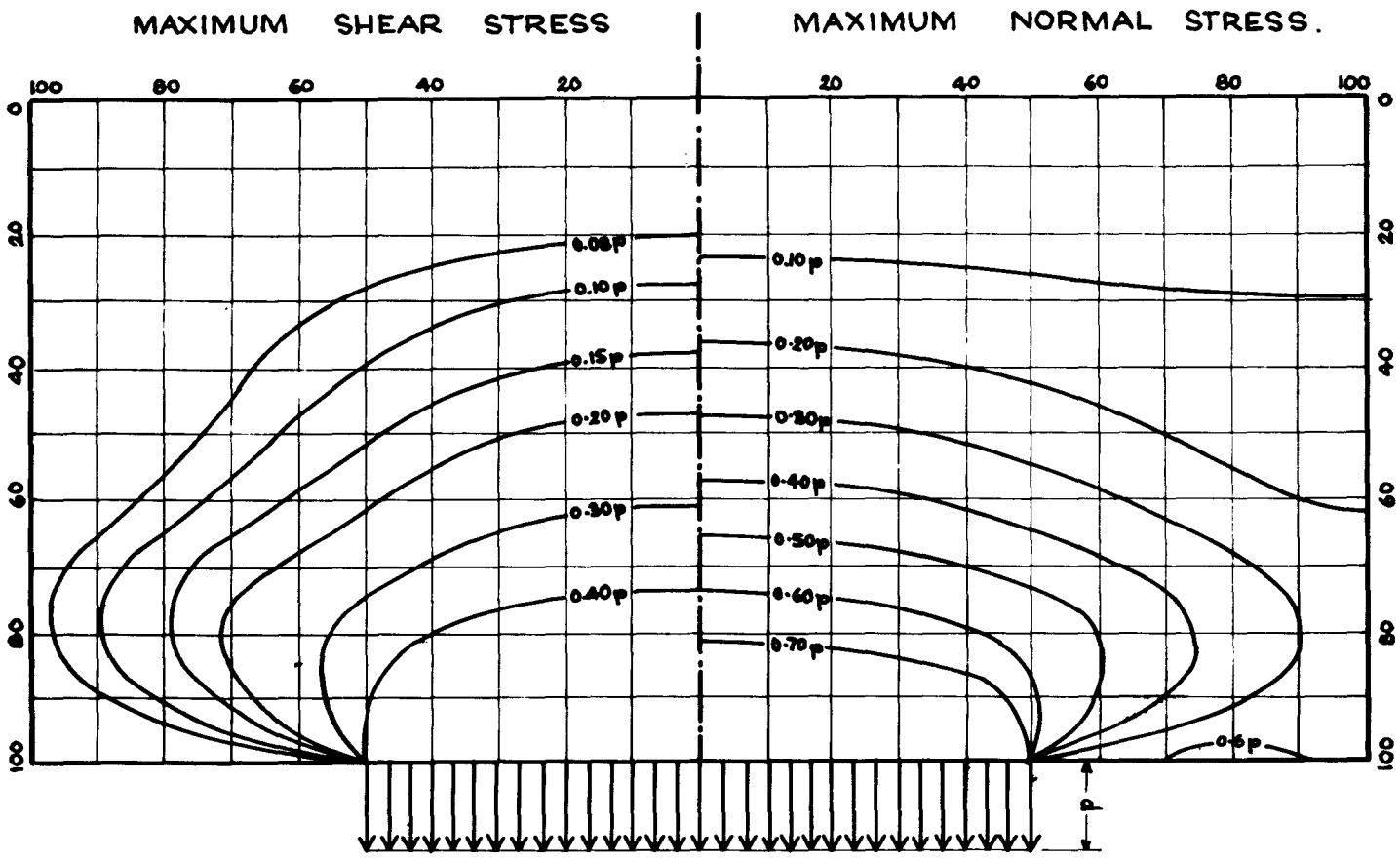

FIGURE 2.7.5

STRESSES IN A TYPICAL INFLUENCE VOLUME DUE TO THE REPLACMENT OF BODY FORCES BY A SURFACE LOAD IF THE HEIGHT t EQUALS THE HALFSPAN ℓ.

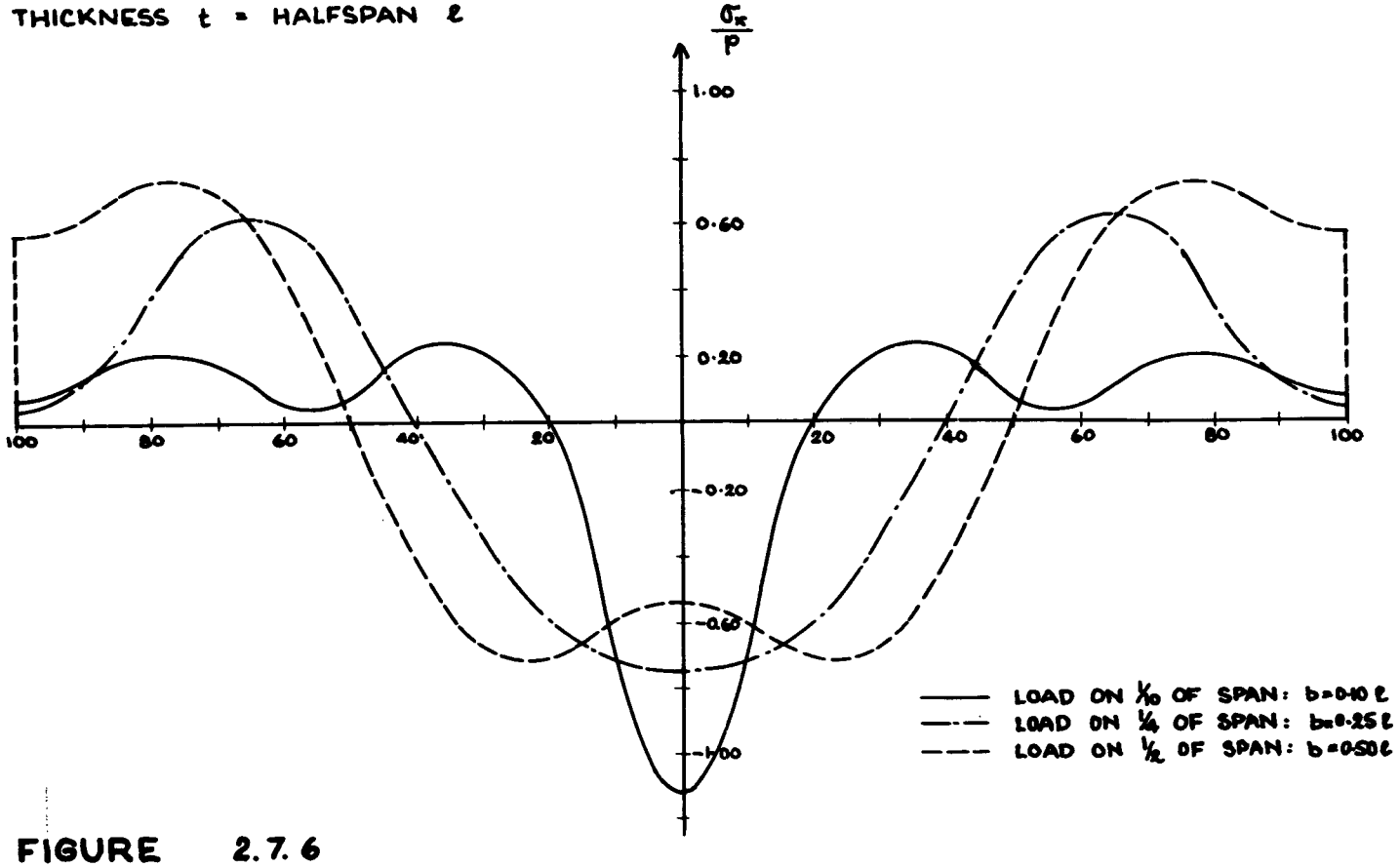

FIGURE 2.7.6

STRESSES IN A TYPICAL INFLUENCE VOLUME ALONG THE FACE ON WHICH THE SURFACE LOAD IS APPLIED.

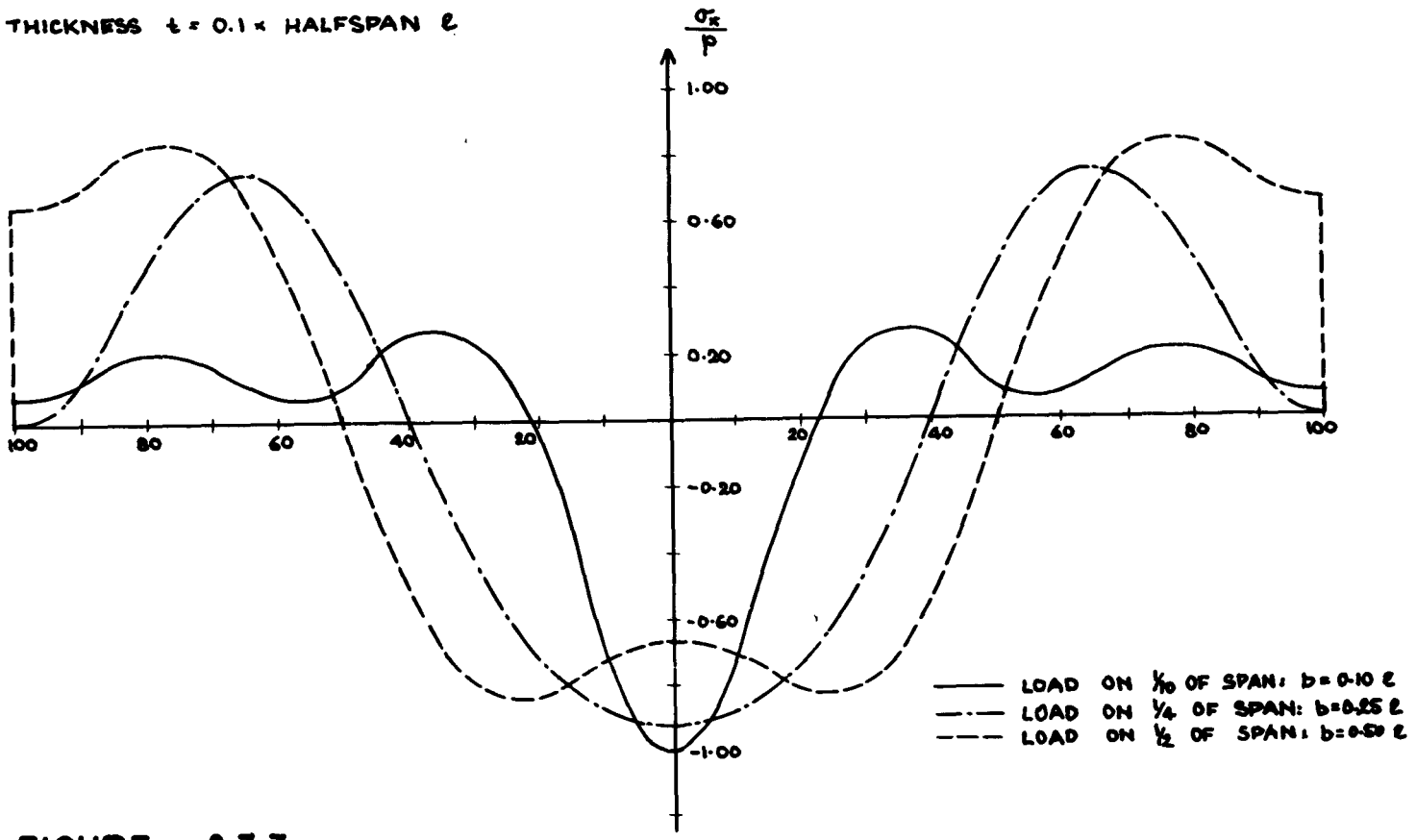

FIGURE 2.7.7

STRESSES IN A TYPICAL INFLUENCE VOLUME ALONG THE FACE ON WHICH THE SURFACE LOAD IS APPLIED.

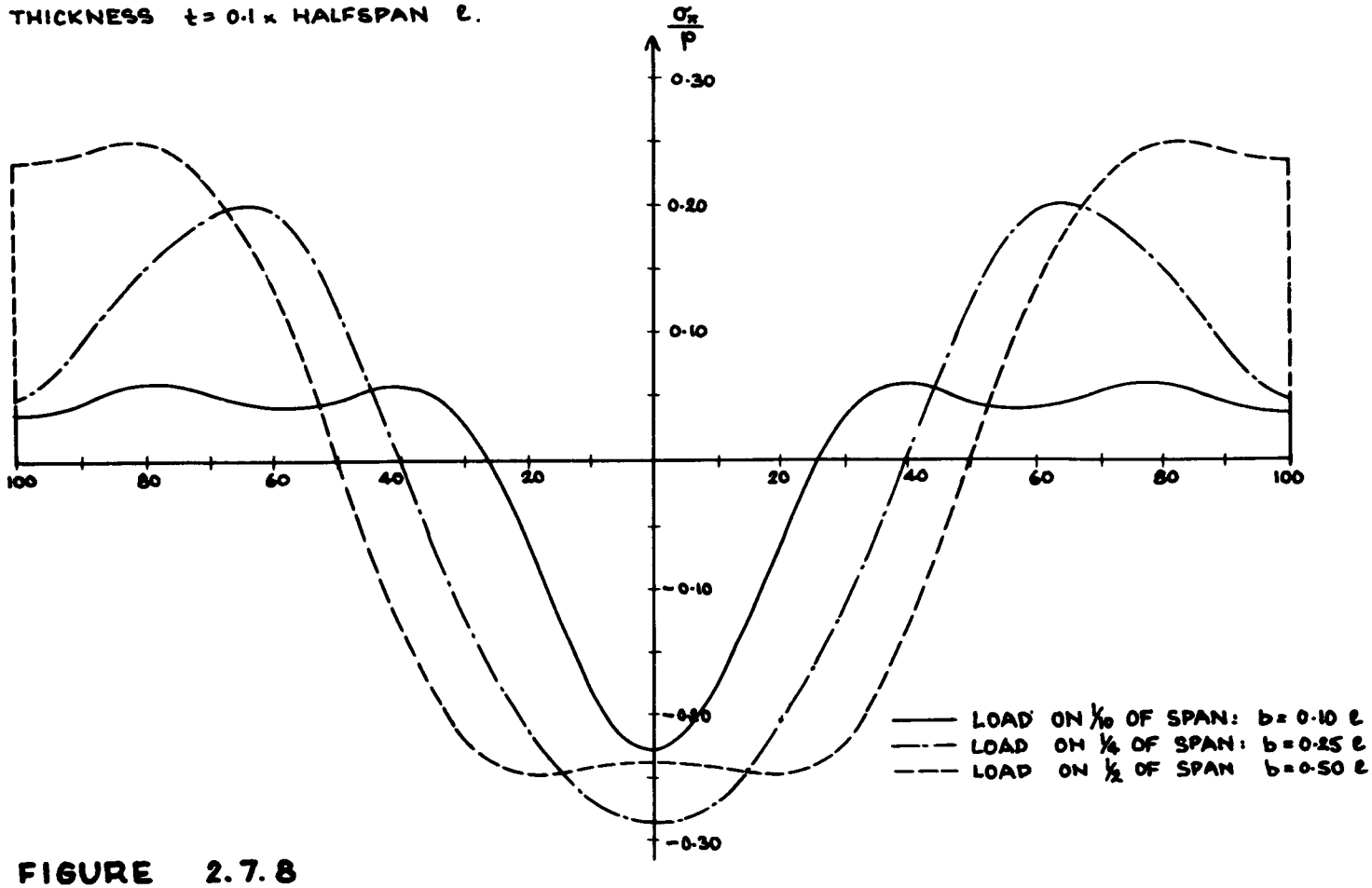

FIGURE 2.7.8

STRESSES IN A TYPICAL INFLUENCE VOLUME ALONG THE FACE OPPOSITE TO THAT ON WHICH THE SURFACE LOAD IS APPLIED.

iii) The replacement of body forces by surface loads may considerably affect the results of ultimate strength studies of mass concrete or lightly reinforced structures. The additional tensile stresses may lead to premature crack formation in the model, or they may cause the model to crack in places where the prototype will not crack. Figures 2.7.3 to 2.7.5 do, however, show that the influence of the surface load attenuates rapidly inside the mass, so that a slight strengthening of the material in the vicinity of the load point will eliminate the harmful effects. Since the stress distribution is known, the amount of additional reinforcment required is readily calculated.

iv) The effect of the body force simulation on the buckling behavior is not studied since buckling is seldom a problem in massive structures.

2.7.2 Error Stress Field if Height t = 0.1 times Half-span ℓ. The loadpoints are spaced at twenty times the thickness of the element. This is typical of large span bending-type structures. The horizontal stresses σ_x on the upper and lower faces of the element have been calculated from the first four terms of the series solution, except at $x = 0$, $b = 0.1\,\ell$ where further terms were added. The results are given in Table 2.7.5 and are shown in Figures 2.7.7 and 2.7.8

Conclusions

i) As for the case $t = \ell$, the additional stresses introduced into the model by the replacement of body forces by a surface load are of the same order of magnitude as the applied stress p, rather than the total applied load. It is thus again of advantage to distribute the applied load over a large percentage of its influence area.

ii) Strain gage readings on both the upper and the lower face of the element are affected by the replacement of body forces by surface forces ($(\sigma_x)_{max}$ = 30% and 100%

of the applied stress p respectively). It is, however, possible to place the strain gage so that it does not register the error stress field. The exact position in this case depends on the ratio b: ℓ, and varies between the quarter and half points of ℓ (see Fig. 2.7.8).

iii) If the load is transferred to the model with a pad, the stiffness of the model is altered locally. This effect has not been taken into account in the preceding analysis since, in the case of massive structures, the relative stiffness of the distribution pad can be made small.

iv) The effect of the body force simulation on the buckling behavior has not been studied. For normal (not massive) structures where this problem would be of interest, it could be investigated by determining the strain energy locked up in the error stress field

$$S.E. = \int_0^t \int_{-\ell}^{\ell} \left\{ \frac{1}{2E} (\sigma_x^2 + \sigma_y^2) - \frac{\lambda \sigma_x \sigma_y}{E} + \frac{\tau_{xy}^2}{2G} \right\} dx dy$$

This could then be compared to the total strain energy required to buckle the structure. Local snapthrough at the loadpoint would also have to be investigated.

Table 2.7.5

Ratio of horizontal to applied stress for t = 0.1 ℓ

$\frac{x}{\ell}$	y = 0			y = t		
	b=0.10 ℓ	b=0.25 ℓ	b= 0.50 ℓ	b = 0.1ℓ	b=0.25ℓ	b=0.50 ℓ
0	-0.227	-0.285	-0.236	-1.000	-0.910	-0.660
0.125	-0.148	-0.258	-0.247	-0.535	-0.844	-0.752
0.250	-0.008	-0.171	-0.242	0.119	-0.595	-0.844
0.375	0.055	-0.029	-0.160	0.282	-0.108	-0.603
0.500	0.046	0.120	0	0.101	0.452	0
0.625	0.043	0.198	0.160	0.094	0.744	0.603
0.750	0.057	0.171	0.242	0.213	0.594	0.844
0.875	0.049	0.118	0.247	0.159	0.208	0.752
1.000	0.038	0.045	0.236	0.071	0.006	0.660

CHAPTER 3

THE TECHNICAL ASPECTS OF THE MODELING OF STEEL STRUCTURES

3.1 SIMILITUDE REQUIREMENTS

We summarize here for convenience the similitude requirements for the static and dynamic response of structures loaded beyond their elastic limit. We shall assume for simplicity that the correlation functions, f, do not change with position or time as they possibly would in the general case.

3.1.1 Static Case. In the static case assuming that we know our prototype material, in this case structural steel, we must examine the possibility of finding a model material with similar elasto-plastic behavior. The correlation functions obtained from a dimensional analysis together with the compatibility of the material properties of the model to prototype will determine the design of the model and the prediction equations from which the prototype behavior will be extrapolated.

3.1.1.1 Basic Assumptions. In the modeling technique which is proposed here the modeling materials are chosen on a rational basis and then investigated to see how accurately they can predict the prototype behavior as compared to actual tests. The scope of this modeling technique will be limited to structures in which the following assumptions hold:

(i) The gravity stresses due to the dead weight of the structure are not important in the study and if they do become critical, external means will be employed to satisfy similitude.

(ii) The structural members are essentially uniaxial so that Poisson's ratio need not be identical in model and prototype.

(iii) Boundary conditions and loading will be duplicated adequately and are not the source of serious model errors.

(iv) In the static case we assume that there are no important differences between the temperature of the model and the prototype, $f_t = 1$; and that the specific heat of the materials does not enter, thus $f_c = 1$; the coefficient of linear expansion will not come into play so that $f_\alpha = 1$; and also, $f_x = 1$ since thermal conduction is no problem.

3.1.1.2 Correlation Functions. In the static case time is no longer a variable thus we see that the only relationship which must be satisfied since accelerations are also arbitrary is the stress ratio. If the model material is known then the stress ratio is determined from the stress-strain relationship of the model and prototype materials. The length scale is chosen arbitrarily. If body forces come into play, that is gravity stresses must be modeled, then the relation which must be satisfied is:

$$f_\sigma = f_g f_r \qquad (3.1.1)$$

which determines the length scale if a model material is chosen.

3.1.1.3 Stress-strain Relationship. By neglecting the effect of time and temperature, we need only investigate the stress-strain behavior of the materials. We shall consider the behavior of homologous points in model and prototype which in most cases will be the most highly stressed points which are of interest.

We assume further that the stress-strain relations for a tension specimen will be representative of all stress-strain relations for compression and shear connecting all shear strain components to the respective stress components in the general case. Knowing the stress-strain relation for the model material chosen one can then determine the correlation functions which make it compatible to the prototype material.

3.1.1.4 The Use of Phosphor Bronze as a Modeling Material for Structural Steel. The first example considers the stress-strain relations shown in fig. 3.1.1. This figure shows the idealized stress-strain relationship of structural steel and phosphor bronze. The compatibility requirements for the different ranges of strain follow:

When

$$0 \leqslant \epsilon \leqslant \epsilon_y$$

we have,

$$\sigma_m = E_m \epsilon_m \tag{3.1.2}$$

$$\sigma_p = E_p \epsilon_p \tag{3.1.3}$$

Since $\epsilon_m = \epsilon_p$ and $\sigma_m = f_\sigma \sigma_p$, it follows from Equation (2.3.10) that

$$\frac{\partial \sigma_m}{\partial \epsilon_m} = f_\sigma \frac{\partial \sigma_p}{\partial \epsilon_p}. \tag{3.1.4}$$

$$\therefore \quad E_m = f_\sigma E_p \tag{3.1.5}$$

The materials are compatible.

When $\epsilon_y \leqslant \epsilon \leqslant \epsilon_{stm}$

$$\sigma_m = \sigma_{ym} \tag{3.1.6}$$

$$\sigma_p = \sigma_{yp} \tag{3.1.7}$$

It follows from equations (3.1.2), (3.1.3), and (3.1.5) that

$$\frac{\sigma_{ym}}{\sigma_{yp}} = \frac{E_m \epsilon_y}{E_p \epsilon_y} = f_\sigma .$$

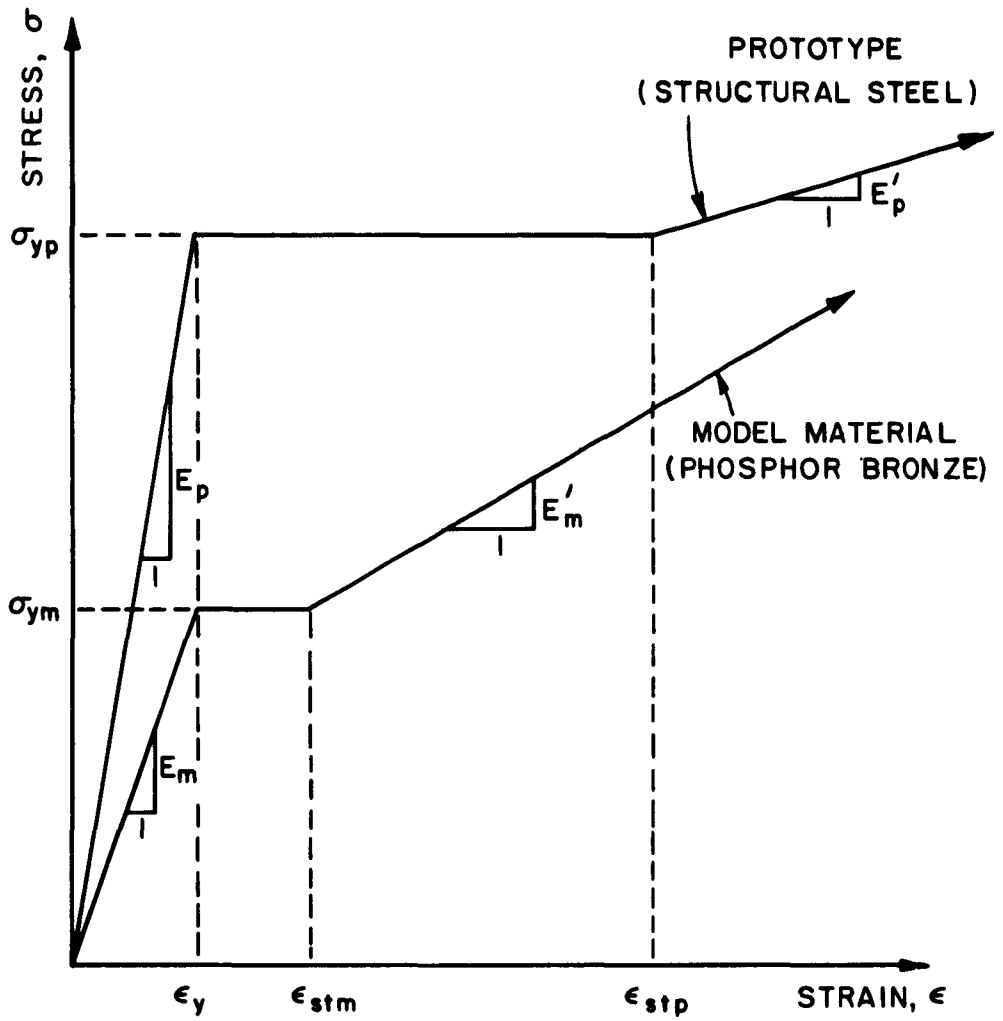

FIG. 3.1.1 IDEALIZED STRESS–STRAIN RELATIONS FOR STRUCTURAL STEEL AND PHOSPHOR BRONZE.

It follows from equations (3.1.6) and (3.1.7) that

$$\frac{\sigma_m}{\sigma_p} = \frac{\sigma_{ym}}{\sigma_{yp}} = f_\sigma \qquad (3.1.8)$$

The materials are thus compatible.

When $\epsilon_{stm} \leqslant \epsilon \leqslant \epsilon_{stp}$

$$\sigma_m - \sigma_{ym} = E'_m (\epsilon_m - \epsilon_{stm}) \qquad (3.1.9)$$

$$\sigma_p = \sigma_{yp} \qquad (3.1.10)$$

Since $\epsilon_m = \epsilon_p$, substitution of equation (3.1.8) into equation (3.1.9) yields

$$f_\sigma (\sigma_p - \sigma_{yp}) = E'_m (\epsilon_p - \epsilon_{stm}) = 0 \qquad (3.1.11)$$

Since $\epsilon_p > \epsilon_{stm}$, this requirement cannot be fulfilled i.e., the two materials are incompatible at this range. Therefore we arrive at the conclusion that above $\epsilon \geqslant \epsilon_{stm}$ the model stress-strain curve should have zero slope. This means that both model and prototype material should strain harden at the same strain. If the plastic deformations

are not excessive it may still be possible to use this modeling material up to strains in the range of ϵ_{stm} however it is unlikely that the full plasticity of a member could be developed unless plastic strains of the order of magnitude of ϵ_{stp} are available. We shall see from actual tests that the plastic strain range is enough to develop full plasticity of the member.

3.1.1.5 The Use of Ethyl Cellulose as a Model Material for Structural Steel. However, if a material such as ethyl cellulose is used to model steel the stress-strain relations will be as shown in fig. 3.1.2. Looking at fig. 3.1.2 and using the results of section 3.1.1.4 we can deduce that for

$$0 \leq \epsilon \leq \epsilon_{yp} ,$$

$$f_{\sigma} = \frac{E_m}{E_p} \qquad (3.1.12)$$

For

$$\epsilon_{yp} \leq \epsilon \leq \epsilon_{stp}$$

there is no compatibility unless $E_m = 0$. In other words for strains beyond ϵ_{yp} but less ϵ_{stp} the flatter the slope of E_m (the weaker the material used for the model) the better is the compatibility of prototype and model materials. However, in all such cases there will be discrepencies in the model, i.e., the model will be "distorted" and the degree of distortion will be a direct function E_m. In such cases the model results cannot be expected to be of a quantitative nature if the model is strained beyond the yield strain of the prototype.

When $\epsilon_{stp} \leq \epsilon \leq \epsilon_{ym}$ there will be a change in the value of f_{σ}. It is now given by

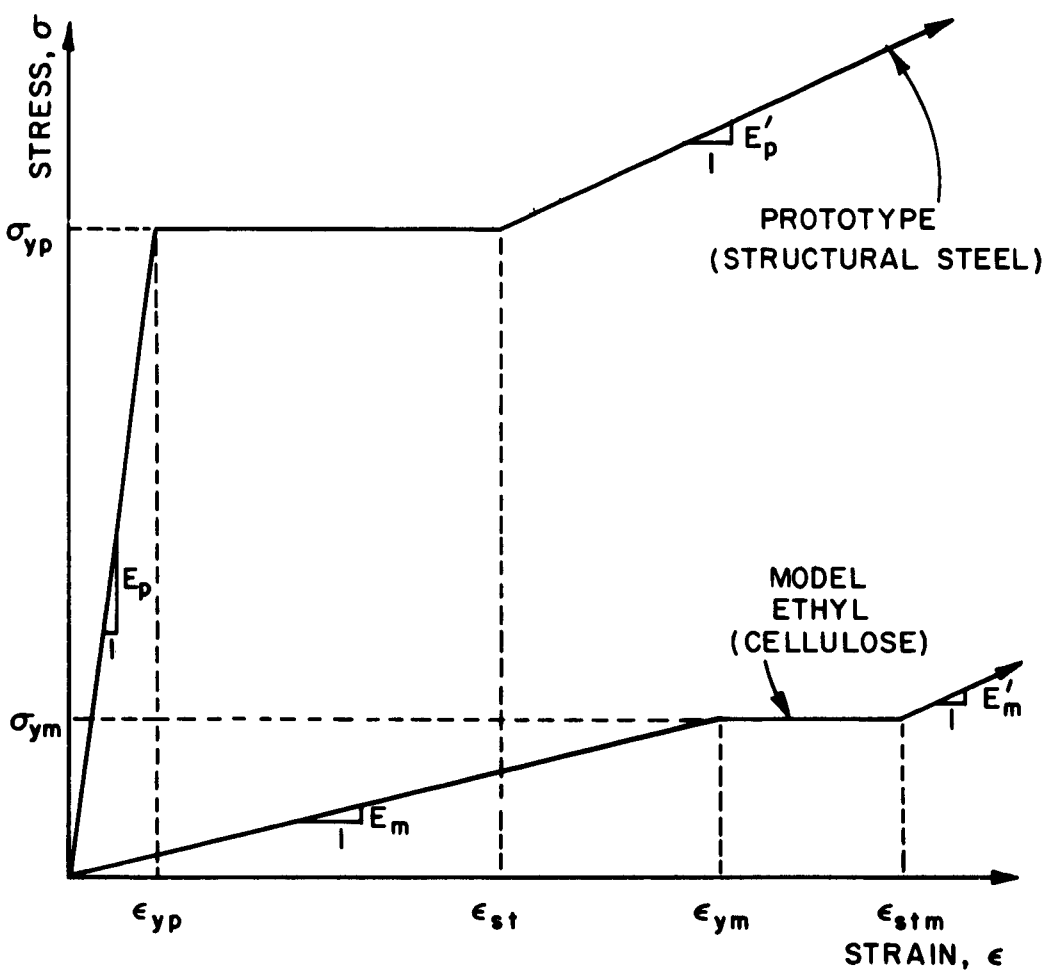

FIG. 3.1.2 IDEALIZED STRESS-STRAIN CURVES FOR STRUCTURAL STEEL AND ETHYL CELLULOSE.

$$f_{\sigma} = \frac{E_m}{E'_p} \qquad (3.1.13)$$

If $\epsilon_{ym} \leq \epsilon < \epsilon_{stm}$ then the smaller the strain hardening modulus of the steel stress-strain curve the better the correlation. It is unlikely that the prototype will be able to strain more than the early part of the strain hardening range at the critical sections where plastic deformations are taking place before the structure fails by local or lateral buckling. Thus ϵ_{stm} is probably the upper limit of strain to be considered.

It should be apparent from the discussion and fig. 3.1.2 that the relative distortion in the model will depend on the positions of ϵ_{ym} with respect to ϵ_{yp}. The closer these two values are the better the correlation. Also, the closer the values of ϵ_{stp} and ϵ_{stm} the better the correlation.

3.1.2 The Dynamic Case. Our main concern in this study is the dynamic response of structures on which the dynamic loads are a result of an air blast.

The similitude requirements covering this phenomenon are derived in Chapter 2. Although similitude does not necessarily impose a stress ratio of unity in the general case, the phenomenon of the air blast in order to be modeled with confidence imposes a stress ratio of one, i.e., the model and the prototype must be tested at the same pressure. This means that in most cases the same material must be used in model and prototype since the stress-strain relationship for the two materials must be identical. However, there may be situations where this restriction is not necessary. If the structure is made of open or frangible type construction such as bridges, towers, trusses and frames the main dynamic loading which results is of the drag type. In such cases the complications resulting from the reflected overpressures as functions of the angle of

incidence and the peak overpressure do not arise. It will be possible then to test the model at a smaller pressure than the prototype. This means that a weaker material than the prototype can be used for the model. It is for such cases that the modeling technique using phosphor bronze was developed in the study of steel structures.

From the basic relation,

$$f_\sigma = f_g f_a f_r \qquad (3.1.14)$$

in the case of phosphor bronze we have:

$$f_r = \frac{1}{15}, \quad f_g \cong 1, \quad f_\sigma = \frac{1}{2}$$

$$f_a = f_r^{-1} f_g^{-1} f_\sigma$$

$$= 15 \times 1 \times \frac{1}{2} = 7.5$$

This implies that the inertial accelerations in the model will be 7.5 times those in the prototype. The result will be a faster rate of strain of the model material.

3.2 CHOICE OF MATERIALS

The modeling of steel structures is a comparatively new phase in model analysis. Whereas in the past many elastic model studies of steel structures have been made these were done mainly in plexiglass or some other easily shaped plastic. Small scale model studies in metal are therefore relatively scarce in the literature. The concept of loading the model beyond the elastic range to predict the ultimate behavior of the prototype and the other restrictions imposed by similitude requirements in the study of the dynamic response of structures cannot be attempted without a clear understanding of the mechanical

properties of the materials involved. In this section the materials of both the prototype and the proposed models will be investigated.

3.2.1 Structural Steel. The mechanical properties of a material are greatly influenced by its microstructure a knowledge of which is very essential in the choice of a model material which will be compatible with the prototype. However, we shall leave this realm of material behavior to the specialists in this newly expanding science and as structural engineers concentrate on the mechanical properties which are of the most immediate use to us.

3.2.1.1 Definition of Structural Steel. Steel is basically an alloy of iron and less than 2% of carbon by weight. Many other metals can be alloyed with it to give steels of various characteristics. We shall be concerned here with structural steels which owe their strength and other properties chiefly to carbon. According to the AISC specifications of November 1961, Section 2.2 defines "structural steel" as follows:

> "Structural steel shall conform to one of the following specifications, latest edition:
>
> Steel for Bridges and Buildings, ASTM A7
> Structural Steel for Welding, ASTM A373
> Structural Steel, ASTM A36"

Table 2.1 summarizes the properties of the structural carbon steels which we shall attempt to model.

Of late a new series of steels which have made their appearance on the market seem to show great promise in imaginative applications in structures resulting in more economical designs. These are the high strength and high strength low alloy steels described in table 2.2. The methods which we shall propose of modeling steel structures can be expanded very easily to fit any of these steels. The stress-strain curves for the steels of

TABLE 3.1 STRUCTURAL CARBON STEELS (U. S. Steel Co.)

Steel (ASTM Designation)	Section Thickness (in)	Min. Yield Pt. (psi)	Min. T.S. (psi)	Suitability for Welding
A7 - 61T	All	33,000	60,000	No*
A373 - 58T	to 4" incl.	32,000	58,000	Yes
A36 - 61T	to 4" incl.	36,000	60,000	Yes

No* - To one inch inclusive

Yes - Over one inch, varies for different specifications

TABLE 3.2 HIGH STRENGTH AND hIGH STRENGTH, LOW-ALLOY STEELS (U. S. Steel Co.)

Steel (ASTM Designation)	Section Thickness (in)	Min. Yield Pt. (psi)	Min. T.S. (psi)	Suitability for Welding
A242 High-strength Low-Alloy Steel	To ¾, incl.	50,000	70,000	Yes
	Over ¾ to 1½, incl.	46,000	67,000	
	Over 1½ to 4, incl.	42,000	63,000	
A440 High-strength Structural Steel	To ¾, incl.	50,000	70,000	No*
	Over ¾ to 1½, incl.	46,000	67,000	
	Over 1½ to 4, incl.	42,000	63,000	
A441 High-Strength Manganese Vanadium Steel	To ¾, incl.	50,000	70,000	Yes
	Over ¾ to 1½, incl.	46,000	67,000	
	Over 1½ to 4, incl.	42,000	63,000	

No* - To one inch inclusive

Yes - Over one inch, varies for different specifications

tables 3.1 and 3.2 are shown in figure 3.2.1. These are taken from U.S. Steel Co. figures and indicate the minimum guaranteed yield points. Note that the plastic range of steel decreases as the yield strength increases. In comparing tables 3.1 and 3.2 note that because the chemical composition of structural steels varies with thickness the mechanical properties such as yield and tensile strength are about the same for all thicknesses. However, in high strength steels the chemical composition is the same and thus the strength properties are a function of the thickness as shown in table 3.2.

3.2.1.2 "Static" Properties of Steel.

The most important mechanical properties of structural steel can be inferred from a close study of the stress-strain curve which results when a standard specimen is pulled in tension at a specified rate of strain. In fig. 3.2.2 we see such a curve.

(a) shows the whole stress-strain behavior.

(b) a magnification of its early portion will concern us most and

(c) the idealization of the early portion which is often made for analysis.

The slope of the elastic portion of the curve is known as Young's modulus and is often approximated at 30×10^6 psi. The most important peculiarity of this stress-strain diagram is the distinct yield point which is almost unique to this material. The upper yield point σ_{yu} is unstable and the large plastic deformation which takes place is at a constant value, σ_{yl}, or the lower yield point. After a strain of about 1.6% the material begins to strain harden but does not fracture except after considerable elongation.

The uniqueness of the yield point in structural steel can be explained on the basis of its microstructure. It seems that carbon atoms strain the iron latice which upon the application of an external stress

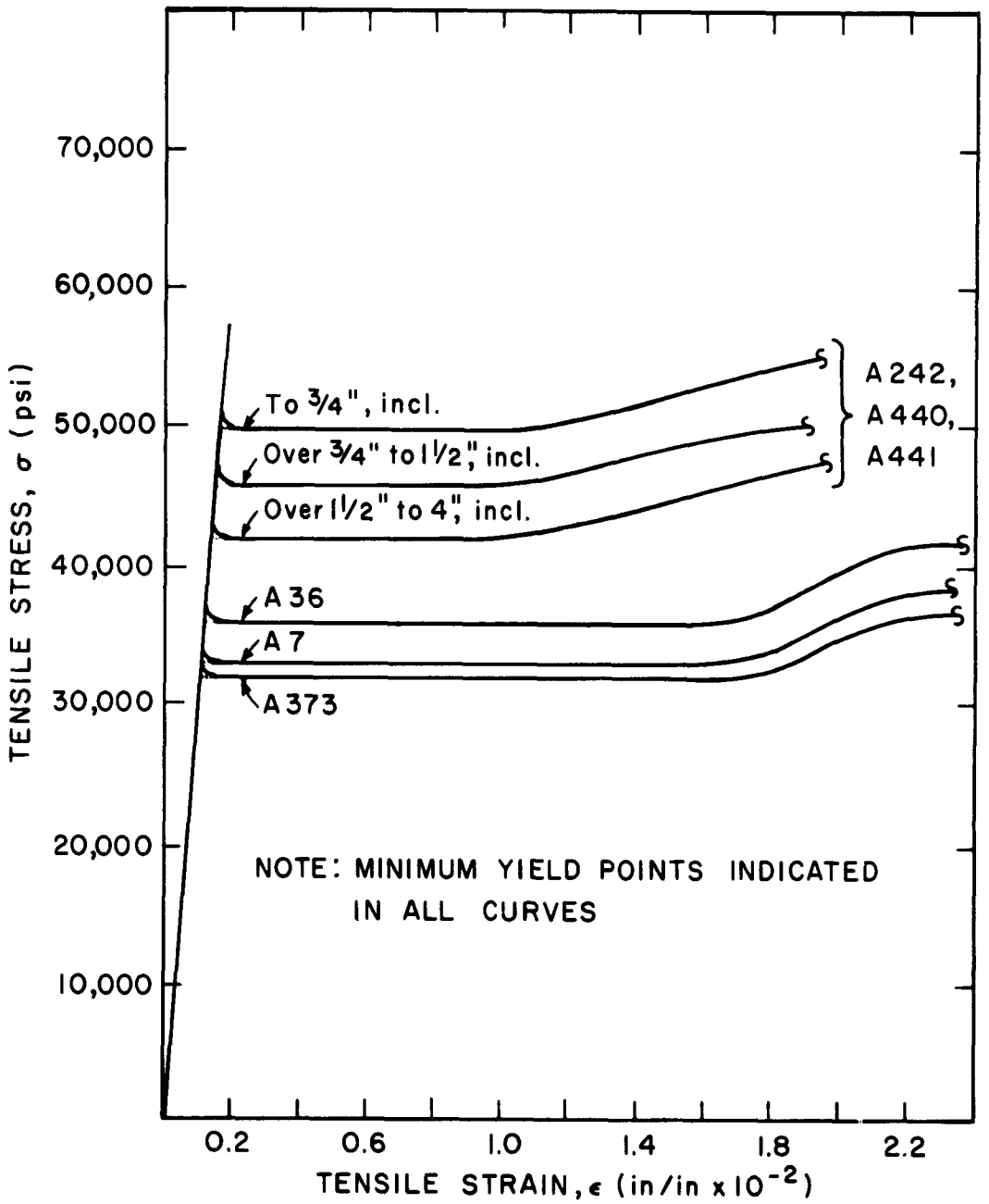

FIG. 3.2.1 IDEALIZED STRESS-STRAIN CURVES FOR ASTM STEELS

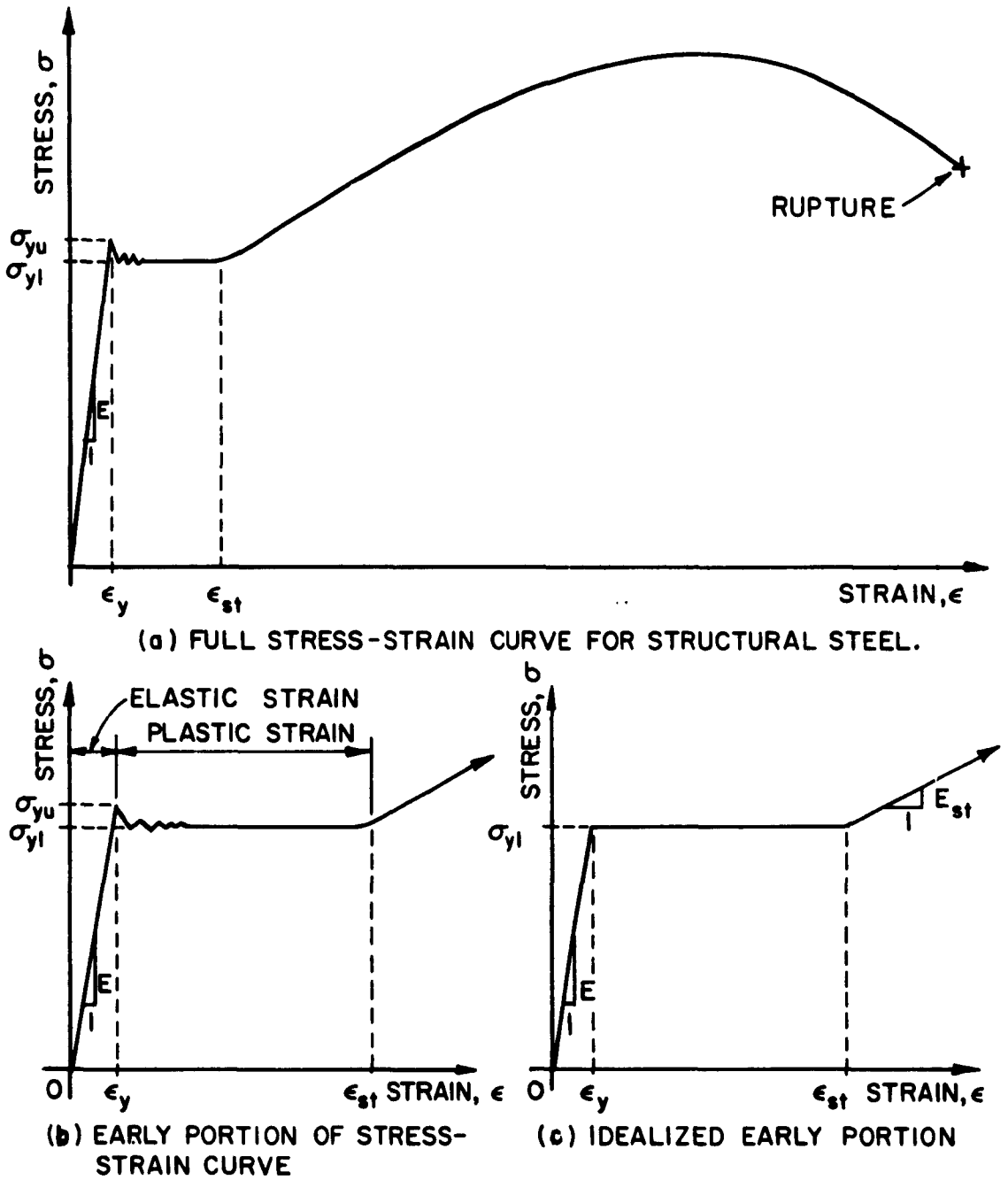

FIG. 3.2.2 TYPICAL STRESS-STRAIN CHARACTERISTICS OF STRUCTURAL STEEL.

field the strains are partly relieved and will cause plastic yielding at a constant value of stress. This phenomenon is also observed in other multiphase systems such as phosphor bronze but not to as pronounced a degree.

The three basic methods of increasing steel strength are adding alloys, heat treating, and cold working. Of these, alloying is the basic method of controlling the properties of structural steels. The yield point and the ultimate tensile strength rise with an increase in the carbon content of steel but a loss in ductility and weldability accompanies these strength gains. This is why carbon content in structural steels is usually limited to 0.28%, the specified maximum for A373, A36 and A440. A7 steel is unique among ASTM-specified structural steels in having no specified limit on carbon content. Manganese and silicon, the most important alloying elements apart from carbon, also increase yield and ultimate tensile strength with a smaller relative loss in ductility and weldability for a given percentage of element added. Copper and nickel are the principal alloying elements used to improve the corrosion resistance of high strength steels. It should be pointed out that all the high-strength structural steels resist atmospheric corrosion better than carbon steels.

3.2.1.3 Dynamic Properties of Steel.

Experimental evidence indicates that the strength behavior of most materials depends among other things on the rate of strain during testing. In steel these changes are shown in fig. 3.2.3 for the case of ASTM A-7 structural steel.

The effects of increasing rate of strain can be summarized as follows, looking at fig. 3.2.3:

1. The yield stress increases to some dynamic value, σ_{dy}.
2. The yield point strain ϵ_y increases.
3. E, the modulus of elasticity, in the elastic range remains constant.

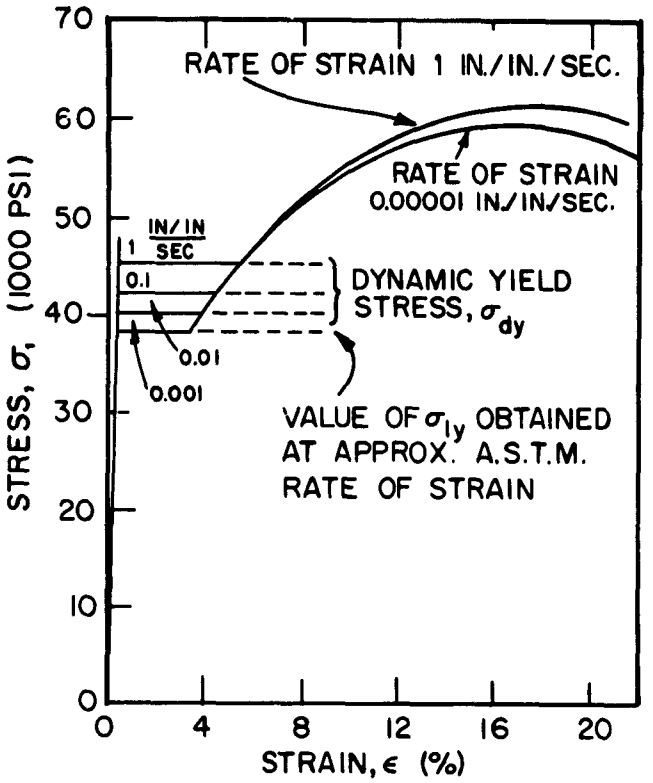

FIG. 3.2.3 EFFECT OF RATE OF STRAIN ON STRESS-STRAIN CURVE FOR STRUCTURAL STEEL (REF. 30)

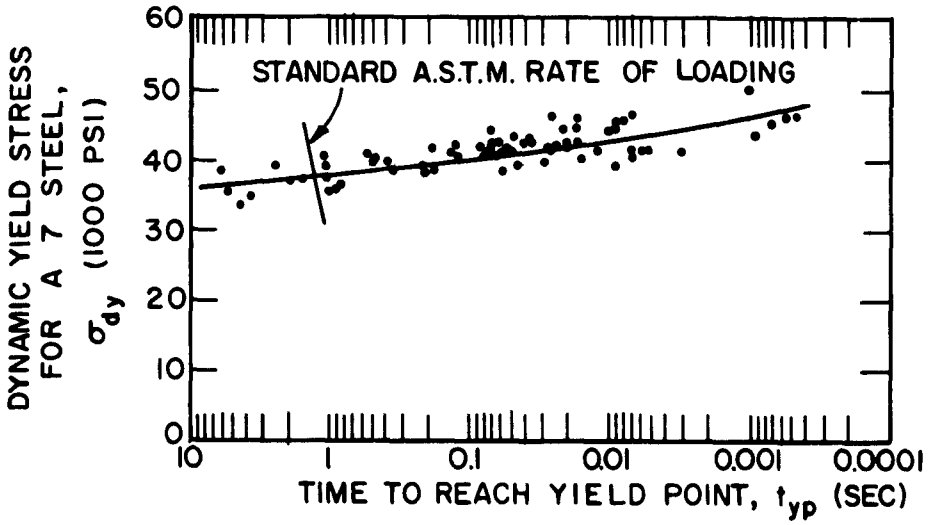

FIG. 3.2.5 EFFECT OF RATE OF STRAIN ON YIELD STRESS (REF. 30)

4. The strain at which strain hardening begins, ϵ_{st} also increases.

5. The ultimate strength increases slightly.

The most important effect which will influence the design of steel structures to resist dynamic loads, is the increase in the yield stress. In fig. 3.2.4 the percentage increase is yield stress is given as a function of the rate of strain for two steels of different static yield stress. It is evident from the figure that the increase in dynamic yield point is greater for steels with lower static yield points as is shown by the higher slopes of curve A. Figure 3.2.5 shows the dynamic yield stress as a function of the time required to reach that value of stress (t_{yp}) for ASTM A7 steel. From this curve values of design yield stress could be found knowing the time to reach yield stress in a particular structure.

3.2.2 The Copper Base Alloys as Model Materials.

Our first investigation in the possibility of finding an appropriate model material which could be used to model steel structures is the family of metals known as the copper base alloys. The similitude requirements for the case of blast loads acting on structures indicate that if the surface loads must be kept the same, which may be the case in some structures such as shells and other non-uniform surfaces, then the same material must be used for model and prototype since strain must be equal also. However, in many structures made of thin exposed members or frangible sidings it is the drag forces which are important and therefore in testing models of such structures it is possible to use lower pressures than in the prototype. This makes it possible to use a large number of materials which have less strength than steel but still compatible to its stress-strain diagram. It is for this class of problems of welded construction in steel for which the modeling technique described in subsequent sections was developed.

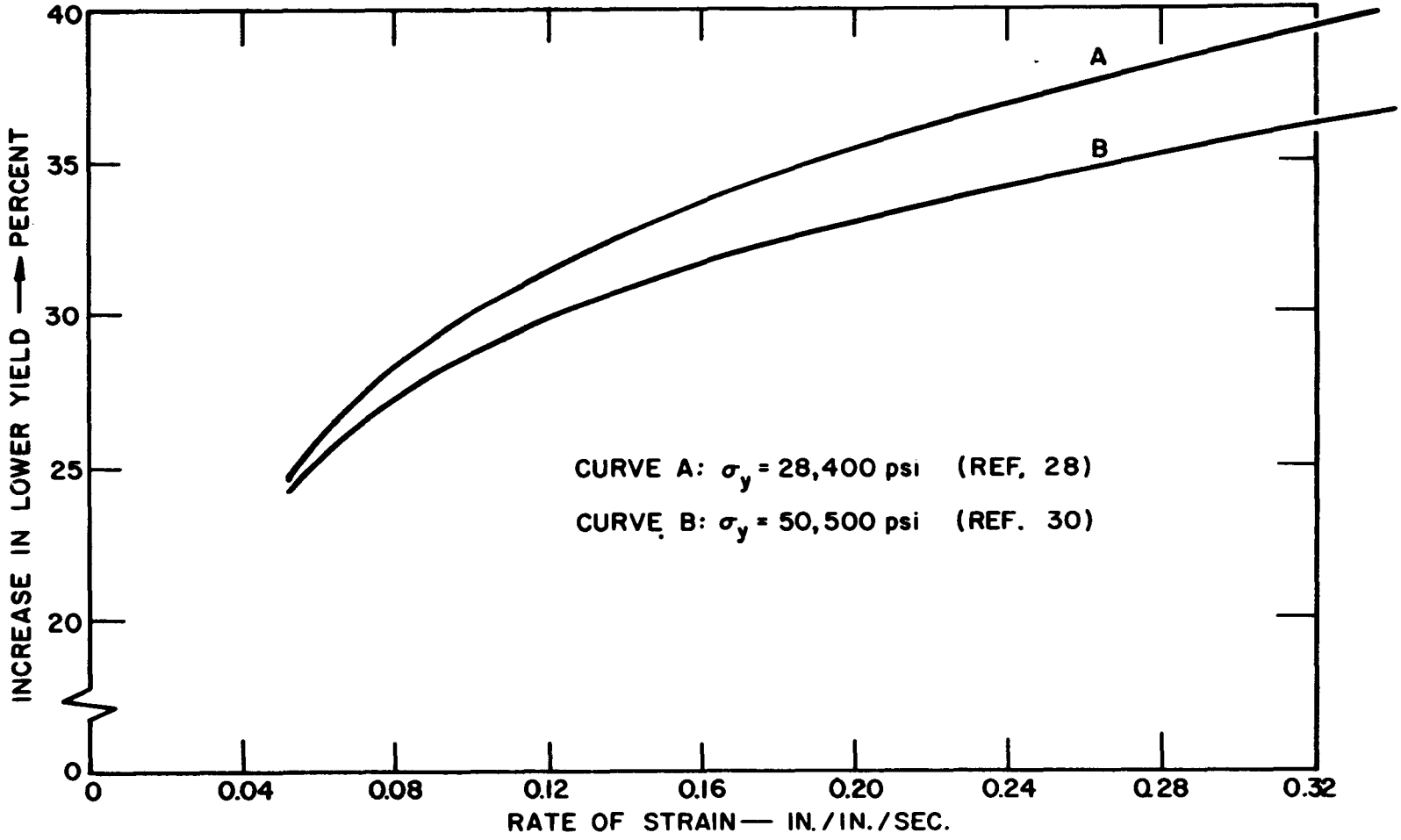

FIG. 3.2.4. INCREASE OF LOWER YIELD POINT OF STEEL WITH STRAIN RATE. (REF.42)

3.2.2.1 Properties. Alloys having copper as a base are on the whole the most readily machinable metals and the ease with which they can be milled into various shapes may be of great advantage in model making. In addition the ease of jointing them by the relatively simple process of silver soldering adds greatly to their favor in cases where welded structures are to be investigated or where a large number of parts must be assembled. An examination of the stress-strain properties of most of these alloys indicates that a distinct yield point as in the case of structural steel does not exist. However, in two commerical alloys namely phosphor bronze and silver nickel a definite yield point can be established after annealing. The important difference, however, is that the plastic yielding in these materials is not as pronounced as in steel.

3.2.2.2. Phosphor Bronze. Of the two commercially available copper base alloys that could be investigated as possible substitutes to steel in model making, phosphor bronze is chosen on the basis of lower cost and better machinability. The "free cutting" phosphor bronze which is investigated contains 4% lead (added to improve machinability), 4% tin, 4% zinc and 88% copper.

To obtain a definite yield point in phosphor bronze a cold drawn specimen must be carefully annealed to control the crystal size. The percent cold work or the amount of reduction in cross-sectional area during the rolling process must be between 50% and 75%. In the case of 50% cold worked samples stress-strain curves from strips indicate an optimum annealing temperature of 675°C for one half hour. The effect of cold work on the yield stress of phosphor bronze is shown in fig. 3.2.6 and the effect of annealing temperature in fig. 3.2.7.

These curves were established by annealing 1/4 inch rods of two hardnesses (50% and 75%) at various temperatures for one half hour. The composition

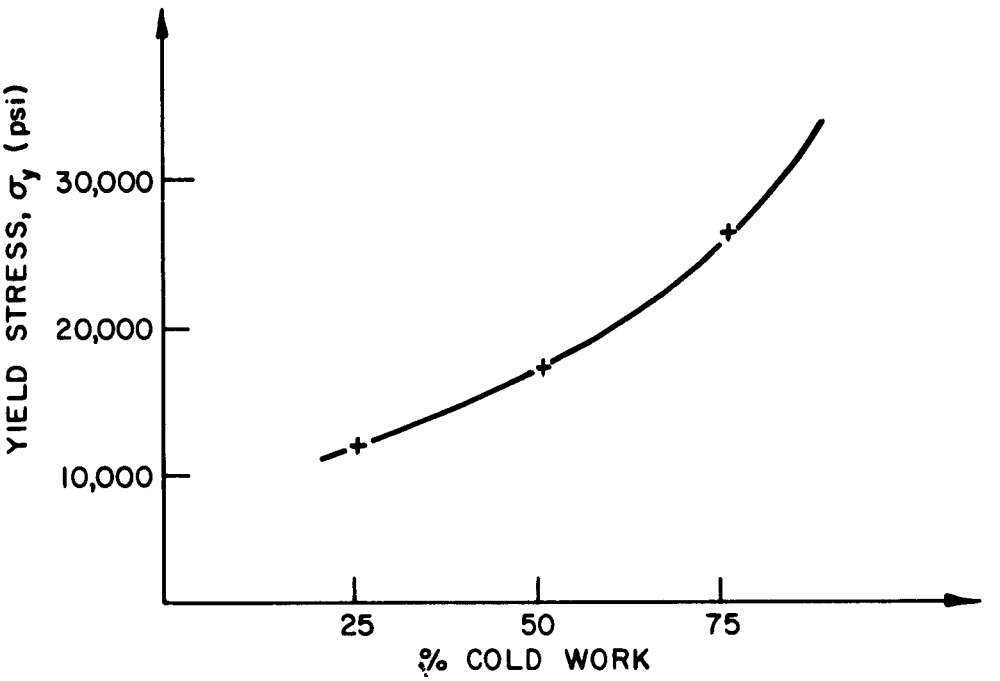

FIG. 3.2.6 EFFECT OF COLD WORK ON THE YIELD STRESS OF PHOSPHOR BRONZE.

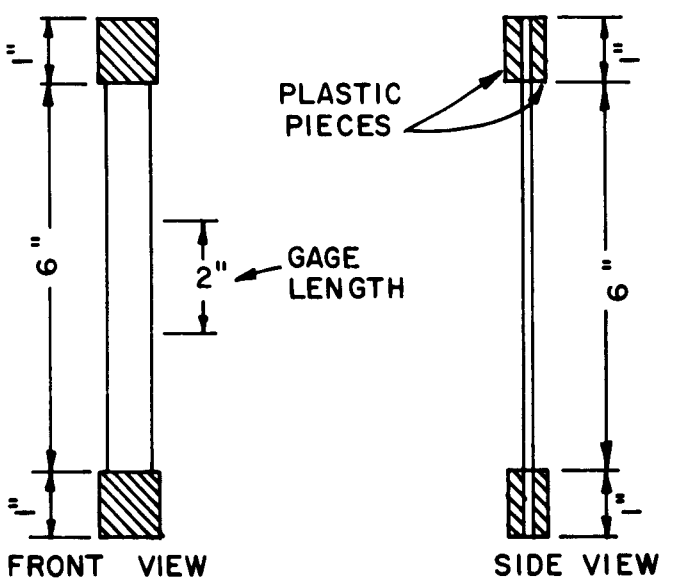

FIG. 3.2.8 DIMENSIONS OF PHOSPHOR BRONZE STRIPS USED AS TENSILE SPECIMENS.

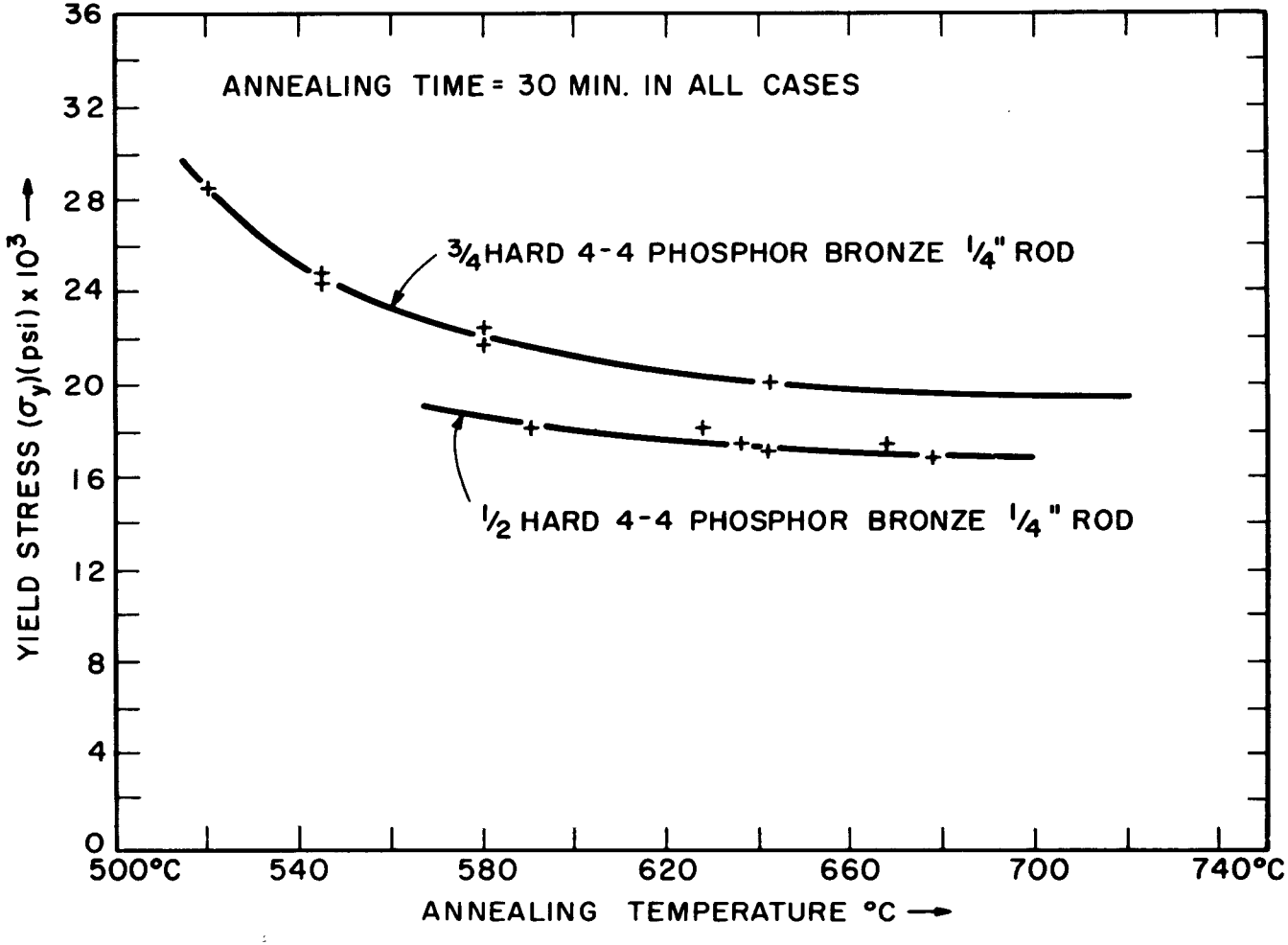

FIG.3.2.7. YIELD STRESS vs ANNEALING TEMPERATURE

of the phosphor bronze was that described above. The stresses quoted in fig. 3.2.7 as "yield stresses" are actually the stresses at which the load was observed to remain approximately constant during the test. It is interesting to note that the annealing has a greater influence in lowering the yield stress in samples of larger cold work. This may be due to the fact that in this case the crystals are left more distorted and strained by the rolling processes.

3.2.2.2.1 Static Stress-Strain Relations.

The stress-strain properties of phosphor bronze are not readily available in the literature. It becomes necessary then to test actual strips the size of the flanges of the wide flange model beams which were machined for the various tests. Fig. 3.2.8 shows the dimensions of the test strips and the precautions taken at the end to prevent failure at the ends by the jaw grips of the testing machine. The tests are made on the constant rate of strain "Ingtrom" type of machine of the Plastics Research Lab. at M.I.T. A gage length of 2 inches was used and externally controlled to define the points on the stress-strain diagram. This is a definite improvement over other constant rate of strain machines where strain is measured from the jaw travel of the machine. Two important errors arise from tests of this type. First, there may be slippage in the jaws which cannot be accounted for on the usual plot which the machine gives as output and, second, if the whole length of the specimen between the two jaws is used as a gage length there will be errors because of the stress distortions at the ends of the specimen. A uniform stress field will exist only in the centeral portion of the specimen which is the region far enough from the ends to allow this uniform field to develop.

The material from which the strips are cut has a cold work hardness of 50%. It is then annealed for one half hour at various temperatures and then tested. The results of three tests at a strain rate of

1×10^{-5} in/in/sec are shown in figures 3.2.9, 3.2.10, and 3.7.11. These results indicate that the optimum annealing temperature is 675°C for the time interval chosen. This is therefore adopted for all the model specimens.

A comparison of the stress-strain properties of phosphor bronze with ASTM A7 steel is made in fig. 3.2.12. We see from the two curves that yielding takes place at about the same strain. This is very important in model studies since a strain ratio of unity will not result in distorted models. However, we notice that although phosphor bronze shows some plastic yield at constant stress it does not possess the uniquely large plastic range of structural steel. Strain hardening begins much earlier in phosphor bronze than in steel so that at very large strains the two materials are not fully compatible. More will be said about this point when actual test results are discussed.

3.2.2.2.2 Dynamic Stress-strain Relations. Strips of the same dimensions as in fig. 3.2.8 are strained at various rates of strain to see how the yield point is affected. These specimens are also annealed at 675°C for one half hour and then pulled to failure at the rates indicated in fig. 3.2.13. The yield point definitely increases with increasing rate of strain in this material. Fig. 3.2.14 shows the effect of the strain rate on the yield point stress of phosphor bronze. Knowing the rate of strain of the model we can estimate the yield stress of the critically stressed points where plastic deformations will take place. The comparison is made in fig. 3.2.14 between structural steel and phosphor bronze yield stresses as affected by strain rate. It can be seen that in steel the effect is more pronounced, but since the rates of strain used are of a different range no definite conclusions can be drawn.

3.2.3 Using Plastics to Model Steel Structures. The possibility of using plastics as a model material for the structural elements of steel is also investigated. It

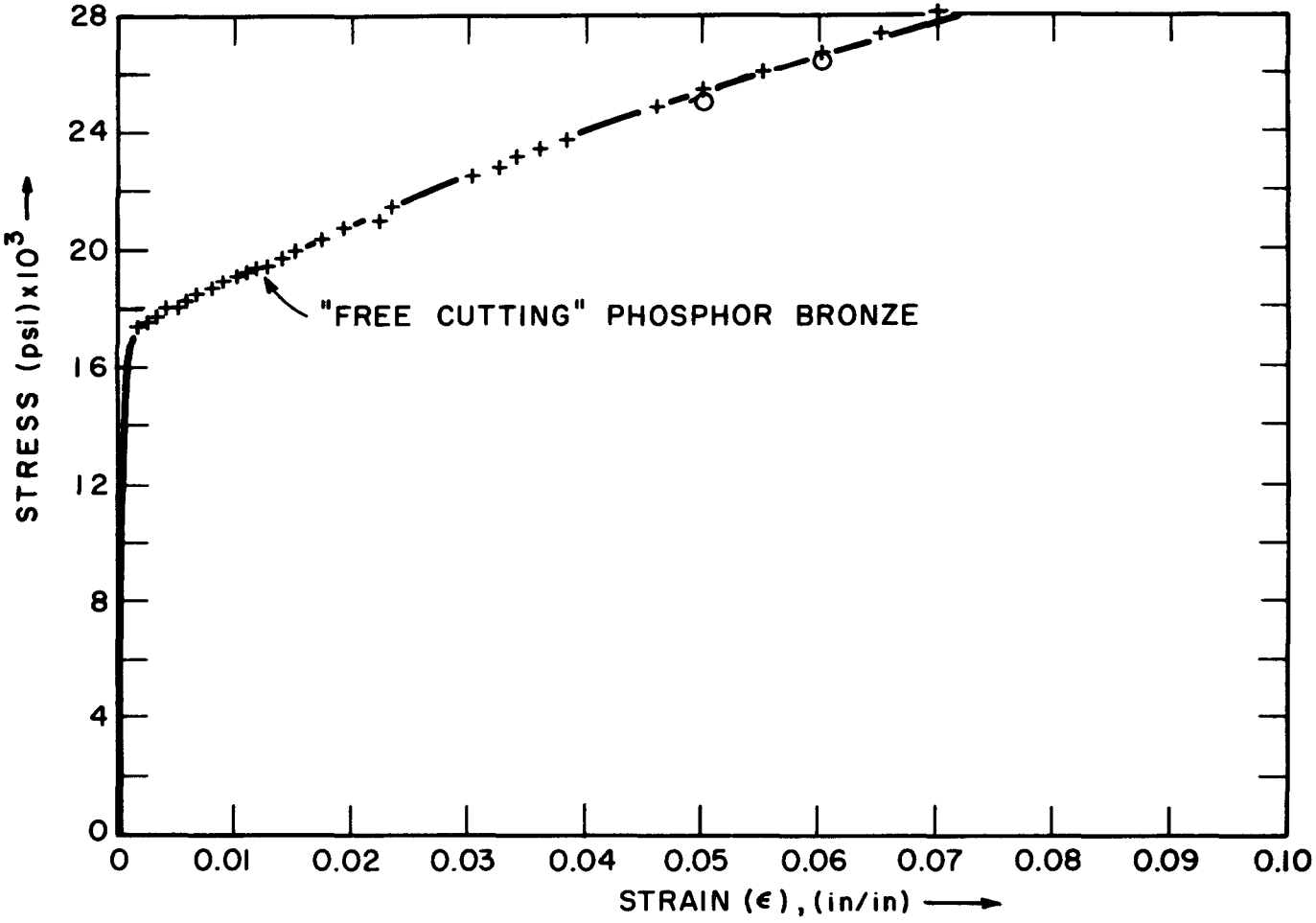

FIG.3.2.9 STRESS vs STRAIN CURVE FOR PHOSPHOR BRONZE STRIP ANNEALED AT 650°C

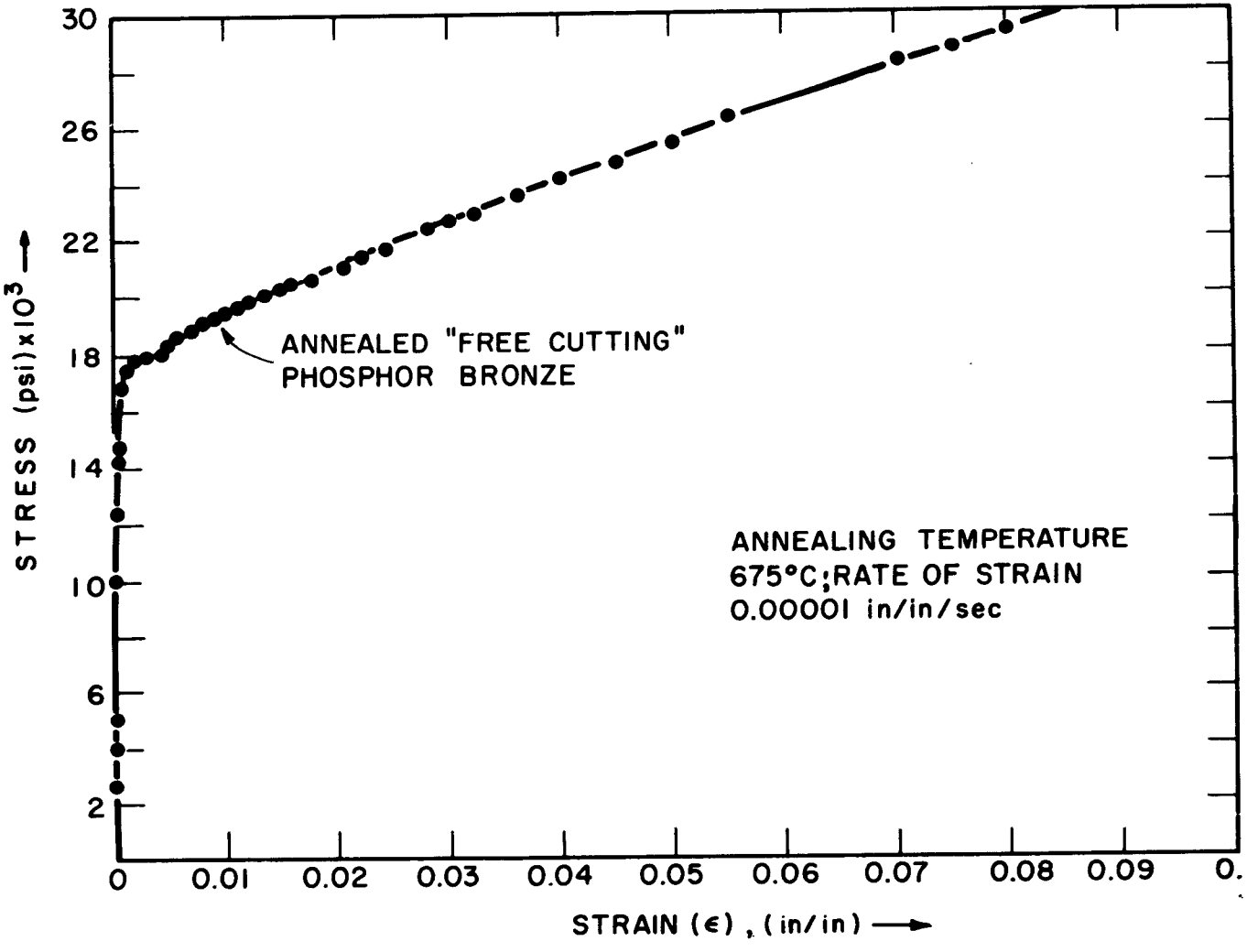

FIG.3.2.10 STRESS vs STRAIN CURVE FOR PHOSPHOR BRONZE STRIP ANNEALED AT 675°C

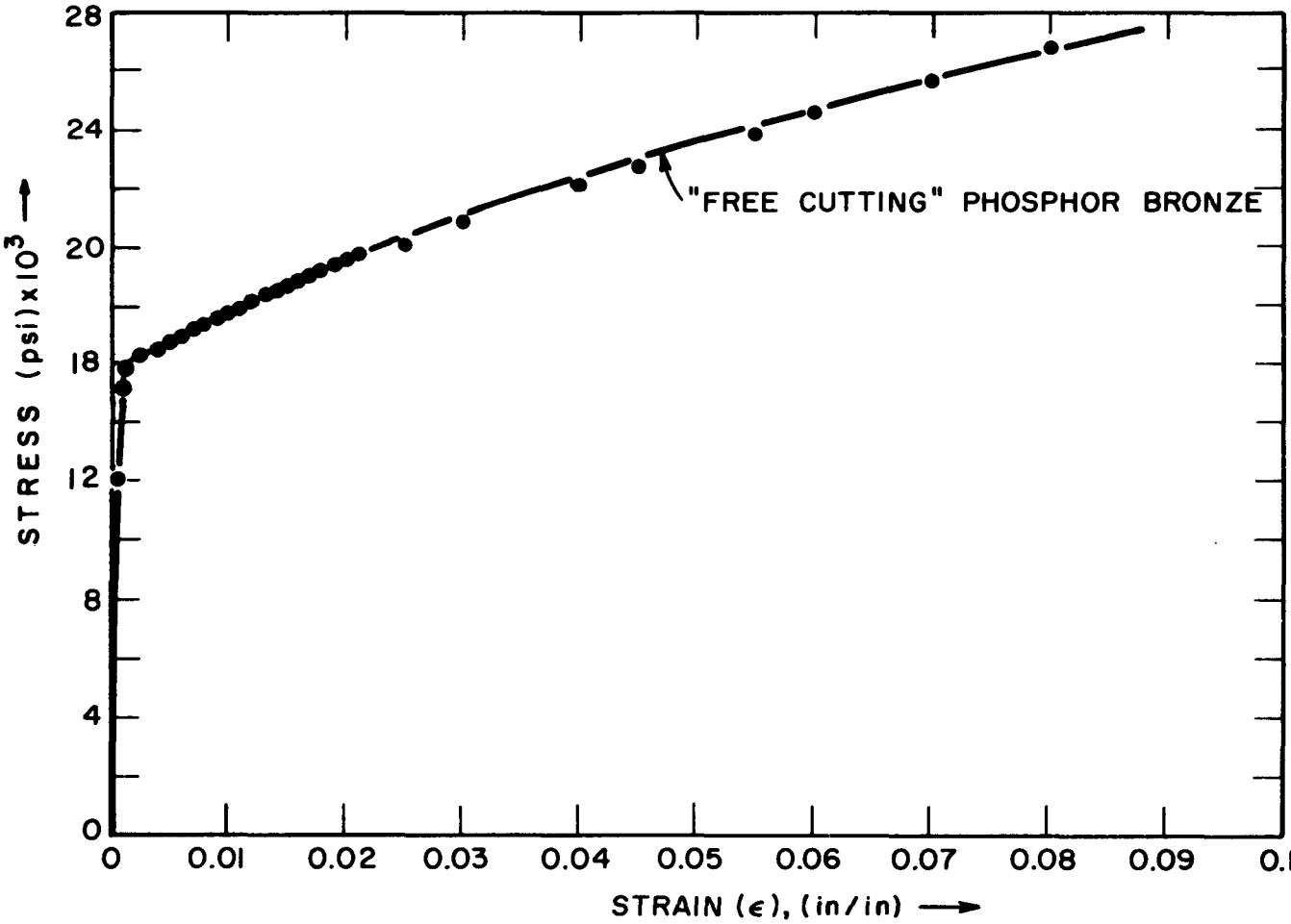

FIG.3.2.11. STRESS vs STRAIN FOR PHOSPHOR BRONZE STRIP, ANNEALING TEMPERATURE AT 712 °C

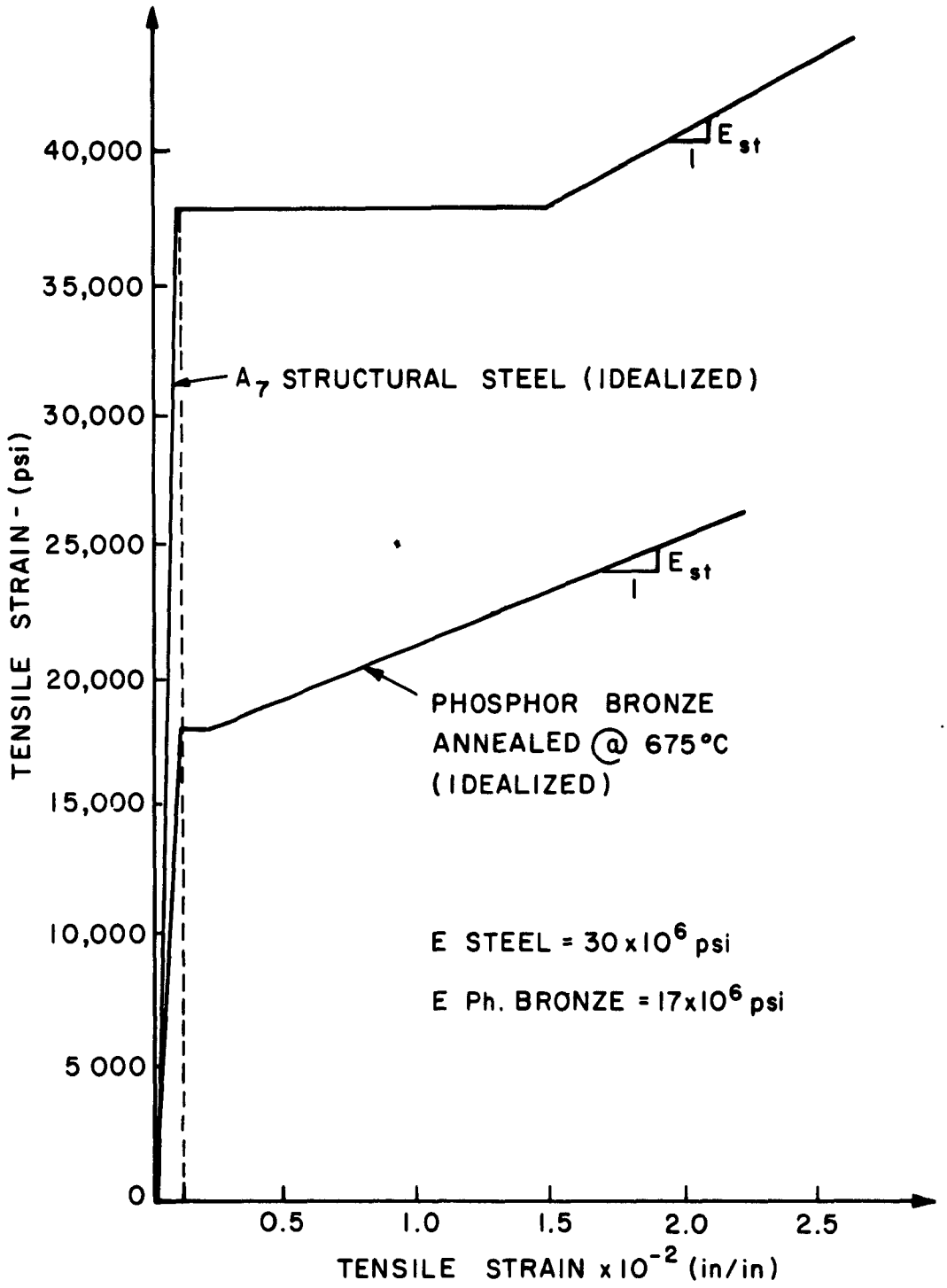

FIG. 3.2.12 COMPARATIVE STRESS-STRAIN CURVES FOR STRUCTURAL STEEL AND PHOSPHOR BRONZE

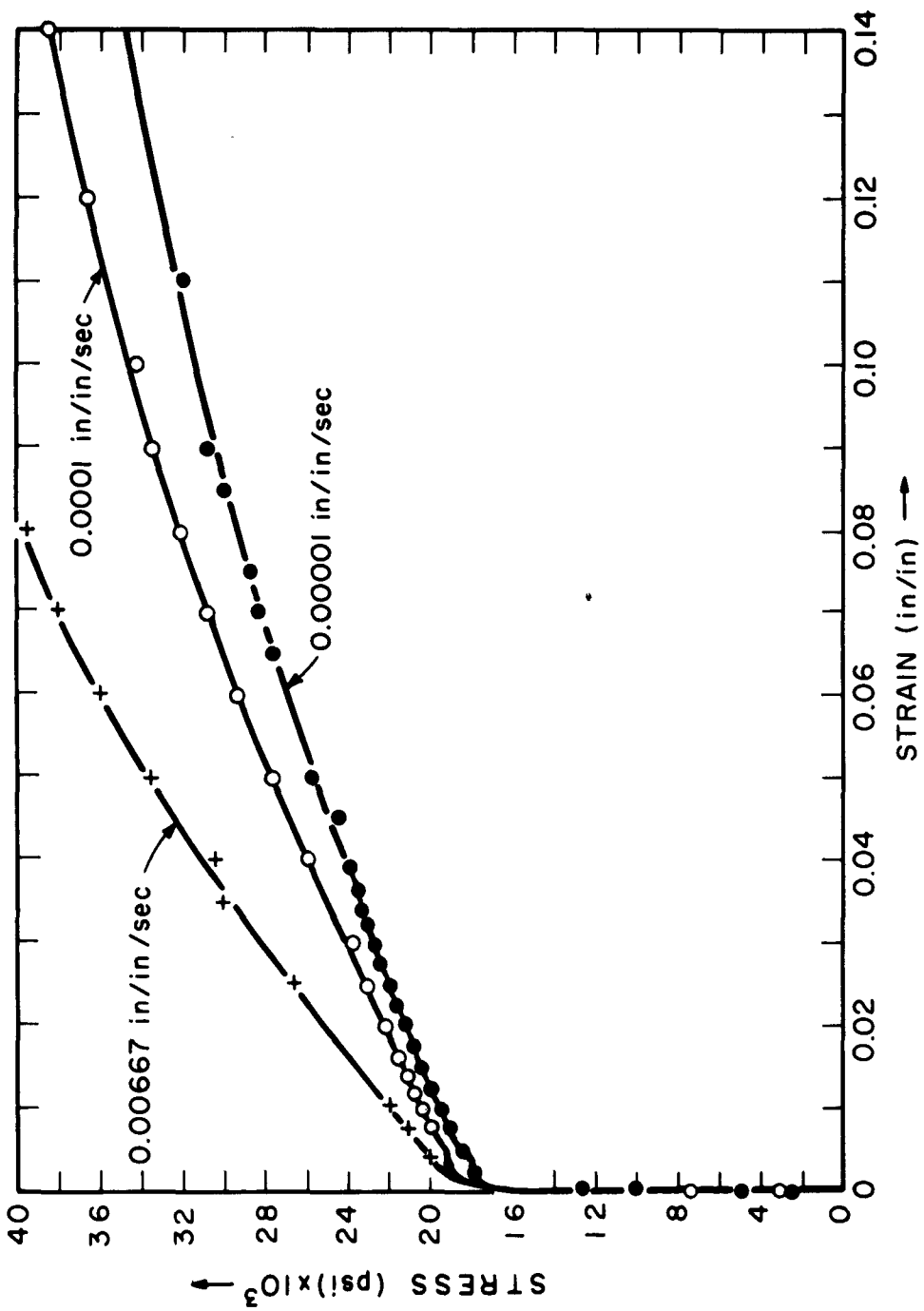

FIG. 3.2.13 EFFECT OF RAPID STRAINING OF PHOSPHOR BRONZE STRIPS ANNEALED AT 675 °C FOR 30 MIN.

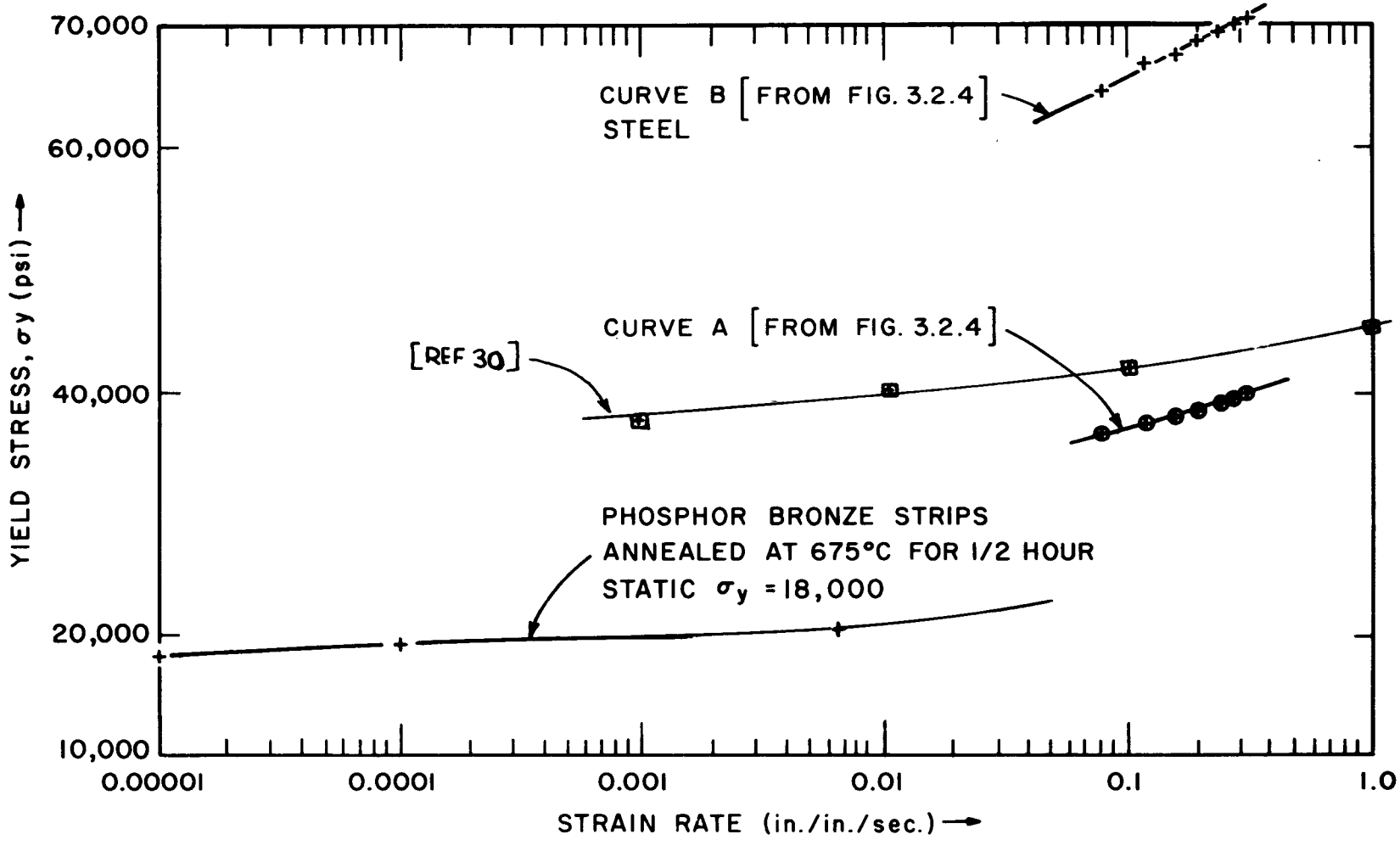

FIG.3.2.14 EFFECT OF STRAIN RATE ON THE YIELD STRESS OF PHOSPHOR BRONZE AND STRUCTURAL STEEL

is observed that most of the plastics are characterised by a non-linear stress-strain relationship throughout the entire range of loading, low initial modulus of elasticity, lack of ductility and a marked degree of creep. Most plastics, in general, provide a considerable contrast to the mechanical properties of structural steel. However, unlike other plastics, ethyl cellulose, a thermo-plastic material, has a remarkably similar stress-strain curve to that of structural steel (ASTM A7).

3.2.3.1 Properties of Ethyl Cellulose.

Ethyl Cellulose, an ethyl ether of cellulose, is a thermo-plastic material. Its chief characteristics are high impact strength, toughness and a considerable degree of ductility. Fluctuations in its dimensions due to normal changes in temperatures and effect of humidity are quite small. In spite of its application in various electric appliances, radio housings, tooth-brushes and other industries, its manufacturers are relatively very few.

Tests on standard specimens of ethyl cellulose subjected to standard rates of strain gave the average stress-strain curve, as shown in fig. 3.2.15. On idealising such a stress-strain relationship, the salient points are:

Modulus of Elasticity	=	0.184×10^6 psi
Yield Stress	=	4.15×10^3 psi
Strain at Yield Stress	=	0.0225 in/in
Ultimate Strain	=	0.172 in/in

The specific gravity of ethyl cellulose is 1.10. A comparison of the idealized stress-strain curve of ethyl cellulose is made to that of steel in fig. 3.2.16.

3.3 MODEL MANUFACTURE

The choice of the materials from which the model is made according to similitude requirements is the most

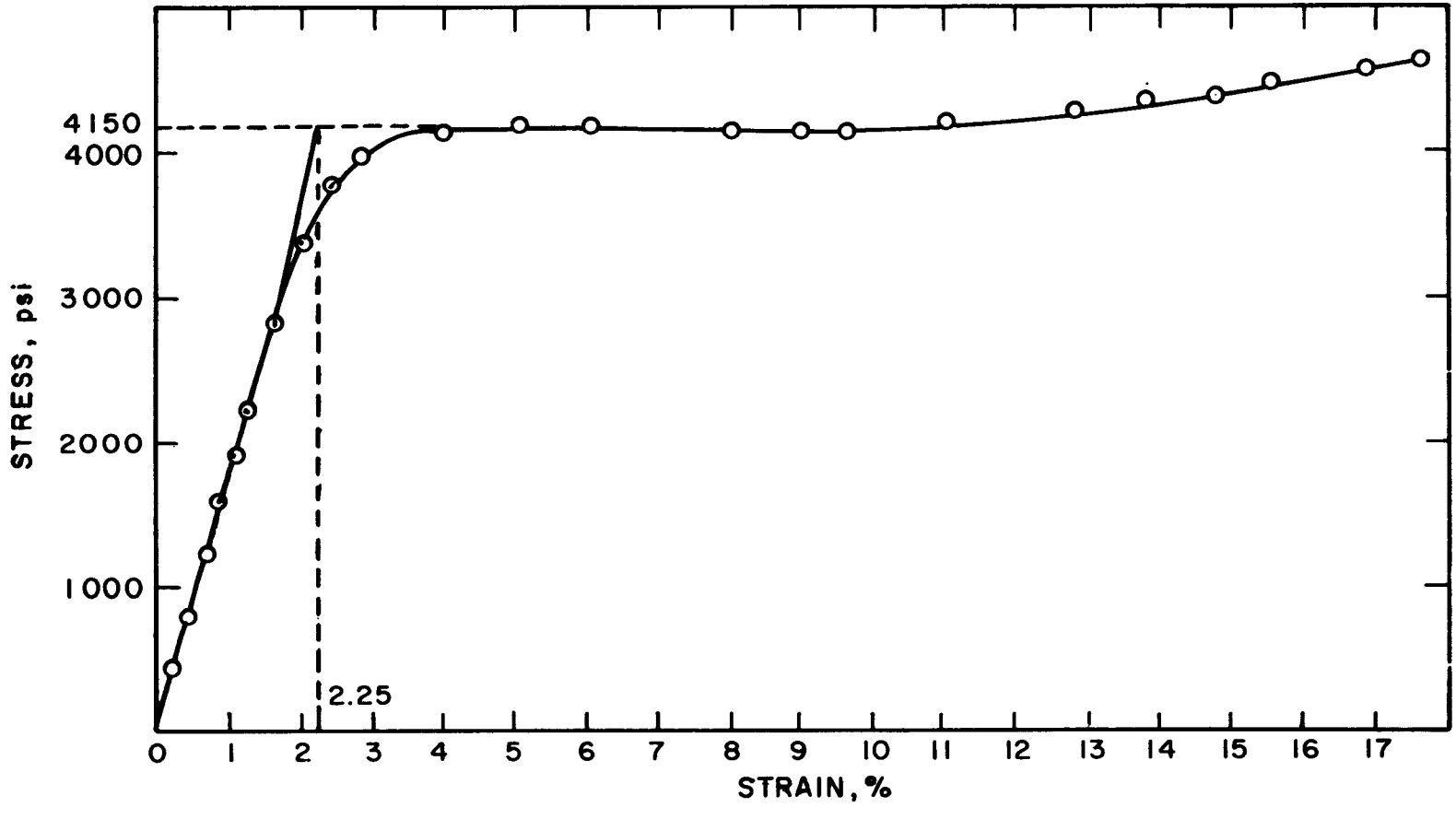

FIG. 3.2.15 STRESS - STRAIN CURVE OF ETHYL CELLULOSE

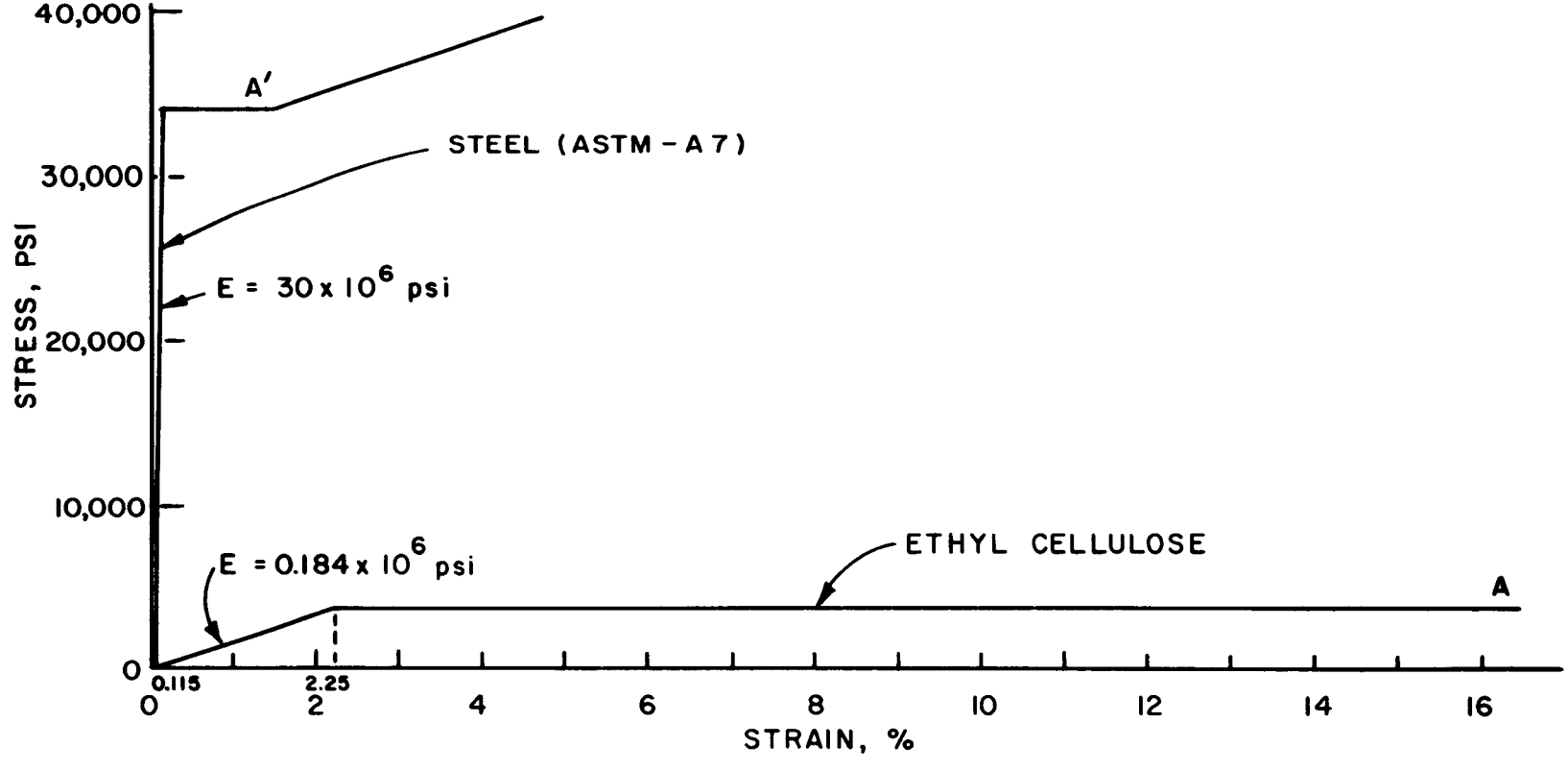

FIG. 3.2.16 COMPARISON OF STRESS-STRAIN CURVES OF STRUCTURAL STEEL AND ETHYL CELLULOSE.

important step in the structural model analysis. The second most important aspect is the actual process of making the model. During this step many considerations must be evaluated before an efficient modeling technique can evolve. In this section some of the considerations on which the decisions of the analyst depend will be examined. Also the details of the modeling technique for steel structures will be described.

3.3.1 Some Considerations in Model Making. When small scale models are to be built the accuracy of the dimensions must be very high. The difficulty of achieving this increases as the scale of length decreases. At some point it may become very hard or even impossible to get good results from a small scale model. The accuracy to be achieved in the model also depends on the results required from the model and the time and funds available for the model study. If the model is to be used to predict the ultimate behavior of the prototype, then boundary conditions and other details, such as joints, also become important. If time and money were not limited then the model could be refined to any degree with increasing chances of giving more accurate results provided of course that similitude requirements are satisfied.

It may also be possible to use many alternate materials for the model especially in cases where elastic behavior is to be considered. Some materials are much easier to work with than others so a careful consideration of all available methods may save considerable amount of time and effort. Since in general model studies are on the high side with respect to time consumption, any effort on the part of the analyst to minimize this is highly advantageous.

3.3.2 Specific Examples of Modeling. We shall consider here some examples of modeling of steel structures in which plastic behavior during the dynamic response is of primary concern. Tests on actual full scale structures and structural elements afford an excellent opportunity for comparisons

with extrapolations from model studies. So far little has been done in the study of the dynamic response of actual full scale structures or structural elements although some model studies have been reported.[26] The case of static loads has received more attention and a host of data from actual full scale structures and structural elements in steel have been reported by many investigators especially the Lehigh University group.[22,25,37,41,46] Before a modeling technique can be generalized as an efficient solution to a class of structural problems, correlation tests must be made to prove its accuracy in predicting the behavior of the prototype. Comparisons are thus made with actual tests on prototype, not with analytical solutions, since the aim of the model study is to bypass these. At any rate the behavior of the real structure will not be the same as the analytical solution would indicate and will be closer to the model prediction depending on the relative accuracy of the basic assumptions made in each case.

3.3.2.1 Phosphor Bronze Models. A decisive advantage of using this material is its ease of handling. Machining operations, fitting and especially jointing are easily performed by the inexperienced analyst. It should be remembered, however, that a modeling technique is by nature specific in that one attempts to solve the immediate problems of the structure to be modeled. In some cases the method may be easily applied. To other problems it may not. Keeping this in mind then, we realize that the phosphor bronze modeling technique of making models of steel structures is not claimed to be the best nor the most general.

3.3.2.1.1 Machining the Shapes. Assuming that most structures will be designed from existing rolled sections and not be predominantly built up, although occasion may require some such sections, we shall try to duplicate through machining the rolled sections in smaller scales. For convenience one section is chosen for duplication of some of the Lehigh tests. The section used mostly there

is the 8WF40 which is shown in fig. 3.3.1(a). A scale of 1:15 is chosen as the basis of being the smallest practical scale on which the technique would be evolved and also a scale in which the joints and boundary conditions could be duplicated faithfully. In order to facilitate machining and to cut down on the cost the exact dimensions to 1:15 scale were modified as shown in fig. 3.3.1(c), assuming that corrections could be applied to the results to overcome the geometric discrepencies. Machining of the sections was done in 30 inch pieces from ½ inch square stock by the Chicago firm of Milled Shapes Inc. The tolerances are less than ±.005" on any dimension. Machining always tends to warp thin sections and the machined phosphor bronze pieces as received showed some signs of warpage but this was not excessive. Another consideration in the choice of the length scale of 1:15 was the maximum capacity of the dynamic loading machine of 4 kips and the size of portal frame which could be handled by the machine dimensions with comparative ease.

3.3.2.1.2 Annealing of Phosphor Bronze. The annealing of the machined shapes is carried out before the components are assembled. The optimum annealing temperature of this material is found to be 675°C for one half hour, from the stress-strain curves on thin strips. Since the annealing temperature and the time of annealing strongly influence the yield point stress in phosphor bronze, it is necessary to find a silver solder with a lower flowing temperature than 675°C to prevent double annealing upon assembly of the parts. During annealing there may be variations in the temperature and this must be guarded against since only a short time interval is used.

3.3.2.1.3 Silver Soldering. The biggest single advantage of using phosphor bronze in model making is the ease with which strong accurate jointscan be made. It is this advantage that prompted the use of this material in the small scale modeling of steel structures although

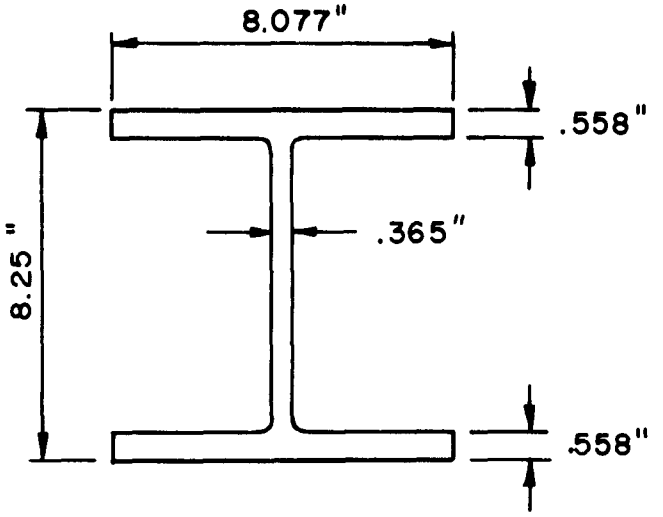

(a) 8 WF 40 (NOMINAL)

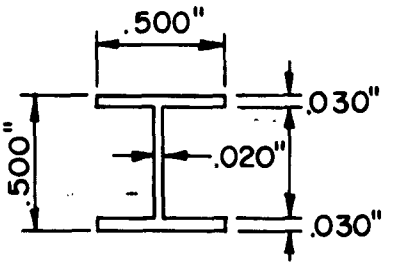

(c) APPROXIMATE SECTION
(PHOSPHOR BRONZE)

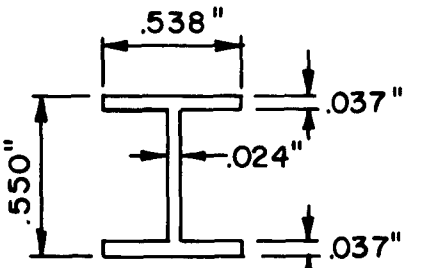

(b) 8 WF 40 (1/15 SCALE)

FIG. 3.3.1 THE SECTIONS OF THE PROTOTYPE AND MODEL STRUCTURES INVESTIGATED.

as seen from the stress-strain curves the compatibility of the two materials does not extend over the whole strain range. If the method proves satisfactory then small scale model studies for shock tube tests where size is an important consideration could be made of structures in the 1/15 - 1/30 scale range very easily. The problems presented by welding of steel sections at these scales are beyond the capabilities of the average models laboratory. Special equipment must be available which may hinder the making of small scale models of welded steel structures. In fact is is highly improbable that a normal size weld as used in steel structures could be modeled at such small scales.

As shown by fig. 3.3.2 the process of silver soldering is extremely simple with a minimum of equipment necessary. All that is required is a gas torch, silver solder wire and a borax flux. The technique can be very easily adopted by technicians and the joints can be done with excellent control as to thickness of weld. The accuracy to be maintained in silver soldering is high even for a scale of 1:15 as shown by fig. 3.3.3 where the stiffeners which go into the wide flange beams are shown before its assembly and below it is a finished beam ready for instrumentation and subsequent testing.

It is important in the assembly to make the joints as quickly as possible so that overheating of the member in the vicinity of the weld will be avoided and the material will not be weakened. The annealing temperature of the models is 675°C and the flowing temperature of the silver solder used was 628°C so that we see that if excessive overheating occurs it could affect the strength of the model at the local point of soldering.

3.3.2.2 Fabrication of Ethyl Cellulose Models.

It is a simple process to bond ethyl cellulose to itself. The following considerations are necessary for a good bond:

i) Design and Fabrication
ii) Selection of Adhesive
iii) Application and Assembly Technique

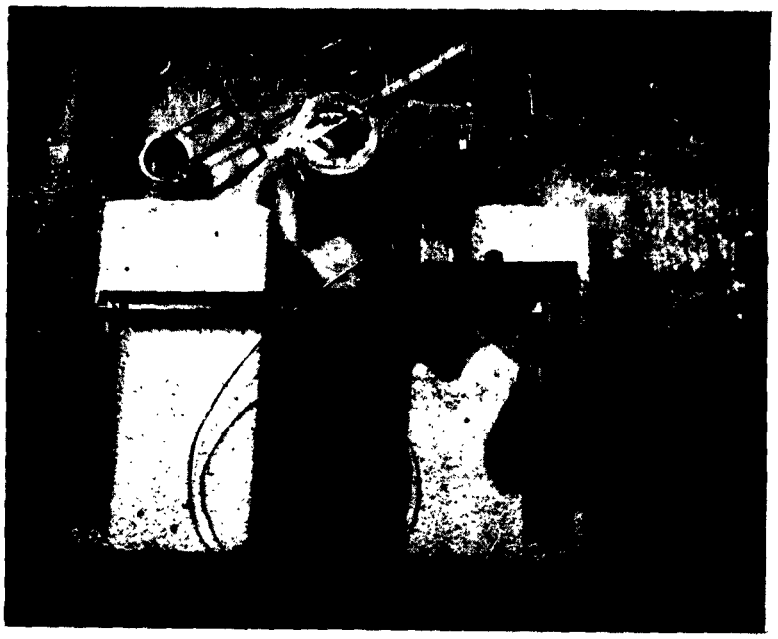

FIG. 3.3.2 EQUIPMENT NEEDED FOR SILVER SOLDERING

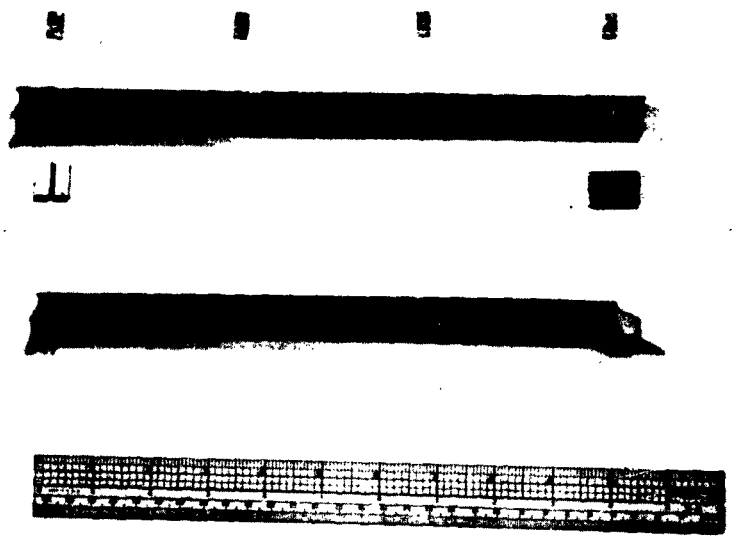

FIG. 3.3.3 PARTS WHICH GO INTO THE MAKING OF A SIMPLE WIDE FLANGE BEAM SCALE 1/15.

i) Design and Fabrication: Strength and ductility are important factors in the design of joints. The tensile strength of adhesive bond is slightly lower than that of ethyl cellulose. Therefore, it is necessary to increase the bonding area in order that the joint will be as strong as the molded part of the material. This can be done either by thickening the wall section around a butt joint or by using a special type of joint. Surface contamination or poor contact of mating surfaces should be avoided in order to obtain good bond.

ii) Selection of Adhesive: There are three available adhesives especially suited for Ethyl Cellulose. They are known commercially as P-34, P-34A and P-35*. These are all the solvents for the material. The first two adhesives have the composition of Alcohol and Toulene in different proportions. The last one is essentially Ethylene Dichloride.

iii) Application and Assembly Techniques: Stronger bonds result when the adhesive is applied to both pieces of an assembly rather than to only one of the mating surfaces. This can be explained by considering that, when only one piece is coated, the solvent first softens the coated plastic and then begins to thicken before the non-coated piece is pressed against it. Thus the solvent does not have as great a chance to soften the second piece and usually a weaker bond results.

The adhesive itself may be applied by various methods, such as saturated felt pad, flow gun, dripping or brush. High vapor concentrations of the adhesives should not be inhaled. Good ventilation at the place of fabrication is desirable, therefore.

3.4 TESTING APPARATUS AND INSTRUMENTATION

To test the small scale models made from phosphor bronze

---

* Dealer - Dow Chemical Co., Midland, Michigan.

special loading and supporting devices are needed. The static tests are performed in the Models Laboratory of the Civil Engineering Department of M.I.T. where a special lever mechanism is available. The dynamic tests are performed with the aid of the impulsive loading machine of the Soil Mechanics Division of the same department. A description of this apparatus and the instrumentation used in the model tests is given below.

3.4.1 Loading Frame for Static Tests. The loading frame for carrying out static tests shown in fig. 3.4.1 has a maximum capacity of 5 kips concentrated load. At the lower bound any small load of a few pounds only could be applied since the friction in the system was found to be very small. The frame is basically a beam pivoted at one end through a roller bearing passing through its center of gravity as shown in the detail of fig. 3.4.1. The load is applied in increments at the furthest extremity from the fulcrum and the model is positioned at any point in between the fulcrum and the point of load application. By varying the position of the model from the fulcrum a variety of multiplication factors can be achieved for the applied load. As point B in fig. 3.4.1 approaches A the multiplication factor increases with a practical maximum of about 10 for this setup.

Since most of the structures to be tested are of a planar nature a rectangular box made of aluminum plates is used to support the small scale models in one plane. Fig. 3.4.2 shows the dimensions of the box and the method of supporting of portal frames which are tested to ultimate failure. Thin brass wires of 1/16" diameter are used for lateral supports of beams and frames to allow the model to reach its full plastic moment. It should be noted that the prototype structures which were modeled are also supported laterally but of course the details vary in model and prototype since size limitations do not allow in many cases the reproduction of details in exactly the same way. In

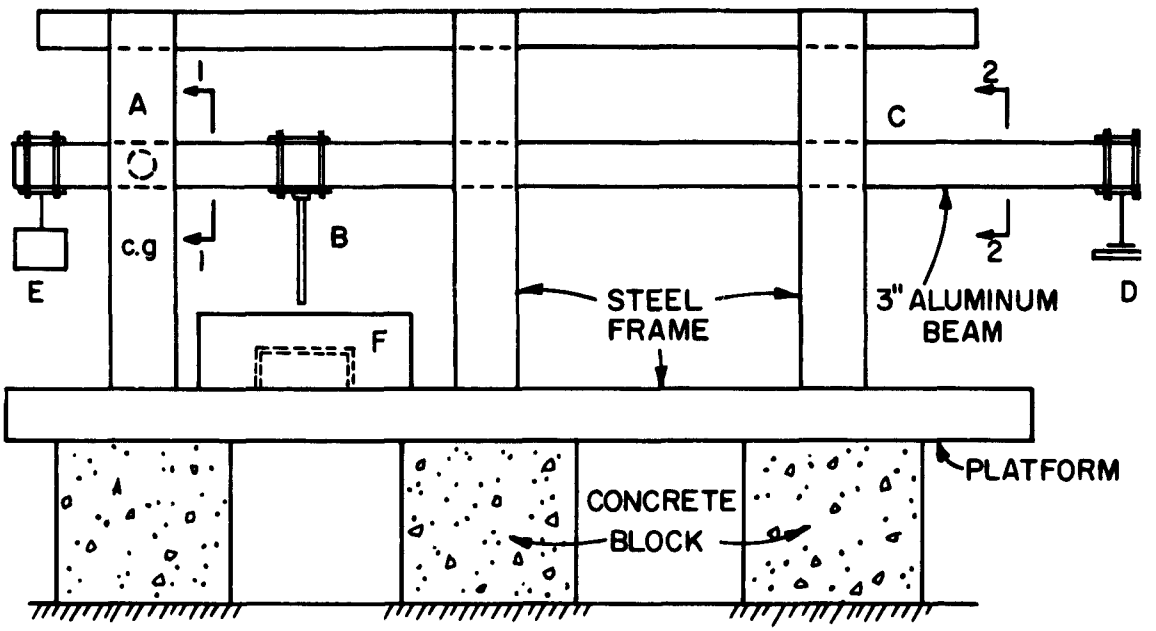

A. ROLLER BEARING PIVOT THROUGH WEB OF BEAM (SECTION 1-1).

B. POINT OF LOAD APPLICATION TO MODEL.

C. ROLLER BEARING GUIDES (SECTION 2-2).

D. POINT OF LOAD APPLICATION AT END OF BEAM.

E. COUNTER BALANCING WEIGHTS CAUSING c.g. PASS THROUGH POINT A

F. ALUMINUM SUPPORTING BOX FOR MODELS

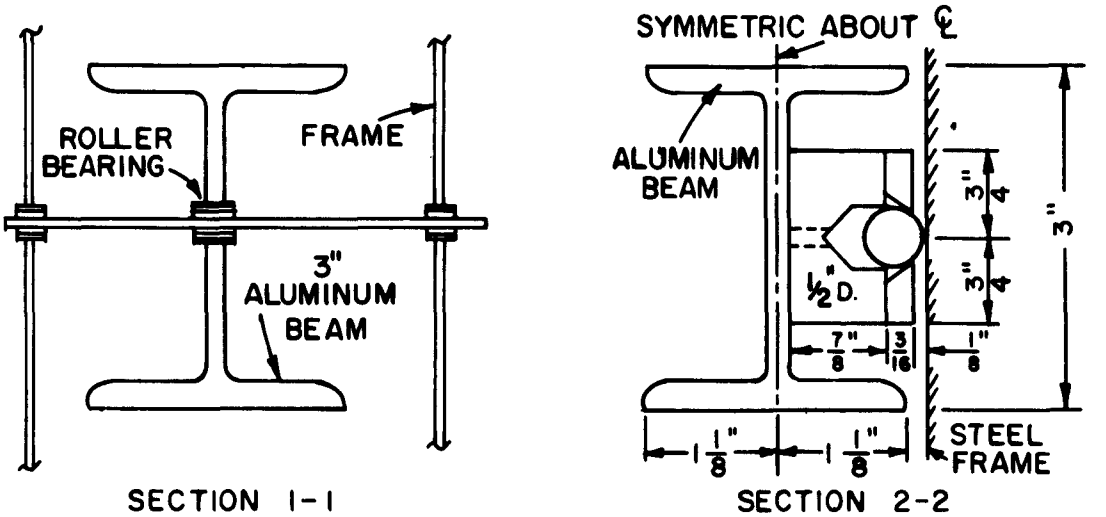

FIG. 3.4.1 SCHEMATIC DRAWING OF STATIC LOADING FRAME.

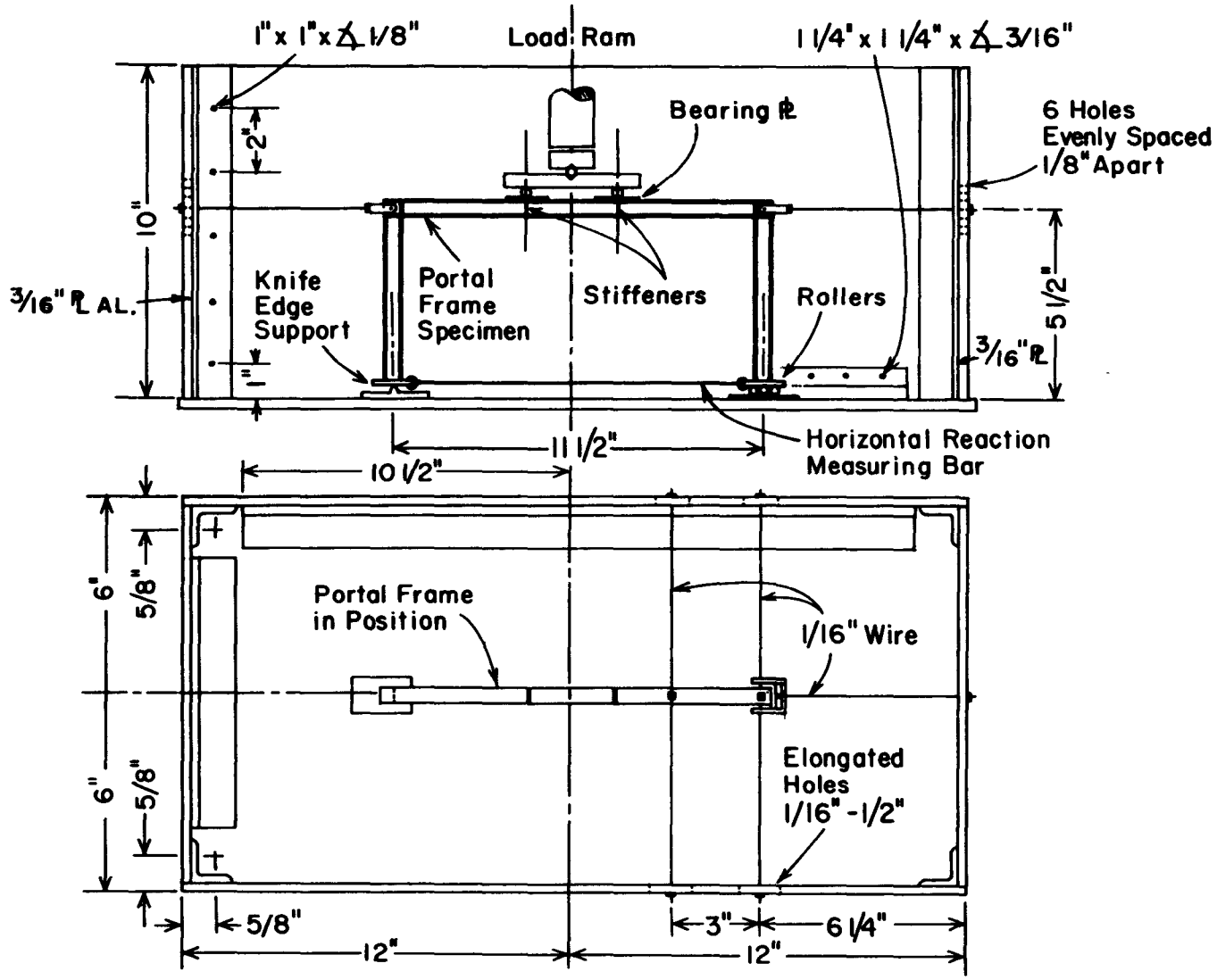

FIG. 3.4.2 DRAWING SHOWING THE DETAILS OF THE SUPPORTING BOX FOR THE SMALL SCALE MODELS

Fig. 3.4.3 a simply supported model beam is being tested in the above mentioned box. Note the lateral supports given by the brass wires.

3.4.1.1 Method of Load Application on Models. Loads on beams and frames were applied through small brass bearing plates placed on the top flange. At points of load application stiffeners were provided. Fig. 3.4.3 shows a close up of the loading and supporting arrangement for a simply supported beam. The concentrated single load of the loading frame is distributed to two or more points by small stiff beams as shown in figs. 3.4.4 and 3.4.5. The method of load application is the same for some of the prototype tests. However, in cases where the load was applied through the web of the beam an exact reproduction on the model was not attempted and all loads are applied through bearing plates on the top flange. Since the load increments are applied by hand at the end of the beam the load variation with time is a step variation rather than a smooth one. Unloading of the specimen during testing is avoided as much as possible especially after the model passes its elastic limit.

3.4.1.2 Deflection Measurements. All deflection measurements for the static tests are taken with Ames dial gages with an accuracy of 0.001 inch. Usually the mid-span deflection is of particular interest in the test but in some cases curvatures are computed from deflection measurements. Figs. 3.47 and 3.48 show the mode of deflection measurements for different model tests. Since the scale of these tests is 1:15 the deflection readings on the model are 1/15 of those of the prototype. The gages used are of sufficient accuracy to allow good extrapolation to the prototype.

3.4.1.3 Strain Measurements. Strain measurements are made by means of SR-4 foil type strain gages with an epoxy backing. Readings are taken with a Baldwin-Lima-Hamilton Strain Indicator. A typical test setup is shown in Fig. 3.4.6.

FIG. 3.4.3 CLOSEUP OF FRAME SHOWING MODEL BEAM READY FOR TEST

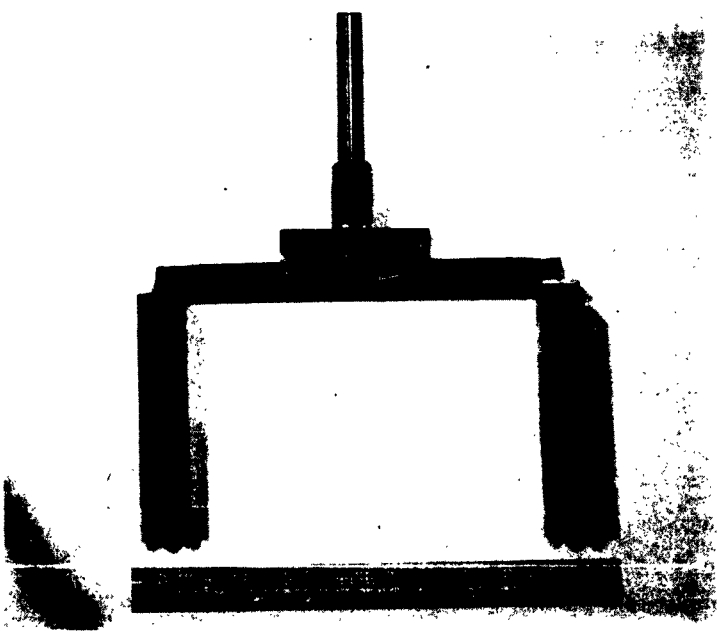

FIG. 3.4.4 CLOSEUP VIEW OF THE LOAD APPLICATION AND THE SUPPORT OF A SIMPLY SUPPORTED MODEL BEAM

FIG. 3.4.5 PORTAL FRAME IN POSITION TO BE TESTED. NOTE THE LOAD APPLICATION AND SUPPORT DETAILS.

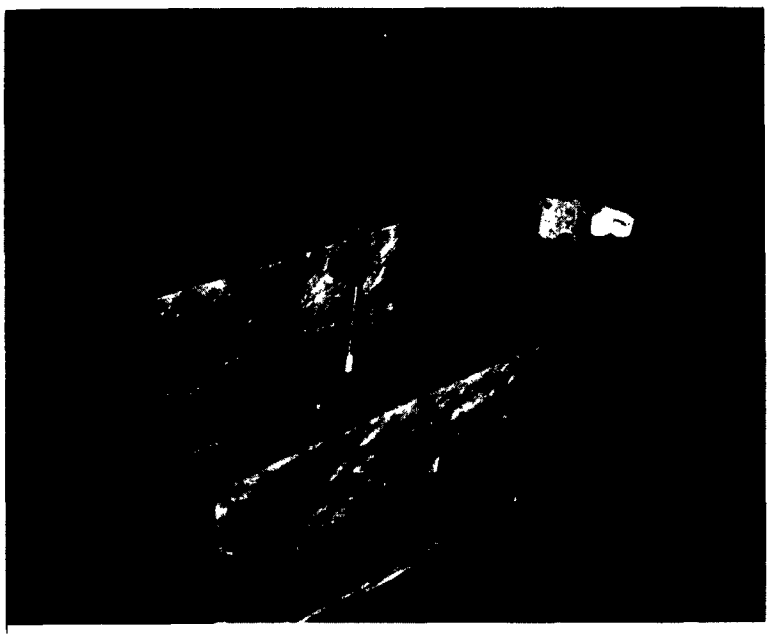

FIG. 3.4.6 CLOSEUP OF SUPPORTING BOX SHOWING THE LATERAL SUPPORTS FOR A PORTAL FRAME, THE METHOD OF LOAD APPLICATION AND THE STRAIN INDICATOR.

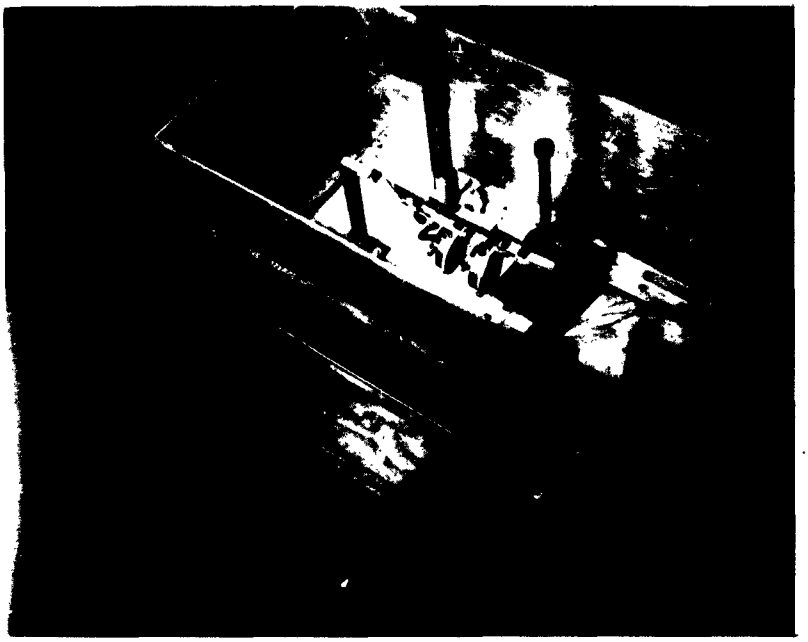

FIG. 3.4.7 CLOSEUP OF LOADING FRAME SHOWING A PORTAL FRAME READY FOR TEST. NOTE LATERAL SUPPORTS.

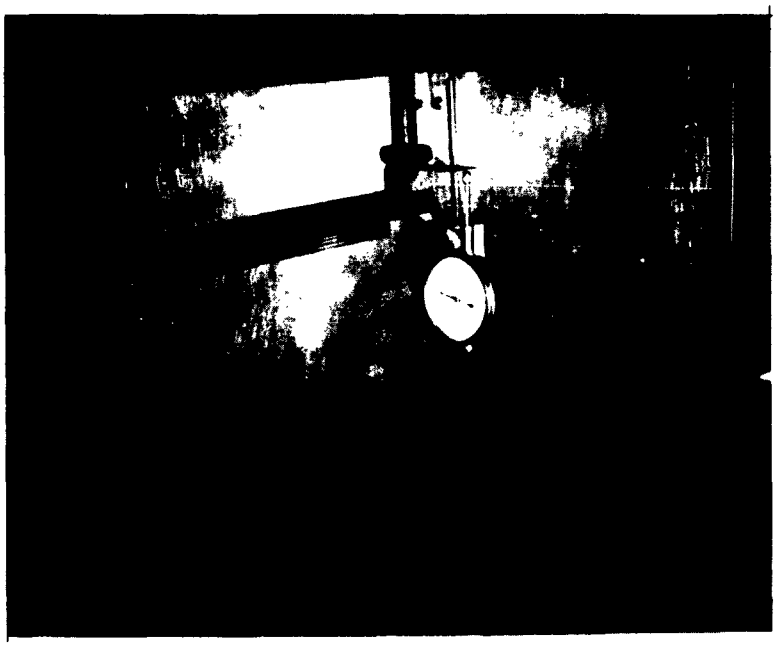

FIG. 3.4.8 DEFLECTION MEASUREMENTS OF JOINT TEST WITH AN AMES DIAL.

The foil gages used varied in length from 3/16" to 1" and are bonded with EPY-150 cement according to the recommended procedure of the manufacturer. This cement is chosen for its relatively fast cure. However, from observations it appears that some of the gages began to creep at strains much less than the maximum range of about 1%. This is thought to be caused by failure of the bond between the gage and the model material and measurements on such gages should be taken only after the creeping has ceased. Whereas the metal material responds quickly to an increment of stress, the same is not true of the epoxy which is a thermo setting plastic. When enough time is allowed for creep to occur the strain measurements give better results.

The gages are temperature compensated for 1018 Steel but since these are used with phosphor bronze with a different coefficient of expansion a dummy gage is used in all the tests.

3.4.2 The Dynamic Loading Machine. The machine used to test the model structures is one built for high speed triaxial tests of soil samples. Fig. 3.4.9 shows a drawing of the machine and Fig. 3.4.10 shows its mode of operation in a schematic form. Since the system had no feedback control on the load rate, the obtained load time curve is the result of interaction between the specimens and the machine and as such the applied load is an impact rather than a predetermined impulse.

Loads up to 5 kips are obtained with this machine and load rise times ranging from 3 milliseconds up.

3.4.2.1 Support Frame. A simple braced frame was built to hold the specimens to be tested. Fig. 3.4.11 shows the frame with a model phosphor bronze portal frame ready to be tested. The support frame is clamped to the platform of the machine during the test.

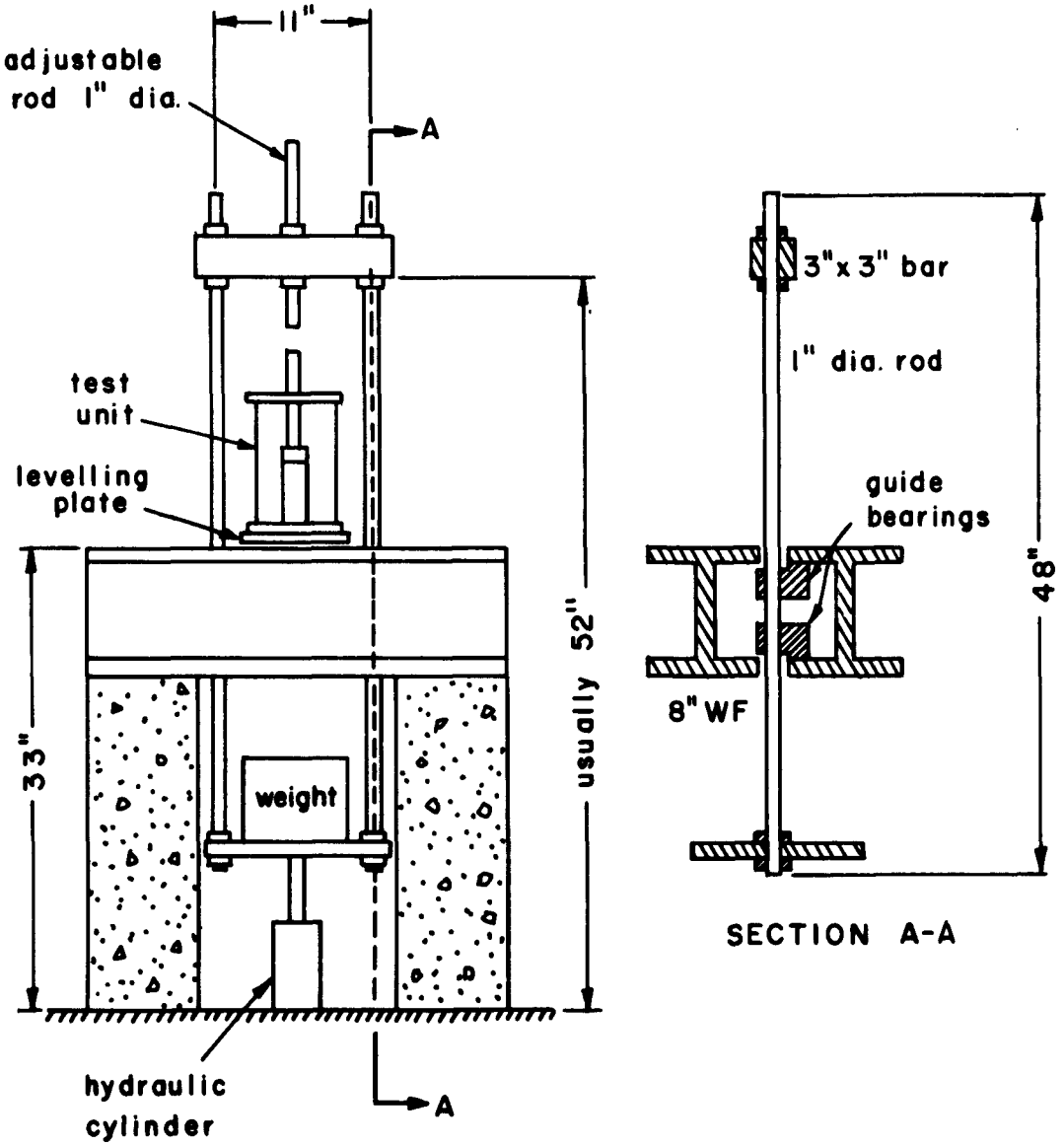

FIG. 3.4.9 THE DYNAMIC LOADING MACHINE USED IN MODEL TESTING.

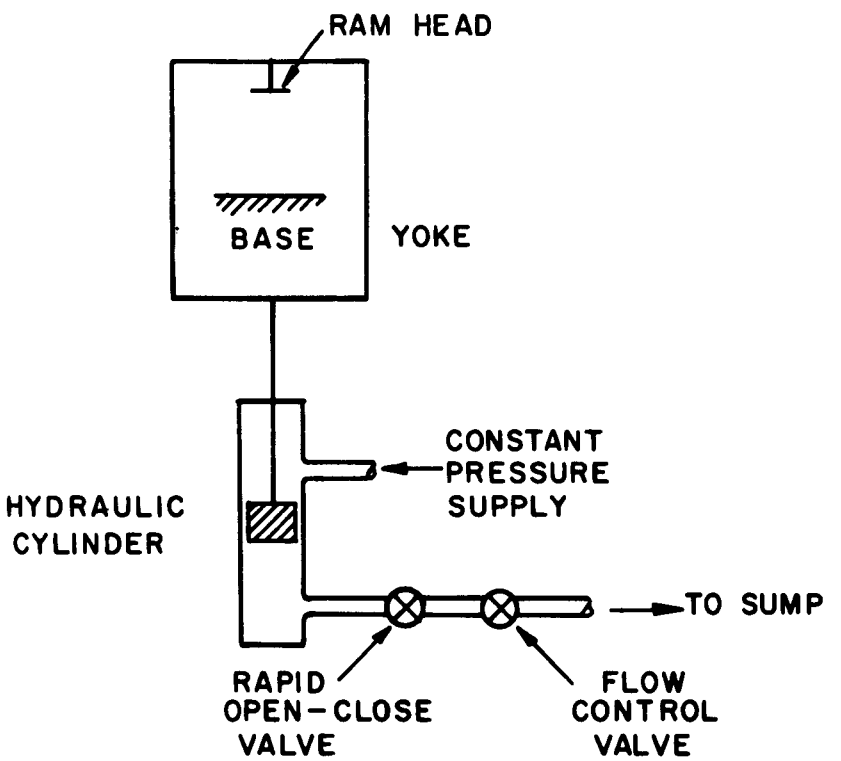

FIG. 3.4.10 BASIC UNITS OF MODEL LOADING MACHINE

3.4.2.2 The Load Cell. The load cell is attached to the ram and the load applied to the model through it. It consisted of a ½ inch diameter aluminum shaft, 2 inches long onto which are bonded two strain gages (Baldwin-Lima-Hamilton Type C7). The gages are laid along diametrically opposed generators of the cylindrical shaft and wired to form two opposite arms of a Wheatstone bridge. The other two arms of the bridge consisted of two dummy gages attached inside an unloaded aluminum box. This system caused the portions of strains due to bending to cancel each other out and the bridge output voltage to be proportional to the axial load in the load cell. The circuit is excited by a 22½ volt battery and the output signal displayed on a cathode ray oscillograph.

3.4.2.3 Recording Equipment. The oscillograph as shown in Fig. 3.4.12 is a Tektronics Type 502 which had a calibrated time sweep and could be triggered by the load signal itself. Permanent records are obtained by using Dumont Type 287 oscillograph record cameras operating with Polaroid-land film.

A Twin Vise Model 60-1300 Sanborn Recorder is used during calibration of the load cell.

The load cell is calibrated in a standard beam type testing machine, the output signal being recorded on a Sanborn unit. The signal due to a known load is compared to the signal due to a fixed unbalance in a Wheatstone bridge. After each test the signal due to this fixed unbalance would be recorded giving a load scale for the data obtained.

The deflections are measured with a Linear Variable Differential Transformer (L.V.D.T), the signal is converted to D.C. and displayed on the Oscillograph. Thus two signals are recorded with time on the same picture. For any time during the response the load deflection relation would be obtained.

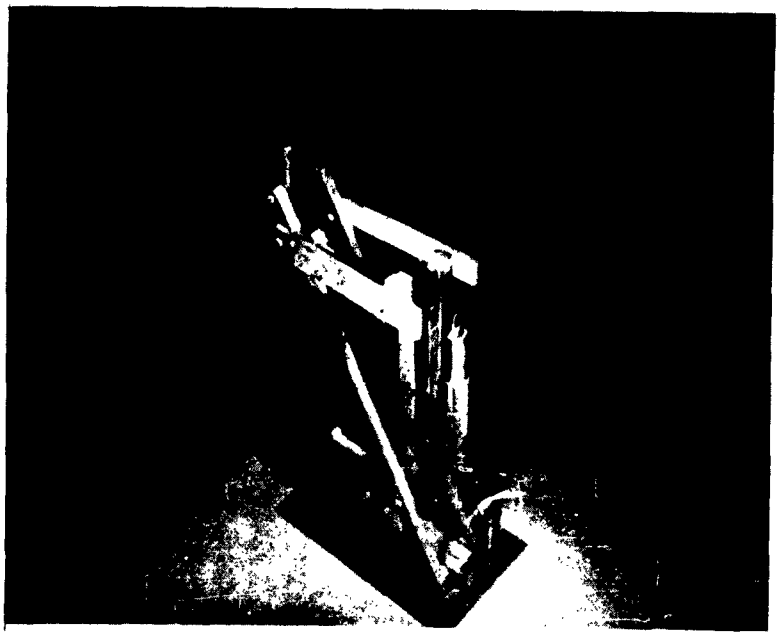

FIG. 3.4.11 SUPPORTING FRAME FOR MODEL FRAMES. NOTE THE L.V.D.T. FOR THE DEFLECTION MEASUREMENTS.

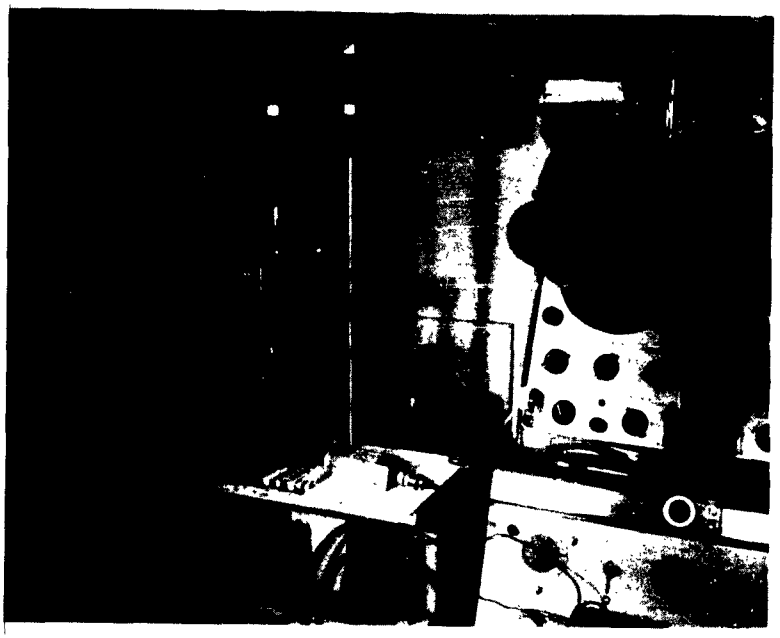

FIG. 3.4.12 SETUP SHOWING THE DYNAMIC LOADING MACHINE AT THE LEFT AND INSTRUMENTATION.

The L.V.D.T. is calibrated with an Ames dial and a plot of signal v.s. deflection is obtained for every test. From this plot the deflections for the response signal recorded by the camera could be obtained.

CHAPTER 4

PHOSPHOR BRONZE MODEL STUDIES OF WELDED STEEL STRUCTURES

Tests were made on wide flange beams, portal frames, and connections for the static loads, and portal frames in the case of dynamic loads. In all these tests a scale of 1:15 was used for convenience and the section used closely approximates an 8WF40 rolled section. In the static tests comparisons are made between the model predictions and the actual prototype tests but in the dynamic case no prototype results were available.

4.1 STATIC TESTS ON MODELS BEYOND THE ELASTIC LIMIT

4.1.1 Wide Flange Beams. A series of seven tests were performed on wide flange beams with simple supports and fixed ends from which load deflection and moment curvature relations were obtained. The test results of the model beams are summarized in table 4.1. Using the full scale results of tests performed at Lehigh University the predicted behavior of the prototype from the model test is compared.

4.1.1.1 Prototype Tests. The simply supported wide flange beams are of two different types. The difference is in both length and mode of loading as shown in Figs. 4.1.1 and 4.1.2.

The "pilot" tests were made on an 8WF40 beam of 12-ft. span, simply supported and loaded at the third points. The load was applied to the beam through bearing blocks resting on the top flange and the web was stiffened under the load with 3/8 in. plates welded perpendicular to the web. From this test it was observed that a non-linear strain variation exists at the mid-span after the elastic limit was exceeded. This caused the neutral

TABLE 4.1 SUMMARY OF BEAM TESTS

Model Beam	Length		Prototype Section	Type of Load	Boundary Conditions	Total Ultimate Load From Prototype Test (Kips)	Total Predicted Model Ultimate Load (Kips)
	Model	Prototype					
B1	9.6"	12'-0"	8WF40	2 Concentrated Loads at L/3	Simply Supported	52	54
B2	11.2"	14'-0"	8WF40	2 Concentrated Loads at L/3	Simply Supported	50.4*	46
B3	11.2"	14'-0"	8WF40	2 Concentrated Loads at L/3	Simply Supported	50.4	50
B4	11.2"	14'-0"	8WF40	2 Concentrated Loads at L/3	Fixed Ended	93**	92
B5	11.2"	14'-0"	8WF40	2 Concentrated Loads at L/3	Fixed Ended	93	91
B1A	9.6"	12'-0"	8WF40	2 Concentrated Loads at L/3	Simply Supported	52	57
B1B	9.6"	12'-0"	8WF40	2 Concentrated Loads at L/3	Simply Supported	52	55

* This is the value for the as delivered beam. The value for the annealed beam is 49 kips.

** This is the value for support condition (a) as shown in Fig. (4.1.12). The value for support condition (b) is 108 kips.

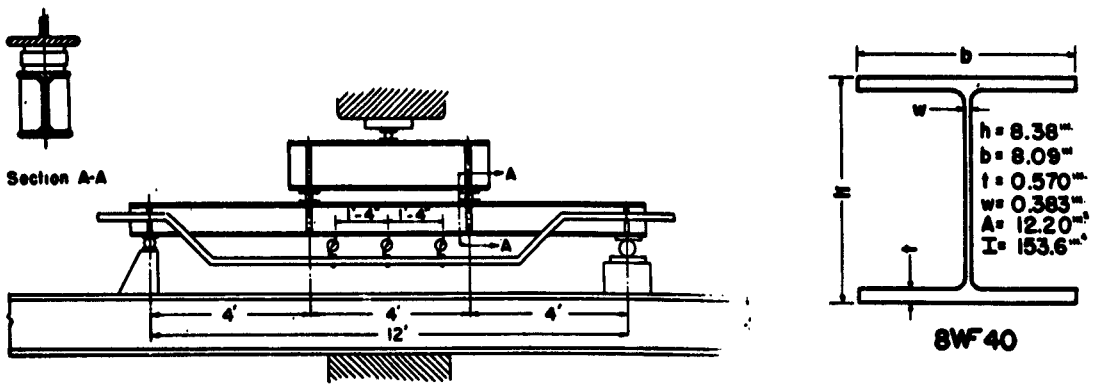

FIG. 4.1.1 PROTOTYPE PILOT TEST OF 8WF40 SIMPLY SUPPORTED BEAMS LOADED ON THE FLANGE AS SHOWN PERFORMED AT LEHIGH (REF. 25).

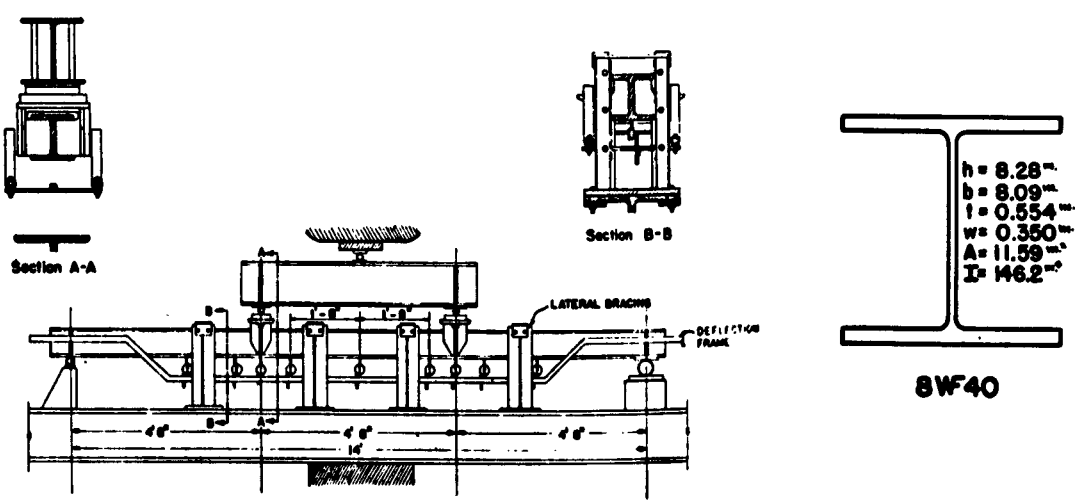

FIG. 4.1.2 PROTOTYPE 8WF40 SIMPLY SUPPORTED BEAMS WITH LOADS APPLIED THROUGH THE WEB AS SHOWN ABOVE TESTED AT LEHIGH (REF. 25).

axis to move towards the tension flange but at higher per cent strains it moved back towards the centroidal axis. The pilot test developed less plastic strength than that calculated.

The "regular" tests were made on 8WF40 beams of 14-ft. span simply supported and loaded at the third points. One test was done on the beam in the as delivered condition and the other was stress-relief annealed prior to testing. The method of load application was made to simulate a beam-to-girder connection by bringing the load directly onto the web. This method of load application could not be duplicated in the model tests without undue loss of time. Thus the method of load application in all the model tests was done through bearing blocks on the top flange as shown in Fig. 4.1.3. The beams were laterally braced to prevent lateral bucking upon passing of the elastic limit.

From the results of these simply supported beams the agreement between the theoretical and experimental results was better for the annealed beam in the "regular" test. The "pilot" beams were not annealed nor laterally supported and also loaded on the top flange through bearing blocks. These may be the causes of the lower than predicted moment of the pilot tests. Annealing although lowering the residual stresses considerably also lowered the yield stress and thus the strength of the annealed specimens was less. It is concluded from the test results that the moment curvature curves for structural steel beams, laterally supported, can be predicted from the stress-strain tensile test curves and the usual theory of plastic bending based on the assumptions of a linear strain variation across the section and a uniform distribution of yield.

The prototype for the continuous beams were also of 14-ft. span. However, the "fixity" in these tests results from the 2 side spans of 7-ft. each of a 3 span continuous beam. The central span of 14-ft is considered fixed ended. Two types of tests are reported from the

Lehigh series on continuous beams.[45] One has the reaction applied to the flange through a bearing plate and the other the reaction is transmitted to the web by a beam to column simulated connection. The test results indicate that the latter support detail has more stiffness and thus the beam mobilized higher loads.

4.1.1.2 The Model Tests. The models of the simply supported beams were of 1:15 scale and are soown in Figs. 4.1.3 and 4.1.4. The cross-sectional geometry was only approximately scaled, however, due to machining difficulties (see Appendix C). The phosphor bronze sections machined from square stock were first annealed as described earlier and then assembled. Fig. 4.1.5 shows a beam before testing and below it a failed simply supported beam, failure due to excessive deflection. In beam tests B1 to B5 only centerline deflections were recorded with load increase. Beams B1A and B1B were instrumented with strain gages at the mid-span section and also in B1B deflections were measured at 2 other points so that moment curvature relations could be established from the model test. The position of the strain gages is shown in Fig. 4.1.3. The beams B1A and B1B are shown in Fig. 4.1.6 after failure. Beam B2 and B3 are shown in Fig. 4.1.7.

For the fixed ended beams B4 and B5 the fixity was achieved in the model by silver soldering the ends to a tube in the case of B4 and pouring molten lead in a similar tube in the case of beam B5. The ends were then fastened to the supports with two screws on each support. The detail of the model "fixed" support is shown in Fig. 4.1.12. The fixed ended model beams are shown after failure in Fig. 4.1.8.

4.1.1.3 Test Results. The results of the model beams representing the "pilot" test of the prototype are given in Tables 4.2, 4.3, and 4.4. These are for model beams B1, B1A and B1B respectively. The explanations following each of these tables gives the procedure followed in obtaining the numerical values in each column. Tables 4.5 and 4.6 give the test results of model beams B2 and B3 and Tables 4.7 and 4.8 give the results on the"fixed" end model beams B4 and B5.

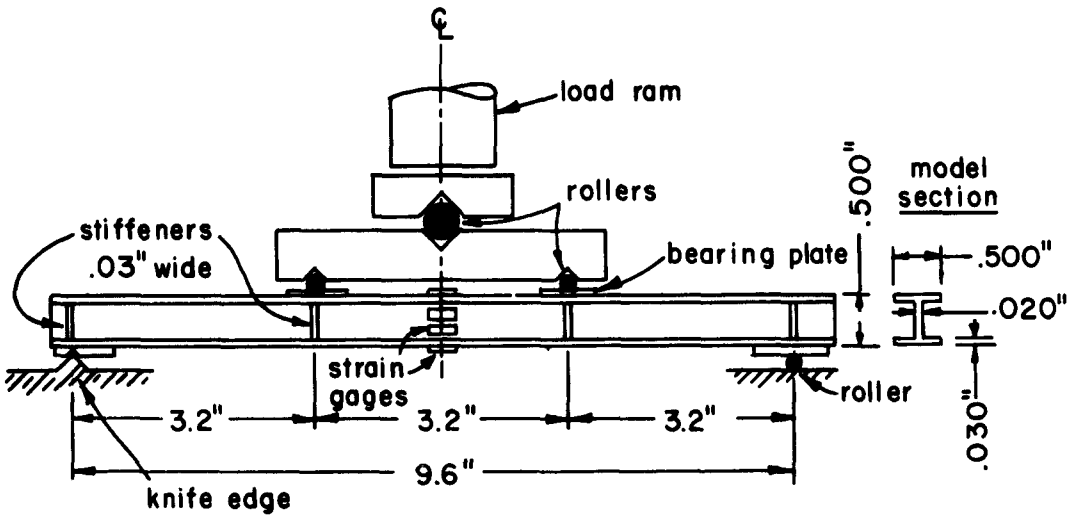

FIG. 4.1.3 MODEL BEAM OF THE "PILOT" PROTOTYPE TEST AT 1:15 SCALE.

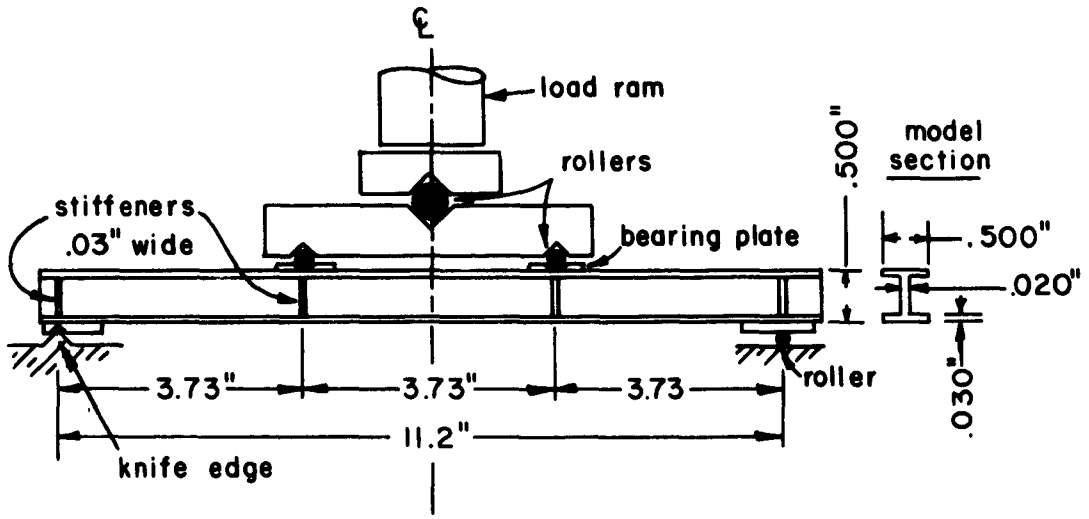

FIG. 4.1.4 MODEL BEAM OF THE "REGULAR" PROTOTYPE TEST AT 1:15 SCALE.

FIG. 4.1.5 MODEL BEAM B1 AFTER FAILURE. SCALE 1:15: MATERIAL, PHOSPHOR BRONZE.

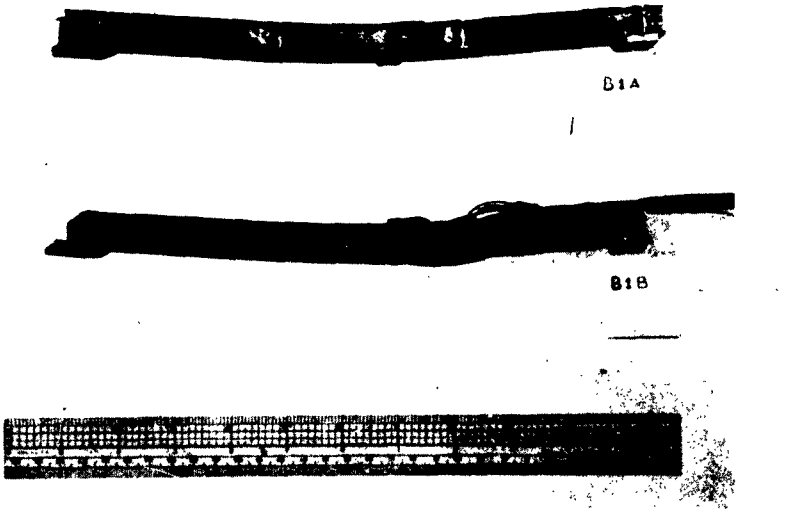

FIG. 4.1.6 MODEL BEAMS B1A AND BIB AFTER FAILURE. NOTE THE STRAIN GAGES AT THE CRITICAL SECTION.

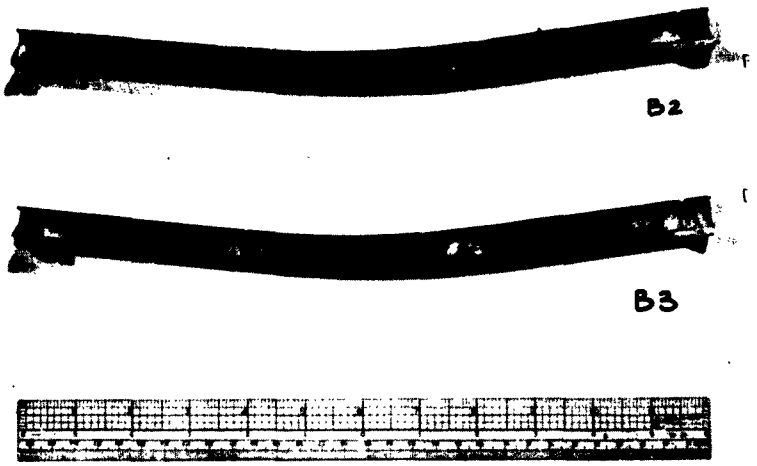

FIG. 4.1.7 SIMPLY SUPPORTED MODEL BEAM 1:15 SCALE AFTER FAILURE.

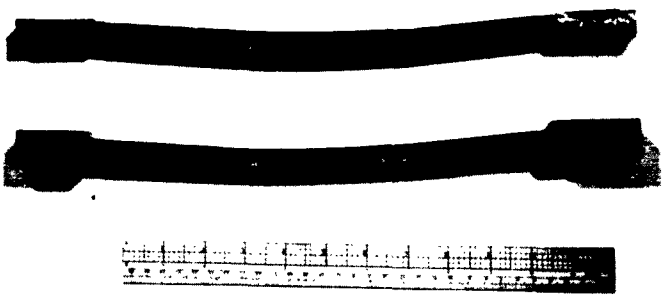

FIG. 4.1.8 FIXED ENDED MODEL BEAM AFTER FAILURE.

Comparison of these results with the prototype tests is given in Fig. 4.1.9 for the "pilot" test or the 8WF40 simply supported beam of 12-ft. span. This figure shows the M-ϕ curves obtained from strain gage readings and also deflection readings in the case of beam B1B.

Fig. 4.1.10 is a load deflection curve for the predicted behavior of the prototype from 3 model tests. This shows the method that could be used to predict ultimate failure loads in more complicated structures from a few model tests. From this figure the predicted failure load is conservatively picked at 56 kips. Backfiguring the ultimate moment of Fig. 4.1.9 (the load deflection curve is not given by Luxion et al.)[25] we get a value of 52 kips for the ultimate load.

Fig. 4.1.11 shows the load deflection curves from model beams B2 and B3 together with the prototype results.

Fig. 4.1.12 shows the load deflection prediction curves from model tests B4 and B5 as compared to two prototype tests of different boundary conditions.

4.1.1.4 Conclusions from the Model Comparisons. From the few tests which are reported herein a number of conclusions could be drawn concerning the correlation of model predictions and actual prototype tests.

1. It is obvious from all the load deflection and the moment curvature plots that the model material strain hardens at earlier values of strain than steel. This was anticipated and the tests verify it. However, as shown by Figs. 4.1.11 and 4.1.12 the ultimate loads on these beams could have been predicted within the accuracy required for design purposes.

2. The results of the two simply supported model beams B2 and B3 which modeled the "regular" tests of 14-ft. spans indicate that the model results approach closer the annealed 8WF40 beam rather than that as delivered as shown by the values of Table 4.1. The failure criterion chosen for the beams is of excessive deflections due to bending deformations.

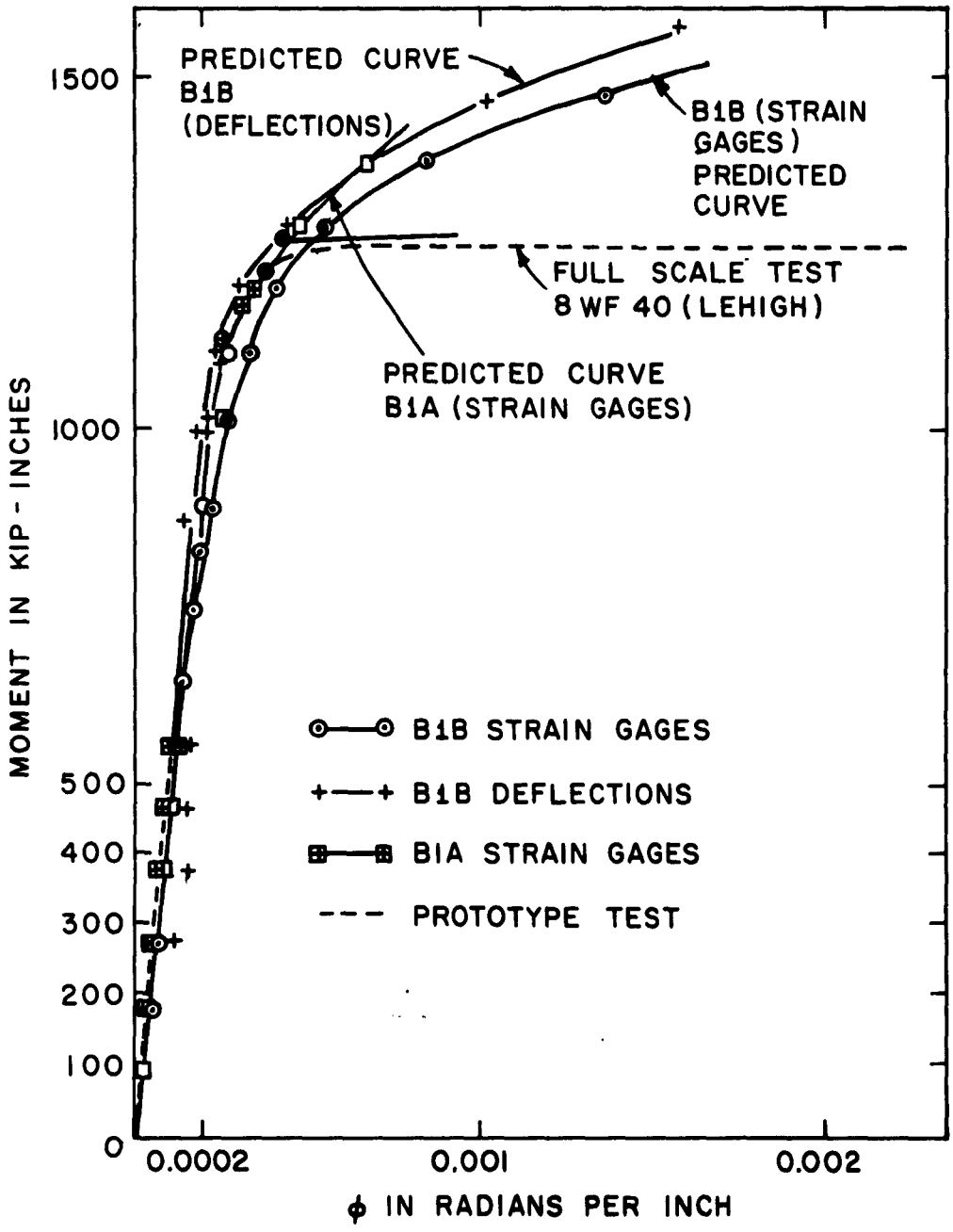

FIG. 4.1.9 SIMPLY SUPPORTED BEAMS M-ϕ RELATIONS

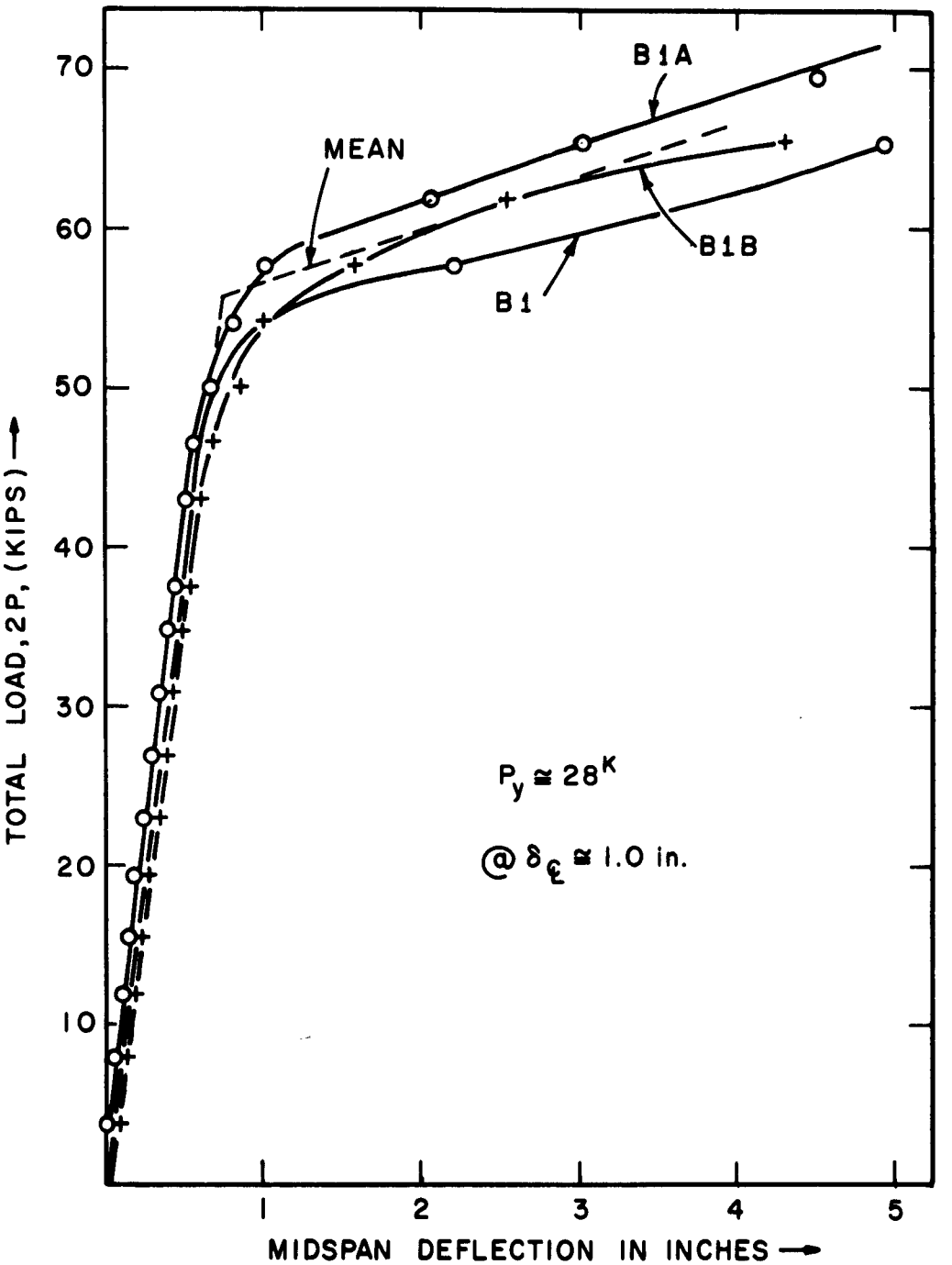

FIG. 4.1.10 LOAD DEFLECTION CURVES PREDICTED FROM MODEL TESTS (1:15) SCALE OF SIMPLY SUPPORTED WIDE FLANGE BEAMS

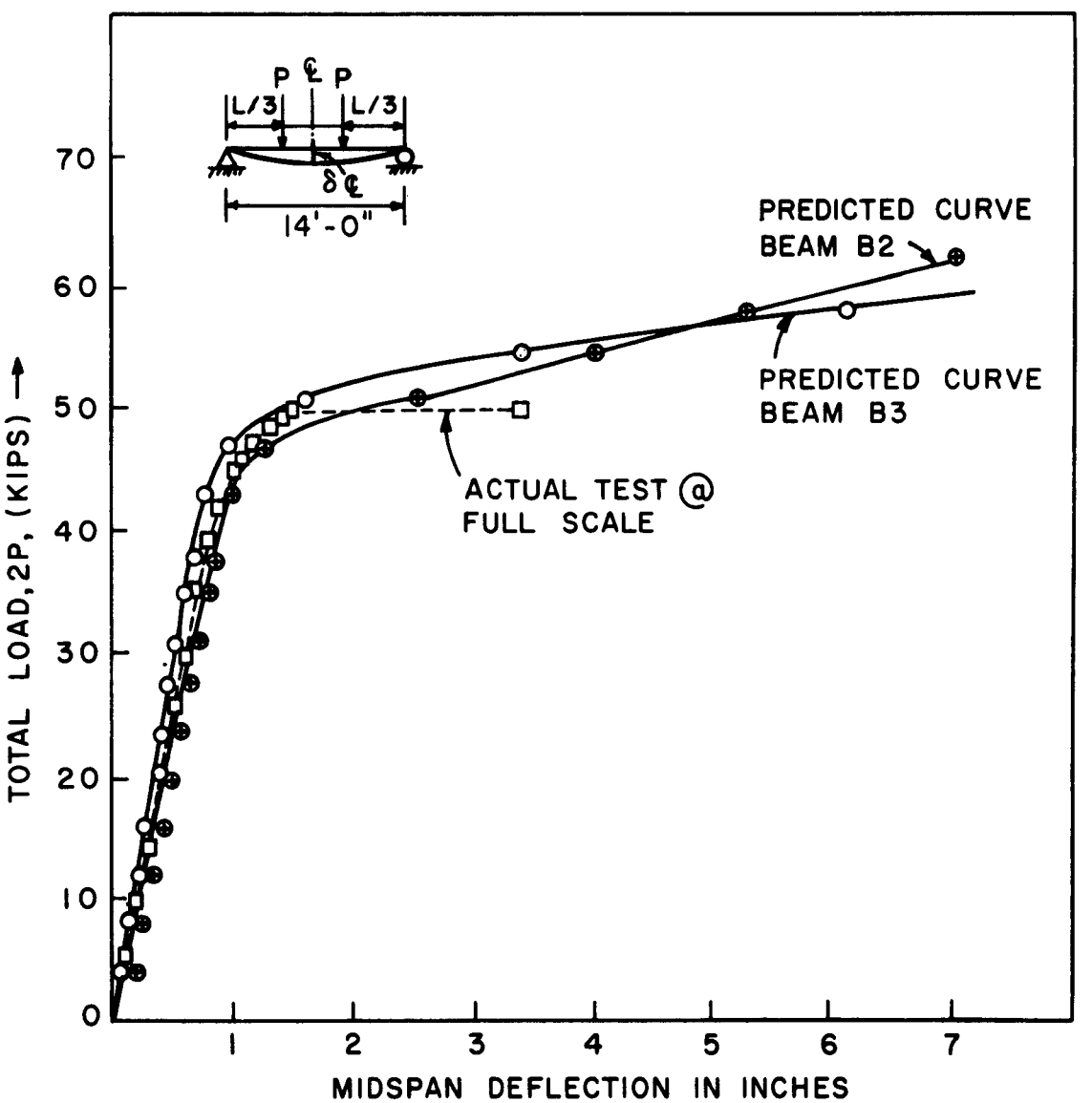

FIG. 4.1.11 LOAD DEFLECTION CURVES FOR SIMPLY SUPPORTED WIDE FLANGE BEAMS

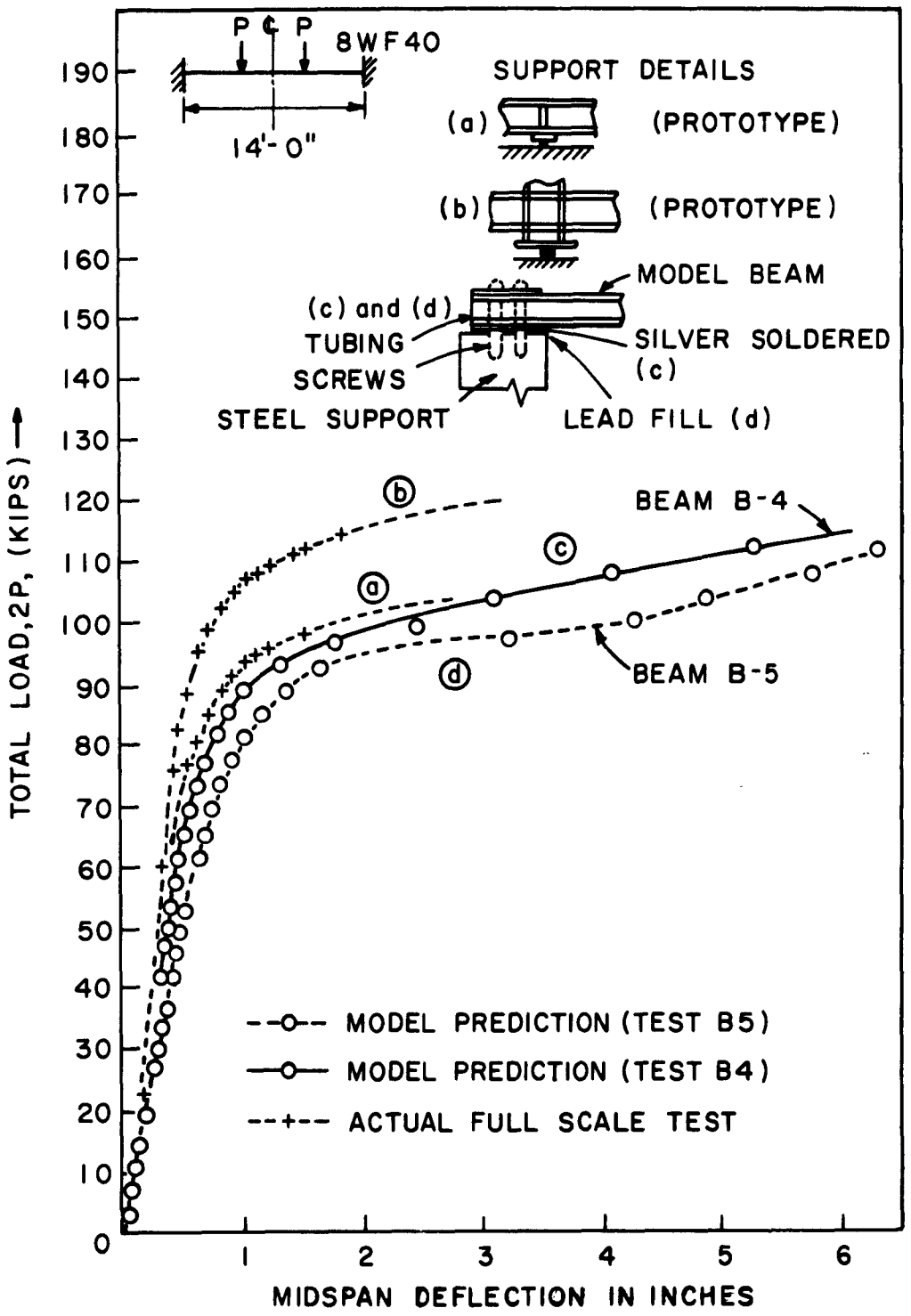

FIG.4.1.12 LOAD DEFLECTION CURVES FOR FIXED ENDED WIDE FLANGE BEAMS

TABLE 4.2 TEST RESULTS FOR MODEL BEAM B1

Load at End of Beam (Lbs.)	Mid-Span Deflection (inches)	Total Load 2P on Model (Lbs.)	Predicted Prototype Load (Kips)	Predicted Prototype Deflection (inches)
1	.004	5.92	3.88	.06
2	.006	11.84	7.74	.09
3	.008	17.76	11.6	.12
4	.01	23.68	15.5	.15
5	.013	29.60	19.3	.195
6	- - -	- - -	- - -	- - -
7	.019	41.44	27.0	.285
8	.0215	47.36	30.9	.324
9	.024	53.28	34.8	.36
10	.028	59.20	37.4	.42
11	.031	65.12	42.8	.465
12	.035	71.04	46.4	.525
13	.0395	76.96	50.2	.593
14	.046	82.88	54.0	.69
15	.069	88.80	57.7	1.035
16	.148	94.72	61.8	2.22
17	.267	100.64	65.5	4.00
18	.329	106.56	69.4	4.94

Explanation of Table 4.2.

Col. 1 gives the load increments on the beam of the loading frame.

Col. 2 is the midspan deflection read on the Ames dial.

Col. 3 gives the total load on the model beam or the sum of the 2 third point concentrated loads. Col. 3 gives the values of Col. 1 times 5.92, the ratio of lengths on the beam or the load multiplication factor of the loading frame.

Col. 4 is the predicted load of the prototype. It is obtained from the following relation:

$$P_p = P_m \times f_r^{-2} \times f_\sigma^{-1} \times (G.F.) \qquad (4.1.1)$$

where

f_r is the length scale

f_σ is the ratio of stresses

G.F. is a geometric factor to account for the difference in moment of inertia as explained in Appendix C.

$$f_r^{-2} \times f_\sigma^{-1} \times G.F. = (15)^2 \times 2 \times 1.45 = 652$$

$$P_p = .652\, P_m \quad \text{(kips)} \qquad (4.1.2)$$

Ccl. 5 gives the predicted defection at mid span of the prototype. The values are obtained from the expression:

$$\vec{U}_p = \vec{U}_m f_r^{-1} \qquad (4.1.3)$$

where

$\vec{U}_p$ is a vector displacement in the prototype.

$\vec{U}_m$ is a vector displacement at the same point and direction in the model.

f_r is the length scale which is 1/15 in this case.

TABLE 4.3 TEST RESULTS OF MODEL BEAM B1A

1 Load at End of Beam in (Lbs.)	2 Midspan Deflection in (Inches)	3 Total Load on Model (Lbs.)	4 Predicted Prototype Total Load (Kips)	5 Predicted Prototype Deflection (Inches)	6 Midspan Moment in Model (Lb.-in)	7 Predicted Prototype Moment (Kip-in)
1	.002	5.92	3.88	.03	9.46	93
2	.004	11.84	7.74	.06	18.92	180
3	.007	17.76	11.6	.105	28.40	358
4	.011	23.68	15.5	.165	37.90	373
5	.014	29.60	19.3	.21	47.30	463
6	.017	35.52	23.2	.255	56.80	556
7	.020	41.44	27.0	.30	66.20	645
8	.023	47.36	30.9	.345	75.60	741
9	.027	53.28	34.8	.405	85.20	835
10	.030	59.20	37.4	.450	94.80	895
11	.033	65.12	42.8	.495	104.20	1028
12	.0375	71.04	46.4	.562	113.6	1113
13	.044	76.96	50.3	.66	122.8	1205
14	.055	82.88	54.0	.825	132.2	1295
15	.070	88.80	57.7	1.05	142.00	1383
16	.138	94.72	61.8	2.07	151.2	
17	.200	100.64	65.5	3.00	160.0	
18	.300	106.56	69.5	4.50	170.0	

TABLE 4.3 (CONT.) TEST RESULTS OF MODEL BEAM B1A

8 Top Flange Strain (μin/in)	9 Upper Web Strain (μ in/in)	10 Lower Web Strain (μ in/in)	11 Bottom Flange Strain (μ in/in)	12 Midspan Curvature in Model (in^{-1})	13 Midspan Curvature in Prototype (in^{-1})
48	30	20	50	.000195	.000013
110	75	35	100	.000365	.0000244
180	110	75	155	.000673	.000045
255	140	105	235	.000930	.000062
330	170	140	300	.001265	.000843
400	210	185	400	.001605	.00107
465	240	220	570	.002127	.00141
540	290	255	835	.00250	.00167
615	325	300	1115	.00287	.00191
690	365	365	1675	.00332	.00221
840	430	410	2840	.0039	.0026
990	525	500	- -	.0041	.00274
1155	645	665	- -	.00524	.0035
- -	895	845	- -	.00696	.00464
- -	1355	1145	- -	.010	.0067

TABLE 4.3 (CONT.). TEST RESULTS OF MODEL BEAM B1A

8 Top Flange Strain (μin/in)	9 Upper Web Strain (μ in/in)	10 Lower Web Strain (μ in/in)	11 Bottom Flange Strain (μ in/in)	12 Midspan Curvature in Model (in^{-1})	13 Midspan Curvature in Prototype (in^{-1})
48	30	20	50	.000195	.000013
110	75	35	100	.000365	.0000244
180	110	75	155	.000673	.000045
255	140	105	235	.000930	.000062
330	170	140	300	.001265	.000843
400	210	185	400	.001605	.00107
465	240	220	570	.002127	.00141
540	290	255	835	.00250	.00167
615	325	300	1115	.00287	.00191
690	365	365	1675	.00332	.00221
840	430	410	2840	.0039	.0026
990	525	500	- -	.0041	.00274
1155	645	665	- -	.00524	.0035
- -	895	845	- -	.00696	.00464
- -	1355	1145	- -	.010	.0067

Explanation of Table 4.3.

Col. 1 - Col. 5 are the same as in Table 4.2.

Col. 6 gives the midspan moment in the model. This is obtained from ½ x Col. 2 x L/3, where L/3 = 3.2".

Col. 7 gives the midspan moment in the prototype. The expression for this value is:

$$M_p = M_m \times f_r^{-3} \times f_\sigma^{-1} \times G.F. \qquad (4.1.4)$$

where, f_r = the length scale

f_σ = the ratio of stresses

G.F. = the correction factor due to discrepencies in the moment of inertia as given in Appendix C

M_p = Prototype moment at midspan.

M_m = Model moment at midspan

$$f_r^{-3} \times f_\sigma^{-1} \times G.F. = (15)^3 \times 2 \times 1.45 = 976$$

therefore,

$$M_p = .976\ M_m \text{ (Kip-in)} \qquad (4.1.5)$$

Col. 8 - Col. 11 give the strain as read on the strain indicator from one SR4 strain gage.

Col. 12 gives the curvature or the rotation per unit length at midspan. The expression used to calculate this as derived in Appendix D from the strain measurements:

$$\frac{1}{R} = \frac{-5\epsilon_1 + 2\epsilon_2 - 2\epsilon_3 + 5\epsilon_4}{4d} \qquad (4.1.6)$$

Col. 13 gives the predicted curvature or rotation per unit length of the prototype at midspan. It is obtained from

$$(1/R)_p = (1/R)_m \times f_r \qquad (4.1.7)$$

where the subscripts indicate prototype and model respectively and f_r is the length scale.

TABLE 4.4. TEST RESULTS OF MODEL BEAM B1B

1 Load at End of Beam in (Lbs.)	2 Deflection at Left Third Point (Inches)	3 Deflection At Midspan (Inches)	4 Deflection At Right Third Point (Inches)	5 Total Load on Model (Lbs.)	6 Predicted Total Prototype Load (Kips)	7 Predicted Prototype Midspan Deflection (Inches)	8 Midspan Moment on Model (Lbs-in)
1	.005	.004	.002	5.92	3.88	.06	9.46
2	.0075	.008	.0035	11.84	7.74	.12	18.92
3	.0105	.0112	.008	17.76	11.6	.167	28.40
4	.0135	.015	.011	23.68	15.5	.232	37.90
5	.0165	.018	.014	29.60	19.3	.270	47.30
6	.0195	.021	.017	35.52	23.2	.315	56.80
7	.0225	.024	.020	41.44	27.0	.360	66.20
8	.0255	.0275	.023	47.36	30.9	.413	75.60
9	.0285	.0305	.027	53.28	34.8	.465	85.20
10	.0325	.0345	.031	59.20	37.4	.525	94.80
11	.0365	.0395	.035	65.12	42.8	.60	104.20
12	.0425	.046	.040	71.04	46.4	.69	113.6
13	.0515	.057	.050	76.96	50.2	.852	122.8
14	.0655	.073	.063	82.88	54.0	1.095	132.2
15	.0945	.106	.090	88.80	57.7	1.59	142.0
16	.1525	.170	.145	94.72	61.8	2.55	151.2
17	.259	.285	.250	100.64	65.5	4.28	160.0

TABLE 4.4. TEST RESULTS OF MODEL BEAM B1B

9	10	11	12	13	14	15	16	17
Predicted Midspan Moment Prototype (Kip-in)	Top Flange Strain (μin/in)	Upper Web Strain (μin/in)	Lower Web Strain (μin/in)	Bottom Flange Strain (μin/in)	Curvature at Midspan Model		Curvature at Midstan in Prototype	
					Deflection (in^{-1})	Strain (in^{-1})	Deflection (in^{-1})	Strain (in^{-1})
93	75	35	30	85	.00039	.000335	.000026	.0000223
180	130	70	75	170	.00117	.000605	.000078	.0000404
248	220	85	110	265	.00152	.001018	.000101	.0000679
373	290	120	140	340	.00215	.001310	.0001435	.0000874
463	350	155	200	420	.00215	.001570	.0001435	.000105
556	450	185	225	450	.00215	.001815	.0001435	.000121
645	520	225	270	590	.00234	.00228	.000156	.000152
741	590	245	310	690	.00273	.002645	.000182	.000176
835	685	295	360	790	.00273	.003035	.000182	.000202
895	780	335	420	900	.00273	.003445	.000182	.00023
1028	880	355	530	1065	.00312	.003997	.000208	.000266
1113	1030	405	595	1320	.00351	.004875	.000234	.000325
1205	1250	505	810	1720	.00468	.00611	.000312	.000407
1295	1610	735	1030	2410	.00663	.00828	.000442	.000550
1383	2450	1325	1450	3680	.01053	.01255	.000703	.000838
1483	3880	2145	2160	5960	.01638	.02029	.00109	.00135
1570	8250	4335	3530	12280	.02341		.00156	

Explanation of Table 4.4.

Col. 1 - Col. 13 are obtained in the same manner as indicated for Table 4.3.

Col. 14 is the curvature or the rotation per unit length at midspan as obtained from the 3 measured deflections. Since the moment is constant over the middle third of the beam, the curvature is constant and has the shape of a circular arc. The rate of change of slope at the center line is then given by the following expression as derived in the Appendix E

$$\frac{1}{R} = \frac{\delta_L - 2\delta_C - \delta_R}{(\Delta X)^2} \qquad (4.1.8)$$

where,

δ_L = the deflection at left third point

δ_C = the deflection at the center line

δ_R = the deflection at the right third point

ΔX = One sixth of span of the beam.

TABLE 4.5. TEST RESULTS OF MODEL BEAM B2

1 Load at End of Beam (Lbs.)	2 Midspan Deflection (Inches)	3 Total Load on Model (Lbs.)	4 Predicted Total Load on Prototype (Kips)	5 Predicted Prototype Midspan Deflection (Inches)
1	.0115	5.92	3.88	.172
2	.017	11.84	7.74	.255
3	.022	17.76	11.6	.33
4	.027	23.68	15.5	.405
5	.0315	29.60	19.3	.472
6	.036	35.52	23.2	.54
7	.042	41.44	27.0	.63
8	.046	47.36	30.9	.69
9	.052	53.28	34.8	.78
10	.0575	59.20	37.4	.862
11	.067	65.12	42.8	1.005
12	.085	71.04	46.4	1.275
13	.170	76.96	50.2	2.55
14	.265	82.88	54.0	3.98
15	.3515	88.80	57.7	5.27
16	.464	94.72	61.8	6.96

TABLE 4.6. TEST RESULTS OF MODEL BEAM B3

1	2	3	4	5
Load at End of Beam (Lbs.)	Midspan Deflection (Inches)	Total Load on Model (Lbs.)	Predicted Total Load on Prototype (Kips)	Predicted Prototype Midspan Deflection (Inches)
1	.005	5.92	3.88	.075
2	.01	11.84	7.74	.15
3	.015	17.76	11.6	.225
4	.019	23.68	15.5	.287
5	.0225	29.60	19.3	.336
6	.027	35.52	23.2	.406
7	.0315	41.44	27.0	.473
8	.036	47.36	30.9	.54
9	.041	53.28	34.8	.615
10	.046	59.20	37.4	.68
11	.052	65.12	42.8	.78
12	.063	71.04	46.4	.95
13	.107	76.96	50.2	1.61
14	.255	82.88	54.0	3.38
15	.403	88.80	57.7	6.06
16	.592	94.72	61.8	8.90

TABLE 4.7 TEST RESULTS OF MODEL BEAM B4

1	2	3	4	5
Load at End of Beam (Lbs.)	Midspan Deflection (Inches)	Total Load on Model (Lbs.)	Predicted Total Load On Prototype (Kips)	Predicted Midspan Deflection Prototype (Inches)
1	.002	5.92	3.88	.03
2	.003	11.84	7.74	.045
3	.0045	17.76	11.6	.0676
4	.006	23.68	15.5	.09
5	.008	29.60	19.3	.12
6	.0095	35.52	23.2	.1425
7	.0115	41.44	27.0	.1725
8	.013	47.36	30.9	.195
9	.015	53.28	34.8	.225
10	.017	39.20	37.4	.255
11	.019	65.12	42.8	.285
12	.021	71.04	46.4	.315
13	.023	76.96	50.2	.345
14	.025	82.88	54.0	.375
15	.029	88.80	57.7	.436
16	.031	94.72	61.8	.465
17	.033	100.64	65.5	.496
18	.036	106.56	69.6	.54
19	.040	112.48	74.0	.60
20	.044	118.40	77.1	.66
21	.049	124.32	81.2	.736
22	.057	130.24	85.0	.856
23	.065	136.16	89.0	.975
24	.085	142.08	92.8	1.275
25	.117	148.00	96.6	1.755
26	.163	153.92	100.0	2.44
27	.206	159.84	104.0	3.09
28	.272	165.76	107.8	4.08
29	.363	171.68	111.8	5.45

TABLE 4.8 TEST RESULTS OF MODEL BEAM B5

1 Load at End of Beam (Lbs.)	2 Midspan Deflection (Inches)	3 Total Load on Model (Lbs.)	4 Predicted Total Load On Prototype (Kips)	5 Predicted Midspan Deflection Prototype (Inches)
1	.0015	5.92	3.88	.0225
2	.003	11.84	7.74	.045
3	.005	17.76	11.6	.075
4	.007	23.68	15.5	.105
5	.009	29.60	19.3	.135
6	.0115	35.52	23.2	.1725
7	.014	41.44	27.0	.21
8	.017	47.36	30.9	.255
9	.0195	53.28	34.8	.292
10	.0225	39.20	37.4	.337
11	.025	65.12	42.8	.375
12	.0275	71.04	46.4	.412
13	.0305	76.96	50.2	.457
14	.0335	82.88	54.0	.502
15	.036	88.80	57.7	.54
16	.040	94.72	61.8	.60
17	.043	100.64	65.5	.645
18	.048	106.56	69.6	.72
19	.053	112.48	74.0	.795
20	.061	118.40	77.1	.915
21	.068	124.32	81.2	1.02
22	.077	130.24	85.0	1.155
23	.091	136.16	89	1.365
24	.110	142.08	92.8	1.65
25	.214	148.00	96.6	3.21
26	.284	153.92	100.0	4.26
27	.323	159.84	104	4.85
28	.380	165.76	107.8	5.70
29	.420	171.68	111.8	6.3

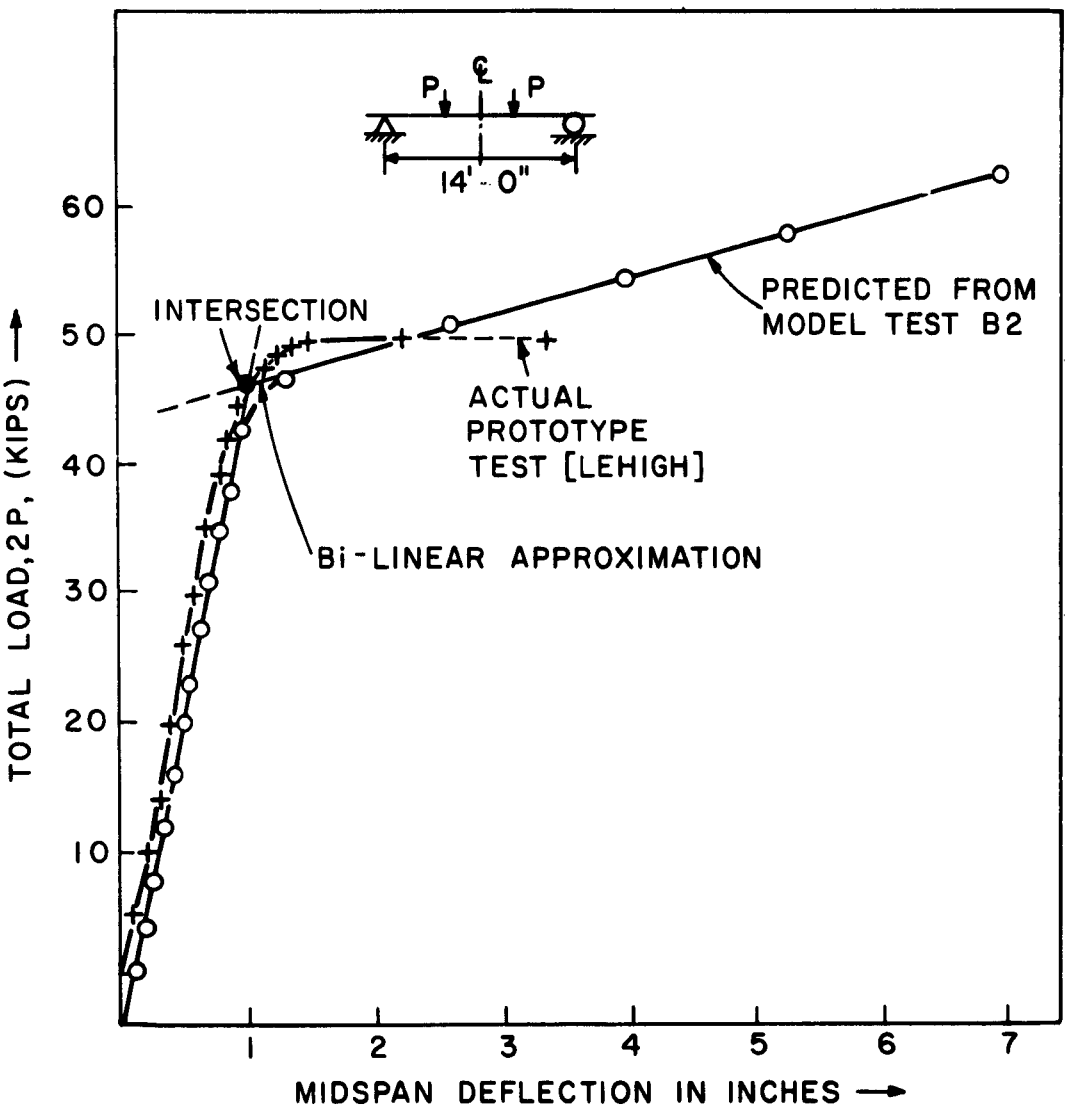

FIG. 4.1.13 CRITERION FOR ULTIMATE LOAD PREDICTION

3. The agreement in the case of the two "fixed" ended beams is closer to the prototype test with support conditions (a) as shown in Fig. 4.1.12. Since the model boundary conditions in the model are simulated in a different way it is hard to draw any conclusions as to which type of boundary conditions the model beams approached. However, it should be noted that there was some rotation at the supports of the model and the extra heat applied in the manufacture of the model at the two ends may have weakened the material at those two points considerably more than the yield stress of 18,000 psi of the regular annealing process.

4. The criterion used in picking the ultimate loads from the load deflection curve will be illustrated with the idealized bi-linear load deflection curve of beam B2 shown in Fig. 4.1.13. At the intersection of the two linear approximations to the predicted load deflection curve we read a total load of 46 Kips and a midspan deflection of 1 inch. This is actually the minimum value of a so-called "ultimate load" since at a larger deflection the correlation between the model test and the prototype test will be better. In fact at a midspan deflection of 2.25 inches the total ultimate load is the same for both or 48.5 Kips. Thus if the maximum allowed deflection of the prototype structure is known (which is the case in most structural problems) then it is a simple matter to pick the ultimate load from the predicted load deflection curve obtained in a model study.

4.1.2 Portal Frames. In order to test the modeling technique better in cases of real structures with more elaborate boundary conditions, it was decided to make model tests of singly redundant portal frames as tested at full scale at Lehigh University[37]. The results from the model test were then used to predict the behavior of the prototype and a comparison was made between this prediction and the actual prototype results.

4.1.2.1. Prototype Tests. The dimensions of the prototype and the loading set up are shown in Fig. 4.1.14 . The rolled section used for beams and columns are the 8WF40

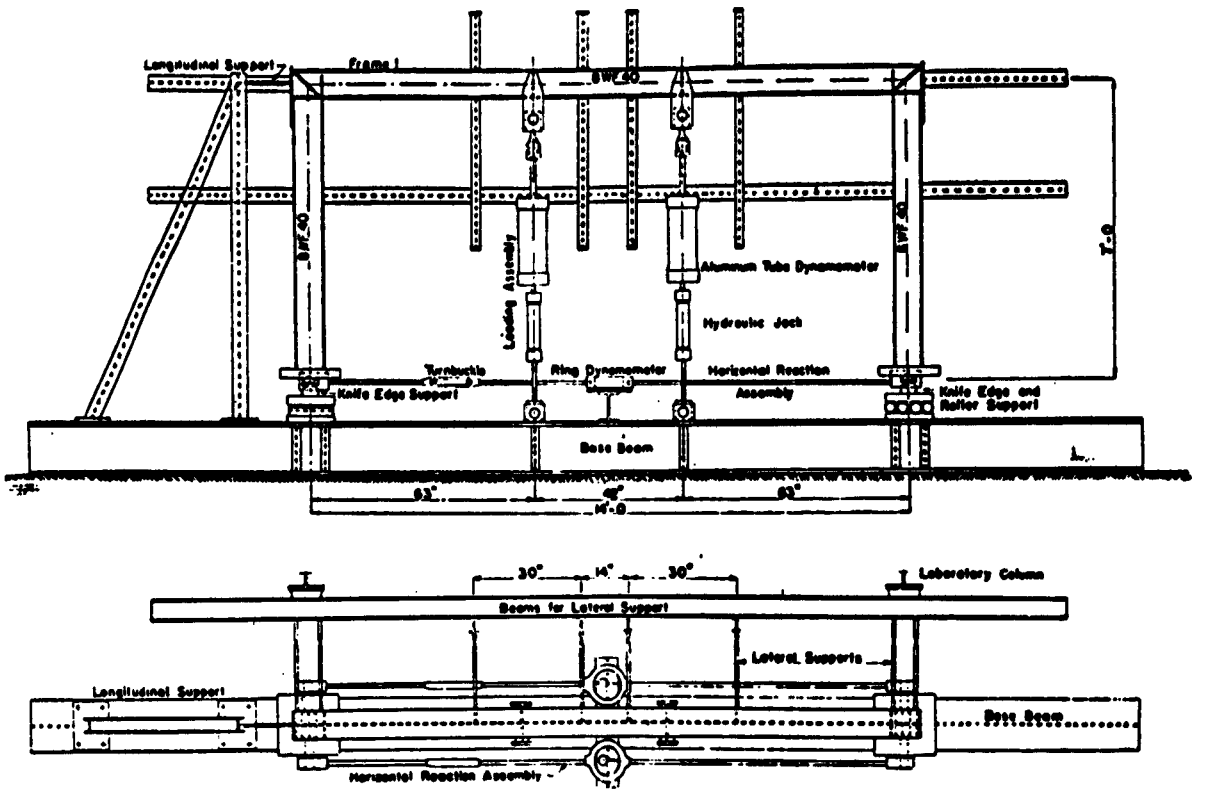

FIG. 4.1.14 TEST SET UP FOR THE PROTOTYPE TEST ON PORTAL FRAMES (REF. 37).

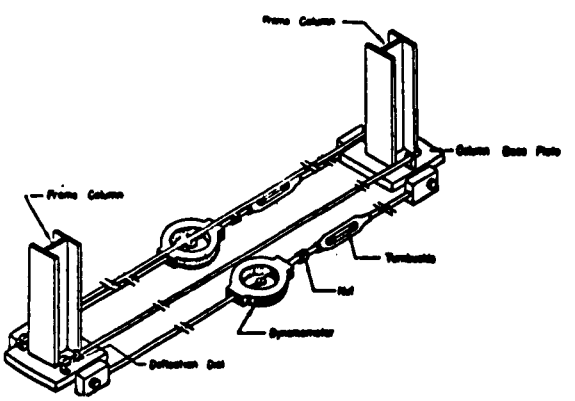

FIG. 4.1.15 HORIZONTAL REACTION ASSEMBLY

section used before in the wide flange beams. The loads applied were two vertical concentrated loads at the 3/8 points. Side-sway and lateral buckling were prevented in these tests. The boundary conditions used are shown in Fig. 4.1.14. They simulate pin ended supports at the base of the columns. The detail of the horizontal reaction measureing assembly is shown in Fig. 4.1.15. Side-sway was prevented by a longitudinal support on one of the knees. Lateral supports were provided at the corner connections and at 4 points along the length of the beam where severe plastic straining was expected. The loads were transferred to the web of the beam as in the case of the beam tests described in the previous section.

4.1.2.2 The Model Tests. The model frame was fabricated from the phosphor bronze section shown in Fig. 4.1.16 and was at a scale of 1:15 of the prototype. Lateral supports were provided by means of thin brass wires attached to the stiffeners of the beam and knees as shown in Fig. 4.1.17. The joints used are a modified version of the prototype. This and other types of connections will be discussed in a section that follows. The horizontal reaction was measured by reading the strain on a stiff steel bar 1" x .03" in cross section. The bar together with other details of the test can be seen in Fig. 4.1.17. The position of the strain gages is shown in Fig. 4.1.16 together with the horizontal reaction measuring bar.

Loads were applied to the frame by means of bearing plates at the top flange as seen in Fig. 4.1.17. Side-sway was prevented by attaching a thin brass wire to the right hand side. However, this proved to be inadequate under very large deflections and the ultimate failure of the frame, after considerable plastification took place, was a side-sway failure to the right. This is shown very clearly in Figs. 4.1.19 and 4.1.20 of the failed specimen.

Deflections were measured at midspan by means of an Ames dial as shown in Fig. 4.1.18.

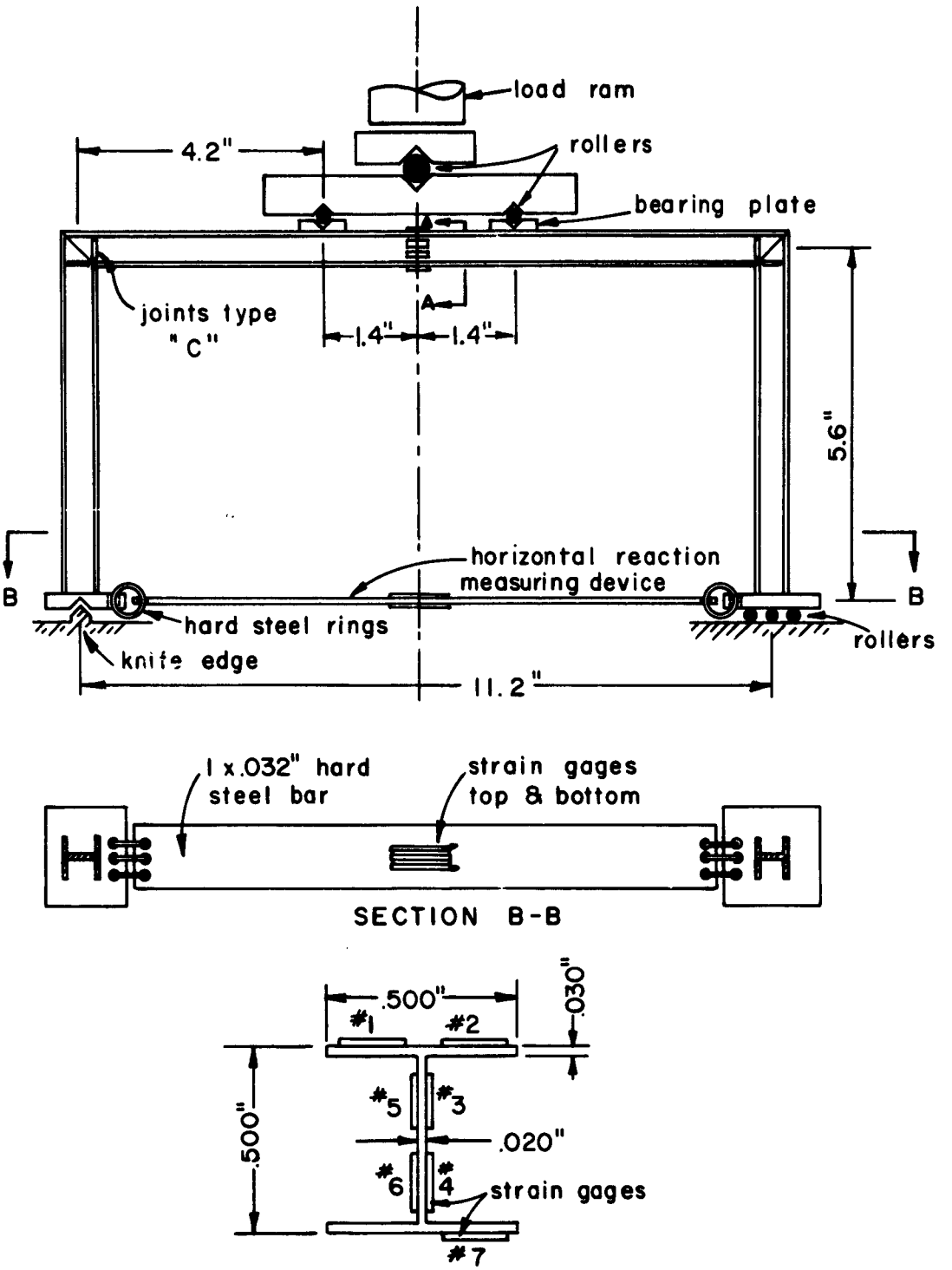

FIG. 4.1.16 MODEL FRAME, 1:15 SCALE, SHOWING HORIZONTAL REACTION MEASURING DEVICE AND POSITION OF STRAIN GAGES.

FIG. 4.1.17 POSITIONING OF THE MODEL PORTAL FRAME IN SUPPORTING BOX, SHOWING LOADING METHOD.

FIG. 4.1.18 TEST SET UP FOR MODEL FRAME

FIG. 4.1.19 MODEL FRAME AFTER TEST.

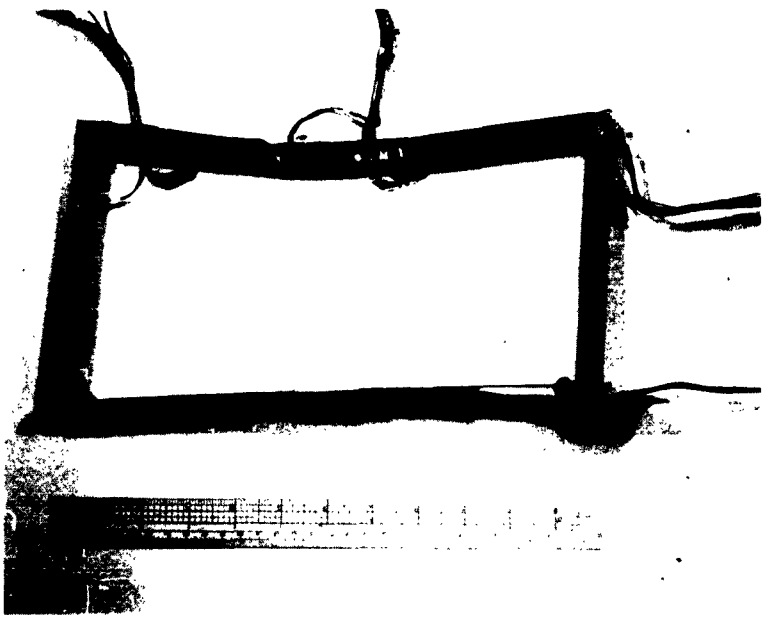

FIG. 4.1.20 MODEL FRAME SHOWING A LATERAL SWAY FAILURE INITIATED BY LOCAL BUCKLING OF THE TOP FLANGE AT LARGE DEFORMATION DUE TO BENDING.

4.1.2.3 Test Results. The results of the test on the model frame are given in Table 4.9 and the explanation of the method of obtaining these results follows. Fig. 4.1.21 shows the horizontal reaction variation with half the total vertical load obtained experimentally from the strain reading on the steel bar. The experimental curve was used to calculate the midspan moment. Fig. 4.1.22 is a comparison of the moment curvature relation at midspan obtained from the model test and the prototype test. In Fig. 4.1.23 the load deflection results are compared from the model and the prototype results.

4.1.2.4 Conclusions from the Portal Frame Test. The results of this test proved a very fundamental point which was not brought out convincingly by the beam tests, namely that the full plastic moment could be developed in phosphor bronze models as it is in structural steel. Fig. 4.1.22 shows that the M-ϕ curves of model and prototype agree very well considering the model was at 1:15 scale. This close agreement as compared to the discrepancy in the simply supported beams is due to the better instrumentation of the frame where strains were based on average values rather than a single reading.

The load deflection predicted curve is in poorer agreement in this case but still the error is less than about 10%. Again it should be emphasized that the agreement in predicting ultimate load is a function of the maximum deflection to be tolerated in the prototype. Once this is known then Pult can be read off the predicted curve. Fig. 4.1.23 emphasizes this point since at deflections of the order of magnitude of 4 to 6 inches the predicted load is in closer agreement to the prototype test.

From the test of the model frame it was found that the horizontal reaction measuring device was too stiff and its strain response was low. This is believed to be the main reason for the large deviation of the experimental curve from the theoretical at relatively low loads as shown in Fig. 4.1.21.

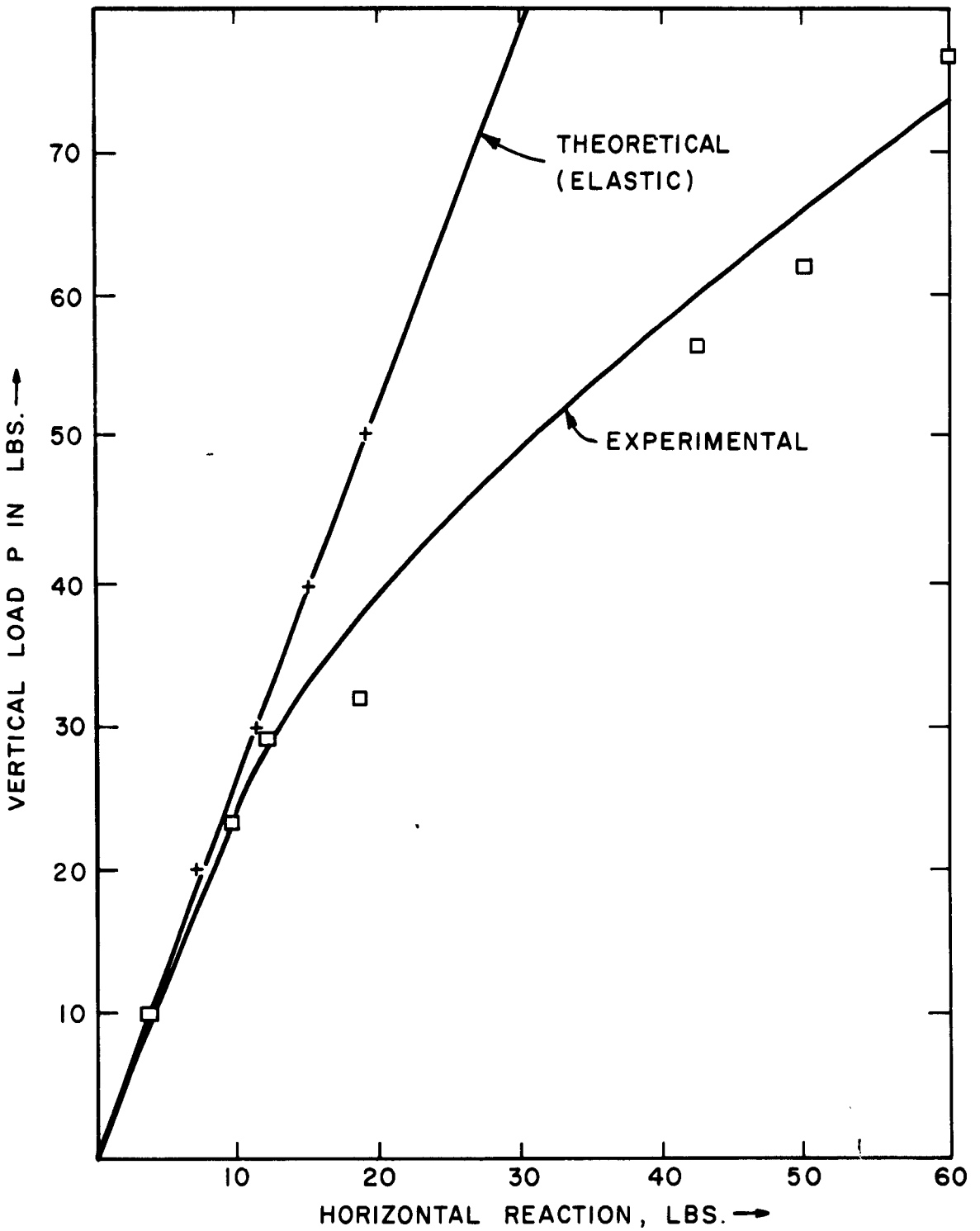

FIG.4.1.21 VERTICAL LOAD vs. HORIZONTAL REACTION FOR THE MODEL FRAME

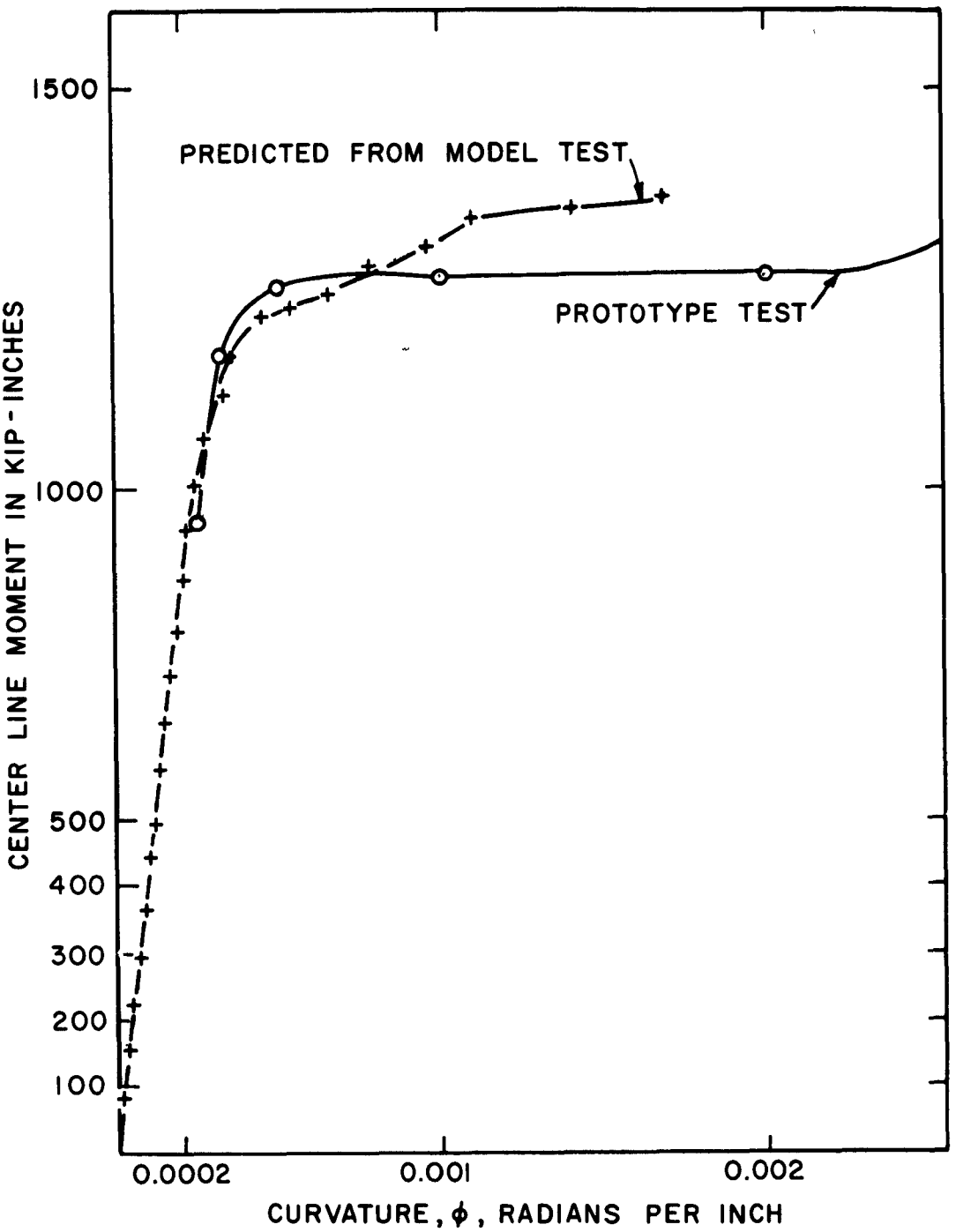

FIG.4.1.22 MOMENT-CURVATURE RELATIONSHIP FOR MODEL FRAME

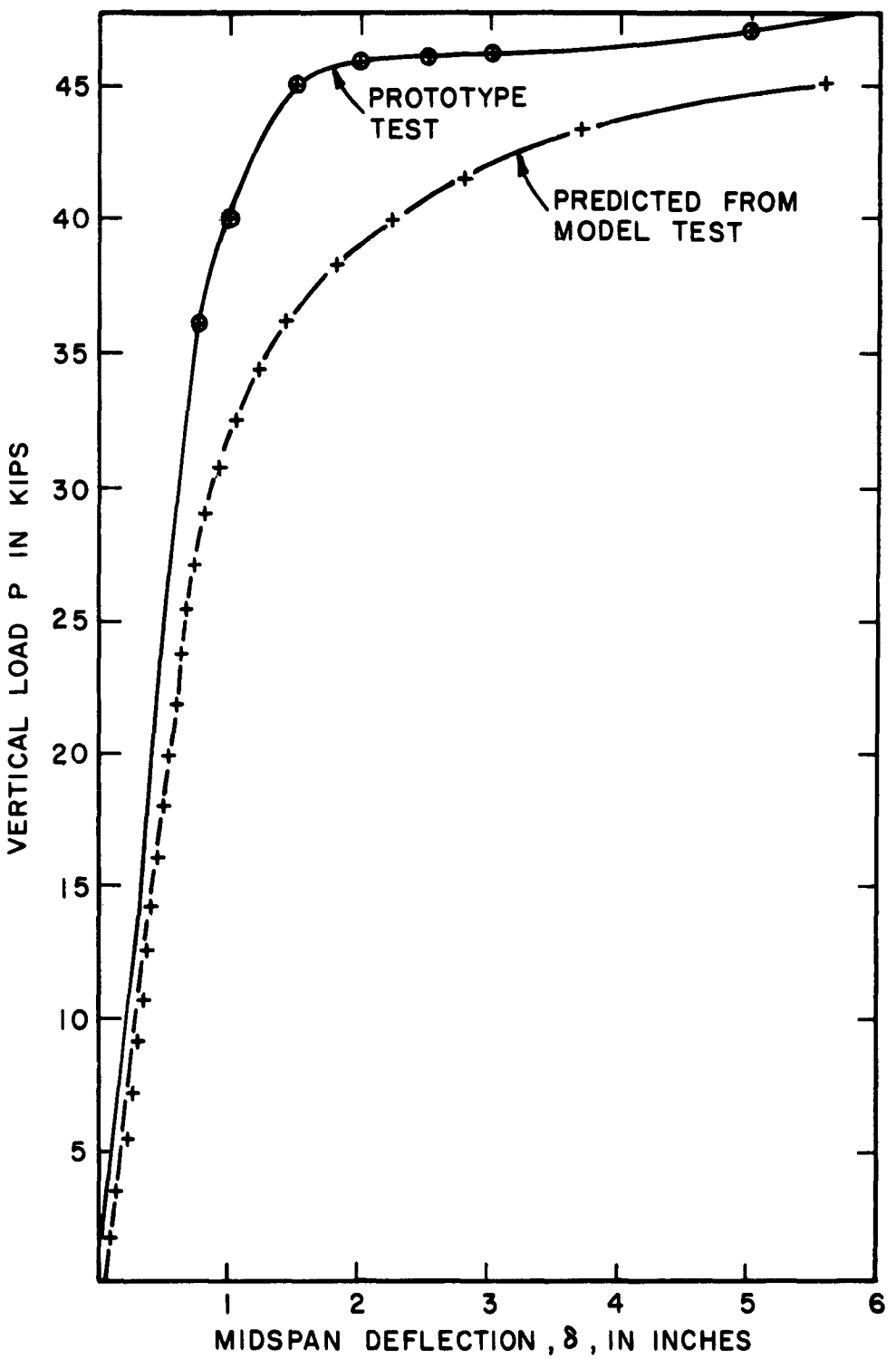

FIG.4.1.23 LOAD DEFLECTION RELATIONSHIP FOR MODEL FRAME

TABLE 4.9 RESULTS OF PORTAL FRAME TESTS

1	2	3	4	5	6	7
Load at End of Beam in (Lbs.)	Deflection in (Inches)	Strain Measurements				Model $\frac{1}{R}$ ($inch^{-1}$)
		Top Flange (μ in/in)	Bottom Flange (μ in/in)	Web Upper (μ in/in)	Web Lower (μ in/in)	
1	.004	- 58	+ 60	- 24	+ 45	.000226
2	.0095	- 103	+ 125	- 14	+ 63	.000493
3	.014	- 123	+ 175	+ 06	+ 91	.000660
4	.017	- 181	+ 255	+ 10	+ 126	.000974
5	.020	- 231	+ 347	- 06	+ 165	.001274
6	.0235	- 288	+ 405	- 10	+ 196	.001526
7	.026	- 326	+ 467	+ 10	+ 218	.001775
8	.028	- 396	+ 521	- 20	+ 195	.002077
9	.0308	- 439	+ 569	- 36	+ 211	.002273
10	.033	- 503	+ 653	- 56	+ 245	.002589
11	.0362	- 565	+ 706	- 77	+ 275	.002826
12	.0385	- 671	+ 780	- 102	+ 327	.003073
13	.041	- 681	+ 850	- 118	+ 367	.003342
14	.044	- 775	+ 925	- 158	+ 375	.003717
15	.050	- 855	+ 997	- 185	+ 394	.004051
16	.055	-1022	+1225	- 260	+ 426	.004932
17	.061	-1157	+1330	- 328	+ 451	.005438
18	.0708	-1371	+1715	- 363	+ 573	.006774
19	.082	-1608	+2035	- 426	+ 671	.008010
20	.095	-1934	+2565	- 510	+ 838	.009899
21	.1225	-2350	+2965	- 641	+ 933	.011713
22	.151	-2919	+3690	- 746	+1123	.014403
23	.189	-3282	+4115	- 816	+1200	.016477
24	.247	-4259	+4975	- 815	+1250	.021020
25	.372	-5186	+5185	- 808	+1600	.025269

TABLE 4.9 (CONT.) RESULTS OF PORTAL FRAME TESTS

8	9	10	11	12	13	14	15
Prototype $\frac{1}{R}$ ($Inch^{-1}$)	2P on Model (Lbs.)	Predicted 2P (Kips)	P (Kips)	Predicted Deflection (Inches)	Horizontal Reaction (Lbs.)	Moment in Model (Lb-In)	Predicted Moment (Kip-In)
.0000151	5.56	3.62	1.81	.06	.6	8.32	81.3
.0000329	11.12	7.26	3.63	.1423	1.4	15.46	151.1
.000044	16.68	10.88	5.44	.210	2.1	23.24	228
.000065	22.24	14.50	7.25	.255	3.0	29.8	291.5
.000085	27.80	18.15	9.07	.30	3.75	37.4	366
.0001015	33.36	21.75	10.87	.352	4.5	45.8	448
.0001182	38.92	25.40	12.70	.39	5.5	50.8	497.5
.0001382	44.48	29.00	14.50	.42	6.2	58.8	576
.0001515	50.04	32.65	16.3	.462	7.0	65.8	644
.0001725	55.60	36.30	18.15	.495	7.75	73.1	715
.0001885	61.16	39.90	19.95	.543	8.5	80.4	786
.000205	66.72	43.5	21.75	.578	9.25	88.2	863
.000223	72.28	47.2	23.6	.615	10.0	95.5	934
.000247	77.84	50.75	25.37	.66	10.75	102.8	1005
.000270	83.40	54.40	27.20	.75	11.6	110	1075
.000329	88.26	58.00	29.00	.825	12.5	116.6	1140
.000362	94.52	61.60	30.80	.915	13.5	122.9	1200
.000452	100.08	65.1	32.55	1.065	14.5	128.8	1260
.000534	105.64	68.8	34.4	1.23	16.5	129.5	1268
.00066	111.20	72.5	36.25	1.425	18.0	132.7	1296
.000782	116.76	76.6	38.3	1.835	19.4	136.5	1335
.000960	122.32	79.8	39.9	2.26	21.0	139	1360
.0011	127.88	83.2	41.6	2.84	22.1	144.2	1410
.0014	133.44	87.0	43.5	3.7	24.1	145	1420
.001685	139.00	90.5	45.3	5.58	26.0	147	1436

Explanation of Table 4.3.

Col. 1 gives the load in lbs. at the end of the beam of the loading frame.

Col. 2 gives the observed deflection of the model frame at midspan.

Col. 3 shows the average strain from two gage readings on the top flange at midspan.

Col. 4 gives the strain in on the bottom flange at midspan. One gage reading only.

Col. 5 is the average of two gage readings at the upper quarter depth of the web at midspan.

Col. 6 gives the average of two readings of the lower quarter of the web at midspan.

Col. 7 gives the curvature or rate of change of the slope at midspan. It is calculated from the following expressions. (See Fig. D.1)

$$\frac{1}{R} = \frac{-5\epsilon_1 + 2\epsilon_2 - 2\epsilon_3 - 5\epsilon_4}{4d}$$

as derived in the Appendix (D.2)

Col. 8 is the values of Col. 7 multiplied by the scale factor of 1/15.

Col. 9 gives the total load, 2P, acting on the model in lbs. It is obtained by multiplying Col. 1 by 5.56 the ratio of lever lengths for the particular test.

Col. 10 is the predicted total load of a prototype structure 15 times larger than the model. It is obtained from the following relation:

$$P_p = P_m \times f_r^{-2} \times f_\sigma^{-1} \text{ (G.F.)}$$

where f_r is the length scale and f_σ is the ratio of stresses as previously defined. G.F. is a geometric factor to account for the difference in moment of inertia as explained in Appendix C.

$$f_r^{-2} \times f_\sigma^{-1} \times G.F. = (15)^2 \times 2 \cdot 1.45 = 652$$

Col. 11 is the value of one half of Col. 10.

Col. 12 is Col. 2 times 15 or f_r^{-1} the length scale.

Col. 13 is the horizontal reaction induced by the vertical load on the frame. It is obtained from measurements of strain on a stiff bar. The plot of P vs H is given in Fig. 4.1.21.

Col. 14 gives the midspan moment of the frame in lb.-in. It is obtained from the expression:

$$M = 4.2P - 5.6H$$

as derived in Appendix F.

Col. 15 gives the predicted midspan moment in Kip inches. It is obtained from Col. 14 by multiplying with the factor .652 as found for Col. 10 times 15 because the units of moment are length x force. The expression therefore is

$$M_p = M_m \times f_r^{-3} \times f_\sigma^{-1} \times (G.F.)$$

The factors are the same as stated previously.

4.1.3 Connections. Welded steel structures have become increasingly more popular because of the continuity of framed structures which ensues when joints and connections are carefully welded. In the model studies in phosphor bronze it was demonstrated that the full plastic moment of the prototype could be predicted from model studies at reduced scales. This can occur in a framed structure only if the connections can withstand the relatively large rotations imposed by plastic design. To verify the adequacy of various joints model connections were made and tested in a manner similar to the tests on connections at Lehigh University[46]. These were not model reproductions of the prototype tests however since an 8B13 section was used in the "prototype". This did not allow correlation with the approximate phosphor bronze section used in the model connections.

4.1.3.1 Prototype Tests. Since the sections of the prototype tests could not be duplicated in the model only the method of testing was of real interest in the Lehigh test series. Some of the model joints were made in a similar fashion as the prototype. The loading arrangement shown in Fig. 4.1.24 was modified and used in the model tests.

4.1.3.2 The Model Tests. The joints which were modeled are shown in Figs. 4.1.25 and 4.1.26. The joint in Fig. 4.1.26 is a typical beam to column connection whereas the joints of Fig. 4.1.25. show the same section in beam and column.

The method of making the joints is illustrated in Fig. 4.1.27 which shows the various pieces which are silver soldered together to make connection K. Figs. 4.1.28 - 4.1.30 show the model joints after testing.

Fig. 4.1.31 shows the method of loading and support of the model frames. The horizontal bar gave the necessary alignment so that the load could be applied concentrically. In Fig. 4.1.32 the whole supporting frame is shown during a test. Only deflections were measured in these tests. From these the rotation of the joint could be approximated. Fig. 4.1.33 shows a closeup of a test specimen in which the method of support is clearly shown.

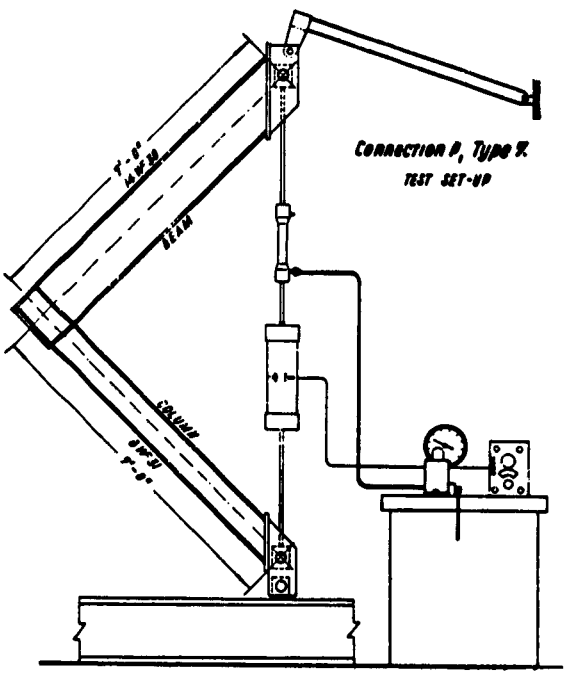

FIG. 4.1.24 TEST SETUP FOR CONNECTION P (REF. 46)

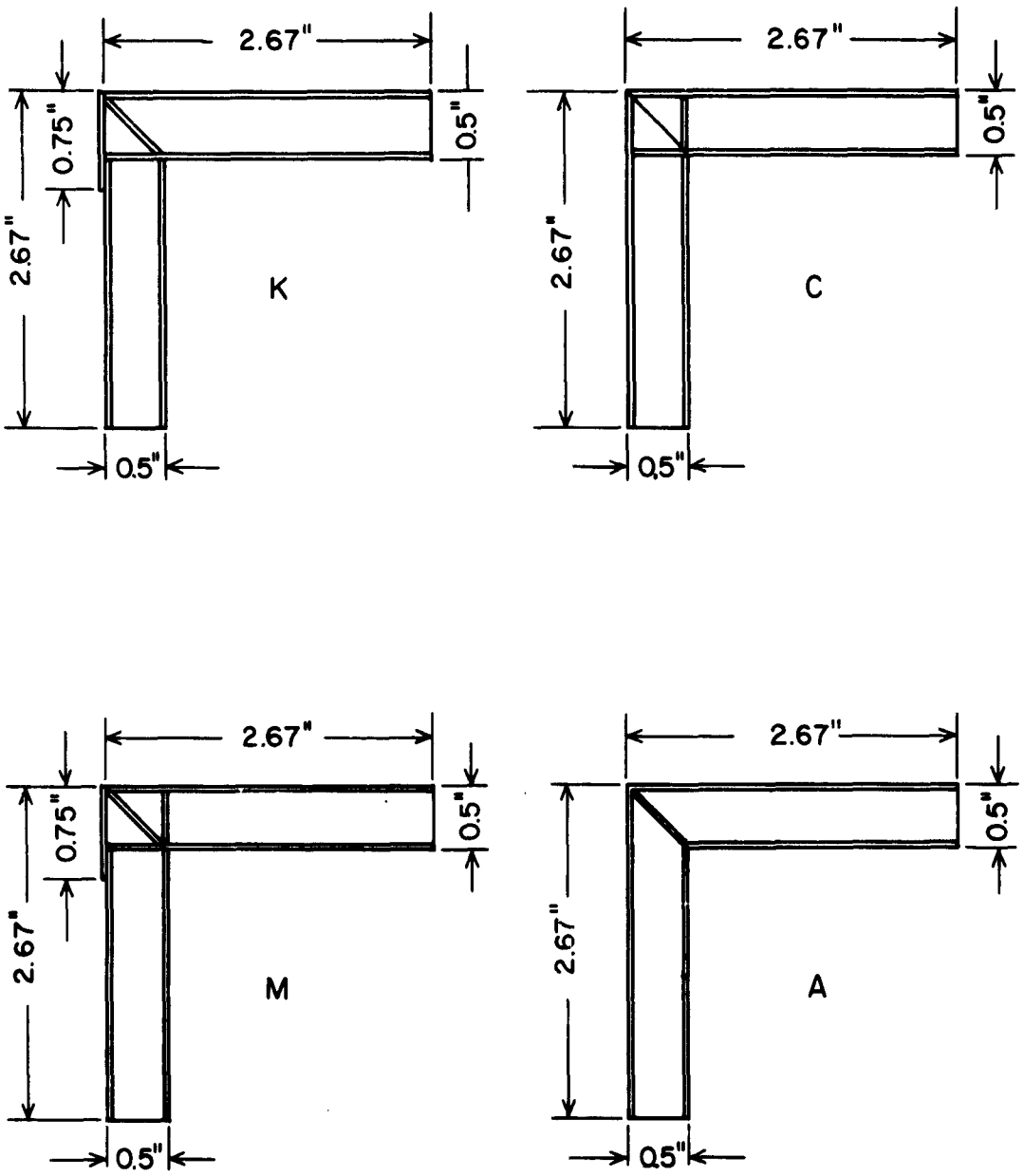

FIG. 4.1.25 DIMENSIONS OF THE MODEL JOINTS TESTED

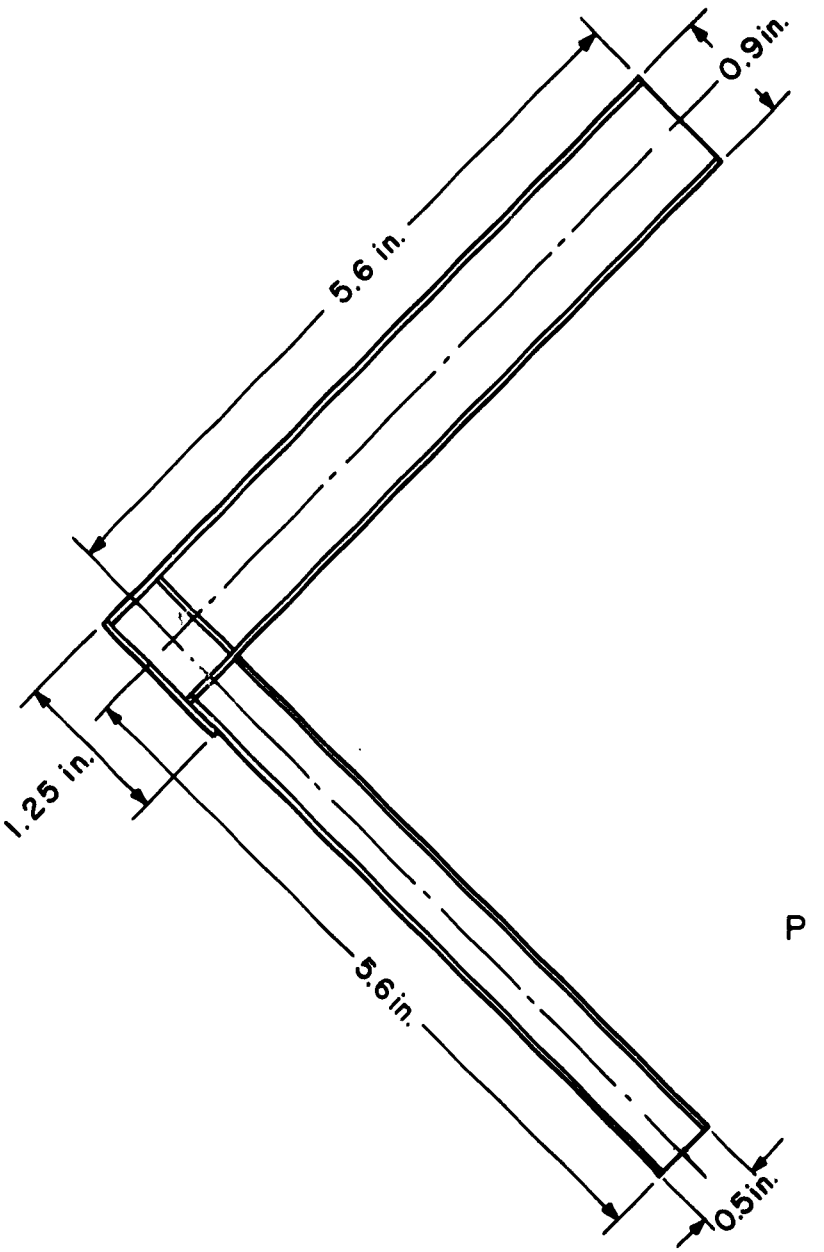

FIG.4.1.26 BEAM TO COLUMN MODEL CONNECTION

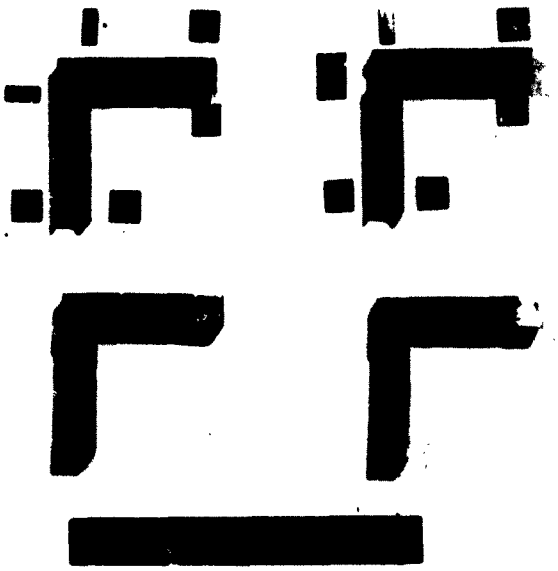

FIG. 4.1.27 PARTS WHICH GO INTO THE MAKING OF A MODEL JOINT.

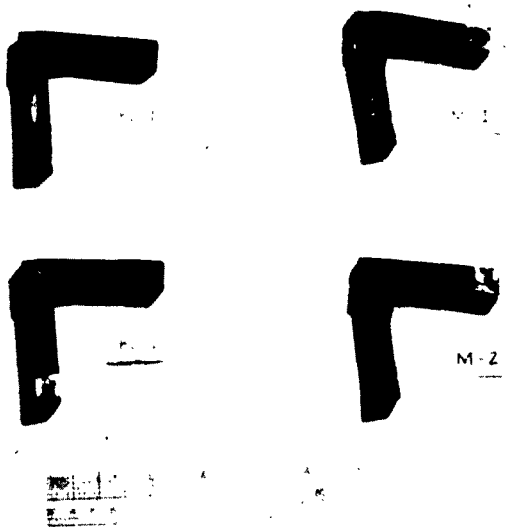

FIG. 4.1.28 MODEL JOINTS AFTER FAILURE. NOTE THE MODE OF FAILURE IN EACH.

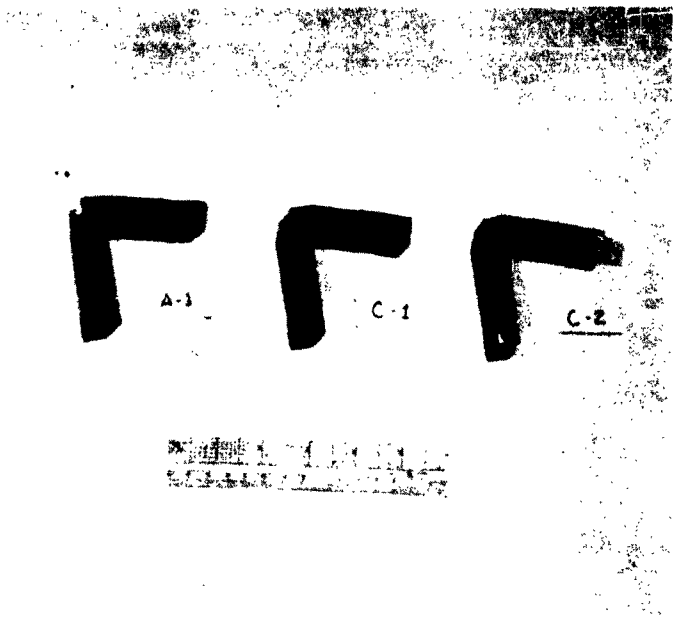

FIG. 4.1.29 TYPES A AND C JOINTS AFTER FAILURE. TYPE C JOINTS WERE USED IN THE PORTAL FRAMES.

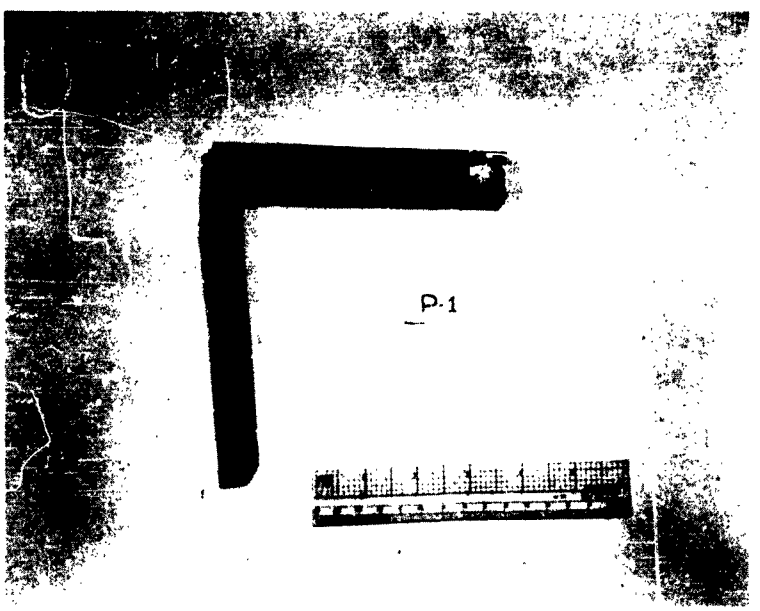

FIG. 4.1.30 TYPE P JOINT AFTER FAILURE.

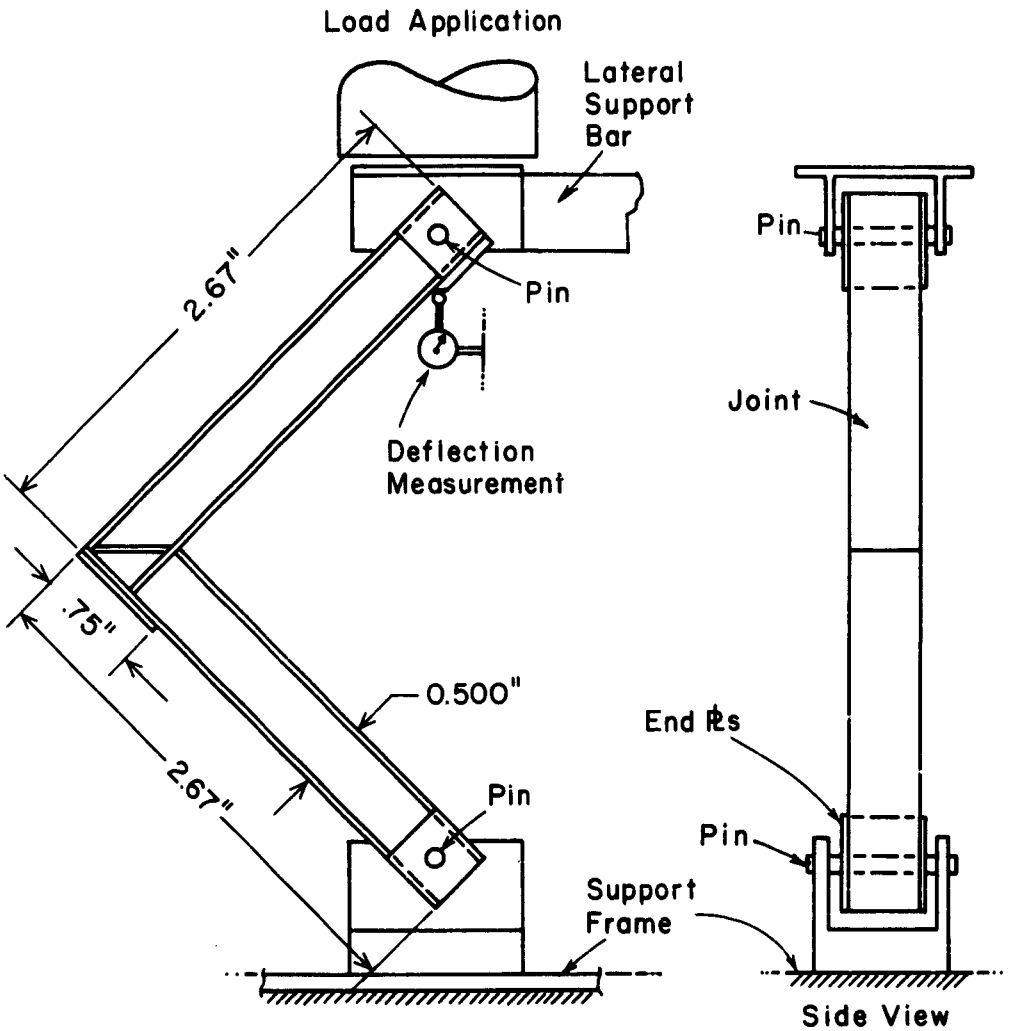

FIG. 4.1.31 TYPE "K" JOINT IN SUPPORTING FRAME

FIG. 4.1.32 MODEL JOINT IN THE SUPPORTING FRAME DURING TEST.

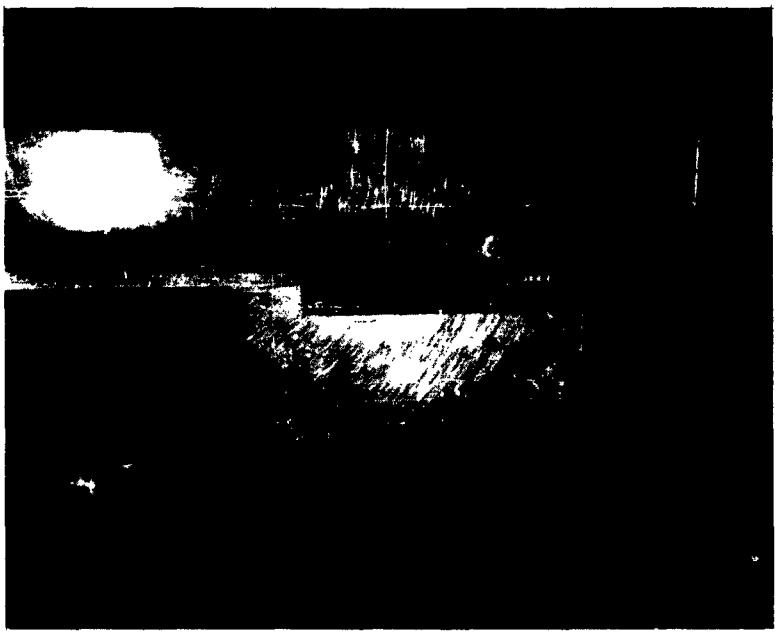

FIG. 4.1.33 CLOSEUP OF MODEL JOINT K-1 AFTER FAILURE. NOTE THE BUCKLING OF THE LOWER BEAM FLANGE.

4.1.3.3 Test Results. Tables 4.10 to 4.17 give the test results on the 8 tests made on model joints. Explanations of the values in the various columns of the tables are also given. The notations used for these calculations is given in Fig. 4.1.34. The moment vs. joint rotation curves are plotted in Fig. 4.1.35 for all the joints except P-1. All the joints depicted in this figure had the same dimensions, the same cross sectional area and were tested in the same manner. The only variable was the configuration of the corner. In Fig. 4.1.36 the moment rotation curve for joint P-1 is given. On the same plot the moment curvature relation for the phosphor bronze section is given. Joint P-1 failed on the column side which was apparently much weaker. This can be observed in Fig. 4.1.30.

4.1.3.4 Conclusions from the Connection Tests. Looking at Fig. 4.1.35 a number of conclusions may be drawn.

1. Except for connection A-1 all the joints can mobilize considerable joint rotations. Joint A-1 was the unstiffened joint.

2. The scatter from only two tests of each joint is not bad in the case of joint M and C but it is bigger in the case of joint K. This is due mainly to variation in workmanship.

3. The strongest joints were type M which had the most stiffeners.

4. Joints of type C show a lower value of moment capacity than type M but since they have proved adequate in the case of the frame tests they should be recommended since they are considerably easier to manufacture.

5. Type K joints are considerably stronger than C but these are as hard to make as type M as shown in Fig. 4.1.25 so they have no decisive advantage over type C.

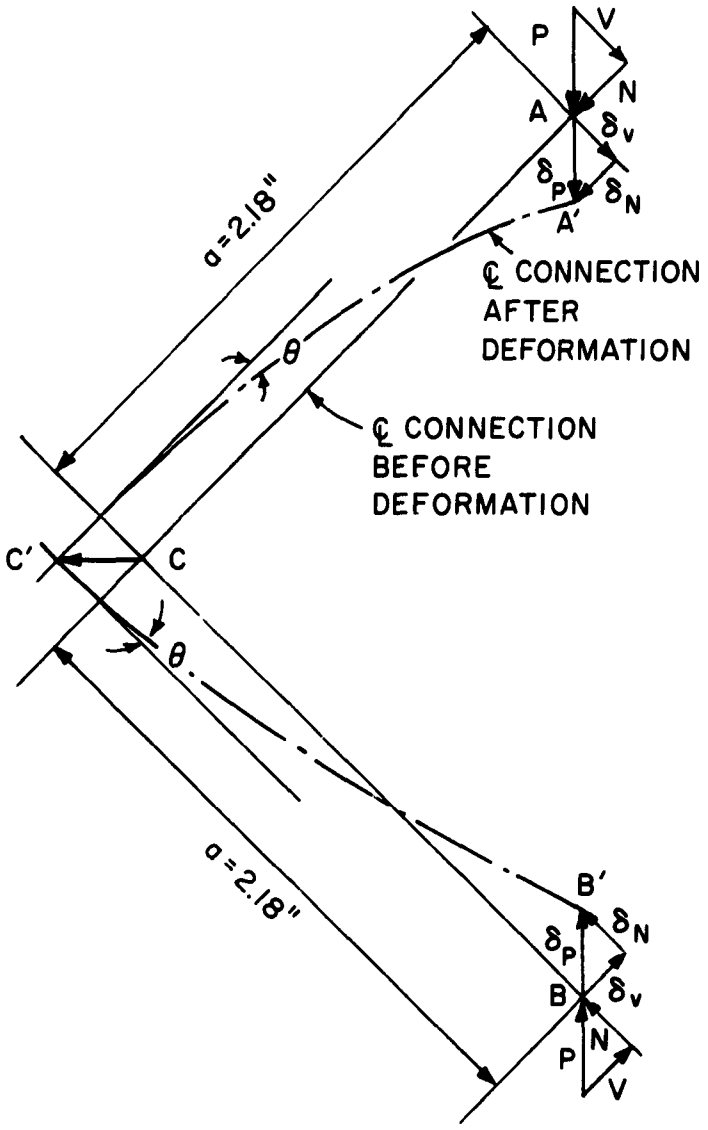

NOTATION:

P VERTICALLY APPLIED LOAD

N AXIAL COMPONET OF P

V SHEARING COMPONENT OF P

δ_P VERTICAL DEFLECTION

δ_V DEFLECTION ALONG V

δ_N DEFLECTION ALONG N

θ HALF THE JOINT ROTATION

a MOMENT ARM TO JOINT CENTER

M_P JOINT MOMENT CAUSED BY P

FIG. 4.1.34 TYPICAL CONNECTION BEFORE AND AFTER BENDING DEFORMATION CAUSED BY TWO COLINEAR FORCES

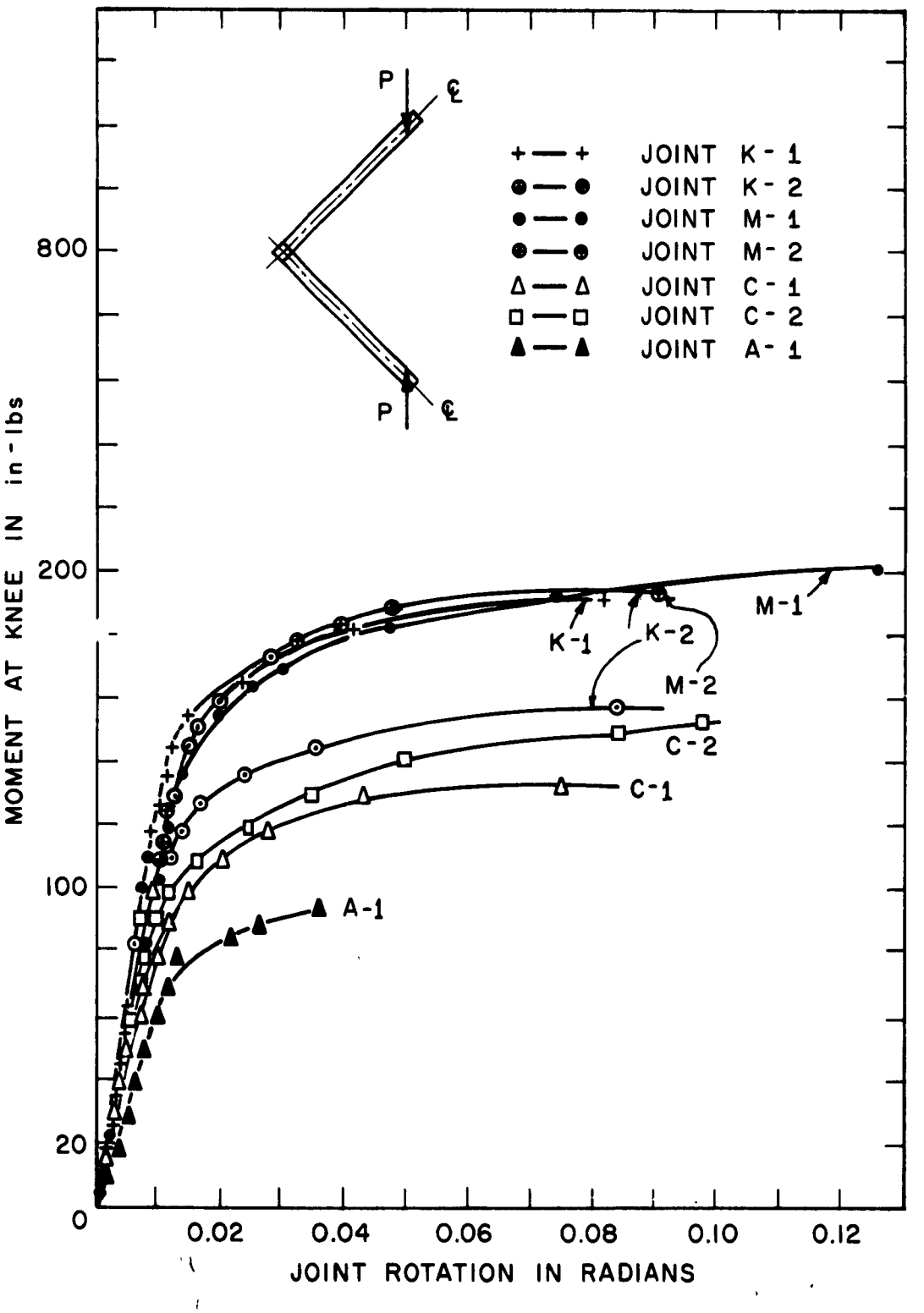

FIG. 4.1.35 MOMENT ROTATION CURVES OF MODEL JOINTS

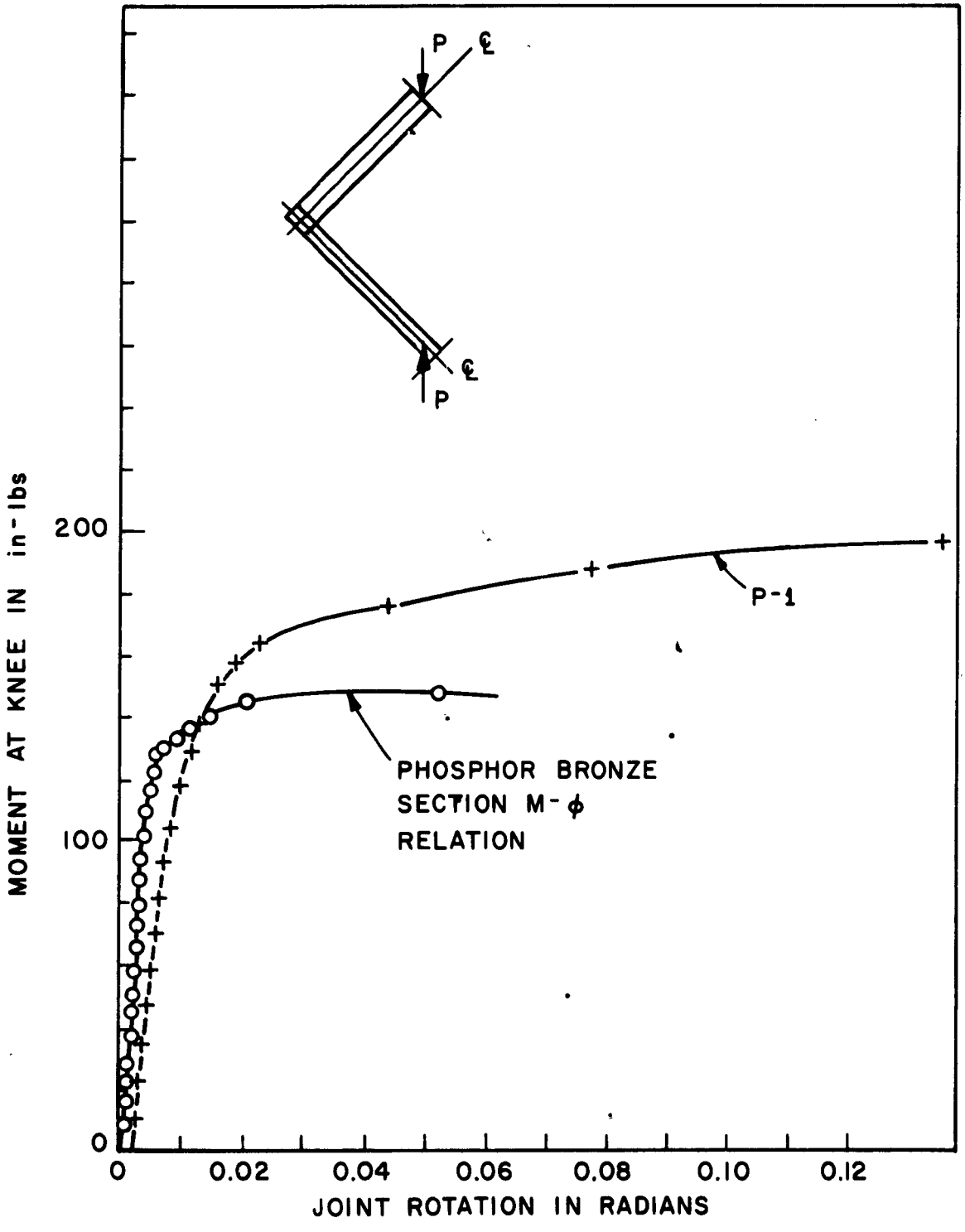

FIG.4.1.36 MOMENT ROTATION RELATIONS FOR JOINT P-1

TABLE 4.10 TEST RESULTS OF MODEL JOINT K-1

1 Load at End of Beam in (Inches)	2 Vertical Deflection δ_P (Inches)	3 δ_v (Inches)	4 Total Joint Rotation (Radians)	5 P Load on Joint (Lbs.)	6 Moment at Joint (Lbs-In)
1	.0045	.00318	.00146	5.91	9.1
2	.006	.00424	.00195	11.82	18.2
3	.008	.00565	.00259	17.73	27.3
4	.009	.00636	.00292	23.64	36.4
5	.011	.00777	.00354	29.55	45.5
6	.012	.00846	.00388	35.46	54.6
7	.0142	.0100	.00459	41.37	63.7
8	.0165	.01165	.00535	47.28	72.8
9	.0188	.0133	.0061	53.19	82.0
10	.021	.01482	.0068	59.10	91.0
11	.023	.01625	.00746	65.01	100.0
12	.026	.01835	.00832	70.92	109.0
13	.0285	.02015	.0092	76.83	118.0
14	.0314	.0222	.0102	82.74	127.2
15	.034	.024	.011	88.65	136.5
16	.038	.02682	.01235	94.56	145.8
17	.0465	.03282	.0151	100.47	154.8
18	.0535	.0378	.01735	106.38	164
19	.072	.0508	.0234	112.29	173
20	.127	.090	.0414	118.20	182
21	.25	.177	.0811	124.11	191

Explanation of Table 4.10

Col. 1 is the load at the end of the beam of the loading frame. This load was applied in increments of one pound and in such a manner that enough time was given to the specimen to allow for creep beyond the yield point.

Col. 2 is the deflection in the direction of the applied load P on the joint. This was measured with an Ames dial gage which reads to the nearest one thousandth of an inch. Since the bottom leg of the joint was prevented from moving vertically at Point B (Fig. 4.1.34) the upper leg at the point of load application A (Fig. 4.1.34) moved down 2 x δ_p.

Col. 3 is the component of the vertical deflection of Col. 2 in the direction of the shearing component of force V.

Col. 4 is the total joint rotation or 2 θ as shown on the Fig. 3.1.34. This was obtained approximately by dividing the deflection δ_v by the moment arm a.

Col. 5 is the load P on the joint which is obtained from the load at the end of the beam by multiplication with the factor of the loading frame depending on the position of the specimen along the beam.

Col. 6 is the moment at the knee or the intersection of the 2 center lines of the members forming the joint. It is obtained by multiplying the shearing component of P by the moment arm a. Note that the axial force N has no moment component at the knee.

$$M = (.707P)(2.18) = 1.54P \text{ (in-lb.)}$$

TABLE 4.11 TEST RESULTS OF MODEL JOINT K-2

1 Load at End of Beam in (Lbs.)	2 Vertical Deflection δ_p (Inches)	3 δ_v (Inches)	4 Total Joint Rotation (Radians)	5 P Load on Joint (Lbs.)	6 Moment at Joint (Lbs-In)
1	.0018	.00127	.000582	5.91	9.1
2	.004	.00282	.001295	11.82	18.2
3	.007	.00494	.00227	17.73	27.3
4	.009	.00635	.00292	23.64	36.4
5	.0112	.0079	.00362	29.55	45.5
6	.0138	.00975	.00448	35.46	54.6
7	.0174	.0123	.00565	41.37	63.7
8	.0194	.0137	.00629	47.28	72.8
9	.0218	.0154	.00707	53.19	82.0
10	.024	.017	.0078	59.10	91.0
11	.028	.0198	.0091	65.01	100.0
12	.032	.02262	.0104	70.92	109.0
13	.036	.02545	.0117	76.83	118.0
14	.0406	.0287	.0132	82.74	127.2
15	.050	.0353	.01622	88.65	136.5
16	.0595	.0421	.01935	94.56	145.8
17	.0735	.052	.0239	100.47	154.8
18	.111	.0785	.0361	106.38	164
19	.258	.1825	.0836	112.29	173

TABLE 4.12 TEST RESULTS OF MODEL JOINT M-1

1 Load at End of Beam in (Lbs.)	2 Vertical Deflection δ_p (Inches)	3 δ_v (Inches)	4 Total Joint Rotation (Radians)	5 P Load on Joint (Lbs.)	6 Moment at Joint (Lbs.-In)
1	.004	.00283	.0013	5.91	9.1
2	.0075	.0053	.00243	11.82	18.2
3	.010	.00707	.00324	17.73	27.3
4	.011	.00777	.00356	23.64	36.4
5	.014	.0099	.00454	29.55	45.5
6	.0165	.01165	.00535	35.46	54.6
7	.019	.0134	.00615	41.37	63.7
8	.0215	.0152	.00698	47.28	72.8
9	.0235	.0166	.00762	53.19	81.9
10	.0265	.0187	.00859	59.10	91.0
11	.029	.0205	.0094	65.01	100.0
12	.0315	.0222	.0102	70.92	109.0
13	.0345	.0244	.0112	76.83	118.0
14	.0375	.0265	.01215	82.74	127.2
15	.041	.029	.0133	88.65	136.5
16	.047	.0332	.01522	94.56	145.8
17	.060	.0424	.01945	100.47	154.8
18	.0745	.0526	.02415	106.38	164
19	.109	.077	.0354	112.29	173
20	.145	.1025	.047	118.20	182
21	.227	.161	.074	124.11	191
22	.390	.276	.1265	130.02	200.5

TABLE 4.13 TEST RESULTS OF MODEL JOINT M-2

1 Load at End of Beam in (Lbs.)	2 Vertical Deflection δ_p (Inches)	3 δ_v (Inches)	4 Total Joint Rotation (Radians)	5 P Load on Joint (Lbs.)	6 Moment at Joint (Lbs-In)
1	.0025	.00177	.000812	3.22	4.96
2	.0035	.00248	.00114	6.44	9.82
3	.005	.00354	.001625	9.66	14.9
4	.007	.00495	.002275	12.88	19.83
5	.0085	.0060	.002755	16.10	24.80
6	.0100	.00707	.00325	19.32	29.80
7	.0115	.00815	.00374	22.54	34.70
8	.0128	.00905	.00416	25.76	39.70
9	.0135	.00955	.00439	28.98	44.60
10	.0145	.01025	.0047	32.2	49.60
11	.0159	.01125	.00516	35.42	54.60
12	.017	.012	.0055	38.64	59.60
13	.018	.01275	.00585	41.86	64.5
14	.019	.01345	.00617	45.08	69.5
15	.0205	.0145	.00665	48.30	74.5
16	.022	.01555	.00713	51.52	79.5
17	.023	.01625	.00745	54.74	84.4
18	.0245	.01732	.00795	57.96	89.2
19	.0258	.01825	.00837	61.18	93.4
20	.027	.0191	.00875	64.40	99.2
21	.0285	.0202	.00927	67.62	104.2
22	.030	.0212	.00972	70.84	109
23	.032	.02263	.0104	74.06	114.2
24	.0336	.0238	.0109	77.28	119
25	.0352	.0249	.0114	80.50	124
26	.0375	.0265	.01215	83.72	129
27	.0395	.0280	.01285	86.94	133.8
28	.0424	.03	.01375	90.16	139.0
29	.045	.0318	.0146	93.38	143.7
30	.050	.0354	.0162	96.60	149
31	.054	.0382	.0175	99.82	153.5
32	.060	.0424	.01945	103.04	159
33	.066	.0466	.0214	106.26	163.5
34	.0775	.0548	.0251	109.48	168.5
35	.087	.0615	.0282	112.70	173.5
36	.100	.0707	.0324	115.92	178.2
37	.1215	.086	.0394	119.14	183.5
38	.146	.1032	.0473	122.36	188.5
39	.280	.198	.0907	125.58	193.2

TABLE 4.1[illegible] TEST RESULTS OF M[illegible]DEL JOINT C-1

1 Load at End of Beam in (Lbs.)	2 Vertical Deflection δ_p (Inches)	3 δ_v (Inches)	4 Total Joint Rotation (Radians)	5 P Load on Joint Lbs.)	6 Moment at Joint (Lbs-In)
1	.001	.000707	.000324	[illegible]3.22	4.96
2	.002	.[illegible]1414	.00065	[illegible].44	9.82
3	.0035	.[illegible]248	.00114	[illegible].66	14.9
4	.005	.[illegible]53	.00162	[illegible]98	19.83
5	.0065	.[illegible]6	.00211	[illegible]10	24.80
6	.0082	.[illegible]8	.00266	[illegible]2	29.80
7	.01	.[illegible]07	.00324	[illegible]	34.70
8	.0115	.[illegible]12	.00372	25.76	39.70
9	.0128	.[illegible]05	.00415	28.98	[illegible]
10	.0148	.[illegible]48	.00481	32.6	[illegible]
11	.0162	.[illegible]	.00528	35.42	[illegible]
12	.018	.[illegible]2	.00584	38.64	59.[illegible]
13	.020	.[illegible]4	.0065	[illegible].86	64.5
14	.0228	.[illegible]	.00747	45.08	69.5
15	.025	.[illegible]	.00812	48.30	74.5
16	.028	.[illegible]	.00907	51.52	79.5
17	.031	.[illegible]195	.0102	54.74	84.4
18	.[illegible]	.0248	.0114	57.96	89.2
19	.[illegible]	.02725	.0125	61.18	93.4
20	.0445	.0315	.01445	64.40	99.2
21	.0525	.0372	.0171	67.62	104.2
22	.0615	.0435	.0200	70.84	109
23	.072	.051	.0234	74.06	114.2
24	.0865	.0612	.0281	77.28	119
25	.102	.0722	.031	80.50	124
26	.1365	.0965	.0433	83.72	129
27	.230	.163	.075	86.94	133.8

TABLE 4.15 TEST RESULTS OF MODEL JOINT C-2

1 Load at End of Beam in (Lbs.)	2 Vertical Deflection δ_p (Inches)	3 δ_v (Inches)	4 Total Joint Rotation (Radians)	5 P Load on Joint (Lbs.)	6 Moment at Joint (Lbs-In)
1	.001	.000707	.000325	3.22	4.96
2	.0015	.00106	.000486	6.44	9.82
3	.0022	.00155	.000712	9.66	14.9
4	.003	.00212	.00974	12.88	19.83
5	.004	.00282	.00129	16.10	24.80
6	.0052	.00367	.001685	19.32	29.80
7	.0065	.00459	.00211	22.54	34.70
8	.008	.00565	.00259	25.76	39.70
9	.01	.00707	.0032	28.98	44.60
10	.0115	.00815	.00374	32.6	49.60
11	.0135	.00955	.00438	35.42	54.60
12	.0155	.011	.00505	38.64	59.60
13	.0178	.0126	.00579	41.86	64.5
14	.020	.01414	.0065	45.08	69.5
15	.0242	.0171	.00785	48.30	74.5
16	.025	.0177	.00813	51.52	79.5
17	.0266	.0188	.00862	54.74	84.4
18	.0292	.02062	.00946	57.96	89.2
19	.032	.0226	.0104	61.18	93.4
20	.0356	.0252	.0115	64.40	99.2
21	.042	.0297	.0136	67.62	104.2
22	.0502	.0355	.0165	70.84	109
23	.0618	.0438	.201	74.06	114.2
24	.075	.053	.0243	77.28	119
25	.0872	.0616	.0283	80.50	124
26	.106	.075	.0344	83.72	129
27	.127	.0898	.0412	86.94	133.8
28	.151	.1068	.049	90.16	141
29	.1835	.13	.0596	93.38	143.6
30	.2585	.183	.084	96.60	148.8
31	.300	.212	.0972	99.82	153.5

TABLE 4.16 TEST RESULTS OF MODEL JOINT A-1

1 Load at End of Beam in (Lbs.)	2 Vertical Deflection δ_p (Inches)	3 δ_v (Inches)	4 Total Joint Rotation (Radians)	5 P Load on Joint (Lbs.)	6 Moment at Joint (Lbs-In)
1	.002	.001414	.00065	3.22	4.96
2	.0055	.0039	.00179	6.44	9.82
3	.0076	.00536	.00246	9.66	14.9
4	.0102	.0072	.0033	12.88	19.83
5	.0128	.00905	.00416	16.10	24.30
6	.015	.0106	.0046	19.32	29.80
7	.017	.012	.0055	22.54	34.70
8	.019	.0134	.00615	25.76	39.70
9	.021	.01482	.0068	28.98	44.70
10	.0232	.0164	.00753	32.6	49.60
11	.026	.0184	.00845	35.42	54.60
12	.0285	.0201	.00923	38.64	59.60
13	.0316	.0224	.0103	41.86	64.5
14	.035	.0247	.0113	45.08	69.5
15	.046	.0325	.0149	48.30	74.5
16	.054	.0382	.0175	51.52	79.5
17	.066	.0466	.0214	54.74	84.4
18	.082	.058	.0266	57.96	89.2
19	.110	.0777	.0357	61.18	93.7

TABLE 4.17 TEST RESULTS OF MODEL JOINT P-1

1 Load at End of Beam in (Lbs.)	2 Vertical Deflection δ_p (Inches)	3 δ_v (Inches)	4 Total Joint Rotation (Radians)	5 P Load on Joint (Lbs.)	6 Moment at Joint (Lbs-In)
1	.0065	.0046	.00211	3.22	11.7
2	.009	.00635	.00291	6.44	23.4
3	.0105	.00742	.00341	9.66	35.2
4	.013	.0092	.00422	12.88	46.8
5	.0155	.01095	.00502	16.10	58.5
6	.018	.01270	.00582	19.32	70.2
7	.0202	.01425	.00655	22.54	82
8	.0232	.0164	.00755	25.76	93.6
9	.027	.0191	.00875	28.98	105.2
10	.0315	.0222	.0102	32.6	118.5
11	.0365	.0258	.01182	35.42	129.0
12	.0425	.03	.01375	38.64	140.8
13	.050	.0353	.0162	41.86	152.2
14	.0715	.0505	.02318	45.08	164
15	.136	.096	.044	48.30	175.8
16	.239	.169	.0775	51.52	187.2
17	.430	.304	.1395	54.74	199

4.2 DYNAMIC TESTS ON MODEL PORTAL FRAMES MADE OF PHOSPHOR BRONZE

Tests on fixed ended portal frames were performed to check the dynamic response of simple structures and compare the increase in strength to that of a static test. In these dynamic tests the impulsive loading machine used is described in Section 3.4.2. The static test was performed in the beam loading apparatus.

4.2.1 Type of Pulse Possible. The impulsive loading machine has the capability of giving rise times down to 3-4 milliseconds. However, these are more impactive rather than impulsive type loads since to achieve these small rise times the ram must not be in contact with the structure but must have an initial travel. A typical load pulse experienced by a frame is shown in Fig. 4.2.1 where a rise time of about 3 milliseconds was achieved.

4.2.2 The Model. The portal frame was made of the same phosphor bronze section which approximates the 8WF40 rolled section at 1:15 scale. The dimensions and the details of obtaining the necessary fixity are shown in Fig. 4.2.2. The model was supported in a special frame shown in Fig. 3.4.11 which was placed in the machine in such a way so that the vertical travel of the machine ram produced the lateral load on the model. Load was measured by the load cell described earlier and the lateral displacement by an L.V.D.T. Both of these outputs were displayed on a cathode ray oscilloscope and a permanent record was taken photographically. Fig. 4.2.3 shows the model frame before and after the test.

4.2.3 The Test Results. The load time variation as experienced by the model frame is plotted from the photographic record in Fig. 4.2.4. Fig. 4.2.5 gives the displacement time variation for the same frame. From these two plots we can find the load displacement curve of the frame as shown in Fig. 4.2.6. This is the dynamic response of the model frame covering the early part of the response.

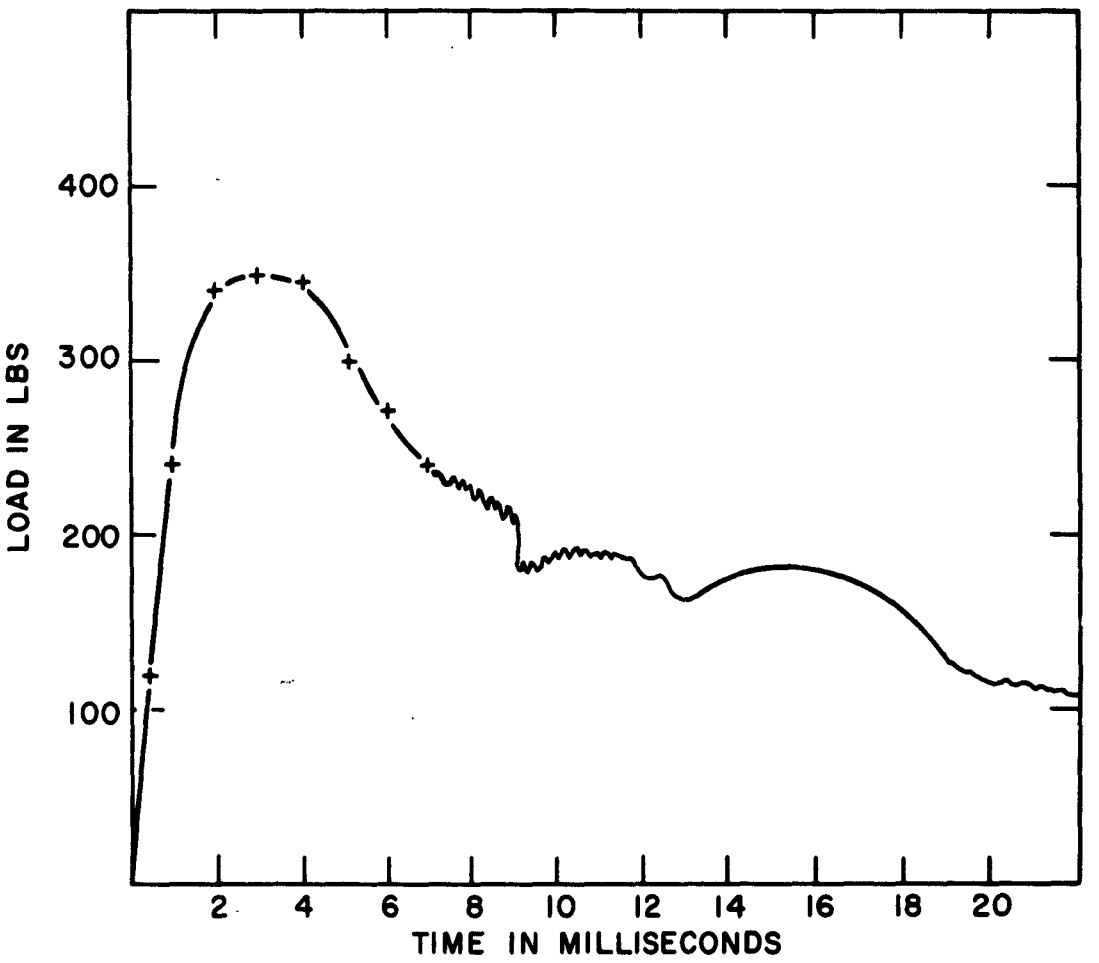

FIG. 4.2.1 TYPICAL TIME LOAD PULSE EXPERIENCED BY FRAME

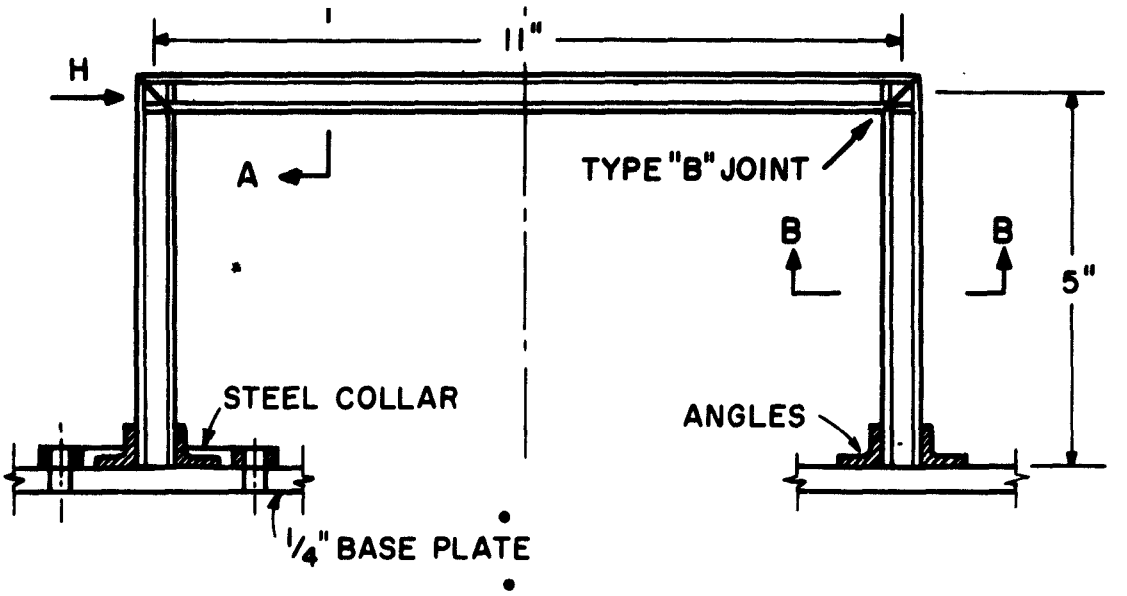

a. DIMENSIONS OF MODEL PHOSPHOR BRONZE FRAME AT 1:15 SCALE

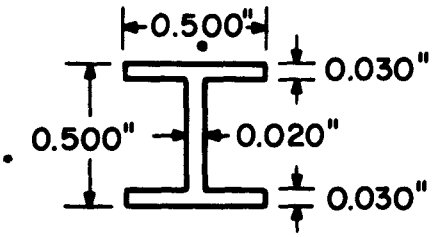

b. SECTIONS A-A & B-B

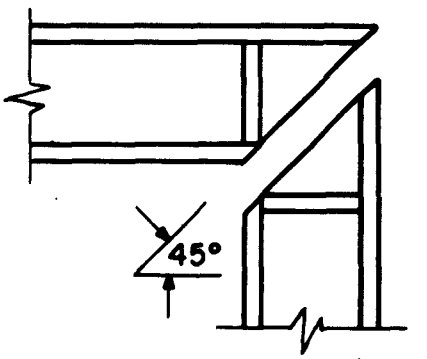

c. DETAIL OF TYPE "B" JOINT BEFORE ASSEMBLY

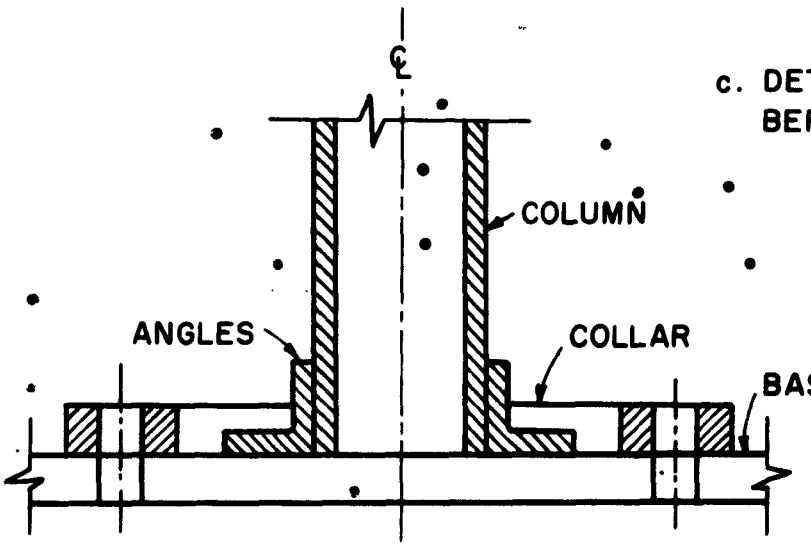

d. DETAIL AT BASE OF COLUMN TO INSURE FIXITY

FIG.4.2.2 DRAWING OF 1:15 SCALE MODEL SHOWING CONSTRUCTION DETAILS

a. BEAM AND COLUMN PARTS BEFORE ASSEMBLY

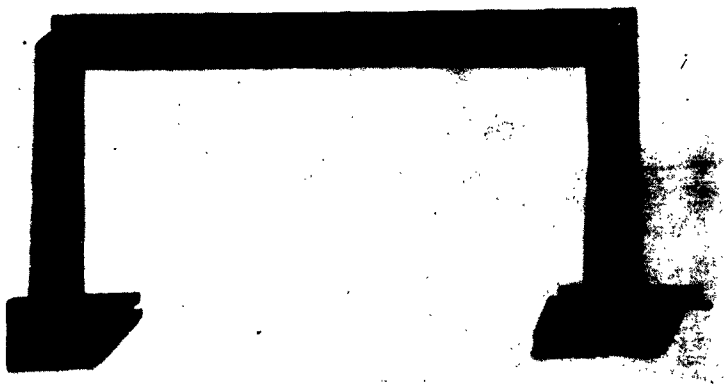

b. WELDED FRAME BEFORE TESTING

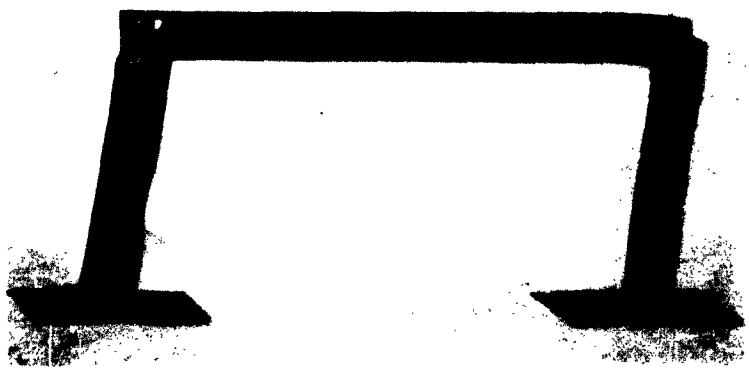

c. FRAME #1, AFTER TESTING

FIC. 4.2.3 PICTURES SHOWING THE MODEL BEFORE AND AFTER THE DYNAMIC TEST

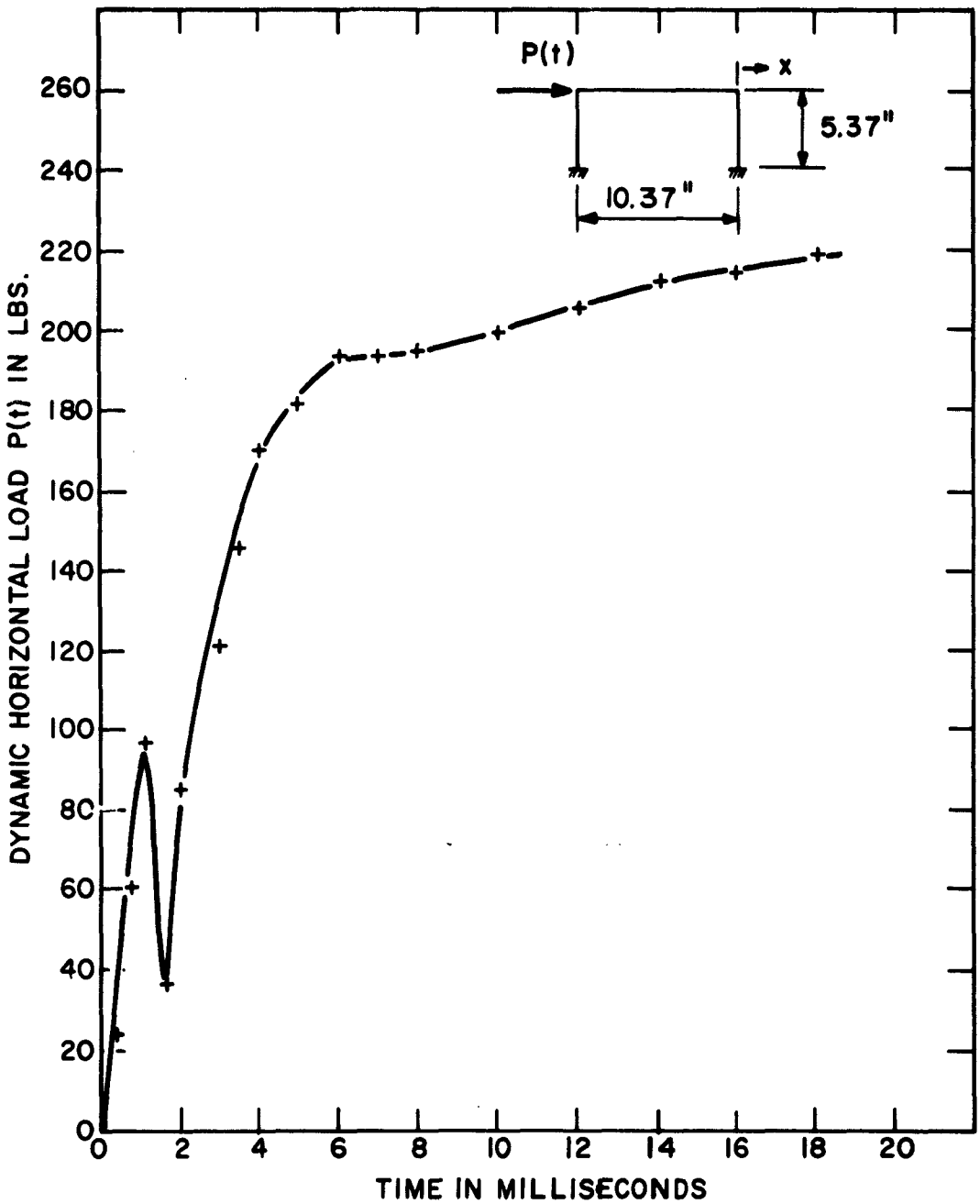

FIG. 4.2.4 LOAD TIME RELATION FOR MODEL FRAME

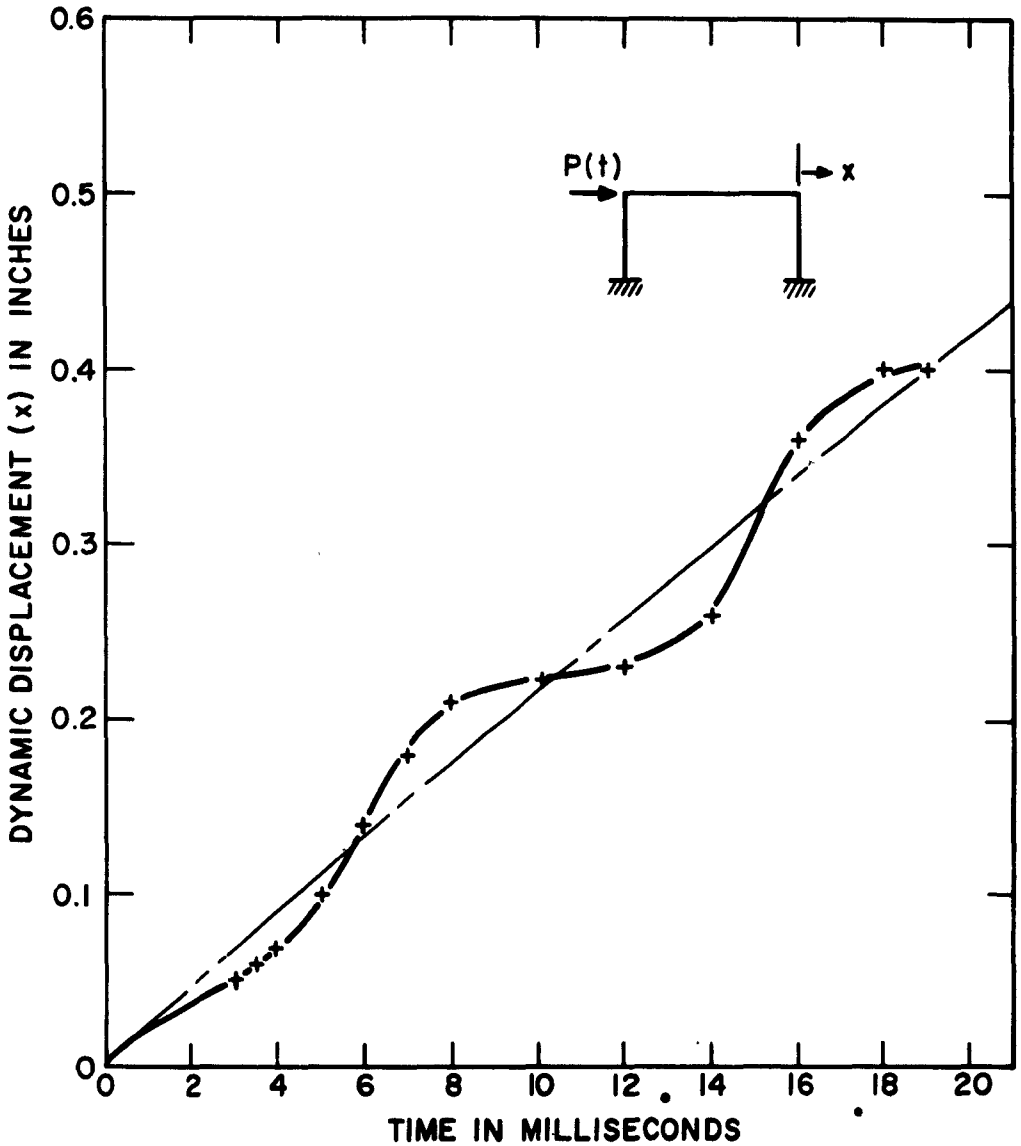

FIG. 4.2.5 DISPLACEMENT TIME RELATION FOR MODEL FRAME

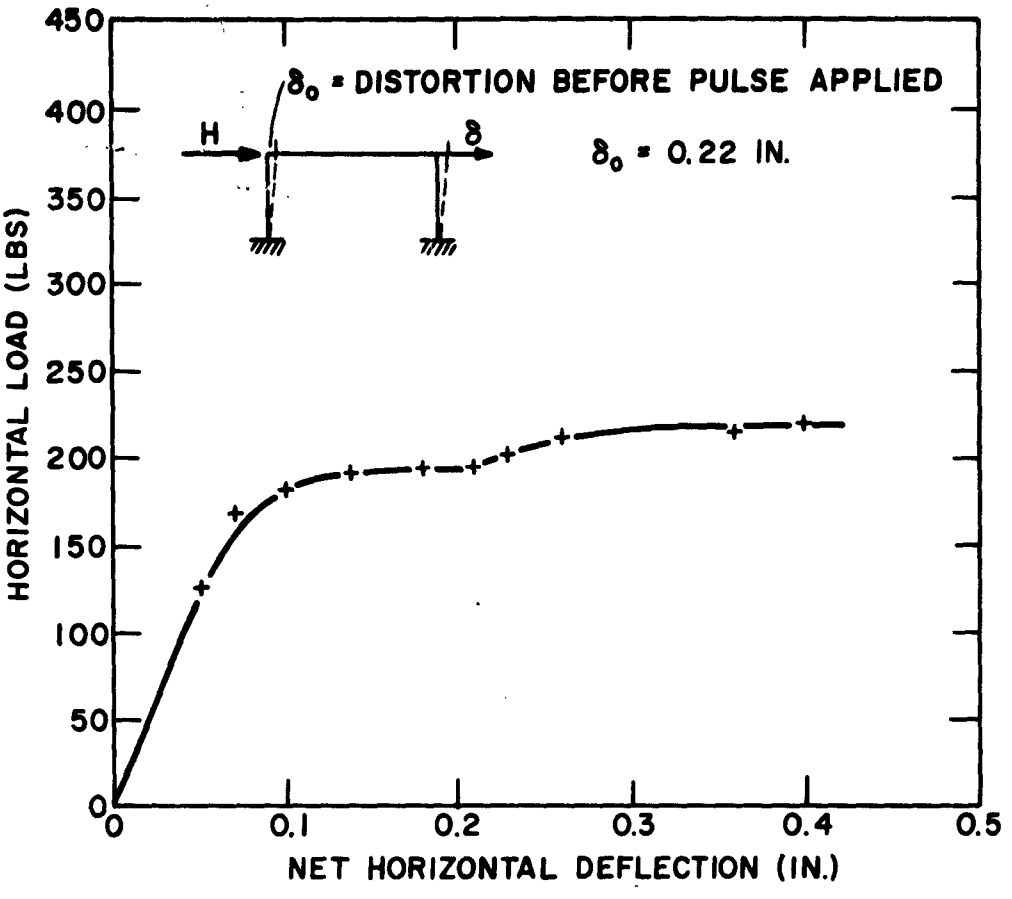

FIG. 4.2.6 LOAD DEFLECTION CURVE FOR MODEL FRAME, DYNAMIC TEST

A static test was also made on a similar frame and the results are given in Table 4.18. The load deflection curve for this model is given in Fig. 4.2.7.

4.2.4 Conclusions from the Dynamic Tests. No correlation between model and prototype could be obtained in this case since there were no known full scale tests to model. However, some conclusions could be drawn from this limited study of dynamic behavior.

1. It can be seen that the dynamic load taken by the model frame is considerably larger than the static test value. The dynamic Pult. is about 220 lbs. and the static is about 130 lbs. where equal deflections were used as a criterion of finding the static Pult.

2. The mode of failure in both static and dynamic tests was essentially the same.

TABLE 4.18 RESULTS OF STATIC LATERAL FORCE ON MODEL FRAME

Load at End Of Beam (Lbs.)	Horizontal Deflection (Inches)	Horizontal Force (Lbs.)
1	.006	5.91
2	.071	11.82
3	.014	17.73
4	.017	23.64
5	.0216	29.55
6	.0265	35.46
7	.0315	41.37
8	.0389	47.28
9	.045	53.19
10	.053	59.10
11	.0625	65.01
12	.0745	70.92
13	.090	76.83
14	.102	82.74
15	.1182	88.65
16	.1302	94.56
17	.1485	100.47
18	.174	106.38
19	.2215	112.29
20	.2825	118.20
21	.351	124.11
22	.461	130.02
23	.600	135.93
24	.815	141.84
25	.986	147.75

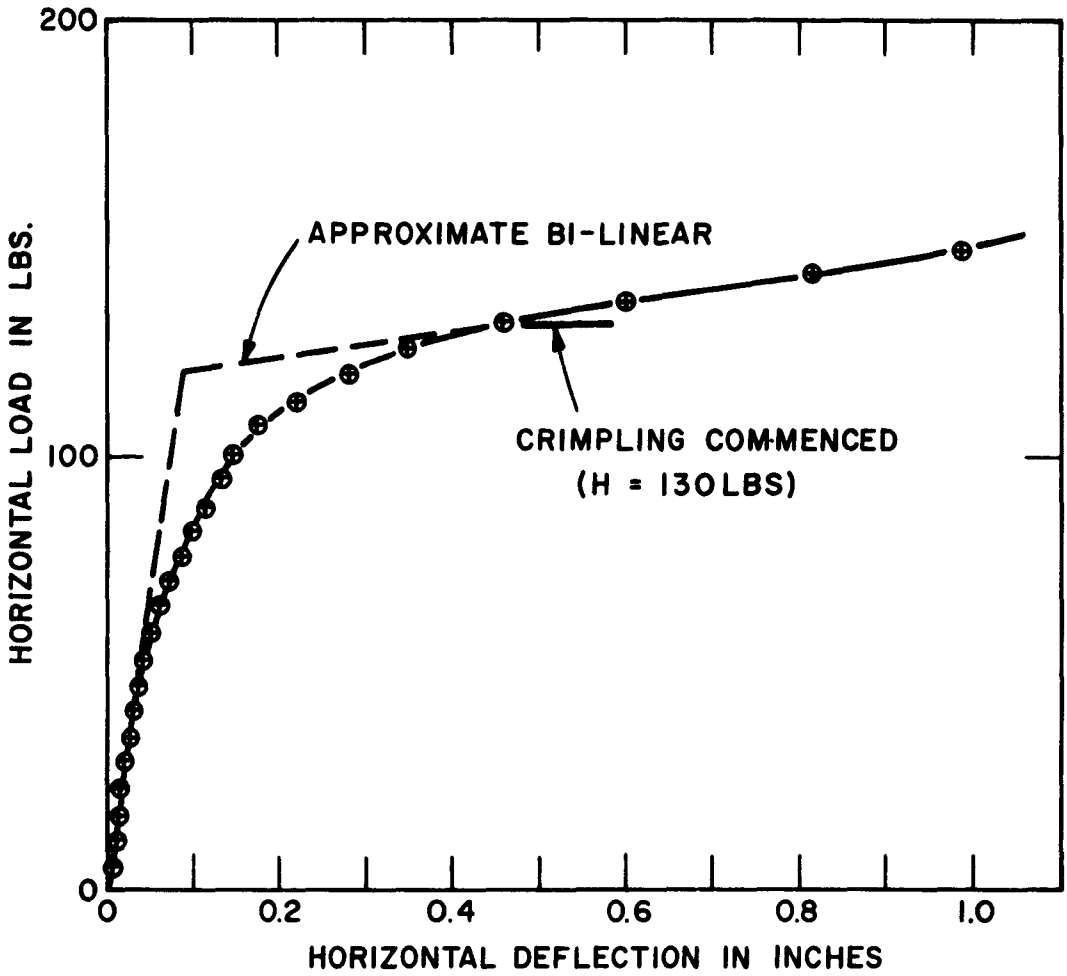

FIG. 4.2.7 LOAD DEFLECTION CURVE FOR MODEL FRAME, STATIC TEST

APPENDIX A

Consider a linearly elastic beam of length L, stiffness EI, coefficient of damping d and mass ς per unit length. The beam is subjected to a solid body acceleration $\ddot{z}$ by the application of constant forces $F = \frac{1}{2} \varsigma \ddot{z} L$ to its two ends. It is desired to determine the deviation at time t of the bending moment of points along the beam from their steady state value

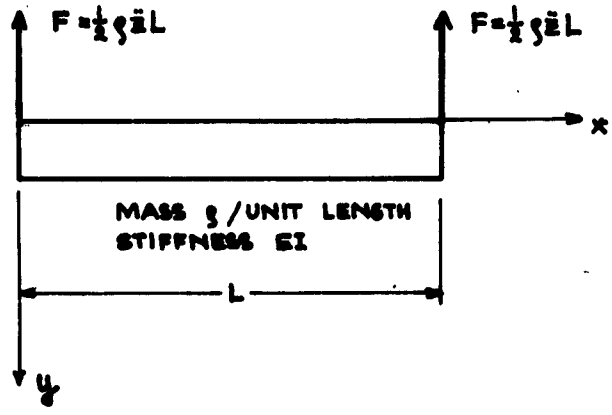

Fig. A.1

Let the x - and y- axes of Figure A.1 move with the beam. Then the governing equation for dynamic equilibrium of the beam is

$$EI \frac{\partial^4 y}{\partial x^4} = \varsigma \ddot{z} - \varsigma \frac{\partial^2 y}{\partial t^2} - d \frac{\partial y}{\partial t} \qquad (A1)$$

Initial conditions: $y = \frac{\partial y}{\partial t} = 0$ for $t = 0$ (A2)

Bound. conditions: $y = \frac{\partial^2 y}{\partial x^2} = 0$ for $x = 0$ and $x = L$ (A3)

Since the governing equation is not homogeneous, substitute $y(x,t) = Y(x,t) + \varphi(x)$ (A4)

and Eqn. (A1) becomes

$$EI\left[\frac{\partial^4 Y}{\partial x^4} + \frac{\partial^4 \varphi}{\partial x^4}\right] = \rho\ddot{z} - \rho\frac{\partial^2 Y}{\partial t^2} - d\frac{\partial Y}{\partial t} \quad (A5)$$

Equation (A5) is homogeneous if $\frac{d^4\varphi(x)}{dx^4} = \frac{\rho}{EI}\ddot{z}$ (A6)

$$\text{i.e. } EI\frac{\partial^4 Y}{\partial x^4} = -\rho\frac{\partial^2 Y}{\partial t^2} - d\frac{\partial Y}{\partial t} \quad (A7)$$

The boundary conditions of the new governing eqn. (A7) are homogeneous if, according to (A3) and (A4)

$$\varphi = \frac{\partial^2 \varphi}{\partial x^2} = 0 \quad \text{for } x=0 \text{ and } x=L \quad (A8)$$

Equation (A6) with boundary conditions (A8) represents a uniformly loaded simply supported beam so that

$$\varphi = \frac{\rho\ddot{z}}{24EI}\left[x^4 - 2Lx^3 + L^3x\right] \quad (A9)$$

It remains to solve (A7) subject to the initial conditions

$$\begin{aligned} Y(x,o) &= -\varphi(x) \\ \frac{\partial Y}{\partial t}(x,o) &= 0 \end{aligned} \quad (A10)$$

and boundary conditions

$$\begin{aligned} Y(o,t) &= Y(L,t) = 0 \\ \frac{\partial^2 Y}{\partial x^2}(o,t) &= \frac{\partial^2 Y}{\partial x^2}(L,t) = 0 \end{aligned} \quad (A11)$$

A trial solution $Y = f(x)\,g(t)$ leads to

$$\frac{f''''}{f} = -\frac{\frac{\rho}{EI}g'' + \frac{d}{EI}g'}{g} = k^4$$ where k is real, and f is differentiated with respect to x, g with respect to t.

$$\therefore Y = e^{-\frac{d}{2\rho}t}\left[c_1' \cos \omega t + c_2' \sin \omega t\right]\left[c_1 \cos kx + c_2 \sin kx + c_3 \cosh kx + c_4 \sinh kx\right]$$

According to the boundary conditions (A11)

$$c_1 = c_3 = c_4 = 0$$

and $\sin kL = 0$

$$\therefore\ k = \frac{n\pi}{L} \qquad n = 0, 1, 2, \ldots$$

$$\text{also } w = \sqrt{\frac{n^4\pi^4 EI}{\rho L^4} - \frac{d^2}{4\rho^2}} \tag{A12}$$

Generally thus

$$Y = \sum_{n=1}^{\infty} e^{-\frac{d}{2\rho}t} \left[c_1' \cos wt + c_2' \sin wt \right] \sin \frac{n\pi x}{L} \tag{A13}$$

From the second of initial conditions (A10):

$$c_2 = \frac{d}{2\rho w} c_1$$

so that (A13) becomes

$$Y = \sum_{n=1}^{\infty} c_n \, e^{-\frac{d}{2\rho}t} \left[\cos wt + \frac{d}{2\rho w} \sin wt \right] \sin \frac{n\pi x}{L}$$

The first initial condition yields

$$\sum_{n=1}^{\infty} c_n \sin \frac{n\pi x}{L} = -\varphi(x) = \frac{\ddot{z}}{24EI} \left[2Lx^3 - x^4 - L^3 x \right]$$

The Fourier coefficients, determined in the normal fashion, are

$$c_n = \frac{2\rho \ddot{z} L^4}{EI \pi^5 n^5} \left[(-1)^n - 1 \right].$$

The general solution for the deflection of the beam is thus

$$y = \frac{\rho \ddot{z}}{EI} \left\{ \frac{x^4}{24} - \frac{Lx^3}{12} + \frac{L^3 x}{24} + \frac{2L^4}{\pi^5} \sum_{n=1}^{\infty} \left[\frac{\left[(-1)^n - 1 \right]}{n^5} e^{-\frac{d}{2\rho}t} \times \right.\right.$$

$$\left.\left. (\cos wt + \frac{d}{2\rho w} \sin wt) \sin \frac{n\pi x}{L} \right] \right\}$$

The first three terms inside the bracket represent the static deflection of the beam, and the last term is an oscillation the amplitude of which is decreasing with time.

The moment in the beam at time t is

$$M = -EI\frac{\partial^2 y}{\partial x^2} = -\rho\ddot{a}\left\{\frac{x^2}{2} - \frac{Lx}{2} + \frac{2L^2}{\pi^3}\sum_{n=1}^{\infty}\frac{[1-(-1)^n]}{n^3}\, e^{-\frac{d}{2\rho}} \right.$$

$$\left. (\cos wt + \frac{d}{2\rho w}\sin wt)\sin\frac{n\pi x}{L}\right\}$$

At midspan,

$$M = \rho\ddot{a}\left\{\frac{L^2}{8} + \frac{2L^2}{\pi^3}\sum_{n=1}^{\infty}\frac{[(-1)^n-1]}{n^3}\, e^{-\frac{d}{2\rho}t}(\cos wt + \frac{d}{2\rho w}\sin wt)\sin\right.$$

(

It is desired to give the variation of M with time for various percentages p of critical damping. From (A12)

$$d_{cr} = \frac{2n^2\pi^2}{L^2}\sqrt{\rho EI} \qquad (A$$

and

$$w = \frac{n^2\pi^2}{L^2}\sqrt{\frac{EI}{\rho}(1-p)} \qquad (A$$

$$\frac{d}{2\rho} = \frac{n^2\pi^2}{L^2}p\sqrt{\frac{EI}{\rho}} \qquad (A$$

Substitution of (A16) and (A17) into (A14) yields all the desired results.

Table B.1

Appendix B: Computations for Section 2.7.1

$\frac{x}{\ell}$	y = 0			y = t		
	b = 0.1 ℓ	b=0.25 ℓ	b=0.50 ℓ	b=0.10 ℓ	b=0.25 ℓ	b=0.50 ℓ
0	-0.0041	-0.0093	-0.0128	-1.128	-0.753	-0.559
0.125	-0.0038	-0.0085	-0.0118	-0.447	-0.704	-0.642
0.250	-0.0028	-0.0064	-0.0090	0.119	-0.506	-0.721
0.375	-0.0014	-0.0034	-0.0049	0.228	-0.106	-0.516
0.500	0.0001	0.0002	0	0.050	0.361	0
0.625	0.0016	0.0036	0.0049	0.070	0.616	0.516
0.750	0.0028	0.0064	0.0090	0.201	0.509	0.721
0.875	0.0036	0.0083	0.0118	0.149	0.149	0.642
1.000	0.0039	0.0089	0.0128	0.063	0.031	0.559

Values of the ratio $\frac{\sigma_x}{p}$ for $t = \ell$.

Table B.2

$\frac{x}{\ell}$	$\frac{\sigma_x}{p}$	$\frac{\sigma_y}{p}$	$\frac{\tau_{xy}}{p}$	α	$\frac{\tau_{max}}{p}$	$\frac{\sigma_1}{p}$	$\frac{\sigma_2}{p}$
			$y = 0.8\ t, \quad b = 0.1\ \ell$				
0	-0.1851	0.2490	0	90	0.317	0.249	-0.185
0.125	-0.1342	0.1990	0.0968	105	0.193	0.225	-0.160
0.250	-0.0388	0.1113	0.1171	119	0.139	0.180	-0.098
0.375	0.0187	0.0624	0.0839	127	0.087	0.127	-0.046
0.500	0.0362	0.0514	0.0656	132	0.066	0.110	-0.022
0.625	0.0531	0.0164	0.0535	145	0.057	0.091	-0.021
0.750	0.0682	0.0189	0.0317	154	0.040	0.084	0.003
0.875	0.0642	0.0213	0.0072	170	0.022	0.064	0.020
			$y = 0.8\ t, \quad b = 0.25\ \ell$				
$\frac{x}{\ell}$	$\frac{\sigma_x}{p}$	$\frac{\sigma_y}{p}$	$\frac{\tau_{xy}}{p}$	α	$\frac{\tau_{max}}{p}$	$\frac{\sigma_1}{p}$	$\frac{\sigma_2}{p}$
0	-0.291	0.456	0	90	0.373	0.456	-0.291
0.125	-0.259	0.429	0.198	105	0.397	0.482	-0.312
0.250	-0.169	0.353	0.195	108	0.325	0.417	-0.233
0.375	-0.039	0.240	0.234	120	0.273	0.373	-0.173
0.500	0.087	0.125	0.208	132	0.209	0.315	-0.102
0.625	0.162	0.055	0.131	146	0.142	0.250	-0.033
0.750	0.169	0.047	0.048	161	0.067	0.175	0.041
0.875	0.136	0.076	0.005	176	0.030	0.136	0.076
1.000	0.056	0.094	0	180.	0.019	0.094	0.056

Table B.3

$\frac{x}{\ell}$	$\frac{\sigma_x}{p}$	$\frac{\sigma_y}{p}$	$\frac{\tau_{xy}}{p}$	α	$\frac{\tau_{max}}{p}$	$\frac{\sigma_1}{p}$	$\frac{\sigma_2}{p}$
	$y = 0.8\ t, \quad b = 0.50\ \ell$						
0	-0.2896	0.6564	0	90	0.473	0.656	-0.290
0.125	-0.2802	0.6502	0.0786	95	0.470	0.655	-0.285
0.250	-0.2389	0.6170	0.1711	101	0.461	0.650	-0.282
0.375	-0.1434	0.5316	0.2577	109	0.424	0.618	-0.230
0.500	0	0.4000	0.2944	118	0.355	0.555	-0.155
0.625	0.1434	0.2684	0.2577	128	0.265	0.471	-0.059
0.750	0.2389	0.1821	0.1711	138	0.194	0.404	0.017
0.875	0.2802	0.1498	0.0786	155	0.104	0.319	0.111
1.000	0.2896	0.1436	0	180	0.073	0.290	0.144
	$y = 0.6\ t, \quad b = 0.10\ \ell$						
$\frac{x}{\ell}$	$\frac{\sigma_x}{p}$	$\frac{\sigma_y}{p}$	$\frac{\tau_{xy}}{p}$	α	$\frac{\tau_{max}}{p}$	$\frac{\sigma_1}{p}$	$\frac{\sigma_2}{p}$
0	-0.0652	0.1093	0	90	0.087	0.109	-0.065
0.125	-0.0560	0.1013	0.0224	98	0.082	0.105	-0.059
0.250	-0.0340	0.0844	0.0361	105	0.069	0.095	-0.044
0.375	-0.0083	0.0651	0.0382	113	0.053	0.081	-0.025
0.500	0.0117	0.0505	0.0327	120	0.038	0.069	-0.007
0.625	0.0247	0.0413	0.0248	126	0.026	0.059	0.007
0.750	0.0335	0.0356	0.0171	134	0.017	0.052	0.017
0.875	0.0395	0.0323	0.0090	146	0.010	0.046	0.026
1.000	0.0418	0.0300	0	180	0.012	0.042	0.030

Table B.4

$\frac{x}{\ell}$	$\sigma_y = 0.6\ t$ $b = 0.25\ \ell$						
	$\frac{\sigma_x}{p}$	$\frac{\sigma_y}{p}$	$\frac{\tau_{xy}}{p}$	α	$\frac{\tau_{max}}{p}$	$\frac{\sigma_1}{p}$	$\frac{\sigma_2}{p}$
0	-0.1334	0.2493	0	90	0.191	0.249	-0.133
0.125	-0.1191	0.2391	0.0398	96	0.184	0.244	-0.124
0.250	-0.0828	0.2116	0.0708	103	0.163	0.229	-0.099
0.375	-0.0322	0.1728	0.0859	110	0.133	0.203	-0.063
0.500	0.0200	0.1335	0.0822	118	0.100	0.177	-0.023
0.625	0.0604	0.1040	0.0628	127	0.067	0.149	0.016
0.750	0.0828	0.0884	0.0387	133	0.039	0.125	0.047
0.875	0.0909	0.0841	0.0172	151	0.018	0.107	0.072
$\frac{x}{\ell}$	$y = 0.6\ t$ $b = 0.50\ \ell$						
	$\frac{\sigma_x}{p}$	$\frac{\sigma_y}{p}$	$\frac{\tau_{xy}}{p}$	α	$\frac{\tau_{max}}{p}$	$\frac{\sigma_1}{p}$	$\frac{\sigma_2}{p}$
0	-0.1593	0.4169	0	90	0.288	0.417	-0.159
0.125	-0.1486	0.4068	0.0403	94	0.280	0.409	-0.151
0.250	-0.1176	0.3867	0.0778	98	0.264	0.398	-0.129
0.375	-0.0653	0.3485	0.1062	104	0.233	0.375	-0.091
0.500	0	0.3000	0.1171	109	0.190	0.340	-0.040
0.625	0.0653	0.2515	0.1062	114	0.140	0.298	0.018
0.750	0.1176	0.2133	0.0778	119	0.091	0.257	0.074
0.875	0.1486	0.1932	0.0403	121	0.046	0.217	0.125
1.000	0.1593	0.1832	0	90	0.012	0.183	0.159

Table B.5

$\frac{x}{\ell}$	$\frac{\sigma_x}{p}$	$\frac{\sigma_y}{p}$	$\frac{\tau_{xy}}{p}$	α	$\frac{\tau_{max}}{p}$	$\frac{\sigma_1}{p}$	$\frac{\sigma_2}{p}$
			y = 0.4 t		b = 0.1 ℓ		
0	-0.0245	0.0569	0	90	0.041	0.057	-0.025
0.125	-0.0219	0.0551	0.0067	95	0.039	0.056	-0.022
0.250	-0.0154	0.0505	0.0117	100	0.035	0.053	-0.018
0.375	-0.0065	0.0443	0.0141	105	0.029	0.048	-0.010
0.500	0.0026	0.0380	0.0139	109	0.022	0.043	-0.002
0.625	0.0101	0.0329	0.0115	113	0.016	0.038	0.005
0.750	0.0154	0.0295	0.0079	114	0.011	0.033	0.012
0.875	0.0183	0.0277	0.0041	111	0.006	0.029	0.017
1.000	0.0193	0.0271	0	90	0.004	0.027	0.019
			y = 0.4 t		b = 0.25 ℓ		
$\frac{x}{\ell}$	$\frac{\sigma_x}{p}$	$\frac{\sigma_y}{p}$	$\frac{\tau_{xy}}{p}$	α	$\frac{\tau_{max}}{p}$	$\frac{\sigma_1}{p}$	$\frac{\sigma_2}{p}$
0	-0.0544	0.1374	0	90	0.096	0.137	-0.054
0.125	-0.0492	0.1338	0.0143	95	0.092	0.134	-0.049
0.250	-0.0352	0.1240	0.0254	99	0.084	0.128	-0.039
0.375	-0.0222	0.1106	0.0313	103	0.073	0.118	-0.029
0.500	0.0044	0.0966	0.0315	107	0.056	0.106	-0.005
0.625	0.0222	0.0846	0.0267	110	0.041	0.094	0.012
0.750	0.0352	0.0760	0.0188	112	0.028	0.083	0.028
0.875	0.0430	0.0710	0.0097	108	0.017	0.072	0.040
1.000	0.0456	0.0694	0	90	0.012	0.069	0.046

Table B.6

	y = 0.4 t b = 0.25 ℓ						
$\frac{x}{\ell}$	$\frac{\sigma_x}{p}$	$\frac{\sigma_y}{p}$	$\frac{\tau_{xy}}{p}$	α	$\frac{\tau_{max}}{p}$	$\frac{\sigma_1}{p}$	$\frac{\sigma_2}{p}$
0	-0.0708	0.2482	0	90	0.1595	0.248	-0.071
0.125	-0.0652	0.2442	0.0170	93	0.1550	0.245	-0.066
0.250	-0.0498	0.2339	0.0314	96	0.1450	0.237	-0.053
0.375	-0.0265	0.2183	0.0411	99	0.1295	0.225	-0.034
0.500	0	0.2000	0.0466	102	0.1100	0.210	-0.010
0.625	0.0265	0.1818	0.0411	104	0.0875	0.192	0.017
0.750	0.0498	0.1661	0.0314	104	0.0659	0.174	0.042
0.375	0.0652	0.1557	0.0170	100	0.0481	0.154	0.057
1.000	0.0708	0.1518	0	90	0.0405	0.152	0.071

APPENDIX C

As discussed earlier, the cross section chosen for the phosphor bronze models was only an approximation of the prototype at the length scale used. This was done in order to faciliatate the machining operations and to cut down on the cost. It was also assumed that geometric corrections could be easily applied to the model results.

The most significant geometric property involved in the type of tests performed was the moment of inertia. This was the case because bending moments were of primary concern. The effects of axial forces and shearing distortions were neglected.

We define the geometric factor, G.F., as follows:

$$G.F. = \frac{\text{Geometric property of Exact Model}}{\text{Geometric property of Actual Model}} \qquad (C.1)$$

For cases involving the moment of inertia of the section the following correction should be used to the values predicted from the model test:

$$G.F. = \frac{I_p \times f_r^4}{I_m} \qquad (C.2)$$

where,

I_p = moment of inertia of prototype about the strong axis.

I_m = moment of inertia of model section about strong axis.

f_r = length scale.

In the case of the 8WF40 section used as a prototype at a scale of 1:15 the model section had an $I_m = .002\ in^4$ and thus the G.F. is

$$G.F. = \frac{146.2 \times (1/15)^4}{.002} = 1.45$$

This was used in all computations of moment and load prediction from the phosphor bronze model tests.

APPENDIX D

In a section under constant moment we can find the curvature or the change in slope of the elastic curve per unit length from the measurement of strains across the critical section.

From elementary beam theory we know that using the convention of Fig. D.1

$$\frac{1}{R} = -\frac{M}{EI} \qquad (D.1)$$

in the elastic range and where 1/R is usually taken as $\frac{d2y}{dx^2}$. If we measure the strains across the critical section and assume that plane sections before bending remain plane after bending we get:

$$\frac{1}{R} = \frac{d^2y}{dx^2} = \frac{d\phi}{dx} \qquad (D.2)$$

where ϕ is the slope to the elastic curve or the rotation of the critical section.

Assuming that strain measurements are taken at the top and bottom flanges and at the upper and lower quarter points of the web we have looking at Fig. D.1

ϵ_1 = top flange strain (-ve)
ϵ_2 = upper quarter point strain in web
ϵ_3 = lower quarter point strain in web
ϵ_4 = bottom flange strain (+ve)
d = depth of section

For an infinitesimal length of beam at the critical section, say dx, we have,

$$\frac{d\phi}{dx} = \frac{\epsilon_4 - \epsilon_1}{d} = \frac{\epsilon_3 - \epsilon_2}{d/2}$$

$$= \frac{\epsilon_2 - \epsilon_1}{d/4} = \frac{\epsilon_4 - \epsilon_3}{d/4} \qquad \text{(D.3)}$$

The average of these values is taken as the curvature:

$$\frac{1}{R} = \frac{d\phi}{dx} = \frac{\epsilon_4 - \epsilon_1}{4d} + \frac{2(\epsilon_3 - \epsilon_2)}{4d} + \frac{4(\epsilon_2 - \epsilon_1)}{4d}$$

$$+ \frac{4(\epsilon_4 - \epsilon_3)}{4d} \qquad \text{(D.4)}$$

$$\frac{1}{R} = \frac{5\epsilon_1 - 2\epsilon_2 + 2\epsilon_3 - 5\epsilon_4}{4d}$$

APPENDIX E

If deflections are measured along a section of a beam in which the moment is constant or approximately so, then the curvature could be determined. Using the notation of Fig. E.1 , we can derive an expression for the second derivative of the deflection at point 2 as follows.

$$\frac{1}{R} = \frac{-\frac{d^2y}{dx^2}}{\left[1+\left(\frac{dy}{dx}\right)^2\right]^{3/2}} \cong -\frac{d^2y}{dx^2} \qquad (E.1)$$

$$(\text{Second Slope})_2 = \frac{\text{Slope}_{2-3} - \text{Slope}_{1-2}}{\Delta x} \qquad (E.2)$$

where

$$\text{Slope}_{1-2} = \frac{y_2 - y_1}{\Delta x},$$

$$\text{Slope}_{2-3} = \frac{y_3 - y_2}{\Delta x},$$

$$(\text{Second Slope})_2 = (1/R)_2$$

$$= \frac{\frac{y_3 - y_2}{\Delta x} - \frac{y_2 - y_1}{\Delta x}}{\Delta x}$$

$$= \frac{y_3 - 2y_2 + y_1}{(\Delta x)^2} \qquad (E.3)$$

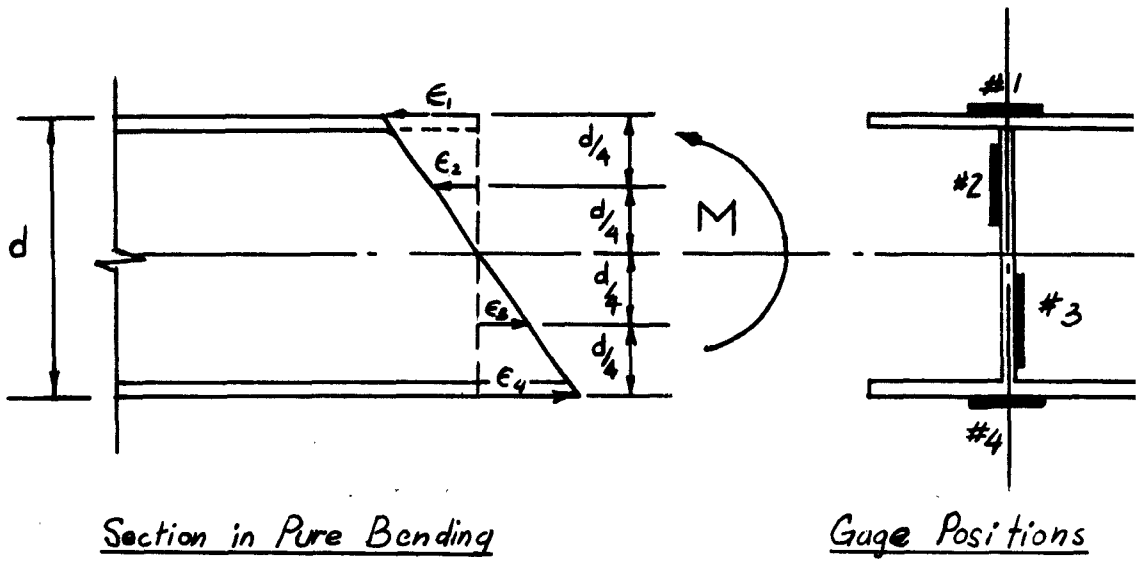

Fig. D.1 Notation for strain readings

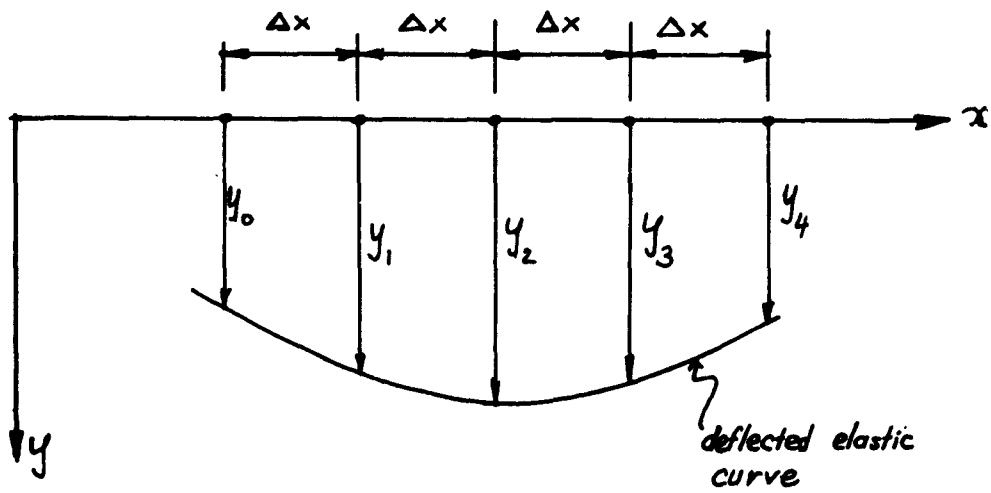

Fig. E.1 Notation for deflections

APPENDIX F

The singly redundant portal frame shown in Fig. F.1 was tested beyond the elastic limit. In order to know the bending moment at the center line, the horizontal reaction must be measured during the entire loading cycle.

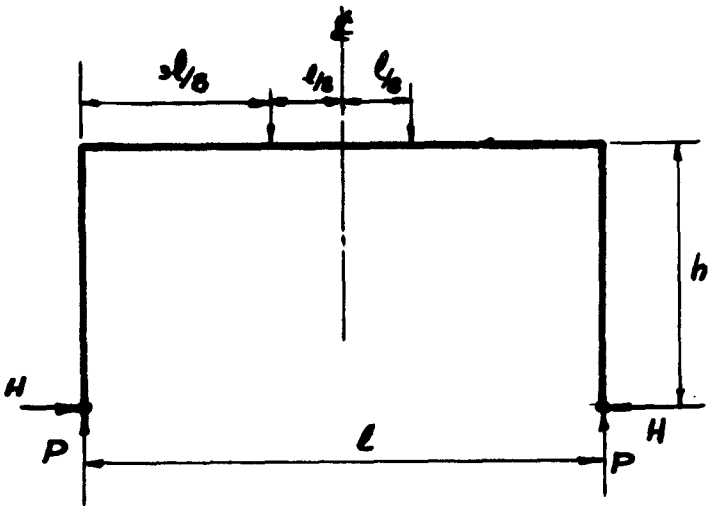

Fig. F.1 Singly Redundant Portal Frame

The bending moment at the centerline section is given by:

$$M = P\frac{\ell}{2} - Hh - P\frac{\ell}{8}$$

$$= P\left(\frac{3}{8}\ell\right) - Hh \qquad (F.1)$$

Substituting the values of $\ell = 11.2"$, $h = 5.6"$

$$M = 4.2\,P - 5.6H \qquad (F.2)$$

The values of H were taken from Fig. 4.1.21.

REFERENCES

1. Antebi, J., Smith, H.D., Hansen, R.J., "Study of the Applicability of Models for the Investigation of Air Blast Effects on Structures", Technical Report to the Defense Atomic Support Agency, M.I.T. Department of Civil Engineering, October 1960.

2. Antebi, J., Smith, H.D., Sharma, S.D., Harris, H.G., Hansen, R.J., "Evaluation of Techniques for Constructing Model Structural Elements", Technical Report to the Defense Atomic Support Agency, M.I.T. Department of Civil Engineering, May 1962.

3. Beaujoint, N., "General Report", RILEM Bulletin No.7, June 1960, p.5.

4. Beaujoint, N., "Modele Reduit en Caoutchouc du Branage de Roselend", RILEM Bulletin No. 8, September 1960, p. 41.

5. Beedle, L.S., Huber, A.W., "Residual Stresses and the Compressive Strength of Steel", Welding Journal, Welding Research Supplement.

6. Beedle, L.S., Plastic Design of Steel Frames , John Wiley and Son, Inc. N.Y. (1958).

7. Biggs, J.M., Hansen, R.J., "Model Techniques used in Structural Engineering Research at M.I.T.," RILEM.

8. Biggs, J.M., Suer, H.S. "The Vibration of Simple Span Highway Bridges", Journal Str. Div. ASCE Vol. 83, No. ST2, March, 1957.

9. Bikhovsky, V.A., et.al., "Tests on Reduced Models of Structures", International Colloquium on Model Scale Structures, Madrid, 1959.

10. Borges, J. Ferry, Lima, Urga E., "Crack and Deformation Similitude in Reinforced Concrete", RILEM Bulletin No.7, June 1960, p.79.

11. Borges, J. Ferry, "Statistical Theories of Structural Similitude", RILEM International Colloquim on Models of Structures, Madrid, June, 1959.

12. Bridgman, P.N., Dimensional Analysis , Yale University Press, 1922.

13. Charlton, T.M., Model Analysis of Structures , London, Spon.

14. "Commentary on Plastic Design in Steel: Connections:" Progress Report No. 6 of the Joint WRC-ASCE Committee on Plasticity Related to Design, April 1960, Mechanic Section ASCE Journal.

15. "Commentary on Plastic Design in Steel: Deflections:" Progress Report No. 7 of the Joint WRC-ASCE Committee on Plasticity Related to Design, April 1960, Mechanic Section ASCE Journal.

16. Fraser, D., Statistics: An Introduction. John Wiley & Sons, Inc.

17. Goodier, J.N. and Thomson, W.T., "Applicability of Similarity Principles to Structural Models", NACA Technical Note No. 933, 1944.

18. Hansen, R.J., "Controlled Impulsive Load Testing Machine", Proceedings, Society for Experimental Stress Analysis, Vol. 6, No. 2, p.64, 1948.

19. Hergenröder, A., Rüsch, H., "Recent Findings in the Testing of Models", Proceedings of the Symposium on Shell Research, Delft, August 1961, p. 316, North Holland Publishing Company.

20. Johnson, B.G., Yang, C.H., and Beedle, L.S., "An Evaluation of Plastic Analysis as Applied to Structural Design", Welding Journal, Welding Research Supplement Vol. XVIII, 1953, p. 224.

21. Ketter, R.L., "The Influence of Residual Stresses on the Strength of Structural Members", Welding Research Council Bulletin No. 44, 1958.

22. Knudsen, K.E., Yang, C.H., Johnson, B.C., "Plastic Strength and Deflections of Continuous Beams". Welding Journal, May, 1953.

23. Langhaar, H.L., Dimensional Analysis and Theory of Models. John Wiley & Sons, Inc. New York 1951. Ch. 2.

24. Leonhardt, F., Spannbeton für die Praxis, Wilhelm Ernst & Sohn, Berlin.

25. Luxion, W., Johnson, B., "Plastic Behavior of Wide Flange Beams", Welding Journal 27 (11), p. 538-S, November 1948.

26. Mayerjak, R.J., "A Study of the Resistance of Model Frames to Dynamic Lateral Load", University of Illinois Publication No. 108, August, 1955.

27. Metals Handbook (1960) American Society for Metals.

28. Moisseiff, S.L., "George Washington Bridge: Design of of the Towers", Trans. A.S.C.E., Vol. 97, p. 164, 1933.

29. Murphy, G., "Similitude in Engineering." New York, Ronald Press, 1950.

30. Norris, Hansen, Holley, et al., "Structural Design for Dynamic Loads", McGraw-Hill Book Company, Inc.

31. Oberti, G., "Large Scale Model Testing of Structures Outside the Elastic Limit", ISMES, Bergamo, Italy.

32. Oberti, G., "Arch Dams: Development of Model Researches in Italy", Proc. ASCE, August 1957.

33. Rocha, M., "The Determination of the Safety Factor of Arch Dams by Means of Models", Madrid, June 1959.

34. Rocha, M., Serafim, J.L., Estevis Ferreira, M.J., "The Determination of the Safety Factor of Arch Dams by Means of Models", RILEM Bulletin No. 7, June 1960, p. 68.

35. Rocha, M. "Dimensionnement Experimental des Constructions", Annals de l'I.T.B.T.P., February 1952.

36. Ruge, A.C., "Earthquake Resistance of Elevated Water-tanks", Proceeding ASCE, p.883, May 1937.

37. Ruzek, J.M., Knudsen, K.E., Johnston, E.R., Beedle, L.S., "Welded Portal Frames Tested to Collapse", Welding Journal 33(9), p. 469-S (1954)

38. Serafim, J.L., Azevedo, M.C., "Methods in Use at the Laboratorio Nacional de Engenharia Civil for the Stress Analysis in Models of Dams", Madrid, June 1959.

39. Serafim, J.L., "Methods and Materials for the Study of the Weight Stresses in Dams by Means of Models", Madrid, June 1959.

40. Serafim, J.L., Da Costa, J.P., "Methods and Materials for the Study of the Weight Stresses in Dams by Means of Models", RILEM Bulletin No. 10, March 1961, p.49.

41. Schilling, C.G., Schutz, Jr., F.W., Beedle, L.S., "Behavior of Welded Single-Span Frames Under Combined Loading", Welding Journal 35 (5), p. 235-S, (1956).

42. Shaw, W.A., "Static and Dynamic Behavior of Portal-Frame Knee Connections", U.S. Naval Civil Engineering Laboratory, Port Hueneme, California, May 1962.

43. Simpson, H., "Design and Construction of a Testing Machine for Large Dynamic Loads", M.I.T., February 1959.

44. Timoshenko, Goodier, Theory of Elasticity , Mc-Graw-Hill Book Company, Inc.

45. Topractsoglou, A.A., Johnston, B.G., Beedle, L.S., "Plastic Design and the Deformation of Structures" Welding Journal, N.Y. 30" 348-S - 356-S, 1951.

46. Topractsoglou, A.A., Johnston, B.G., Beedle, L.S., "Connections for Welded Continuous Portal Frames", Welding Journal, 30 (7), p. 359-S (1951); 30(8), p. 237-S (1951), 31 (11) p. 543-S (1952).

47. Van Driest, "On Dimensional Analysis and the Presentation of Data in Fluid Flow Problems", J. Applied Mechanics, Vol. 13, No. 1, p. A34, March 1946.

48. Van Vlack, "Elements of Materials Science", Addison Wesley Publishing Co., Inc. Reading, Mass. 1959

49. Wells, W.M. , "Design, Construction and Operation of a Machine for Testing Reinforced Concrete Slabs under Long Duration Impulsive Loads", M.I.T. 1950, ScD Thesis.

50. Wilbur, J.B., Norris, C.H., Goodier, J.N., "Structural Model Analysis" and "Dimensional Analysis", Handbook of Experimental Stress Analysis, Hetenyi, Editor, New York, John Wiley & Sons, 1950.

51. Wilson, J.S., Gore, W., "Stresses in Dams; An Experimental Investigation by Means of India Rubber Models", Proceedings I.C.E., Paper No. 3705, Vol. 172, Part 2 1908.

52. Winter, G., "Properties of Steel and Concrete and the Behavior of Structures", Journal Str. Div. ASCE, February 1960.

52. Young, J.F., "Materials and Processes", (1958) John Wiley and Sons, Inc. N.Y.

DISTRIBUTION LIST FOR
BLAST & SHOCK
R & D REPORTS

ADDRESSEE	ARMY	NO. OF CYS.
Chief of Engineers, D/A, Washington 25, D. C. Attn:	ENGCW-NE	1
	ENGTE-E	1
	ENGMC-E	1
Commanding General, U. S. Army Materiel Command, Washington, D. C.	Attn: AMCRD-DE-N	2
Commanding General, U. S. Continental Army Command, Ft. Monroe, Virginia		1
President, U. S. Army Air Defense Board, Ft. Bliss, Texas		1
Commandant, Command & General Staff College, Ft. Leavenworth, Kansas, Attn: Archives		1
Commandant, U. S. Army Air Defense School, Ft. Bliss, Texas	Attn: Command & Staff Dept.	1
Director, Special Weapons Development, Hq. CDC, Ft. Bliss, Texas, Atttn: Chester I. Peterson		1
Commanding General, Aberdeen Proving Ground, Aberdeen, Md. Attn: Director, BRL		1
Commanding General, The Engineer Center, Ft. Belvoir, Va. Attn: Asst. Commandant, Engineer School		1
Director, U. S. Army Research and Development Laboratory Ft. Belvoir, Va.	Attn: Chief, Tech. Support Branch	1
Commanding Officer, Picatinny Arsenal, Dover, N.J. Attn:	ORDBB-TK	1

ARMY (Cont'd.)	NO. OF CYS.
Commanding General, USA Electronic R&D Lab. Ft. Monmouth N.J., Attn: Technical Documents Center, Evans Area	1
Commanding General, USA Missile Command, Huntsville, Alabama	1
Commanding Officer, U. S. Army Nuclear Defense Laboratory, Edgewood Arsenal, Edgewood, Md. Attn: Tech. Library	1
Director, Waterways Experiment Station, U. S. Army Corps of Engineers, Vicksburg, Mississippi, Attn: Library	1
Director, U. S. Army Corps of Engineers, Nuclear Cratering Group, Livermore, California	1
NAVY	
Director of Naval Intelligence, ND, Wash. 25, D.C. Attn: OP-922V	1
Chief, Bureau of Naval Weapons, ND, Wash. 25, D.C.	2
Chief, Bureau of Ships, ND, Washington 25, D. C. Attn: Code 372	1
Attn: Code 423	1
Chief, Bureau of Yards and Docks, ND, Wash. 25,D.C. Attn: Code D-400	1
Attn: Code D-440	1
Chief of Naval Research, ND, Washington 25, D.C. Attn: Code 811	1
Superintendent, U. S. Naval Postgraduate School, Monterey, California	1

NAVY (Cont'd.)	NO. OF CYS.
Commanding Officer, Nuclear Weapons Training Center, Atlantic, Naval Base, Norfolk 11, Va. Attn: Nuclear Warfare Dept.	1
Commanding Officer, U. S. Naval Schools Command, U. S. Naval Station Treasure Island, San Francisco, California	1
Commanding Officer, Nuclear Weapons Training Center, Pacific, Naval Station, North Island, San Diego 35, California	2
Commanding Officer, U. S. Naval Damage Control Training Center, Naval Base, Philadelphia 12, Pa. Attn: ABC Defense Course	1
Commander, U. S. Naval Ordnance Laboratory, Silver Spring 19, Maryland	
Attn: EA	1
Attn: EU	1
Attn: E	1
Commander, U. S. Naval Ordnance Test Station, China Lake, Calif.	1
Commanding Officer & Director, U. S. Naval Civil Engineering Laboratory, Port Hueneme, Calif. Attn: Code L31	1
Director, U. S. Naval Research Laboratory Washington 25, D. C.	1
Commanding Officer & Director, Naval Electronics Laboratory, San Diego 52, Calif.	1
Commanding Officer & Director, David W. Taylor Model Basin, Washington 7, D.C. Attn: Library	1

AIR FORCE	NO. OF CYS.
Air Force Intelligence Center, Hq. USAF ACS/I (AFCIN-3K2) Washington 25, D.C.	1
ASD, Wright Patterson AFB, Ohio	1
Commander, Air Force Logistics Command, Wright - Patterson AFB, Ohio	2
AFSC, Andrews Air Force Base, Washington 25, D.C., Attn: RDRWA	1
Director, Air University Library, Maxwell AFB Alabama	2
AFCRL, L. G. Hanscom Field, Bedford, Mass. Attn: CRQST-2	1
AFSWC (SWRS) Kirtland AFB, New Mexico	1
Commandant, Institute of Technology, Wright-Patterson AFB, Ohio, Attn: MCLI-ITRIDL	1
BSD, Norton AFB, California	1
Director, USAF Project RAND, Via: U. S. Air Force Liaison Office, The Rand Corporation, 1700 Main St. Santa Monica, California	1
Director of Civil Engineering, Hq.USAF, Washington 25, D. C. Attn: AFOCE	1
OTHERS	
Director of Defense Research & Engineering, Washington 25, D. C. Attn: Tech. Library	1
Commandant, Armed Forces Staff College, Norfolk 11, Virginia Attn: Library	1
Commander, Field Command, DASA, Sandia Base, Albuquerque, New Mexico	16

OTHERS(Cont'd.)	NO. OF CYS.
Commander, Field Command, DASA, Sandia Base, Albuquerque, New Mexico, Attn: FCWT	1
Attn: FCTG	1
Chief, Defense Atomic Support Agency, Washington 25, D. C.	5
Officer-in-Charge, U. S. Naval School, Civil Engineering Corps Officers, U. S. Naval Contruction Battalion, Port Hueneme, California	1
Los Alamos Scientific Laboratory, P. O. Box 1663, Los Alamos, New Mexico, Attn: Report Librarian (For Dr. A. C. Graves)	1
Administrator, National Aeronautics & Space Administration 1512 H. Street N.W. Washington 25, D. C.	1
Langley Research Center, NASA, Langley Field, Hampton, Va. Attn: Mr. Philip Donely	1
Chief, Classified Technical Library, Technical Information Service, U. S. Atomic Energy Commission, Washington 25, D. C. Attn: Mrs. Jean O'Leary (for Dr. Paul C. Fine)	1
Chief, Classified Technical Library, Technical Information Service, U. S. Atomic Energy Commission, Washington 25, D. C. Attn: Mrs. Jean O'Leary	1
Dr. Walter Bleakney, Forestal Research Center Library, Aeronautical Sciences Bldg. Princeton University, Princeton, N.J. Attn: Librarian	1
Manager, Albuquerque Operations Office, U. S. Atomic Energy Commission P. O. Box 5400, Albuquerque, New Mexico	1
Dr. Robert J. Hansen, Rm. 1-238, Massachusetts Institute of Technology, Cambridge 39, Mass.	1

OTHERS(Cont'd)	NO. OF CYS.
Dr. Bruce G. Johnston, The University of Michigan, University Research Security Office, Lobby 1, East. Eng. Bldg. Ann Arbor, Michigan	1
Sandia Corporation, Sandia Base, Albuquerque, New Mexico, Attn: Classified Document Division (For Dr. M. L. Merritt)	1
Dr. Nathan M. Newmark, University of Illinois, Room 207, Talbot Laboratory, Urbana, Illinois	1
Commander, ASTIA, Arlington Hall Station, Arlington 12, Virginia, Attn: TIPDR	15
Holmes & Narver, Inc., AEC Facilities Division 849 S. Broadway Los Angeles 14, California, Attn: Mr. Frank Galbreth	1
Professor Robert V. Whitman, Massachusetts Institute of Technology, Rm. 1-346A, Cambridge 39, Mass.	1
Professor J. Neils Thompson, University of Texas, Structural Mechanics Research Laboratory, Austin, Texas	1
Mr. Kenneth Kaplan, United Research Services, 1811 Trousdale Drive, Burlingame, California	1
Mr. Fred M. Sauer, Department of Physics, Stanford Research Institute, Menlo Park, California	1
Dr. Robert C. DeHart, Southwest Research Institute, P. O. Box 28281, San Antonio 6, Texas	1
Dr. Neidhardt, General American Transportation Corporation, 7501 N. Natchez Avenue, Niles, Illinois	1

OTHERS (Cont'd.)

Dr. T. H. Schiffman, Armour Research Foundation,
10 West 35th Street, Chicago 16, Illinois

Mr. Marc Peter, E. H. Plesset Associates, Inc.,
1281 Westwood Blvd., Los Angeles 24, Calif.

Professor M. G. Spangler, Iowa State University
Ames, Iowa

Mr. Sherwood Smith, Roland F. Beers, Inc.,
2520 Oakville, Alexandria, Va.

Mr. J. Barton, Space Technology Laboratories, Inc.
5500 West El Segunda Blvd., Los Angeles 1,
Calif.

Dr. Frank Shelton, Kaman Nuclear, Colorado Springs
Colorado

Paul Weidlinger, Consulting Engineer, 770 Lexington
Ave., New York 21, New York,
Attn: Dr. M. Baron

Mr. A. Weiderman, Armour Research Foundation
10 West 35th St. Chicago 16, Illinois